Gas-phase structures of molecules containing heavy *p*-block elements

Derek A. Wann

A thesis presented for the degree of
Doctor of Philosophy
in the College of Science and Engineering
at the University of Edinburgh, 2005

Declaration

This thesis has not been submitted, in whole or in part, for any degree at this or any other university. The work is original and my own, carried out under the supervision of Prof. David W. H. Rankin; where this is not so, credit has been duly given.

Acknowledgements

I would like to thank my supervisor, David Rankin, for all his help, encouragement and guidance in all aspects of my life and work during the past three years. Along with a variety of postdocs, students and visitors who have worked in our group during this period, he has helped to create an atmosphere that is conducive to productive research. Special thanks must go to Heather Robertson for her help and expertise when gathering data with the diffractometer – a task that was often not trivial! Thanks also to Sarah Hinchley and Andy Turner for their tuition during the early years of my PhD and to Andy and Phil McCaffrey for some very useful discussions and help with programming.

There are several other members of the School of Chemistry who have been a great help with various aspects of my research. Carole Morrison's knowledge of computational chemistry in general, and in particular her excellence in the field of solid-state theory, made her an invaluable source of information. Her student Murshed Siddick was kind enough to allow me to use the plethora of molecular dynamics data that he had collected during his PhD. I thank Martin Walker, another of Carole's students, for his help with all things related to molecular dynamics and in particular the visualisation of simulations.

I am grateful to the EPSRC National Service for Computational Chemistry Software (NSCCS) for the award of computer time (and to Sarah Wilsey in particular for her support when things went wrong) and to the Edinburgh Parallel Computing Centre (EPCC) for time on the high-performance computing facilities used to perform some very demanding molecular dynamics simulations.

My final acknowledgement is to my friends in the School of Chemistry who, although too numerous to mention individually, have been a great support. To the lunchtime crew who helped me to hone my cryptic crossword skills and to those who enjoy nothing better than a few beers in KB House on a Friday night, I thank you all!

Abstract

Gas-phase electron diffraction (GED) is the method of choice for determining the structures of molecules containing between 2 and 100 atoms, free from intermolecular interaction. However, for many molecules it becomes necessary to augment the experimental GED data with information from other sources. The SARACEN method, used routinely at Edinburgh when determining structures, allows computed parameters from *ab initio* and density functional theory (DFT) calculations to be used as extra data in the GED refinement process.

This thesis describes the determinations of the gas-phase structures of molecules that contain heavy *p*-block elements, including examples from Groups 13, 14, 15 and 16. Each of the compounds studied was solid at room temperature, requiring heating to produce a suitable vapour pressure and vaporisation rate and testing the existing electron diffraction apparatus to its limits. Use was made of a new heated reservoir, recently developed in Edinburgh by a previous PhD student, which has allowed compounds to be studied that were previously inaccessible. The molecules that were studied during the course of this degree are: $In(P_3C_2Bu^t_2)$, $In(P_2C_3Bu^t_3)$, $Sn(P_2C_2Bu^t_2)$, $Sb_2(C_6F_6)_3$, $Bi_2(C_6F_6)_3$, $Se(SCH_3)_2$ and $Te(SCH_3)_2$.

While determining the structures of these molecules, accurate theoretical geometries have been obtained using both *ab initio* and DFT methods. As a result a better understanding has been achieved of which methods are suitable for use in calculating the structures of molecules with heavy *p*-block elements. The use of pseudopotentials as opposed to all-electron basis sets proved necessary when performing calculations on such large molecules containing heavy atoms. The extent to which these pseudopotentials, especially ones that consider very few electrons to be in the valence shell of an atom, can affect the calculated geometries has been shown to be considerable.

In addition, methods being developed to compute vibrational corrections for gas-phase structure determination have been extended to the crystalline phase. Molecular dynamics simulations have been used to derive the effects of vibrations on average nuclear positions, relative to equilibrium positions. The differences, when applied to coordinates obtained experimentally by neutron diffraction, yield experimental equilibrium structures.

Contents

Contents of Electronic Appendix

List of symbols, terms, abbreviations and acronyms used

$\angle$	angle (in degrees)
a	*anti* conformation
aug-cc-pVQZ-PP	augmented correlation-consistent quadruple-ζ quality basis set with small-core pseudopotential
ASYM	program to determine rectilinear vibrational corrections
Å	Ångstrøm (10^{-10} m, 100 pm)
B	Becke's 1988 exchange functional
B3	Becke's three-parameter hybrid functional
Bu^t	tertiary butyl group
Cp	cyclopentadienyl group ($C_5H_5^-$)
CPU	central processing unit
DFT	density functional theory
DYNAMITE	dynamic interaction of theory and experiment method
E	energy
EA	electronic appendix
ECP	effective core potential
EPSRC	Engineering and Physical Sciences Research Council
EPCC	Edinburgh Parallel Computing Centre
ESD	estimated standard deviation
eV	electron volt
ϕ	torsional angle (in degrees)
fs	femtosecond (10^{-15} s)
f_X	scattering factor for atom X
g	*gauche* conformation
GB	gigabyte
GDIIS	direct inversion in iterative subspace geometry optimisation algorithm
GED	gas-phase electron diffraction
GGA	generalised gradient approximation method of DFT

GTO	Gaussian-type orbital
$\hat{H}$	Hamiltonian operator
HF	Hartree-Fock theory (used synonymously with RHF in this work)
IR	infrared (spectroscopy)
k	perpendicular correction factor
K	Kelvin
kV	kilovolt
LanL2DZ	basis set utilising Los Alamos ECP on heavy atoms
LDA	local density approximation method of DFT
LYP	correlation functional developed by Lee, Yang and Parr
m	metre
MD	molecular dynamics
Me	methyl group
MHz	megahertz
mm	millimetre
MM	molecular mechanics
MOCED	molecular orbital constrained electron diffraction method
MP2	second order Møller-Plesset perturbation series
MW	microwave spectroscopy
nm	nanometre
NMR	nuclear magnetic resonance (spectroscopy)
NSCCS	National Service for Computational Chemistry Software
NVE	type of MD simulation where number of particles, volume and energy are constant
PBE	exchange and correlation functional of Perdew, Burke and Ernzerhof
PE	photoelectron (spectroscopy)
PES	potential energy surface
pm	picometre (10^{-12} m)
PP	pseudopotential
ps	picosecond
PW91	exchange and correlation functional developed by Perdew and Wang
r	interatomic distance

r_a	raw distance obtained from GED
r_α	distance derived from average atomic positions
R_D	goodness of fit (ignoring correlation between parameters)
r_e	equilibrium distance
r_g	vibrationally averaged interatomic distance
R_G	general goodness of fit (including correlation between parameters)
r_{h0}	distance including perpendicular correction determined by ASYM
r_{h1}	distance including perpendicular correction determined by SHRINK
RHF	spin-restricted Hartree-Fock
RMS	root mean square
s	second
SARACEN	structure analysis restrained by *ab initio* calculations for electron diffraction method
SC	supercomputer
SHRINK	program used to determine curvilinear vibrational corrections
T	temperature
tert	tertiary
u	amplitude of vibration
Ψ	wavefunction
ζ	exponent of a basis function

Chapter One

Introduction and background theory

1.1 General introduction

With the size and shape of molecules dictating the chemical and physical properties of compounds, the study of molecular structure is vitally important to chemical research. Traditionally, such structural determinations have been performed using the well-established methods of absorption and emission spectroscopy and diffraction techniques. These methods of structural investigation are ideally carried out in the gaseous phase where sample molecules are free from external constraints and packing forces distorting their structure, as can be the case in the solid state.

Gas-phase electron diffraction (GED) and rotational spectroscopy are the two techniques that are used routinely to determine molecular structures of gases. However, as rotational spectroscopy is suitable only for relatively small molecules, GED may be considered to be the only experimental method for obtaining the gas-phase structures for many of the molecules studied in this thesis.

In recent years, chemists' understanding of theoretical methods of structure determination has greatly improved. It is now acknowledged that quantum chemistry can usefully complement experimental data in the investigation of molecular geometry and that complete structures can be obtained by combining information from different sources. Conversely, accurate gas-phase structures are entirely necessary for the standardisation of some computational methods for isolated molecules.

Ab initio molecular orbital theory and density functional theory are powerful computational tools that can be used to calculate any property of a molecule from first principles. Such theoretical methods of structural determination do have their own limitations. The main factors that can limit *ab initio* calculations are the size of the molecules being studied and the speed and cost of suitable computer hardware. However, the widespread availability of parallel processors and access to the resources of the EPSRC-funded National Centre for Computational Chemistry Software (admin: Department of Chemistry, Imperial College London, South Kensington, London, SW7 2AZ) have further extended the range of molecules that can be studied.

1.2 Gas-phase electron diffraction

Gas-phase electron diffraction (GED) is the principal technique used by chemists to determine molecular structures of gases. The Edinburgh diffraction group is one of only a handful worldwide, including one other in the UK, several in the USA and others in Norway, Russia, Germany, Belgium and Japan. The diffractometers used in each group tend to have been developed in relative isolation and procedures vary significantly. Although the theory underpinning the GED method is consistent, some of the following sections are concerned specifically with the performance of electron diffraction in Edinburgh.

1.2.1 Background

Two fundamental understandings led to the development of the GED technique as a means of investigating structure. In 1801 Thomas Young conducted his double-slit experiment,[1] showing that light possessed wave properties and, therefore, could be diffracted, giving rise to interference phenomena. Young established that when a wave of incident light encounters a narrow slit on a screen, the light diffracts to form a cylindrical wavefront. If this wave encounters a second screen with two parallel slits, further diffraction will occur. Two coherent wavefronts are produced and advance towards a third, solid screen where they combine showing an interference pattern of alternating light and dark areas, due to constructive and destructive interference, respectively.

The other theory that was necessary for the advancement of GED was developed by Louis de Broglie in 1924.[2] Knowing that light behaved as a wave, he suggested that *all* moving particles had an associated wavelength. Thus, a photon of light can be regarded both as a wave and as a particle, and the same can be said for an electron.

In 1927, the American physicists Clinton Davisson and Lester Germer performed a crucial experiment, which demonstrated the diffraction of electrons by a nickel crystal.[3] Meanwhile in Scotland, George Thomson showed that a beam of electrons was diffracted when passing through a thin gold foil.[4]

Very soon after these first electron diffraction experiments a method was developed whereby this diffraction phenomenon could be applied to the determination of molecular structure. Every pair of atoms in a molecule acts like a pair of slits, diffracting a beam of electrons directed at the molecule, which then interfere causing light and dark areas to be recorded on photographic film. A pattern of concentric rings is seen because of the random orientation of the gaseous molecules (see Figure 1). Assuming that the wavelength of the electrons is known, the distance between the atoms can be calculated from the diffraction pattern and consequently the molecular structure can be determined. It was in 1930 that the first diffraction of electrons by gaseous molecules was successfully recorded. Herman Mark and Raimund Wierl determined the structures of some simple, highly symmetrical molecules including carbon tetrachloride, germanium tetrachloride, benzene and cyclohexane.[5]

Figure 1 Electron scattering data recorded on Kodak Electron Image film.

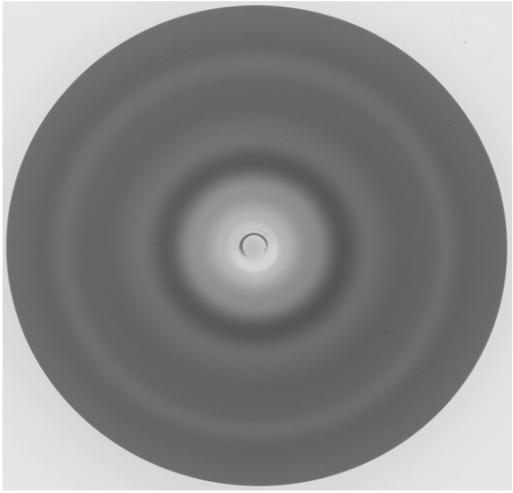

1.2.2 Instrumentation

The general requirements for an electron diffractometer include an electron gun, a method for focusing the electron beam, a nozzle to introduce the sample gas and a detector (Figure 2). A beam of electrons is accelerated from a loop of hot tungsten wire across an accurately measured potential of approximately 40 kV. A series of magnetic lenses and apertures is then used to focus the narrow beam of electrons. The gaseous

sample is introduced through a nozzle, perpendicular to the electron beam that intersects it. The diffracted electrons continue towards a photographic film, which acts as a detector, while the sample is condensed on a cold trap to prevent further interaction with the electron beam. It is common to evacuate the apparatus to 10^{-6} Torr in order that the electrons do not encounter other species which may cause diffraction.

Figure 2 Schematic diagram of a typical gas-phase electron diffraction apparatus.

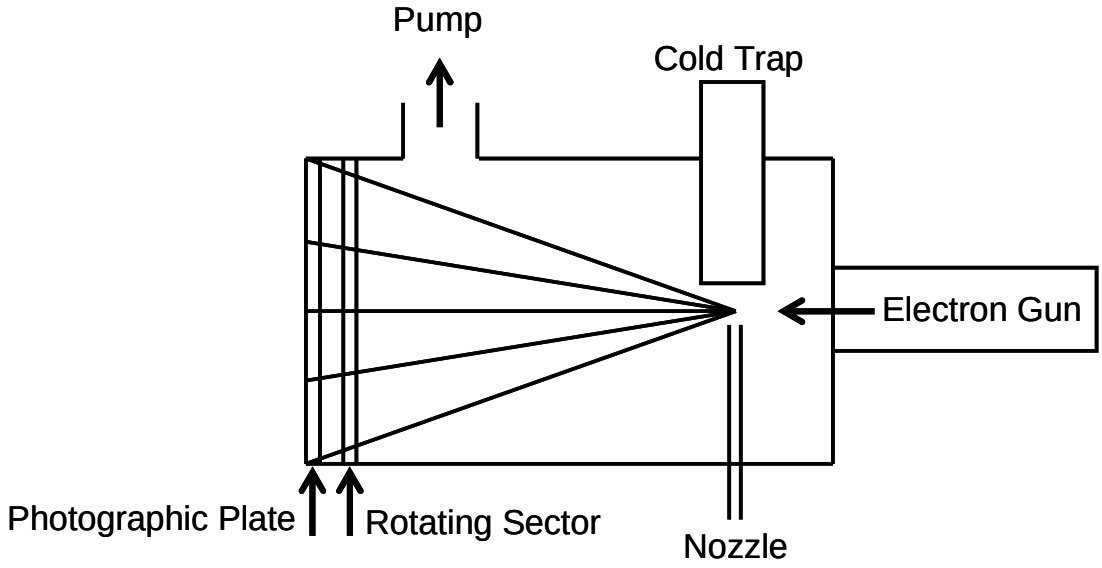

The intensity of scattered electrons decreases steeply (approximately the 4th power of the scattering angle) and, therefore, the range of intensities associated with the diffracted electrons is so large that they cannot be accurately recorded on a photographic plate. To minimise this problem, a rotating sector[6] (Figure 3) is positioned in front of the photographic film. Made from aluminium, the sector has an opening that increases in size (approximately proportional to r^4) on moving away from the centre of the plate. When this plate rotates rapidly, it acts to decrease the effective exposure time at scattering angles where the intensities would normally be too strong to be recorded. Undiffracted electrons are collected by a metal cylinder, found at the centre of the sector, called a beam-stop.

Figure 3 Shape of rotating sector used in Edinburgh (adapted from Ref. 7).

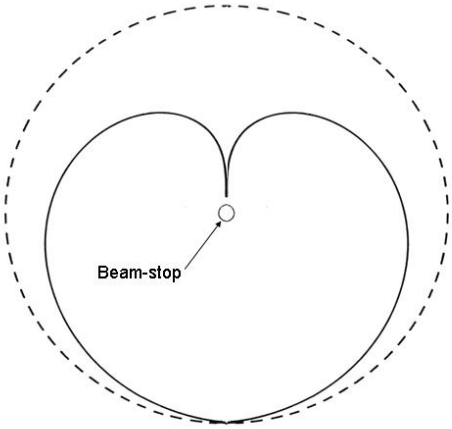

Distances within the apparatus and the wavelength of the electrons are calculated by reference to the scattering pattern for benzene, recorded immediately after the sample has been run. The experiment is usually performed twice, or occasionally three times, at different nozzle-to-film distances, to increase the range of scattering angles (Figure 4) and therefore obtain more data for a more accurate structure determination.

Figure 4 Application of two nozzle-to-film distances, (*a*) short and (*b*) long (adapted from Ref. 7).

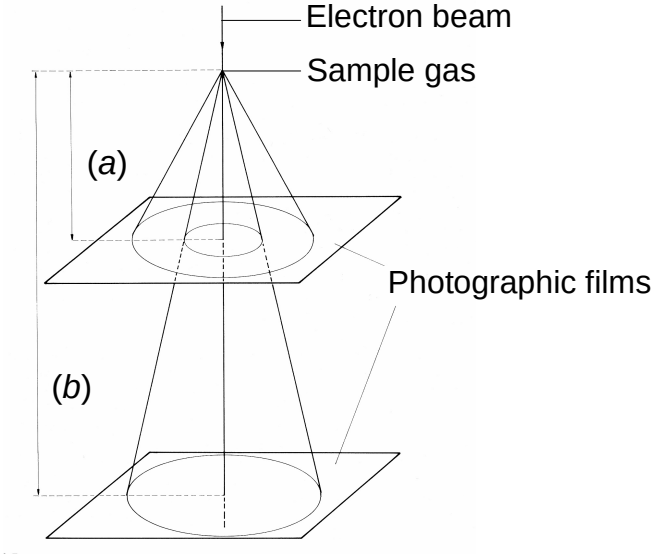

1.2.3 Data analysis

The recorded scattering intensities (see Figure 1 for an example of the photographic film) are measured in-house using an Epson 1600 Pro flatbed scanner and converted to mean optical densities as a function of the scattering variable, *s*, using an established program.[8]

The diffraction pattern recorded on the photographic film represents the overall scattering intensity. Three types of scattering are combined to give the total scattering, as shown in Equation 1.

$$I_{total} = I_{atomic} + I_{molecular} + I_{background} \qquad \text{Equation 1}$$

The molecular-intensity scattering curve is required to obtain the molecular structure and so the atomic and background intensities must be subtracted from the total. The atomic scattering is independent of the molecular structure and the scattering contribution from each of the atoms in the molecule can simply be summed and removed.

Even when the molecular-intensity scattering curve has been obtained, the values for the interatomic distances are not immediately obvious. A sine Fourier transformation must be performed to obtain a useful radial-distribution curve, which, in theory, shows a representation of every bonded and non-bonded distances in the molecule as the centre of a peak in the curve. From the radial-distribution curve it *may* be possible to extract enough information about the bond lengths and angles to determine the structure of a simple molecule.

1.2.4 Limitations of GED – and some solutions

When interatomic distances are very similar, overlapping peaks occur in the radial-distribution curve. When this happens it is often impossible to obtain the correct distance associated with each atom pair. If the distances cannot be correctly assigned then the structure cannot be accurately determined. This is one of the main limitations associated with the GED experiment, and is encountered in every radial-distribution curve displayed in this thesis.

Light atoms scatter electrons less than heavy atoms and this can lead to poor definition of the positions of atoms such as hydrogen. With the positions of these atoms uncertain, it becomes impossible to obtain an accurate structure using GED alone. In such cases, we must look to other techniques to help us solve the structure.

Another problem associated with GED concerns the phase shift of an electron wave as it passes through an atomic field. Attracted to the nucleus, the electron speeds up and its de Broglie wavelength is shortened. On leaving the field of the atom, the electron slows down to its original speed and wavelength. This becomes a problem when a molecule contains atoms with very different atomic numbers. As can be seen in Figure 5, the heavier atom (B) causes a larger contraction of the electron wave than (A). This leads to beating in the molecular intensity curve, which shows up in the experimental radial-distribution curve as a split peak corresponding to the bonded distance *r*A–B. This effect is taken into account in the theoretical curves using complex (*i.e.* containing both a real and imaginary part) scattering factors to calculate the molecular scattering and therefore the radial-distribution curve.[9]

Figure 5 The phase effect, caused by differences in wave contraction as the electron approaches a light atom (A) and heavy atom (B), (adapted from Ref. 10).

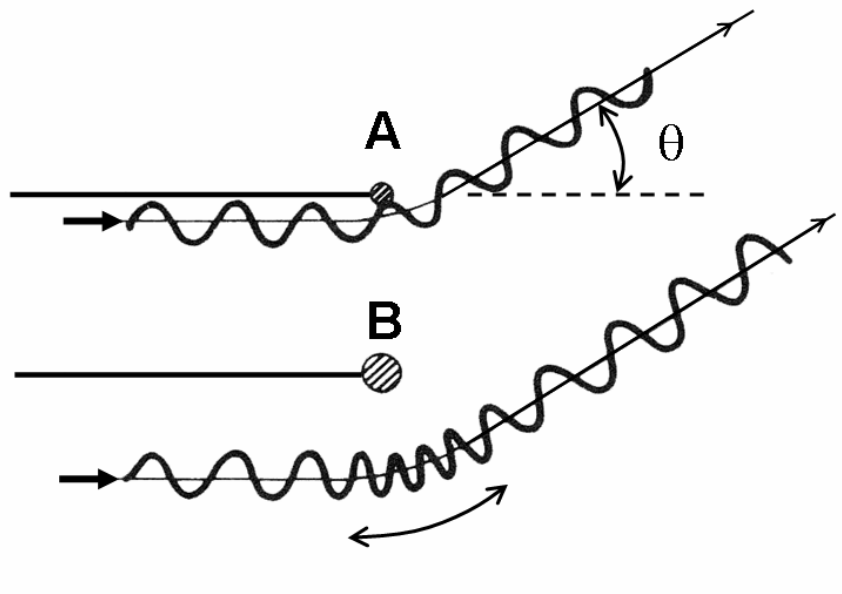

Samples for GED may be solid, liquid or gas at ambient temperature and pressure but must have a suitable vaporisation rate (with heating if necessary) and vapour pressure for significant diffraction to occur. This somewhat limits the range of compounds that can be studied using this technique.

Recently, developments have been made to the experimental procedure so that compounds that do not fit the criteria for vaporisation rate and vapour pressure can still be used.[11] A small reservoir, heated by a flow of hot gas, was used in the collection of some of the data for the compounds in this thesis. This vessel was found to be far better than that used previously, where the heating was performed using heating tape, which was prone to giving hot spots.

The final problem with GED arises because of the fact that the structure obtained is vibrationally averaged. Each individual electron sees the molecule at a single instant in time and millions of electrons contribute to the total picture. Figure 6 depicts a linear, triatomic molecule vibrating. Except for the instant when it is linear, the molecule spends its time bent. This means that the distance between the two black atoms is, on average, less than twice the bond length between the black and white atoms. The two distances would thus imply, incorrectly, that the molecule was bent. A similar phenomenon is found for non-linear systems and is known as the shrinkage effect[12] and must be corrected for in the vibrational model.

Figure 6 Schematic diagram showing the vibration of a triatomic molecule.

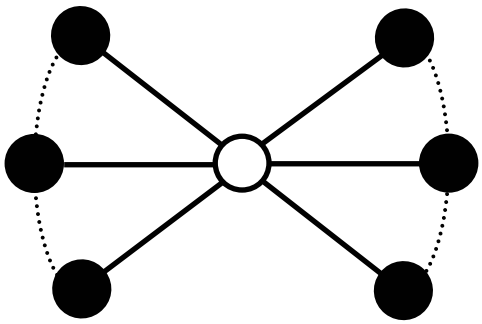

The shrinkage effect can be corrected through the use of calculated force fields. The theoretical force constants are used to calculate either rectilinear or curvilinear corrections. The rectilinear corrections allow for the perpendicular motions of the atoms by increasing the bond lengths when the atoms are not in the linear position. This is intuitively wrong and so in this work curvilinear corrections are used throughout, modelling better the curved motion of the atoms. These corrections are calculated using the SHRINK program.[13]

1.2.5 Experimental equilibrium structures

The vibrational correction described above is one of a number of corrections that are routinely made to the raw distances obtained from the GED experiment. These distances, which are denoted r_a, are modified in order to produce an experimental equilibrium structure that is then independent of the method by which it was determined. The equilibrium structure of a molecule is the structure in a hypothetical vibrationless state at the minimum on the potential energy surface.

The GED distances, r_a, are averaged over all vibrational motions and are the inverse of the inverse distance between a pair of atoms averaged over time, as shown in Equation 2. It is necessary to take the inverse because of the way that the distances are defined in the scattering equations.

$$r_a = \langle r^{-1} \rangle^{-1} \qquad \text{Equation 2}$$

The difference between r_a and the equilibrium distance has four terms. The first is a term allowing for motion along the coordinate between two atoms and gives the average internuclear distance, r_g. Equation 3 shows the connection between r_a and r_g, where u is the root-mean-squared (RMS) amplitude of vibration (which can be calculated) and r_e is the equilibrium distance. Of course, r_e is not known and so r_a must be used as an approximation.

$$r_g = r_a + \frac{u^2}{r_e}$$ Equation 3

This equation describes r_g at the temperature, T, of the experiment and should strictly be written r_g^T. To obtain a value for r_g at 0 K, the correction shown in Equation 4 is applied, where a is an anharmonicity constant used to allow for the anharmonicity of the potential well (Morse curve) and u is the RMS amplitude of vibration.

$$r_g^0 = r_g^T - \frac{3}{2}a(u_T - u_0)^2$$ Equation 4

For diatomic molecules, r_g^0 (the average internuclear distance at 0 K) is equal to another quantity, r_α^0 (the distance between average nuclear positions at 0 K). r_g^0 can be related to r_e by a further anharmonic correction, shown in Equation 5.

$$r_e = r_g^0 - \frac{3}{2}a{u_0}^2$$ Equation 5

When a molecule has three or more atoms, as demonstrated previously, there is a shrinkage effect affecting non-bonded distances and $r_\alpha^0 \neq r_g^0$. A perpendicular amplitude correction term, k, is calculated using SHRINK.[13]

The final term that is required to correct from r_a to r_e is an allowance for centrifugal distortion, δr. This is often negligible and has not been included in the corrections used during the refinements in this thesis.

The whole correction is shown in Equation 6. Note that subscripts hn have now been added and these denote the use of a harmonic force field calculation to obtain the corrections, with the vibrational motions treated at the nth order approximation. In this work the distances reported are of the type r_{h1}, showing that the calculated harmonic force field has been used in conjunction with the SHRINK program to obtain corrections. As mentioned earlier, it was previously common to use rectilinear correction factors and these would be denoted r_{h0}.

$$r_{hn} = r_a + \frac{u_{hn}^2}{r_e} - \frac{3}{2}au_{hn}^2 - k_{hn} - \delta r_{hn} \qquad \text{Equation 6}$$

1.3 *Ab initio* molecular orbital theory

The use of computational methods for structure determination has grown rapidly in recent years. With advances in technological ability at relatively low costs, theoretical techniques have become the natural complement to experiment. A wide range of techniques, both *ab initio* and semi-empirical, has been developed from an understanding of quantum mechanics.

Ab initio molecular orbital theory is a powerful computational method for calculating molecular properties such as geometries, thermodynamic properties, and bond energies from first principles alone. These calculations can be used in conjunction with experimentally obtained results from, for example, GED. They can also be used to obtain data for compounds that cannot be analysed by known experimental methods.

In theory, molecular geometries can be calculated exactly from an exact solution of the time-independent Schrödinger equation,

$$E\Psi = \hat{H}\Psi \qquad \text{Equation 7}$$

where E is the total molecular energy, Ψ is the molecular wavefunction, and $\hat{H}$ is the Hamiltonian operator. However, the equation can only be solved exactly for one-electron systems such as H and He^+. An approximate solution for the equation can be obtained for larger systems by simplifying both $\hat{H}$ and Ψ.

1.3.1 Simplification of the Hamiltonian operator

The Hamiltonian operator is composed of five terms, namely the kinetic energies of the nuclei and of the electrons in the molecule, and the potential energies associated with nuclear repulsion, electronic repulsion and nuclear–electronic attraction.

To simplify the Hamiltonian, the Born-Oppenheimer[14] and adiabatic[15] approximations are employed. The Born-Oppenheimer approximation assumes that the mass of the nuclei in a molecule is considered to be so much greater than the mass of the electrons that the nuclei can be said to be stationary in a field of moving electrons. This makes the nuclear and electronic wavefunctions separable. As a result, the kinetic energy term for the nuclei can be equated to zero, and the value for the potential energy of the nuclear repulsion becomes constant. The adiabatic approximation amounts to neglecting the coupling between electronic states caused by nuclear motion. Now, only the terms of the Hamiltonian relating to electrons must be considered.

The Hartree-Fock (HF) potential is used to replace the electronic repulsion term in the Hamiltonian. Each electron is considered to move in a uniform field, generated by the other electrons present in the molecule. A series of single-electron Schrödinger equations can then be solved, generating a series of one-electron atomic orbitals. This method accounts for about 99% of the energy of the molecule. The deficit is due to the fact that electrons do not move in uniform fields. When more than one electron is present in a system, electron correlation occurs and the HF method must be extended to include the electron correlation energy.

Electron correlation is most pronounced in systems with areas of high electron density, such as molecules with lone pairs of electrons, double bonds or those containing highly electronegative elements. If electron correlation was ignored in such systems, the calculated bond distances would be too short and the bond energies inaccurate. Fortunately there are ways to improve upon the HF method. Most take the HF wavefunction as their starting point and add in extra terms to account for the effects of electron-electron repulsion. The Møller-Plesset (MP) perturbation series[16] is one way of including the electron correlation effects, with the most commonly used one of these being the MP2 level of theory, which is used often in the work presented in this thesis.

1.3.2 Simplification of the molecular wavefunction

The wavefunction, Ψ, describes where in the molecule the nuclei and electrons should be found. This must also be simplified to allow an approximation of the Schrödinger

equation to be solved. Using the Born-Oppenheimer approximation,[14] the nuclei are imagined to be fixed in space and so only the region of space for the electronic motion (*i.e.* the atomic orbitals) need be considered. Commonly, Gaussian-type orbitals (GTO) are used to approximate the atomic radial functions. Figure 7 compares the two functions.

In practice it is necessary to combine many GTOs with different weightings and coefficients in order to represent the atomic radial functions accurately. Such a collection of GTOs is known as a basis set, and each atom in a molecule requires a basis set. Ideally, the basis set would consist of an infinite number of functions to allow for the maximum flexibility for electronic motion. This is not possible in practice and so a truncated series of GTOs is used. Basis sets are defined in terms of the number of GTOs describing each atomic orbital. A single-ζ basis set will allow one function to describe each occupied atomic orbital. A double-ζ basis set will have two functions for each orbital, and so on.

Figure 7 Comparison of a Gaussian function with an atomic radial function.

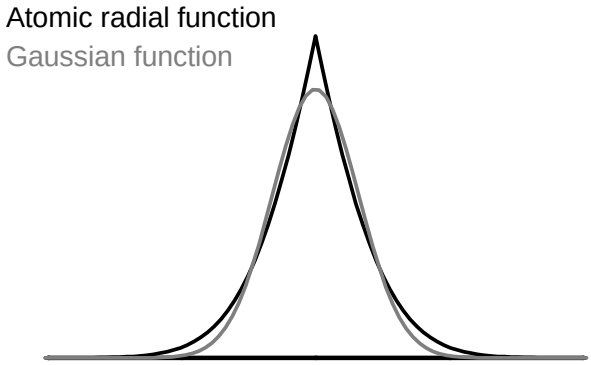

The 3-21G* basis set[17] would normally be used to calculate a starting geometry for further calculations and is a split-valence basis set, with the first term (3) referring to the core electrons, and the second and third terms (2 and 1) referring to the inner and outer valence electrons, respectively. As each individual atom in a molecule has its own basis set, it is often useful to add additional functions to basis sets for atoms that will

significantly change in shape, size or charge on becoming part of a molecule. A polarisation function (*) adds functions with higher angular momentum than would be normal in the atomic ground state. A diffuse function (+) allows the orbitals to fill a larger space, a factor especially important for systems carrying high negative charges.

Basis sets of the type just described have not been optimised for all atoms in the periodic table. The 3-21G*, for instance, is only applicable up to, and including, Xe (Z = 54) and other larger basis sets are even more limited in their application. For larger atoms, with more electrons, basis sets have been developed that allow an effective core potential (ECP) to be applied. The core electrons are unimportant in terms of bonding, and the core is, therefore, replaced by a potential and the valence electrons are expanded as usual. This speeds up the calculations as fewer electrons are explicitly involved.

With the simplification of the Hamiltonian operator, $\hat{H}$, and the wavefunction, Ψ, the Schrödinger equation can be solved to an approximation. The approximation is dependent upon the degree of simplification of $\hat{H}$ and Ψ.

1.4 Density functional theory

Hohenberg and Kohn proved that the ground-state energy of a system can be determined completely by its electron density.[18] This is the basis of density functional theory (DFT), which offers an alternative theoretical approach to the *ab initio* calculations already discussed. As the energy is not calculated from the wavefunction, the 4N variables (atomic coordinates and spin for all N atoms) required for *ab initio* methods can be reduced to the three coordinates of the electron density. This is, therefore, independent of the number of electrons and requires much less computational effort. DFT methods are ideal for use with very large molecules where the time taken for *ab initio* calculations to complete can be prohibitive. The only barrier to carrying out DFT calculations is that the functional relating the electron density to the energy of the electrons is unknown. The functionals available in the literature are developed by fitting parameters to known experimental data and then testing against large sets of reference atoms and molecules for reliability.

It was mentioned earlier that Hartree-Fock theory, while it calculates the electron-exchange energy exactly, ignores electron correlation completely. The functionals used in pure DFT, however, work by approximating both electron exchange and electron correlation.

Early applications of DFT used the local density approximation (LDA), which assumes that the electron density is constant throughout space and can be treated as a uniform electron gas. For metallic systems this approximation is quite relevant and LDA proves to be a fairly good model, but for molecular systems where the electron density varies rapidly it fails. Improvements over LDA can be made by considering a non-uniform electron gas. The generalised gradient approximation (GGA) includes information about the gradient of the charge density. Becke's 1988 exchange functional[19] (B) and that of Perdew, Burke and Ernzerhof[20] (PBE) were developed from GGA and are used in some of the calculations presented in this thesis.

Hybrid DFT methods are often used as they take the exact electron-exchange energy (as calculated by HF) and combine this with the approximate electron correlation energy (as calculated using LDA and GGA). Becke's three-parameter functional[21] (B3) is a commonly used method of including the exact electron-exchange energy and is used often in this work. Among the correlation functionals employed are those of Perdew and Wang[22] (PW91) and Lee, Yang and Parr[23] (LYP).

DFT methods can be combined with the basis sets described earlier to calculate ground-state gas-phase molecular properties. As will be described in Chapter 7, DFT also has major applications in calculating the structures of solid-state molecular systems.

1.5 Structure refinement in practice – combining GED and theoretical data

With *ab initio* and DFT calculations performed on isolated molecules, free from intramolecular interactions, and electron diffraction concerned with gas-phase structures, these techniques are complementary. The calculations are useful for providing extra data in a number of different ways. The theoretical relative energies of conformational isomers can give an indication of their abundance in an experimental sample. In

addition, frequency calculations are used to obtain theoretical harmonic force fields, thus allowing accurate amplitudes of vibration to be used in the refinement. A list of curvilinear vibrational correction terms is also achieved through use of the SHRINK program.[13]

To solve the structure it is also necessary to write a model in Fortran code to define the atomic coordinates of the proposed geometry, from the minimal set of geometrical parameters. The model is defined in terms of parameters (bond lengths, bond angles, torsional angles and, where necessary, weightings of conformers) and describes any local and overall symmetry the molecule possesses. The structure is then refined using a least-squares refinement program, allowing the parameters and amplitudes to vary until the best fit to the experimental data is obtained.

Recently a new GED refinement program has been introduced in Edinburgh. The previous program (called ED96, but really a reincarnation of a program used in the group for many years) was MS-DOS based and required the user to spend a lot of time opening and closing various files in order to follow the refinement process. The newly developed program, called ed@ed,[24] has improved upon its predecessors by incorporating a Windows interface. This allows all the relevant information to be viewed on a single screen.

The goodness of the fit between the calculated and experimental data is assessed by the R_G factor, the value of which should ideally be under 10%, although the value depends on the scattering pattern for the molecule as well as the quality of the data and accuracy of the model. Another measure of the data fit is the difference curve between the experimental and theoretical data sets. When viewed in conjunction with the radial-distribution curve this makes it possible to see where the data fit best and where the greatest discrepancies lie.

1.5.1 SARACEN

The principles of the SARACEN (Structure Analysis Restrained by *Ab initio* Calculations for Electron diffractioN) method[25] have also been used in the refinements presented in this thesis. Parameters that are poorly defined by the GED experiment

(typically bond lengths, angles and torsion angles relating to hydrogen atoms, and parameters that depend on interatomic distances that differ little) tend to refine to chemically unreasonable values. SARACEN allows flexible restraints to be applied to such parameters, thus allowing their inclusion in the refinement. A restraint consists of a value (often the starting value for the parameter taken from the highest-level calculation) and an uncertainty (usually derived from the way that a parameter value has converged during a series of calculations). The inclusion of parameters in the refinement process that would previously have been excluded should lead to the determination of a more reliable structure. The SARACEN method replaced MOCED (Molecular Orbital Constrained Electron Diffraction),[26] a method that used values calculated *ab initio* to constrain parameters in the GED refinement.

1.5.2 DYNAMITE

The DYNAMITE method[27] (DYNAMic Interaction of Theory and Experiment) has recently been developed in Edinburgh and has been utilised in the refinement of the main-group metal polyphospholyl half-sandwich complex described in Chapter 3. DYNAMITE recognises that, even with the SARACEN method, it was still necessary to make some assumptions about the local symmetry of substituent groups. If steric strain is present in a molecule, then assumptions of local symmetry for light-atom groups, such as methyl groups, will affect the heavy-atom positions as they compensate for any inaccuracies in the light-atom positions. DYNAMITE allows real-time theoretical data (at present molecular mechanics) to be incorporated into the GED refinement program.

1.6 Molecular dynamics simulations

Molecular dynamics (MD) is a computational method that allows the behaviour of a system to be modelled over a period of time. It can be applied to situations as diverse as the study of Brownian motion in liquids and hydrogen bonding in crystals. The method combines energy calculations (such as the type described earlier, *e.g.* HF, DFT) with classical Newtonian mechanics, used to move the atoms for small time steps (often in

the order of 1 fs) before the energy gradient is once again calculated. When this process is repeated many times the result is a trajectory that specifies how the positions and velocities of the particles in the system vary with time. Chapter 7 deals with the use of MD simulations as a method for studying atomic motions in crystals and its application to the determination of experimental solid-state equilibrium structures. There will also be more about the method in Chapter 7.

The majority of MD simulations, including those reported in this work, are of the type NVE, indicating that during the simulations the number of particles in the system is kept constant, as are the volume of the system and its total energy.

1.6.1 Plane-wave DFT

In section 1.4 DFT calculations are presented as an alternative to pure *ab initio* calculations for calculating molecular geometries and force fields. In those calculations each atom in the molecule requires a basis set, consisting of a number of functions that describe the electronic motion within that atom.

In addition to its use in single-molecule calculations, DFT has been widely used in the study of solid-state systems such as conductors, semiconductors, insulators, crystals and surfaces. The DFT methods that are used in these applications are identical to those (non-hybrid methods) discussed previously (*e.g.* PW91, PBE), but with one important distinction. When dealing with condensed-phase materials with periodic boundary conditions, electrons can no longer be regarded as pertaining to a single atom, as was the case with, for example, the Gaussian functions representing the atomic radial functions described above. Instead, a plane-wave basis set is used, allowing the electrons to be modelled as (almost) free particles within the bounds of a lattice. A package of plane waves, which take the form of sine or cosine waves, is used. Waves may have different wavelengths (and, therefore, energies) but must be standing waves.

In practice, the number of plane waves that would be required to model the wavefunctions close to the nucleus correctly is unfeasibly large and the core electrons are represented by a pseudopotential with only the valence electrons having a plane-

wave basis set. Thus, the assumption is made that only the valence electrons affect the physical properties of the system.

1.6.2 Choice of time step

The choice of time step used in an MD simulation is of the greatest importance as it ultimately determines how far an atom, which is being subjected to a computed force, will be moved before the energy is recalculated. A time step that is too large will cause an atom to move too far along a trajectory, causing the equations to fail, and poorly modelling the motion of the atom. If too short a time step is chosen then it will be necessary to run more cycles in the MD simulation than would otherwise be necessary. In such a time-consuming, computationally demanding exercise this must be avoided. Ideally the time step should be 10 – 15 times shorter than the timescale of the quickest (highest-energy) vibration.

1.7 References

1. T. Young, *Philos. Trans. R. Soc. London, Ser. A*, 1802, **92**, 12.
2. L. de Broglie, *Philos. Mag.*, 1924, **47**, 446.
3. C. J. Davisson and L. H. Germer, *Nature* (*London*), 1927, **119**, 558.
4. G. P. Thompson, *Nature* (*London*), 1927, **120**, 802.
5. H. Mark and R. Wierl, *Z. Elektrochem.*, 1930, **36**, 675.
6. P. Debye, *Phys. Z.*, 1939, **40**, 404.
7. J. Tremmel and I. Hargittai, Gas Electron Diffraction Experiment, in *Stereochemical Applications of Gas-Phase Electron Diffraction, Part A: The Electron Diffraction Technique*, ed. I. Hargittai and M. Hargittai, VCH, 1988.
8. H. Fleischer, D. A. Wann, S. L. Hinchley, K. B. Borisenko, J. R. Lewis, R. J. Mawhorter and D. W. H. Rankin, *Dalton Trans.*, 2005, 3221.
9. R. Glauber and V. Schomaker, *Phys. Rev.*, 1953, **89**, 667.
10. B. F. Johnston, *Ph.D. Thesis*, University of Edinburgh, 2002.
11. J. T. Schirlin, *Ph.D. Thesis*, University of Edinburgh, 2004.
12. O. Bastiansen and M. Trætteberg, *Acta Crystallogr.*, 1960, **13**, 1108; Y. Morino, S. J. Cyvin, K. Kuchitsu and T. Iijima, *J. Chem. Phys.*, 1962, **36**, 1109; R. Stølevik, H. M. Seip and S. J. Cyvin, *Chem. Phys. Lett.*, 1972, **15**, 263.
13. V. A. Sipachev, *J. Mol. Struct.* (*THEOCHEM*), 1985, **121**, 143; V. A. Sipachev, *J. Mol. Struct.*, 2001, **567**, 67.
14. M. Born and J. R. Oppenheimer, *Ann. Phys.* (*Berlin*), 1927, **84**, 457; W. Kolos and L. Wolniewicz, *J. Chem. Phys.*, 1964, **41**, 3663; B. T. Sutcliffe, *Adv. Quantum. Chem.*, 1997, **28**, 65.
15. N. C. Handy and A. M. Lee, *J. Chem. Phys.*, 1996, **252**, 425.
16. C. Møller and M. S. Plesset, *Phys. Rev.*, 1934, **46**, 618.
17. J. S. Binkley, J. A. Pople and W. J. Hehre, *J. Am. Chem. Soc.*, 1980, **102**, 939; M. S. Gordon, J. S. Binkley, J. A. Pople, W. J. Pietro and W. J. Hehre, *J. Am. Chem. Soc.*, 1982, **104**, 2797; W. J. Pietro, M. M. Francl, W. J. Hehre, D. J. DeFrees, J. A. Pople and J. S. Binkley, *J. Am. Chem. Soc.*, 1982, **104**, 5039.

18. P. Hohenburg and W. Kohn, *Phys. Rev. Sect. B*, 1964, **136**, 864.
19. A. D. Becke, *Phys. Rev. B: Condens. Matter*, 1988, **38**, 3098.
20. J. P. Perdew, K. Burke and M. Ernzerhof, *Phys. Rev. Lett.*, 1996, **77**, 3865; J. P. Perdew, K. Burke and M. Ernzerhof, *Phys. Rev. Lett.*, 1997, **78**, 1396.
21. A. D. Becke, *J. Chem. Phys.*, 1993, **98**, 5648.
22. J. P. Perdew and Y. Wang, *Phys. Rev. B: Condens. Matter*, 1992, **45**, 13244.
23. C. Lee, W. Yang and R. G. Parr, *Phys. Rev. B: Condens. Matter*, 1992, **37**, 785; B. Miehlich, A. Savin, H. Stoll and H. Preuss, *Chem. Phys. Lett.*, 1989, **157**, 200.
24. S. L. Hinchley, H. E. Robertson, K. B. Borisenko, A. R. Turner, B. F. Johnston, D. W. H. Rankin, M. Ahmadian, J. N. Jones and A. H. Cowley, *Dalton Trans.*, 2004, 2469.
25. A. J. Blake, P. T. Brain, H. McNab, J. Miller, C. A. Morrison, S. Parsons, D. W. H. Rankin, H. E. Robertson and B. A. Smart, *J. Phys. Chem.*, 1996, **100**, 12280; P. T. Brain, C. A. Morrison, S. Parsons and D. W. H. Rankin, *J. Chem. Soc., Dalton Trans.*, 1996, 4589; N. W. Mitzel and D. W. H. Rankin, *Dalton Trans.*, 2003, 3650.
26. N. S. Chiu, J. D. Ewbank, M. Askari and L. Schäfer, *J. Mol. Struct.*, 1979, **54**, 185; N. S. Chiu, H. L. Sellers, L. Schäfer and K. Kohata, *J. Am. Chem. Soc.*, 1979, **101**, 5883; V. J. Klimkowski, J. D. Ewbank, C. v. Alsenoy, J. N. Scarsdale and L. Schäfer, *J. Am. Chem. Soc.*, 1982, **104**, 1476.
27. S. L. Hinchley, M. F. Haddow and D. W. H. Rankin, *Dalton Trans.*, 2004, 384.

Chapter Two

The molecular structures of [In($P_3C_2Bu^t_2$)] and [In($P_2C_3Bu^t_3$)] using gas-phase electron diffraction and *ab initio* and DFT calculations

2.1 Introduction

In the past 20 years many unsaturated ring systems have been synthesised using the phospha-alkyne synthon, Bu^{t}CP. A selection of these rings is shown in Figure 1.[1]

Figure 1 A selection of unsaturated rings that can be synthesised from Bu^{t}CP.

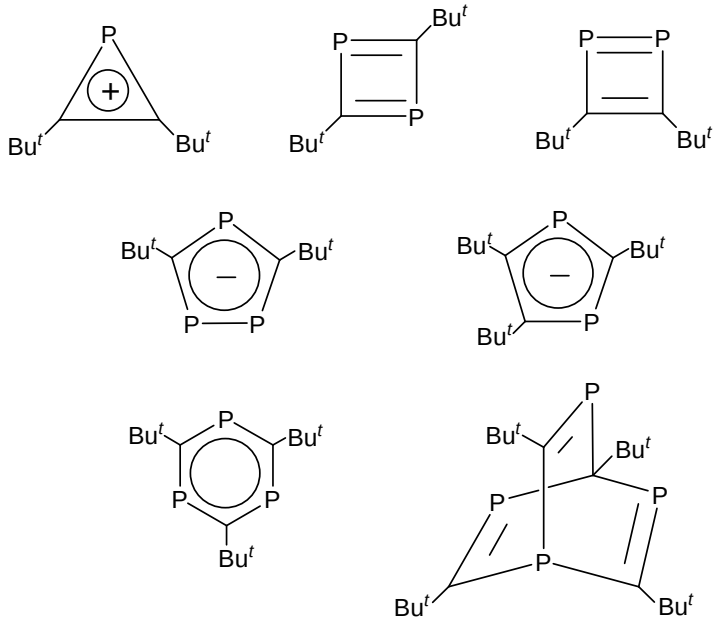

Complexes in which $[P_3C_2Bu^t_2]^-$ and $[P_2C_3Bu^t_3]^-$ have been coordinated to *d*- and *f*-block metals have been studied extensively,[2] but until five years ago little was known about similar complexes with main-group elements. Singly charged anions like $[P_3C_2Bu^t_2]^-$and $[P_2C_3Bu^t_3]^-$ are of interest because of their ability to stabilise monovalent metals. Complexes with the Group 13 metals Ga, In and Tl have been synthesised and have potential uses in the manufacture of III–V semiconductors. The In complexes $[In(P_3C_2Bu^t_2)]$, **1**, and $[In(P_2C_3Bu^t_3)]$, **2**, contain both precursor atoms for the formation of indium phosphide and their volatility could lend themselves to use in chemical vapour deposition (CVD) of semiconducting films.[3]

Compounds **1** and **2** have both previously been studied using X-ray diffraction,[4,5] and both crystal structures show In coordinated to the ring in an η^5-fashion. However, while

the crystal structure of **2** consisted of distinct monomers, the structure of **1** displayed weakly bound chains of molecules. The reason for this difference was explained by the increased steric bulk of **2**, with an extra Bu^t group attached to the ring. This phenomenon is further observed in the crystal structure of [In(η^5-$C_5H_4Bu^t$)], in which the presence of less steric bulk allows the In–centroid distances between an indium atom and the two adjacent rings to be as similar as 253 and 285 pm.[6] The values for the In–centroid distances in the crystal structure of **1** are 259.8 pm to the strongly associated ring and 352.6 pm to the next ring in the chain, thus demonstrating weak aggregation.

In this chapter (and in Chapter 3, which deals with a Group 14 half-sandwich complex) a search is performed for the most suitable *ab initio* and DFT methods for performing calculations on main-group half-sandwich complexes and the calculated geometries are used during the GED structure determinations of [In($P_3C_2Bu^t_2$)], **1**, and [In($P_2C_3Bu^t_3$)], **2**.

2.2 Experimental

2.2.1 Synthesis

Samples of [In($P_3C_2Bu^t_2$)], **1**, and [In($P_2C_3Bu^t_3$)], **2**, were prepared by the co-condensation of indium vapour and $Bu^tC{\equiv}P$ at 77 K by Dr. Matthew Francis and co-workers at the University of Sussex.[4,5]

2.2.2 Theoretical methods

The calculations reported in this work were performed using the Gaussian 03 suite of programs,[7] with the resources of the EPSRC National Service for Computational Chemistry Software. Some of the calculations were carried out using a cluster of six HP ES40 computers, where each Alphaserver ES40 machine has four 833 MHz EV68 CPUs and 8 GB of memory connected with a high-speed, low-latency QSW switch forming an Alphaserver SC. Other calculations were performed using a cluster of 22 Linux Opteron nodes. Each Opteron server has twin 2.4 GHz Opteron 250 CPUs and 8 GB of memory connected with a high-speed, low-latency Myrinet network.

The starting coordinates for the geometry optimisation calculation for [In($P_3C_2Bu^t_2$)], **1**, were taken from the structure obtained from X-ray diffraction.[4] C_s symmetry was imposed and calculations were initially performed at the Hartree-Fock level of theory using first the 3-21G* basis set[8] and then the 6-31G* basis set[9] on the light atoms (H, C and P) and the LanL2DZ basis set,[10] including an effective core potential (ECP), on the indium atom. When geometry optimisations were performed at these levels, it was noted that the calculations had difficulty in reaching convergence as the forces acting on the atoms became too small. This is characteristic of a very shallow potential-energy surface (PES). Force fields were calculated at these levels and had a tendency to return a single imaginary frequency (~ 13*i* cm^{-1}), indicating that a minimum on the PES had not been reached. By visualising the imaginary frequencies using the Molekel graphics program,[11] it was seen that those frequencies were associated with the twists of the symmetry-related *tert*-butyl groups. A modified geometry optimisation was performed using the direct inversion in the iterative subspace (GDIIS) algorithm[12] as this is known to aid convergence in calculations of large molecules, especially those having a shallow PES.

Calculations were also performed at different levels of theory, namely BLYP,[13,14] B3LYP,[14,15] B3PW91[15,16] and MP2.[17] A scan of the PES was performed (B3PW91/LanL2DZ/6-31G*) to gain an insight into its form (Figure 2). The torsional angle C(9)–C(7)–C(3)–P(2) was varied in steps of 5° from a zero-torsion position where the C_{tert}–C_{Me} bond was eclipsing the C(3)–P(2) ring bond (see Figure 3 for atom numbering). When the calculations were started from a position where the C(9)–C(7)–C(3)–P(2) torsion angle was 40°, a structure with real frequencies was obtained, indicating that the optimised geometry represented an energy minimum.

Figure 2 Relative energies upon rotation about the C_{ring}–C_{tert} bond in [In($P_3C_2Bu^t_2$)], **1**. Torsional angles in degrees.

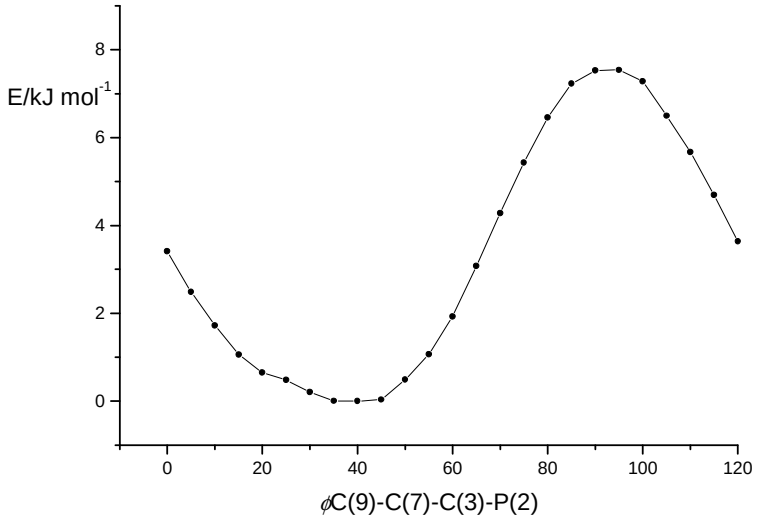

The LanL2DZ pseudopotential that was used above is an example of a large-core ECP. For the indium atom, LanL2DZ considers 46 of the 49 electrons to belong to the atomic core. Recently, small-core pseudopotentials were developed that regard only 28 of the electrons to be in the core ([Ar] + 4*d*) and treat the rest explicitly. A quadruple-ζ basis set of this type[18] (aug-cc-pVQZ-PP) has been tested to see whether the inclusion of more electrons in the valence shell of the atom can produce more reliable theoretical structures. The accuracy of each method will be assessed by comparison with the GED structure for **1**.

Figure 3 Structure of [In($P_3C_2Bu^t_2$)], **1**, with C_s symmetry showing the atom numbering used in calculations and the GED refinement.

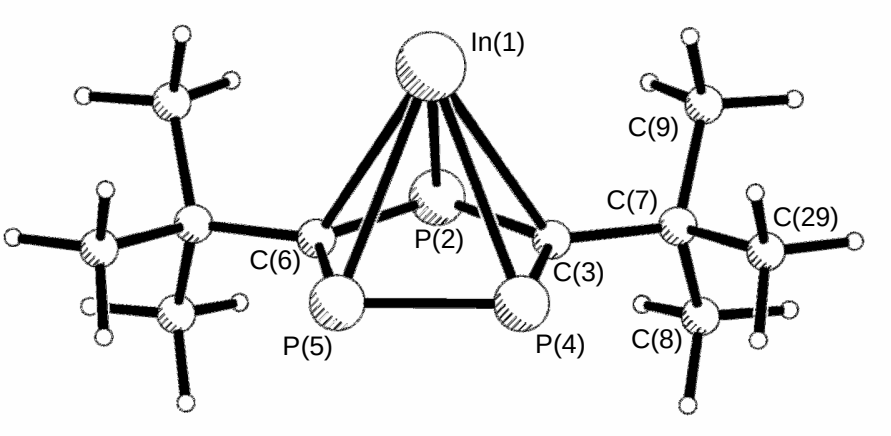

A similar set of calculations was performed for [In($P_2C_3Bu^t_3$)], **2**. Again different methods were tried and a variety of pseudopotentials were used. Unlike **1**, molecule **2** was found to have C_1 symmetry.

Analytical force fields calculated at the RHF/aug-cc-pVQZ-PP/6-31G* level for both **1** and **2** were used with the SHRINK program[19] to calculate accurate amplitudes of vibration (u_{h1}) and curvilinear corrections (k_{h1}) to allow for the shrinkage effect that is associated with the GED experiment.[20]

2.2.3 Gas-phase electron diffraction

Data were collected for **1** and **2** using the Edinburgh gas-phase electron diffraction apparatus.[21] A voltage of approximately 40 kV was used to accelerate the electrons, resulting in an electron wavelength of around 6.0 pm. The intensities of the scattered electrons were recorded using Kodak Electron Image films. Data were collected for **1** at a nozzle-to-film distance of 254.05 mm with sample and nozzle temperatures of 481 and 487 K, respectively, and for **2** at a distance of 252.13 mm with sample and nozzle temperatures of 402 and 438 K.

The weighting points for the off-diagonal weight matrices, correlation parameters and scale factors for both sets of data are given in Table 1. Also included are the exact wavelengths of the electrons as determined from the scattering patterns for benzene that

were recorded immediately after the patterns for compounds **1** and **2**. The scattering intensities were measured using an Epson Expression 1600 Pro flatbed scanner and converted to mean optical densities as a function of the scattering variable, *s*, using an established program.[22] The data reduction and least-squares refinement processes were carried out using the ed@ed program[23] employing the scattering factors of Ross *et al*.[24]

Table 1 Nozzle-to-film distances (mm), weighting functions (nm^{-1}), scale factors, correlation parameters and electron wavelengths (pm) used in the electron diffraction studies of [In($P_3C_2Bu^t_2$)], **1**, and [In($P_2C_3Bu^t_3$)], **2**.

	[In($P_3C_2Bu^t_2$)], **1**	[In($P_2C_3Bu^t_3$)], **2**
Nozzle-to-film distance[a]	254.05	252.13
Δs	2	2
s_{min}	30	20
sw_1	40	40
sw_2	13.2	12.8
s_{max}	15.4	14.0
Scale factor[b]	0.907(24)	1.295(44)
Correlation parameter	0.446	0.360
Electron wavelength	6.020	6.020

[a] Determined by reference to the scattering pattern of benzene. [b] Values in parentheses are the estimated standard deviations.

2.3 Results and discussion

A large amount of work has previously been directed towards calculating the structures of transition-metal complexes incorporating ring systems. A review[25] of the computational chemistry of metallocenes investigated the application of *ab initio* and DFT methods to the modelling of transition-metal complexes and in particular ferrocene. The M–Cp distance was identified as an appropriate parameter on which to judge the suitability of a calculation for such a molecule. *Ab initio* studies[26] of ferrocene at the HF level gave Fe–ring distances that were overestimated by up to 15% compared to experimental parameters and this phenomenon was shown to be independent of basis set. A further study[27] of transition-metal sandwich and half-sandwich compounds was carried out and aimed to investigate the correlation effects involved in optimising the

M–Cp distance. This concluded that the bond length was insensitive to an improvement in basis set beyond double-ζ quality. A later study[28] applied MP2 perturbation theory to the problem with similarly unsatisfactory results. In that instance the Fe–Cp bond length in ferrocene was underestimated by more than 10 pm.

In contrast to the unsuccessful efforts to optimise the geometries of metallocenes *ab initio*, the application of DFT methods to these compounds has proved promising. In a study of ferrocene,[29] the use of a DFT method (LDA) returned an Fe–Cp distance to within 1 pm of experimental values (electron diffraction). DFT methods have also been used to investigate the structures of substituted ferrocenes with good results.[30]

As part of the structure determinations of the Group 13 half-sandwich complexes [In($P_3C_2Bu^t_2$)], **1**, and [In($P_2C_3Bu^t_3$)], **2**, several DFT methods as well as MP2 have been tested for their ability to calculate accurate geometries for this class of compound. The use of both small-core (aug-cc-pVQZ-PP) and large-core (LanL2DZ) ECPs has also been investigated. Selected parameters from those geometry optimisations are given in Table 2 and show that there is a wide variation in the quality of the results when compared to GED values. The parameters were chosen for comparison because they were defined by the GED experiment without the need for restraints, which themselves are derived from calculated values. See Figures 3 and 4 for the atom numbering of **1** and **2**, respectively.

Table 2 Selected parameters from the structures of **1** and **2** determined by experimental and theoretical methods. For each of the theoretical methods both a small-core aug-cc-pVQZ-PP (SC) and large-core LanL2DZ (LC) pseudopotential has been tested on In.[a]

[In($P_3C_2Bu^t_2$)], **1**	XRD[b]	GED	MP2		B3PW91		B3LYP		BLYP		PW91PW91		PBE1PBE	
			SC	LC	SC	LC	SC	LC	SC	LC	SC	LC	SC	LC
*r*In–P(2)	310.8(4)	293.5(20)	301.9	296.8	294.6	296.0	300.2	300.6	304.4	303.7	296.0	297.1	292.9	295.1
*r*In–P(4/5)	303.5(3)	292.7(14)	298.8	300.3	293.1	296.3	297.7	299.9	301.0	302.0	294.4	297.0	291.8	295.4
*r*In–C	298.1(9)	283.2(10)	290.8	281.9	283.0	284.0	288.4	288.5	292.5	291.5	284.0	284.5	281.1	282.6
*r*P(2)–C(3/6)	178.1(10)	177.1(4)	175.7	176.5	176.6	176.6	177.2	177.2	179.0	179.0	177.9	177.9	176.3	176.3
*r*P(4/5)–C(3/6)	174.8(10)	176.5(4)	174.3	177.0	176.0	176.0	176.6	176.5	178.5	178.5	177.4	177.4	175.7	175.7
*r*P–P	211.1(5)	213.2(11)	212.8	212.7	214.2	214.0	215.3	215.1	218.0	217.9	215.9	215.7	213.6	213.3
$\angle C_{ring}–P–C_{ring}$	100.0(7)	100.3(5)	101.3	99.3	100.3	100.0	100.6	100.3	100.7	100.3	100.1	99.8	100.2	99.9
$\angle P–C_{ring}–P$	119.8(6)	120.3(4)	119.6	121.0	120.5	120.7	120.3	120.5	120.4	120.6	120.7	121.0	120.6	120.8
$\angle C_{ring}–P–P$	100.2(3)	99.6(2)	99.7	99.2	99.3	99.3	99.4	99.3	99.3	99.2	99.2	99.1	99.3	99.2
[In($P_2C_3Bu^t_3$)], **2**	XRD[c]	GED	MP2[d]		B3PW91		B3LYP		BLYP		PW91PW91		PBE1PBE	
			SC	LC	SC	LC	SC	LC	SC	LC	SC	LC	SC	LC
*r*In–P[e]	290.8(3)	284.2(11)	—	—	285.4	288.0	290.2	290.6	294.4	293.0	287.5	288.7	285.0	287.0
*r*In–C(2)	281.1(9)	266.1(13)	—	—	275.7	277.2	280.0	280.1	283.8	282.5	277.1	277.9	274.2	276.3
*r*In–C(4/5)[e]	283.5(9)	286.6(10)	—	—	277.3	278.6	284.3	282.8	288.5	285.7	279.9	279.4	276.8	277.4
*r*P(3/6)–C(2)[e]	172.8(9)	183.1(10)	—	—	174.8	174.8	175.3	175.2	177.0	177.0	176.1	176.0	174.5	174.5
*r*P(3/6)–C(4/5)[e]	178.9(10)	181.0(9)	—	—	180.8	180.7	181.7	181.5	183.7	183.5	182.1	182.0	180.3	180.2
$rC_{ring}–C_{ring}$	142.9(11)	140.7(14)	—	—	141.7	141.8	141.8	141.9	142.9	143.0	142.5	142.5	141.5	141.6
$\angle C_{ring}–C_{ring}–P$[e]	114.9(7)	116.4(2)	—	—	115.1	115.2	115.1	115.1	115.1	115.1	115.2	115.3	115.2	115.2
$\angle P–C_{ring}–P$	116.3(5)	110.8(10)	—	—	115.2	115.4	115.0	115.2	115.1	115.3	115.5	115.7	115.3	115.5
$\angle C_{ring}–P–C_{ring}$[e]	97.0(4)	98.2(6)	—	—	97.3	97.1	97.4	97.3	97.4	97.2	97.0	96.8	97.2	97.0

[a] Distances (*r*) are in pm, angles ($\angle$) in degrees. [b] Taken from Ref. 4. [c] Taken from Ref. 5. [d] MP2 calculations proved too computationally demanding for **2**. [e] Average value.

Figure 4 Structure of [In($P_2C_3Bu^t_3$)], **2**, with C_1 symmetry showing the atom numbering used in calculations and the GED refinement.

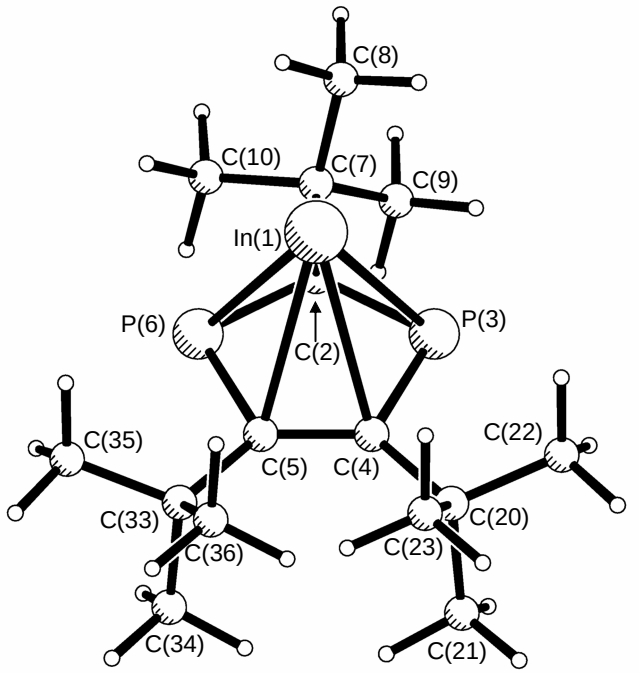

For **1**, the calculations that most closely matched the GED experimental results were performed using the B3PW91 method with the small-core ECP on indium. Using the LanL2DZ ECP with this method overestimated the In–ring distances by between 1 and 3 pm. For MP2, neither the large-core or small-core ECPs gave results concordant with those from experiment. Although MP2/LanL2DZ calculated *r*In–C to within 1.5 pm of the GED value, *r*In–P was overestimated by up to 8 pm. Similarly poor results were obtained for the B3LYP and BLYP methods, which overestimated bond lengths by between 6 and 11 pm for *r*In–P(2), by between 5 and 9 pm for *r*In–P(4/5) and by between 5 and 9 pm for *r*In–C. The PW91PW91 and PBE1PBE methods performed better, generally predicting distances to within a few picometres, especially when using the small-core ECP. Coordinates for each of the calculated geometries are given in Tables 2.1–2.12 in the Electronic Appendix (EA).

[In($P_2C_3Bu^t_3$)], **2**, has more atoms (and therefore more electrons) than **1** and is also of lower symmetry. For these reasons similar calculations for **2** took longer and required

more CPU memory. In fact, despite the powerful resources of the NSCCS Opteron clusters, it proved impossible to run MP2 calculations for **2**. From the calculations that were run (see Table 2) the similarity of parameters to those obtained from GED was poor. Again the parameters chosen for comparison were not restrained in the GED refinement. The discrepancies between theory and experiment are unlikely to be due to the inaccuracy of calculations (which of course worked well for **1**). Instead it is probable that the GED data were of poor quality and this is discussed further later in this section.

The calculated results do, however, show a degree of correlation with the parameters obtained from X-ray diffraction.[5] Ideally calculated parameters should be compared with gas-phase data where structures are not altered by packing forces, but on this occasion some comparisons will be made with the crystal structure. This course of action is supported by the nature of the crystal structure of **2**. Unlike **1**, for which chains of molecules were observed in the crystalline phase[4] and, consequently, the In–ring distances are much longer than the gas-phase distances (Table 2), the molecules of **2** in the crystal are further apart, minimising intermolecular interactions. Thus the molecular structures in the gas phase and solid state will be more similar.

In the case of **2**, the B3LYP calculations give In–ring bond lengths that are within about 1 pm of the X-ray determined values. Here the use of the small-core and large-core basis sets makes less difference to the parameters, with most bond lengths lying within 2 pm of one another. As was found for **1**, the BLYP method overestimated most distances and the PW91PW91 and PBE1PBE methods underestimated them. For **1** there was a definite trend towards the use of small-core ECPs giving more accurate results. Such a trend is not observed for **2**, where sometimes the use of a small-core ECP gives a result closer to an experimental value and sometimes it is further away. This was true when compared to both the GED experimental parameters and the X-ray parameters. Coordinates for each of the calculated geometries are given in Tables 2.13–2.22 (EA).

The SARACEN method[31] was used to determine the structure of [In($P_3C_2Bu^t_2$)], **1**. A C_s-symmetry model was written describing the molecule as a planar ring with an attendant In atom, which was free to move above the ring within the constraints of C_s symmetry. The two *tert*-butyl groups were related through symmetry and were allowed to bend out

of the plane of the ring. In total the geometry was described by 11 distance parameters, seven angle parameters and two torsion angle parameters (see Table 3). The distances included a single C–H bond length (p_1) as the theoretical structure (B3PW91/aug-cc-pVQZ-PP/6-311+G*) showed all the distances to be within 0.2 pm of one another. The four different C–C bond lengths were described by an average and three difference parameters according to the following equations, where Me1 is the methyl group containing C(9), Me2 contains C(8) and Me3 contains C(29). (See Figure 3 for atom numbering.)

$p_2 = [r(C_{ring}–C_{tert}) + r(C_{tert}–C_{Me1}) + r(C_{tert}–C_{Me2}) + r(C_{tert}–C_{Me3})] / 4$

$p_3 = r(C_{ring}–C_{tert}) – \{[r(C_{tert}–C_{Me1}) + r(C_{tert}–C_{Me2}) + r(C_{tert}–C_{Me3})] / 3\}$

$p_4 = r(C_{tert}–C_{Me1}) – \{[r(C_{tert}–C_{Me2}) + r(C_{tert}–C_{Me3})] / 2\}$

$p_5 = r(C_{tert}–C_{Me2}) – r(C_{tert}–C_{Me3})$

Parameters 2–5 were then used to define the four C–C distances.

The two C–P bond lengths were described using the simple average of the two and the difference between them ($p_{6–7}$) and rP–P, which only appears once in the molecule, is p_8. The other distance used to describe the ring was the non-bonded C···C distance (p_9). In order to position the indium atom above the ring, rIn–P(2) and rIn–C_{ring} were included as independent parameters ($p_{10–11}$).

The three different C_{ring}–C_{tert}–C_{Me} angles were described using (i) a simple average of the three, (ii) the angle to Me1 minus the difference between the other two, and (iii) the difference between the angles to Me2 and Me3 ($p_{12–14}$). The angles between the methyl groups, which were needed to describe the asymmetry of the Bu^t groups fully, were defined as $\angle C_{Me1}–C_{tert}–C_{Me3}$ (p_{15}) and $\angle C_{Me2}–C_{tert}–C_{Me3}$ (p_{16}), and a single $\angle C_{tert}–C_{Me}–$H angle was used (p_{17}). Calculations (B3PW91/aug-cc-pVQZ-PP/6-311+G*) showed that the twist of each methyl group (*i.e.* the torsional angle formed by one C–H and $C_{ring}–C_{tert}$) was approximately 180° and these values were not allowed to vary in the final refinement.

$\angle$P(2)–C_{ring}–C_{tert} (p_{18}) determined the angle that the Bu^t groups made with the P(2)–C(3) bond. The dihedral angle providing the twist of the Bu^t groups (applied so that C_s symmetry was preserved) was defined as ϕP(2)–C(3)–C(7)–C(9) (p_{19}), where the zero-

torsion position has C(7)–C(9) eclipsing P(2)–C(3). A positive value for p_{19} relates to a twist of the Bu^t group containing C(7) in a clockwise direction when viewed from C(3) to C(7) and a twist in the opposite direction for the other Bu^t group. ϕP(5)–P(4)–C(3)–C(7) (p_{20}) allowed the Bu^t groups to bend out of the plane of the ring in the opposite direction to In.

Table 3 Refined (r_{h1}) and calculated (r_e) geometric parameters for [In($P_3C_2Bu^t_2$)], **1**, from the GED study using SARACEN.[a,b]

	Parameter	r_{h1}	r_e	Restraint
Independent				
p_1	*r*C–H mean	109.6(4)	109.5	109.5(5)
p_2	*r*C–C average	154.1(3)	154.9	—
p_3	*r*C–C difference 1	0.3(1)	0.3	0.3(1)
p_4	*r*C–C difference 2	–0.2(1)	–0.2	–0.2(1)
p_5	*r*C–C difference 3	0.6(2)	0.6	0.6(2)
p_6	*r*C–P average	176.8(3)	176.3	—
p_7	*r*C–P difference	0.6(2)	0.6	0.6(2)
p_8	*r*P–P	213.2(11)	214.2	—
p_9	*r*C(3)···C(6)	272.0(10)	271.3	—
p_{10}	*r*In–P(2)	293.5(20)	294.6	—
p_{11}	*r*In–C(3/6)	283.2(10)	283.0	—
p_{12}	∠C_{ring}–C_{tert}–C_{Me} average	111.2(6)	110.3	—
p_{13}	∠C_{ring}–C_{tert}–C_{Me} difference 1	2.7(6)	2.1	2.1(7)
p_{14}	∠C_{ring}–C_{tert}–C_{Me} difference 2	–4.5(7)	–4.3	–4.3(8)
p_{15}	∠C_{Me1}–C_{tert}–C_{Me3}	108.0(10)	108.8	108.2(10)
p_{16}	∠C_{Me2}–C_{tert}–C_{Me3}	108.5(10)	108.7	108.9(10)
p_{17}	∠C_{tert}–C_{Me}–H mean	111.5(10)	111.1	111.1(10)
p_{18}	∠P(2)–C_{ring}–C_{tert}	120.5(11)	119.3	—
p_{19}	$\phi$$Bu^t$	48.4(50)	34.0	—
p_{20}	ϕP(5)–P(4)–C(3)–C(7)	3.4(5)	3.3	3.3(5)
Dependent				
p_{21}	*r*In–P(4/5)	292.7(14)	293.1	—
p_{22}	*r*C(6/3)–P(2)	177.1(4)	176.6	—
p_{23}	*r*C(3/6)–P(4/5)	176.5(4)	176.0	—
p_{24}	∠C_{ring}–P–C_{ring}	100.3(5)	100.3	—
p_{25}	∠P–C_{ring}–P	120.3(4)	120.5	—
p_{26}	∠C_{ring}–P–P	99.6(2)	99.3	—

[a] Refers to B3PW91/aug-cc-pVQZ-PP/6-311+G*. [b] Distances (*r*) are in pm, angles (∠) and torsions (ϕ) in degrees. See text for parameter definitions and Figure 3 for atom numbering. The figures in parentheses are the estimated standard deviations of the last digits. Me1 is the methyl group surrounding C(9), Me2 is associated with C(8) and Me3 with C(29).

A total of 20 geometric parameters and nine groups of amplitudes of vibration were refined during the least-squares refinement process. See Table 2.23 (EA) for a list of the amplitudes of vibration. Flexible restraints were employed, using the SARACEN method, for 11 geometric parameters and six amplitudes. The restraints were derived from calculations performed using B3PW91/aug-cc-pVQZ-PP/6-311+G*, which had proved the most accurate of the methods tested for determining this structure.

The success of the refinement, for which $R_G = 0.059$ ($R_D = 0.043$), can be gauged on the basis of the radial-distribution and experimental – theoretical difference curves (Figure 5) and the molecular-scattering intensity curve (Figure 6). The least-squares correlation matrix is given in Table 4 and the coordinates for the GED structure are given in Table 2.24 (EA).

Figure 5 Experimental and difference (experimental – theoretical) radial-distribution curves for [In($P_3C_2Bu^t_2$)], **1**. Before Fourier inversion, the data were multiplied by $s.\exp(-0.00002s^2)/(Z_{In} - f_{In})(Z_C - f_C)$.

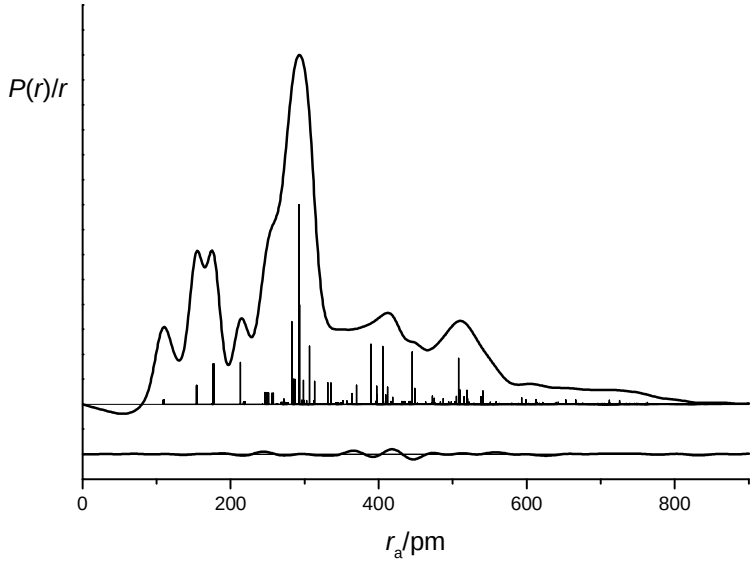

Figure 6 Molecular-scattering intensity and final weighted difference curves for [In($P_3C_2Bu^t_2$)], **1**.

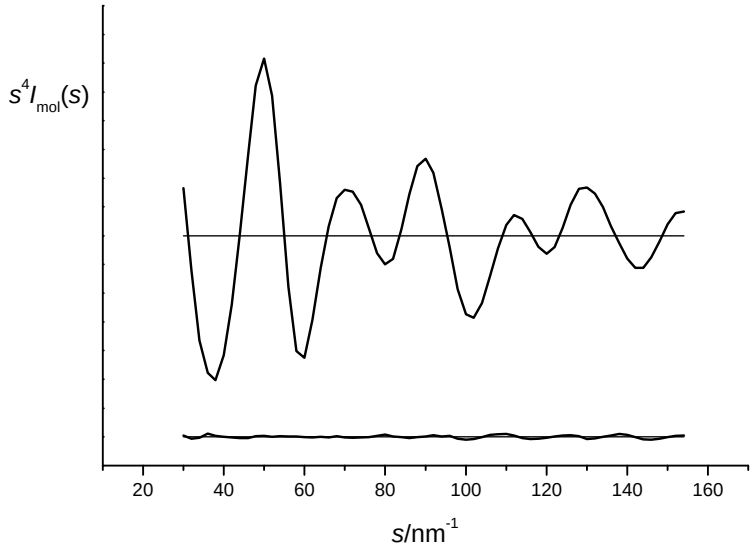

Table 4 Least-squares correlation matrix (×100) for [In($P_3C_2Bu^t_2$)], **1**.[a]

	p_{11}	p_{18}	u_{26}	k_1
p_2				71
p_6			–50	
p_8			–56	
p_{10}	82			
p_{11}			50	
p_{12}				57
p_{13}		51		
u_{17}			60	

[a] Only elements with absolute values ≥ 50% are shown; k_1 is a scale factor.

A C_1-symmetric model was written to describe the coordinates of [In($P_2C_3Bu^t_3$)], **2**, in terms of 30 independent parameters (see Table 5). This allowed for asymmetry in the molecule through the independence of the three Bu^t groups. These groups have been named so that Bu^t1 is the group centred on C(7), Bu^t2 is the group centred on C(20) and Bu^t3 is centred on C(33). Although calculations (B3PW91/aug-cc-pVQZ-PP/6-311+G*) showed that the ring had slight deviations from planarity and that, for example, *r*C(2)–

P(3) and *r*C(2)–P(6) differed by approximately 0.5 pm, the model was written to describe the InP_2C_3 motif with local C_s symmetry. (See Figure 4 for atom numbering.)

Of the eight distance parameters, a single mean value was used for *r*C–H (p_1). The C–C bond lengths were defined by a simple average (p_2) of (i) the short rC_{ring}–C_{ring} and (ii) the average of the other eight C–C bonds (four from Bu^{t}1 and four from Bu^{t}2/3, where the differences in *r*C–C between Bu^{t}2 and Bu^{t}3 were so small they were assumed to be the same), and the difference between (i) and (ii), p_3. Those eight C–C bond lengths were then defined using individual fixed (*i.e.* non-refineable) distances away from the average of the eight. The assumption of a plane of symmetry splitting the ring into two equal halves means that only two P–C distances are required; these were defined as an average and difference ($p_{4–5}$). The final three distance parameters in the model are the non-bonded P···P distance (p_6) and two ring-to-indium parameters *r*In–C(2) and *r*In–P ($p_{7–8}$), which allow the indium atom to move within the mirror plane dividing the ring in two.

As each of the Bu^t groups is different and has little symmetry it was necessary to use many parameters to describe these groups. In terms of the C_{ring}–C_{tert}–C_{Me} angles, each Bu^t group was considered to have three different angles, which were described using an average of the three and two differences ($p_{9–11}$ for Bu^{t}1, $p_{12–14}$ for Bu^{t}2 and $p_{15–17}$ for Bu^{t}3) in the same way as was shown above for the Bu^t groups in **1**. Similarly each group had two independent ∠C_{Me}–C_{tert}–C_{Me} angles ($p_{18–19}$ for Bu^{t}1, $p_{20–21}$ for Bu^{t}2 and $p_{22–23}$ for Bu^{t}3). A single ∠C_{tert}–C_{Me}–H mean value was used, which had been averaged over all 27 angles (p_{24}). ∠P(3)–C_{ring}–C_{tert1} (p_{25}) was used to move Bu^{t}1 away from the ring and for Bu^{t}2/3 the simple average and difference between ∠C(5)–C(4)–C(20) and ∠C(4)–C(5)–C(33) was used ($p_{26–27}$). All three Bu^t groups are defined so that C_{tert}–C_{ring} lies in the plane of the ring.

The final three parameters were dihedral angles, used to describe the torsions applied to the Bu^t groups ($p_{28–30}$). For Bu^{t}1 this was the P(6)–C(2)–C(7)–C(9) dihedral angle, where 0° signifies that P(6)–C(2) and C(7)–C(9) are eclipsed and a positive value relates to a clockwise twist of Bu^{t}1 about the C(2)–C(7) axis when viewed from C(2) to C(7). For Bu^{t}2 the P(3)–C(4)–C(20)–C(22) dihedral angle was used and a positive value

indicates a clockwise rotation of Bu^{t}2 about the C(4)–C(20) bond when viewed from C(4)–C(20) and from the zero-torsion position where P(3)–C(4) and C(20)–C(22) eclipse one another. For Bu^{t}3 the P(6)–C(5)–C(33)–C(35) dihedral angle starts from a zero-position where P(6)–C(5) and C(33)–C(35) eclipse and a positive value is a clockwise rotation of Bu^{t}3 about the C(5)–C(33) bond where, when viewed from C(5) to C(33). No asymmetry was included in the methyl groups, which had C_{3v} local symmetry. The methyl twists of those groups were not allowed to refine and were fixed in positions where a C_{ring}–$C_{\textit{tert}}$–C_{Me}–H value of 180° exists for each methyl group.

Table 5 Refined (r_{h1}) and calculated (r_e) geometric parameters for two refinements of [In($P_2C_3Bu^t_3$)], **2**, from the GED study.[a,b]

		All parameters restrained			Best-fit structure	
	Parameter	r_{h1}	r_e	Restraint	r_{h1}	Restraint
Independent						
p_1	*r*C–H mean	109.5(6)	109.5	109.5(5)	109.6(4)	109.5(5)
p_2	*r*C–C average	147.0(6)	147.8	147.8(6)	145.0(4)	—
p_3	*r*C–C difference	12.4(6)	12.3	12.3(5)	11.9(5)	12.3(5)
p_4	*r*C–P average	176.4(8)	177.8	177.8(10)	180.7(13)	—
p_5	*r*C–P difference	5.8(6)	6.0	6.0(5)	5.9(6)	6.0(5)
p_6	*r*P···P	295.8(12)	295.2	295.2(10)	306.3(34)	—
p_7	*r*In–C(2)	276.8(12)	275.7	275.7(10)	267.4(24)	—
p_8	*r*In–P	287.7(9)	285.4	285.4(10)	289.8(12)	—
p_9	$\angle C_{ring}–C_{tert1}–C_{Me}$ average	111.2(11)	110.3	110.3(10)	110.0(10)	110.3(10)
p_{10}	$\angle C_{ring}–C_{tert1}–C_{Me}$ difference 1	2.2(6)	1.7	1.7(5)	2.1(5)	1.7(5)
p_{11}	$\angle C_{ring}–C_{tert1}–C_{Me}$ difference 2	–3.9(8)	–4.2	–4.2(7)	–4.0(8)	–4.2(7)
p_{12}	$\angle C_{ring}–C_{tert2}–C_{Me}$ average	112.5(11)	111.5	111.5(10)	111.6(10)	111.5(10)
p_{13}	$\angle C_{ring}–C_{tert2}–C_{Me}$ difference 1	5.9(12)	6.2	6.2(10)	6.4(10)	6.2(10)
p_{14}	$\angle C_{ring}–C_{tert2}–C_{Me}$ difference 2	–3.0(9)	–2.9	–2.9(7)	–2.9(8)	–2.9(7)
p_{15}	$\angle C_{ring}–C_{tert3}–C_{Me}$ average	112.9(11)	111.8	111.8(10)	111.9(10)	111.8(10)
p_{16}	$\angle C_{ring}–C_{tert3}–C_{Me}$ difference 1	–0.6(4)	–0.6	–0.6(3)	–0.6(3)	–0.6(3)
p_{17}	$\angle C_{ring}–C_{tert3}–C_{Me}$ difference 2	0.5(4)	0.5	0.5(3)	0.5(3)	0.5(3)
p_{18}	$\angle$C(8)–C_{tert1}–C(9)	108.6(12)	108.5	108.5(10)	108.3(11)	108.5(10)
p_{19}	$\angle$C(9)–C_{tert1}–C(10)	108.6(12)	108.6	108.6(10)	108.4(11)	108.6(10)
p_{20}	$\angle$C(21)–C_{tert2}–C(22)	105.9(12)	106.2	106.2(10)	105.7(11)	106.2(10)
p_{21}	$\angle$C(22)–C_{tert2}–C(23)	104.5(12)	104.4	104.4(10)	104.3(11)	104.4(10)
p_{22}	$\angle$C(34)–C_{tert3}–C(35)	104.9(12)	104.4	104.4(10)	104.3(13)	104.4(10)
p_{23}	$\angle$C(35)–C_{tert3}–C(36)	106.1(12)	106.2	106.2(10)	106.0(11)	106.2(10)

p_{24}	∠C_{tert}–C_{Me}–H mean	110.5(6)	110.5	110.5(10)	110.8(5)	110.5(10)
p_{25}	∠P(3)–C_{ring}–C_{tert1}	122.6(4)	122.6	122.6(5)	123.3(4)	—
p_{26}	∠C_{ring}–C_{ring}–$C_{tert2/3}$ average	132.1(10)	131.8	131.8(10)	133.8(7)	—
p_{27}	∠C_{ring}–C_{ring}–$C_{tert2/3}$ difference	1.0(5)	1.0	1.0(4)	0.9(4)	1.0(4)
p_{28}	ϕBu^{t}1	34.9(58)	36.2	36.2(50)	102.6(35)	—
p_{29}	ϕBu^{t}2	6.9(45)	25.6	25.6(50)	4.6(37)	—
p_{30}	ϕBu^{t}3	31.9(47)	10.1	10.1(50)	5.9(39)	—
Dependent						
p_{31}	*r*In–C(4/5)	280.4(29)	277.3	—	294.7(20)	—
p_{32}	*r*C(2)–P(3/6)	173.5(8)	174.8	—	174.8(11)	—
p_{33}	*r*C(4/5)–P(3/6)	175.9(16)	180.8	—	177.7(13)	—
p_{34}	*r*C_{ring}–C_{ring}	140.8(8)	141.7	—	139.0(6)	—
p_{35}	∠P(3/6)–C(4/5)–C(5/4)	115.5(2)	115.1	—	116.9(4)	—
p_{36}	∠C(4/5)–C(3/6)–C(2)	97.1(5)	97.3	—	96.4(5)	—
p_{37}	∠P(6)–C(2)–P(3)	114.7(8)	115.2	—	113.4(8)	—

[a] Refers to B3PW91 calculation with an aug-cc-pVQZ-PP basis set on In and 6-311+G* on C, P and H atoms. [b] Distances (*r*) are in pm, angles (∠) and torsions (ϕ) in degrees. See text for parameter definitions and Figure 4 for atom numbering. The figures in parentheses are the estimated standard deviations of the last digits. *Tert*1 and Bu^{t}1 refer to the Bu^t group containing C(7), *tert*2 and Bu^{t}2 refer to C(20) and *tert*3 and Bu^{t}3 to C(33).

The refinement of the GED structure of [In($P_2C_3Bu^t_3$)], **2**, proved to be problematic and this was most likely because of the poor quality of the data. Only data at a long nozzle-to-film distance were collected and these data give most information about large-amplitude distances. This means that torsions will be well defined but because long data contain little information about small-amplitude distances it will not be so good at determining bond lengths. The lack of short-distance nozzle-to-film data will also make it difficult to resolve similar distances.

Two separate refinements were performed, the first following the routine SARACEN procedure of restraining parameters that were poorly defined by the data to give the best-fit structure. In total 30 geometric parameters and seven groups of amplitudes of vibration were refined, with 20 parameters and three amplitudes needing to be restrained. A list of amplitudes of vibration is given in Table 2.25 (EA). The final *R* factors were R_G = 0.083 (R_D = 0.058). These, and comparison of the experimental and theoretical radial-distribution curves (Figure 7) and molecular-scattering intensity curves (Figure 8) show that this model is consistent with the experimental data, although these are limited. The coordinates for this best-fit geometry of **2** are given in Table 2.26 (EA) and the least-squares correlation matrix in Table 6. Despite the apparent good fit of these parameters to the experimental data, there are a number of parameters for which the values are questionable. In particular the position of the indium atom above the ring appears to be poorly defined by the data and this is the result of the absence of short nozzle-to-film data.

Figure 7 Experimental and difference (experimental – theoretical) radial-distribution curves for the best-fit refinement of [In($P_2C_3Bu^t_3$)], **2**. Before Fourier inversion, the data were multiplied by $s.\exp(-0.00002s^2)/(Z_{In} - f_{In})(Z_C - f_C)$.

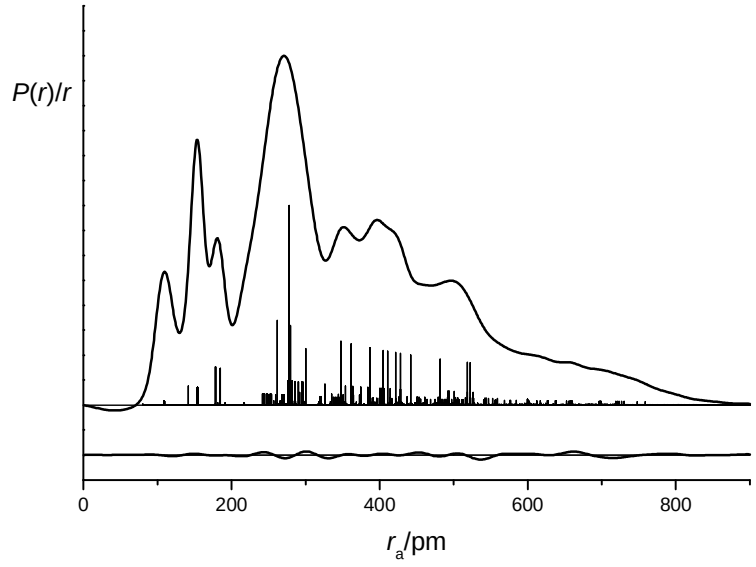

Figure 8 Molecular-scattering intensity and final weighted difference curves for the best-fit refinement of [In($P_2C_3Bu^t_3$)], **2**.

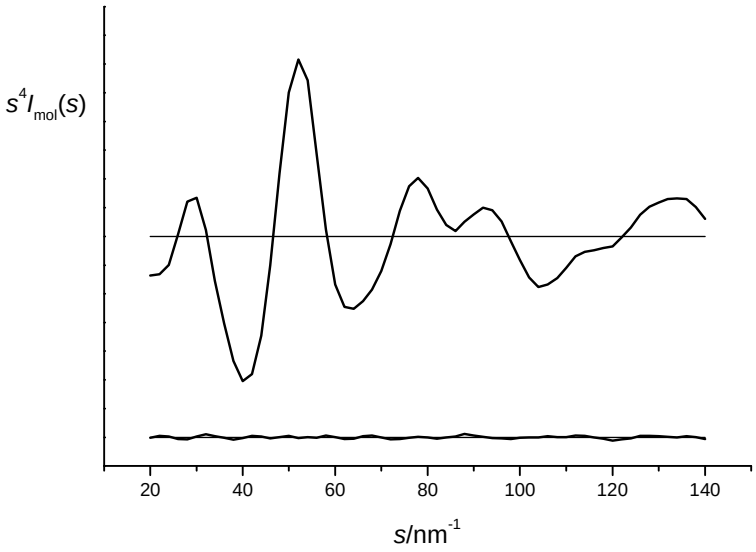

Table 6 Least-squares correlation matrix (×100) for the best-fit refinement for [In($P_2C_3Bu^t_3$)], **2**.[a]

	p_6	p_8	p_{30}	u_{71}	k_1
p_4	98	73		54	67
p_6		80			59
p_{29}			–53		
u_{71}					91

[a] Only elements with absolute values ≥ 50% are shown; k_1 is a scale factor.

The second refinement that was performed for **2** imposed flexible restraints on all of the independent parameters based on the values calculated at B3PW91/aug-cc-pVQZ-PP/6-311+G*. This gave a much worse fit to the data with R_G = 0.161 (R_D = 0.140). The radial-distribution curve for this refinement is shown in Figure 9. The experimental – theoretical difference curve shows that the parameters subject to restraints do not fit well with the experimental data. The amplitudes of vibration from this restrained refinement are given in Table 2.27 (EA) and the geometric coordinates in Table 2.28 (EA).

Figure 9 Experimental and difference (experimental – theoretical) radial-distribution curves for the fully-restrained refinement of [In($P_2C_3Bu^t_3$)], **2**. Before Fourier inversion, the data were multiplied by $s.\exp(-0.00002s^2)/(Z_{In} - f_{In})(Z_C - f_C)$.

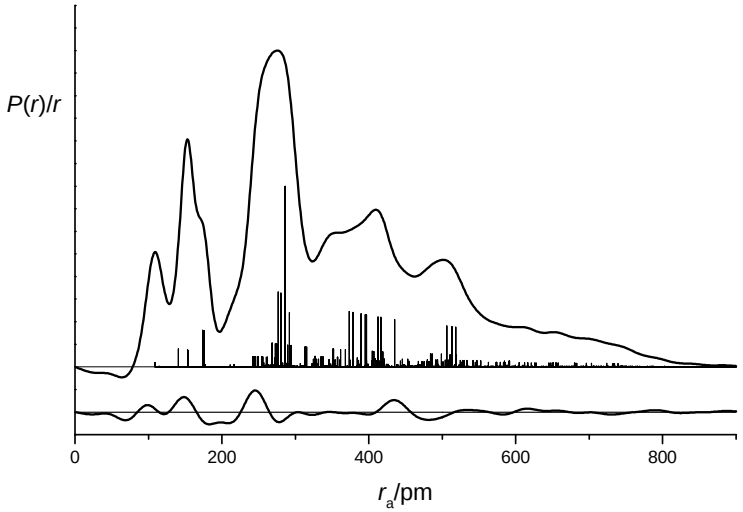

Consulting Table 2, the calculated values for the C–P and C–C ring distances at the various levels of theory are quite close. However, while *r*P(3/6)–C(2) has theoretical values that deviate by about 2 pm over the series of calculations, the unrestrained GED value from the best-fit refinement is between 6 and 8 pm longer than these values. Although it is acknowledged that bond lengths between first and second row elements can be wrongly predicted by theory, these differences are far too great for that to be the sole cause in this case. Again, the evidence suggests that the data are of poor quality.

As mentioned earlier, the fact that the crystal structure of **2** contains monomeric molecules[5] rather than chains of molecules suggests that the gas-phase and solid-state structures should be more similar than in the case of **1**. However, in terms of the ring distances (see Table 2 for selected X-ray and GED parameters), it is seen that these are reasonably close for **1** and much more different for **2**. This adds to the suspicion of bad data for **2**. Unfortunately, no further sample is available, and as the electron diffractometer was taken to its present heating limit this could not be solved.

In conclusion, the calculated geometry for [In($P_3C_2Bu^t_2$)], **1**, using the B3PW91 method with a small-core aug-cc-pVQZ-PP ECP on indium was very close to the geometry obtained from the GED refinement. The calculations also showed that it is advisable to use a small-core ECP wherever it is available as this can have a striking effect on the accuracy of *ab initio* and DFT calculations. It is unfortunate that, due to poor electron diffraction data, it was not possible to extend this study to show that the same method of calculation is as good for [In($P_2C_3Bu^t_3$)], **2**.

2.4 References

1. K. B. Dillon, F. Mathey and J. F. Nixon, *Phosphorus: The Carbon Copy: From Organophosphorus to Phospha-organic Chemistry*, John Wiley and Sons, Chichester, 1998 and references therein.
2. J. F. Nixon, *Coord. Chem. Rev.*, 1995, **145**, 201.
3. A. Schnepf, G. Stößer, D. Carmichael. F. Mathey and H. Schnöckel, *Angew. Chem., Int. Ed. Engl.*, 1999, **38**, 1646.
4. C. Callaghan, G. K. B. Clentsmith, F. G. N. Cloke, P. B. Hitchcock, J. F. Nixon and D. M. Vickers, *Organometallics*, 1999, **18**, 793.
5. G. K. B. Clentsmith, F. G. N. Cloke, M. D. Francis, J. C. Green, P. B. Hitchcock, J. F. Nixon, J. L. Suter and D. M. Vickers, *J. Chem. Soc., Dalton Trans.*, 2000, 1715.
6. O. T. Beachley, Jr., J. F. Lees and R. D. Rogers, *J. Organomet. Chem.*, 1991, **418**, 165.
7. M. J. Frisch, G. W. Trucks, H. B. Schlegel, G. E. Scuseria, M. A. Robb, J. R. Cheeseman, J. A. Montgomery, Jr., T. Vreven, K. N. Kudin, J. C. Burant, J. M. Millam, S. S. Iyengar, J. Tomasi, V. Barone, B. Mennucci, M. Cossi, G. Scalmani, N. Rega, G. A. Petersson, H. Nakatsuji, M. Hada, M. Ehara, K. Toyota, R. Fukuda, J. Hasegawa, M. Ishida, T. Nakajima, Y. Honda, O. Kitao, H. Nakai, M. Klene, X. Li, J. E. Knox, H. P. Hratchian, J. B. Cross, C. Adamo, J. Jaramillo, R. Gomperts, R. E. Stratmann, O. Yazyev, A. J. Austin, R. Cammi, C. Pomelli, J. W. Ochterski, P. Y. Ayala, K. Morokuma, G. A. Voth, P. Salvador, J. J. Dannenberg, V. G. Zakrzewski, S. Dapprich, A. D. Daniels, M. C. Strain, O. Farkas, D. K. Malick, A. D. Rabuck, K. Raghavachari, J. B. Foresman, J. V. Ortiz, Q. Cui, A. G. Baboul, S. Clifford, J. Cioslowski, B. B. Stefanov, G. Liu, A. Liashenko, P. Piskorz, I. Komaromi, R. L. Martin, D. J. Fox, T. Keith, M. A. Al-Laham, C. Y. Peng, A. Nanayakkara, M. Challacombe, P. M. W. Gill, B. Johnson, W. Chen, M. W. Wong, C. Gonzalez and J. A. Pople, *Gaussian 03, Revision C.01*, Gaussian, Inc., Wallingford, CT, 2004.
8. J. S. Binkley, J. A. Pople and W. J. Hehre, *J. Am. Chem. Soc.*, 1980, **102**, 939; M. S. Gordon, J. S. Binkley, J. A. Pople, W. J. Pietro and W. J. Hehre, *J. Am. Chem. Soc.*,

1982, **104**, 2797; W. J. Pietro, M. M. Francl, W. J. Hehre, D. J. DeFrees, J. A. Pople and J. S. Binkley, *J. Am. Chem. Soc.*, 1982, **104**, 5039.

9. W. J. Hehre, R. Ditchfield and J. A. Pople, *J. Chem. Phys.*, 1972, **56**, 2257; P. C. Hariharan and J. A. Pople, *Theor. Chim. Acta*, 1973, **28**, 213; M. S. Gordon, *Chem. Phys. Lett.*, 1980, **76**, 163.
10. P. J. Hay and W. R. Wadt, *J. Chem. Phys.*, 1985, **82**, 270; W. R. Wadt and P. J. Hay, *J. Chem. Phys.*, 1985, **82**, 284; P. J. Hay and W. R. Wadt, *J. Chem. Phys.*, 1985, **82**, 299.
11. P. Flükiger, H. P. Lüthi, S. Portmann and J. Weber, *MOLEKEL 4.0*, Swiss Center for Scientific Computing, Manno, Switzerland, 2000.
12. Ö. Farkas and H. B. Schlegel, *Phys. Chem. Chem. Phys.*, 2002, **4**, 11.
13. A. D. Becke, *Phys. Rev. A*, 1988, **38**, 3098.
14. C. Lee, W. Yang and R. G. Parr, *Phys. Rev. B: Condens. Matter*, 1992, **37**, 785; B. Miehlich, A. Savin, H. Stoll and H. Preuss, *Chem. Phys. Lett.*, 1989, **157**, 200.
15. A. D. Becke, *J. Chem. Phys.*, 1993, **98**, 5648.
16. J. P. Perdew, K. Burke and Y. Wang, *Phys. Rev. B: Condens. Matter*, 1996, **54**, 16533.
17. C. Møller and M. S. Plesset, *Phys. Rev.*, 1934, **46**, 618.
18. K. A. Peterson, *J. Chem. Phys.*, 2003, **119**, 11099.
19. V. A. Sipachev, *J. Mol. Struct.* (*THEOCHEM*), 1985, **121**, 143; V. A. Sipachev, *J. Mol. Struct.*, 2001, **567**, 67.
20. O. Bastiansen and M. Trætteberg, *Acta Crystallogr.*, 1960, **13**, 1108; Y. Morino, S. J. Cyvin, K. Kuchitsu and T. Iijima, *J. Chem. Phys.*, 1962, **36**, 1109; R. Stølevik, H. M. Seip and S. J. Cyvin, *Chem. Phys. Lett.*, 1972, **15**, 263.
21. C. M. Huntley, G. S. Laurenson and D. W. H. Rankin, *J. Chem. Soc., Dalton Trans.*, 1980, 954.
22. H. Fleischer, D. A. Wann, S. L. Hinchley, K. B. Borisenko, J. R. Lewis, R. J. Mawhorter, H. E. Robertson and D. W. H. Rankin, *Dalton Trans.*, 2005, 3221.

23. S. L. Hinchley, H. E. Robertson, K. B. Borisenko, A. R. Turner, B. F. Johnston, D. W. H. Rankin, M. Ahmadian, J. N. Jones and A. H. Cowley, *Dalton Trans.*, 2004, 2469.
24. A. W. Ross, M. Fink and R. Hilderbrandt, *International Tables for Crystallography*, ed. A. J. C. Wilson, Kluwer Academic Publishers, Dordrecht, Netherlands, 1992, vol. C, p.245.
25. N. Fey, *J. Chem. Technol. Biotechnol.*, 1999, **74**, 852.
26. H. P. Lüthi, J. Ammeter, J. Almlöf and K. Korsell, *Chem. Phys. Lett.*, 1980, **69**, 540; H. P. Lüthi, J. Ammeter, J. Almlöf and K. Fægri Jr., *J. Chem. Phys.*, 1982, **77**, 2002.
27. J. Almlöf, K. Fægri Jr., B. E. R. Schilling and H. P. Lüthi, *Chem. Phys. Lett.*, 1984, **106**, 266.
28. W. Klopper and H. P. Lüthi, *Chem. Phys. Lett.*, 1996, **262**, 546.
29. A. Bérces, T. Ziegler and L. Fan, *J. Phys. Chem.*,1994, **98**, 1584.
30. C. A. Morrison, S. F. Bone, D. W. H. Rankin, H. E. Robertson, S. Parsons, R. A. Coxall, S. Fraser, J. A. S. Howell, P. C. Yates and N. Fey, *Organometallics*, 2001, **20**, 2309.
31. A. J. Blake, P. T. Brain, H. McNab, J. Miller, C. A. Morrison, S. Parsons, D. W. H. Rankin, H. E. Robertson and B. A. Smart, *J. Phys. Chem.*, 1996, **100**, 12280; P. T. Brain, C. A. Morrison, S. Parsons and D. W. H. Rankin, *J. Chem. Soc., Dalton Trans.*, 1996, 4589; N. W. Mitzel and D. W. H. Rankin, *Dalton Trans.*, 2003, 3650.

Chapter Three

The molecular structure of [$Sn(P_2C_2Bu^t_2)$] using gas-phase electron diffraction and *ab initio* and DFT calculations

3.1 Introduction

In the past decade the phospha-alkyne synthon, Bu^tCP, has been used as a building block for a number of unsaturated ring systems. As described in Chapter 2, these molecules are analogues of well-known organic ligands in which C–R fragments have been replaced by phosphorus atoms.[1]

Transition-metal complexes of the cyclobutadiene derivative 1,3-diphosphacyclobutadiene were independently reported in 1986 by Nixon[2] and Binger,[3] who synthesised and structurally characterised compounds of the type $[M(\eta^5\text{-}C_5R_5)(\eta^4\text{-}P_2C_2Bu^t_2)]$ (M = Co, Rh, Ir; R = H or Me). Since this early work, several other 1,3-diphosphacyclobutadiene transition-metal complexes that include no ligands apart from the four-membered rings have been reported (see Figure 1).[4–6]

Figure 1 1,3-diphosphacyclobutadiene transition-metal complexes.

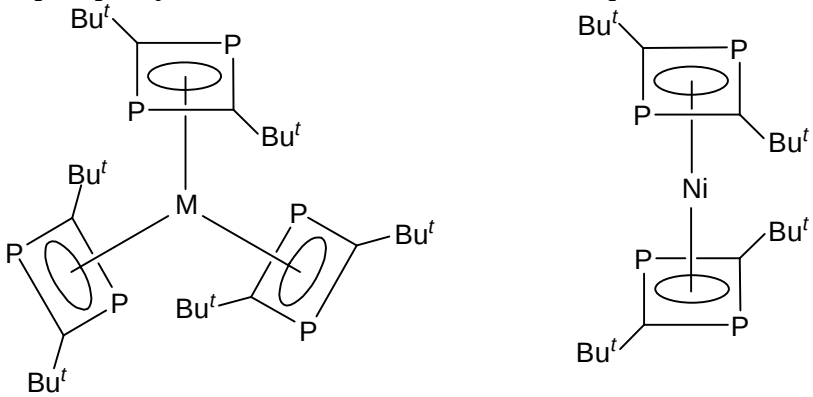

M = Mo, W

In the past three years the first main-group elements have been ligated to a 1,3-diphosphacyclobutadiene ring.[7–9] The series of compounds of the type $[M(\eta^4\text{-}P_2C_2Bu^t_2)]$ (M = Ge, Sn, Pb), **1a**–**c** (Figure 2), were shown by single-crystal X-ray diffraction studies to have the 1,3-diphosphacyclobutadiene ring coordinated to the metal in an η^4-fashion. Since these compounds are derivatives of divalent metals, the ligands should formally be considered as $[P_2C_2Bu^t_2]^{2-}$ dianions.

Figure 2 Half-sandwich main-group metal complexes of 1,3-diphosphacyclo-butadiene.

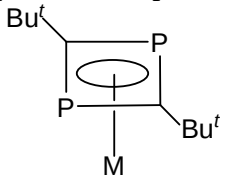

1a M = Ge
1b M = Sn
1c M = Pb

Very recently the synthesis and structural characterisation of the dilithium salt of the analogous silicon-containing dianion,[10] $[P_2C_2(SiMe_3)_2]^{2-}$ has been reported. Also discussed in recent literature is a theoretical study of the aromaticity of the corresponding isoelectronic cyclobutadiene dianion,[11] $[C_4H_4]^{2-}$, and its structurally characterised derivative $[Li_2C_4R_4]$ (R = $SiMe_3$).[12]

$[Sn(\eta^4\text{-}P_2C_2Bu^t_2)]$ is an example of a 24-electron *nido*-cage structure. Replacing the tin atom with a phosphorus gives $[P_3C_2Bu^t_2]^+$, a compound which is known to have a cage structure. This has previously been prepared by Dr. Jason Lynam and co-workers at the University of York.[13]

The gas-phase structure of $[Sn(\eta^4\text{-}P_2C_2Bu^t_2)]$, **1b**, as determined by electron diffraction and theoretical methods should, therefore, provide an interesting complement to these studies.

3.2 Experimental

3.2.1 Synthesis

A sample of $[Sn(P_2C_2Bu^t_2)]$, **1b**, was prepared from $SnCl_2$ and $[Zr(\eta^5\text{-}C_5H_5)_2(PCBu^t)_2]$ according to the literature method by Dr. Matthew Francis and co-workers, University of Sussex.[7]

3.2.2 Theoretical methods

The majority of calculations reported in this work were performed on a Linux 12-Processor Parallel Quantum Solutions (PQS) workstation[14] running the Gaussian 98 suite of programs.[15] Calculations at the PBE1PBE level were run using the Gaussian 03 programs,[16] with the resources of the EPSRC National Service for Computational Chemistry Software, on a cluster of six HP ES40 computers. Each Alphaserver ES40 machine has four 833 MHz EV68 CPUs and 8 GB of memory connected with a high-speed, low-latency QSW switch forming an Alphaserver SC. Calculations using the aug-cc-pVQZ-PP ECP were carried using a newly installed cluster of 22 Linux Opteron nodes, where each Opteron server has twin 2.4 GHz Opteron 250 CPUs and 8 GB of memory connected with a high-speed, low-latency Myrinet network.

A search of the potential-energy surface of **1b** was undertaken at the Hartree-Fock level of theory using a 3-21G* basis set[17] (HF/3-21G*) in order to locate any minima and a single structure with C_{2v} was identified.

A series of calculations was performed in order to gauge the effects of basis set size, use of effective core potentials and treatment of electron correlation on the optimised geometries. At the Hartree-Fock level of theory, where electron correlation is ignored, calculations were performed using the 6-31G* basis set[18] on C, P and H and, firstly, the LanL2DZ basis set[19] on Sn, then the Stuttgart/Dresden/Dunning (SDD) basis set,[20] and finally the SDB-aug-cc-pVTZ basis set,[21] in order to investigate their suitability. Such basis sets were chosen for the tin atom because of their ability to provide a pseudopotential, as relativistic effects become important with heavier atoms, and, given that the effective core potential (ECP) reduces the number of electrons that must be considered, they reduce the time taken for the calculations.

The DFT methods that were used in this work are based on Becke's B3 electron-exchange functional[22] and both the PW91[23] and LYP[24] correlation functionals. The PBE1PBE exchange-correlation functional of Perdew, Burke and Ernzerhof[25] was also used. Calculations comparing LanL2DZ, SDD and SDB-aug-cc-pVTZ on Sn were performed using the B3PW91, B3LYP and PBE1PBE functionals with various basis sets on C, P and H (6-31G*, 6-311G*, 6-311+G* and 6-311++G**).

Calculations at the MP2 level of theory[26] were performed using the same combinations of ECPs on Sn and other basis sets on the lighter atoms as described previously. All MP2 calculations were frozen core.

Based on the effects of different levels of theory and basis sets on the geometry of **1b**, the analytical force field was calculated at the B3PW91/6-31G* (LanL2DZ on Sn) level. This was used to provide estimates of the amplitudes of vibration (u_{h1}) and the curvilinear corrections (k_{h1}), from the SHRINK program,[27] for use in the gas-phase electron diffraction refinements.

An identical approach to that described above was adopted for geometry optimisation calculations to investigate the structures of related molecules and fragments: [Sn($P_2C_2H_2$)], **2**, [($P_2C_2Bu^t_2$)], **3**, [Sn($C_4Bu^t_2H_2$)], **4**, and [$Li_2P_2C_2Bu^t_2$], **5**.

The calculations above were completed before the study of [In($P_3C_2Bu^t_2$)] and [In($P_2C_3Bu^t_3$)], described in Chapter 2, which highlighted the need to consider newly developed small-core ECPs. Calculations have subsequently been performed for **1b** using the aug-cc-pVQZ-PP ECP with all the methods listed above.

3.2.3 Gas-phase electron diffraction

Data were collected for [Sn($P_2C_2Bu^t_2$)], **1b**, using the Edinburgh gas-phase electron diffraction apparatus.[28] An accelerating voltage of around 40 kV was used, equating to an electron wavelength of approximately 6.0 pm. Scattering intensities were recorded on Kodak Electron Image films at nozzle-to-film distances of 86.08 and 255.26 mm, with sample and nozzle temperatures held at 431 and 452 K, respectively, for the shorter distance and 424 and 429 K for the longer distance.

The weighting points for the off-diagonal weight matrices, correlation parameters and scale factors for both camera distances are given in Table 1. Also included are the exact electron wavelengths as determined from the scattering patterns for benzene that were recorded immediately after the patterns for **1b**. The scattering intensities were measured using an Epson Expression 1600 Pro flatbed scanner and converted to mean optical densities as a function of the scattering variable, *s*, using an established program.[29] The

data reduction and the least-squares refinement processes were carried out using the ed@ed program[30] employing the scattering factors of Ross *et al*.[31]

Table 1 Nozzle-to-film distances (mm), weighting functions (nm^{-1}), scale factors, correlation parameters and electron wavelengths (pm) used in the electron diffraction study of $[Sn(P_2C_2Bu^t_2)]$, **1b**.

Nozzle-to-film distance[a]	86.06	255.26
Δs	4	2
s_{min}	80	20
sw_1	120	40
sw_2	230	102
s_{max}	250	110
Scale factor[b]	0.801(42)	0.857(14)
Correlation parameter	0.393	0.119
Electron wavelength	6.020	6.020

[a] Determined by reference to the scattering pattern of benzene. [b] Values in parentheses are the estimated standard deviations.

3.3 Results and discussion

Recently, DFT calculations have been used to give information about the electronic structures of the following phospha-metallocenes $[M(\eta^5\text{-}P_3C_2Bu^t_2)_2]$ (M = Ti, Fe, Ru); $[M(\eta^5\text{-}P_2C_3Bu^t_3)_2]$ (M = Fe); $[Sc(\eta^5\text{-}P_3C_2Bu^t_2)_2\text{-}\mu\text{-}(\eta^2\text{-}P_3C_2Bu^t_2)Sc(\eta^5\text{-}P_3C_2Bu^t_2)]$ and the half-sandwich compounds $[M(\eta^5\text{-}P_3C_2Bu^t_2)\text{-}(CO)_3]$ (M = Mn, Re); and $[M(\eta^5\text{-}P_3C_2Bu^t_2)]$ and $[M(\eta^5\text{-}P_2C_3Bu^t_3]$ (M = In).[32–36]

Much less research has been directed towards calculating structures of *p*-block metallocenes or phospha-metallocenes. In the recently published paper investigating the electronic structure of $[Sn(P_2C_2Bu^t_2)]$, Green *et al*. describe the use of one DFT method.[9] They compare the calculated parameters with the crystal structure[7] in order to assess the reliability of the calculations. While these values compare reasonably, it would have been especially interesting to compare the theoretical parameters with ones determined in the gas phase, where molecules are free from intermolecular interactions.

In this chapter such a structure determination of $[Sn(P_2C_2Bu^t_2)]$, **1b**, is discussed using gas-phase electron diffraction and *ab initio* molecular-orbital calculations and density

functional theory. Many theoretical methods have been tested, and several different effective core potentials have also been evaluated.

The structure of **1b** was investigated using the various levels of theory and basis sets described in the Experimental section. With respect to the ECP to be used on the Sn atom, there was little to choose between the LanL2DZ and SDB-aug-cc-pVTZ pseudopotentials. Both produced Sn–ring bond lengths to within a couple of picometres of the experimental (GED and X-ray) values. The SDD pseudopotential was less successful, generating Sn–P bond lengths that were approximately 5 pm too long. Results for each of the three ECPs that were tested for the tin atom are given in Table 2. From this point on, all calculations will use the LanL2DZ ECP on the Sn atom unless otherwise stated.

Selected principal parameters taken from the geometries calculated at the different levels of theory used in this study are given in Table 3, alongside experimental data for comparison. In general, an improvement in the results of the calculations was noted as the basis set was increased from 6-31G* to 6-311G*. Only a very slight further difference was observed upon the addition of diffuse functions to the non-hydrogen atoms (6-311+G*) and no gain was made by adding diffuse and polarisation functions to the hydrogen atoms (6-311++G**).

It was noted that while the MP2 level of theory did not perform as badly as reported for transition-metal complexes, it had a tendency to overestimate the Sn–P length by up to 9 pm, depending on the pseudopotential used on Sn. Only when using SDB-aug-cc-pVTZ on tin did MP2 give results that were consistent with those determined experimentally. It should also be noted that these calculations took more than four times as long as B3PW91/LanL2DZ to complete on our workstation.

In the months since this work was completed and published,[37] it has become apparent that geometry optimisation calculations can be particularly disadvantaged by the use of large-core pseudopotentials. The recent structural study of indium half-sandwich complexes, described in Chapter 2 and soon to be submitted for publication, showed that the small-core aug-cc-pVQZ-PP basis set for In could sometimes predict the r_{h1} experimental geometry better than LanL2DZ.

For Sn, the pseudopotentials that were tested treat 46 of the 50 electrons as part of the core, with only four electrons in the valence shell. The aug-cc-pVQZ-PP pseudopotential, however, uses a core of ([Ar] + 4*d*) electrons, thus treating 22 electrons explicitly when used for Sn. With the availability of small-core correlation-consistent basis sets up to and including quintuple-ζ quality for all *p*-block elements between Ga and Rn, it now seems wrong to use a large-core ECP for Sn. This is especially true because the availability of supercomputers means that the time taken for two similar calculations, one using a small-core ECP and the other using a large-core ECP, is less than one day (although the calculations with the small-core ECP can take up to twice as long).

In light of these findings, calculations have been run for **1b** at the MP2 level, and using the various DFT methods, with the 6-31G* basis set on H, C and P and aug-cc-pVQZ-PP on Sn. These results are given in Table 2 and show that the use of a small-core basis set on this molecule results in distances that are closer to the experimental values for almost all methods. In particular, the calculation using B3PW91 and aug-cc-pVQZ-PP predicts *r*Sn–P to within 0.5 pm and gives a value for *r*Sn–C_{ring} of 241.8 pm, within the uncertainty of the GED value. Once again MP2 calculations give very reasonable results.

Table 2 Calculated geometries (r_e) at different levels of theory using the 6-31G* basis set on C, P and H atoms and comparing the LanL2DZ, SDD and SDB-aug-cc-pVTZ large-core pseudopotentials and aug-cc-pVQZ-PP (a small-core pseudopotential) on Sn.[a]

	MP2	B3PW91	B3LYP	PBE1PBE	PW91PW91
LanL2DZ					
Sn–C_{ring}	242.2	242.6	243.7	242.0	244.0
Sn–P	266.5	263.3	264.8	262.8	265.5
P–C	181.0	181.2	181.1	180.8	182.0
Ring deformation[b]	10.4	8.4	8.7	8.5	8.5
SDD					
Sn–C_{ring}	247.0	246.3	247.6	245.6	247.8
Sn–P	269.8	266.0	267.6	265.4	268.2
P–C	181.4	181.2	181.8	180.8	182.7
Ring deformation[b]	9.4	7.7	8.0	7.8	7.8
SDB-aug-cc-pVTZ					
Sn–C_{ring}	240.9	243.5	244.7	242.9	244.8
Sn–P	262.4	262.9	264.4	262.3	264.9
P–C	182.3	181.3	181.8	180.7	182.7
Ring deformation[b]	8.2	7.5	7.8	7.5	7.6
aug-cc-pVQZ-PP					
Sn–C_{ring}	242.2	241.8	244.0	240.4	243.1
Sn–P	259.9	261.1	263.3	259.8	262.9
P–C	179.2	180.9	181.7	180.7	182.6
Ring deformation[b]	7.1	7.5	7.5	7.4	7.4

[a] Distances are in pm, angles in degrees. [b] Refers to the angle of deformation from the position where all four ring atoms are coplanar. The C atoms move towards the Sn atom and the P atoms move away from Sn. For definition, see text regarding p_{20}.

Table 3 Comparison of selected ring parameters for GED (r_{h1}), X-ray and theoretical (r_e) methods.[a]

	GED	X-ray[b]	MP2	B3PW91	B3LYP	PBE1PBE
Sn–C_{ring}	241.0(11)	243.2(3)	242.8	242.9	244.0	243.1
Sn–P	261.6(7)	261.1(1)	266.4	262.8	264.3	262.7
P–C_{ring}	180.1(3)	179.8(3)[c]	181.3	180.9	181.5	180.6
P–C_{ring}–P	97.1(8)	97.5(2)	98.9	98.1	98.0	98.0
C_{ring}–P–C_{ring}	82.0(7)	82.1(2)	80.3	81.4	81.5	81.5
Ring deformation[d]	6.4(16)	6.9	9.7	7.7	8.1	7.6

[a] All calculations were performed using the 6-311+G* basis set on all atoms except Sn, where LanL2DZ was used. [b] Taken from Ref. 7. [c] Average value. [d] Refers to the angle of deformation from the position where all four ring atoms are coplanar. The C atoms move towards the Sn atom and the P atoms move away from Sn. For definition, see text regarding p_{20}.

The gas-phase structure has been determined with the help of Dr. Sarah Hinchley using the DYNAMic Interaction of Theory and Experiment (DYNAMITE) method.[38] This new technique has been successfully applied to the gaseous structure determination of sterically crowded molecules[30] and allows ligands to be fully asymmetric during the gas electron diffraction refinement. This is achieved by incorporation of theoretical methods [in this case molecular mechanics (MM)] into the least-squares refinement program.

This theoretical method allows the differences in light-atom positions to be defined accurately, whilst the less-accurate absolute distances, angles and torsions are scaled back to the single refining parameters from the original description. This allows groups to possess C_1 symmetry without the need for many or any extra refining parameters, which would all require restraint in the SARACEN method.[39] If there is steric strain present within a molecule, then assumptions of local symmetry for light-atom groups (*e.g.* methyl groups) affect the heavy-atom positions as they compensate for the inflexibility of the light-atom groups. The application of the DYNAMITE method to [Sn($P_2C_2Bu^t_2$)] allows us to examine whether there are structural consequences of steric strain within this molecule, and also to examine its potential application to other main-group metal half-sandwich complexes.

On the basis of the calculations described above, a geometrical model describing **1b** was written allowing the ring to be non-planar and also permitting two different C_{ring}–P distances. For the initial SARACEN refinement, the geometry was described in terms of 21 independent parameters (see Table 4 and Figure 3 for atom numbering). These comprised five bond lengths, which included the average C–C bond distance (the simple average of the mean C_{tert}–C_{Me} bond and the C_{tert}–C_{ring} distance) and the corresponding difference between these two ($p_{1–2}$). Fixed differences were used to define the separate bond lengths of the three C_{tert}–C_{Me} bonds away from their mean value. A single common C–H length was used throughout (p_3) and the Sn–C_{ring} and C_{ring}–P bond lengths were also included ($p_{4–5}$). Although symmetry implies that two distinct C_{ring}–P distances are possible, all calculations with this symmetry found all C–P distances to be the same and therefore only one C–P distance is actually required. The model also used seven angle parameters. The average C–C–C angle (p_6) is the average of the three values C(3)–C(6)–

C(7/8/9). As C(3)–C(6)–C(8) and C(3)–C(6)–C(9) were calculated to have the same value, the C–C–C difference parameter (p_7) is the difference between this value and that for C(3)–C(6)–C(7). An average value (p_8) of all the C–C–H angles in the molecule is combined with fixed differences to describe each individual angle. Other angles that are used are ∠P–C_{ring}–C_{tert}, ∠Sn–C_{ring}–C_{tert}, ∠P–C_{ring}–P and ∠C_{ring}–P– C_{ring} ($p_{9–12}$). The drop of the butyl groups relative to the PPC half-ring plane is defined as the angle between the mid-point of the two P atoms (PP_{mid}) and the C_{ring} and C_{tert} atoms, ∠PP_{mid}–C(3)–C(6) (p_{13}). The remaining nine parameters are dihedral angles required to place all atoms in position. In all cases, a positive dihedral angle indicates clockwise rotation when viewed along the central bond. The twist of the first methyl group is defined by ∅C(3)–C(6)–C(7)–H(10) (p_{14}), with the other two hydrogen atoms added with the assumption of C_{3v} local symmetry. The twists of the other two methyl groups are defined similarly, using ∅C(3)–C(6)–C(8)–H(13) and ∅C(3)–C(6)–C(9)–H(16) ($p_{15–16}$) respectively. The *tert*-butyl groups were of approximate C_s local symmetry and therefore the positions of the methyl groups were determined relative to the C(7) methyl group using ∅C(8)–C(6)–C(3)–C(7) and ∅C(9)–C(6)–C(3)–C(7) ($p_{17–18}$) to move the respective methyl groups in opposite directions. The twist of the *tert*-butyl group is described by ∅P(2)–C(3)–C(6)–C(7) (p_{19}). Dihedral angle C(3)–P(2)–C(5)–P(4) (p_{20}) is used to define the deformation of the ring from planar to a position where the carbon atoms move towards the tin atom and the phosphorus atoms move away from it. The final dihedral angle that is used in the model is ∅Sn(1)–C(3)–C(6)–C(7) (p_{21}), which describes the twist of the *tert*-butyl group in relation to the position of the Sn atom. By allowing the *tert*-butyl groups to rotate, the molecule can adopt either C_2 or C_{2v} symmetry. A value for p_{21} of 180° corresponds to C_{2v} symmetry.

In total 21 geometric parameters and 14 groups of amplitudes of vibration were refined in the least-squares process. See Table 5 for the list of amplitudes of vibration. Flexible restraints were employed, using the SARACEN method,[39] for 14 parameters and nine amplitudes. For the purposes of SARACEN, the parameter values were set to be those obtained from calculations performed using the B3PW91 level of theory with the

LanL2DZ basis on Sn and 6-311+G* on all other atoms. The uncertainty on each restraint was then based on the change in value of that parameter during a series of graduated calculations. Within experimental error, the molecule was found to have C_{2v} symmetry.

Table 4 Refined (r_{h1}) and calculated (r_e) geometric parameters for [Sn($P_2C_2Bu^t_2$)], **1b**, from the GED study using DYNAMITE. [a,b]

	Parameter	r_{h1}	r_e	Restraint
Independent				
p_1	rC–C average	153.6(2)	152.4	152.4(3)
p_2	rC–C difference	3.0(5)	2.5	2.5(5)
p_3	rC$_{Me}$–H average	110.3(3)	109.5	109.5(5)
p_4	rP–C$_{ring}$	180.1(3)	180.9	—
p_5	rSn–C$_{ring}$	241.0(11)	242.9	—
p_6	∠C$_{ring}$–C$_{tert}$–C$_{Me}$ average	109.6(5)	109.4	—
p_7	∠C$_{ring}$–C$_{tert}$–C$_{Me}$ difference	2.7(5)	2.6	2.6(5)
p_8	∠C$_{tert}$–C$_{Me}$–H average	111.1(8)	111.1	111.1(10)
p_9	∠P–C$_{ring}$–C$_{tert}$	129.4(11)	129.8	129.8(10)
p_{10}	∠Sn–C$_{ring}$–C$_{tert}$	126.8(8)	126.6	126.6(10)
p_{11}	∠C$_{ring}$–P–C$_{ring}$	82.0(7)	81.4	—
p_{12}	∠P–C$_{ring}$–P	97.1(8)	98.1	—
p_{13}	∠PP$_{mid}$–C(3)–C(6)	166.4(16)	167.5	—
p_{14}	ϕH(10)–C(7)–C(6)–C(3)	59.9(17)	60.0	60.0(15)
p_{15}	ϕH(13)–C(8)–C(6)–C(3)	64.0(17)	63.8	63.8(15)
p_{16}	ϕH(16)–C(9)–C(6)–C(3)	56.3(17)	56.6	56.6(15)
p_{17}	ϕC(8)–C(6)–C(3)–C(7)	118.3(16)	119.1	119.1(15)
p_{18}	ϕC(9)–C(6)–C(3)–C(7)	–118.2(16)	–119.1	–119.1(15)
p_{19}	ϕP(2)–C(3)–C(6)–C(7)	–78.0(28)	–79.4	—
p_{20}	Ring deformation	–6.4(16)	–7.7	–7.7(15)
p_{21}	ϕSn(1)–C(3)–C(6)–C(7)	180.3(23)	180.0	180.0(20)
Dependent				
p_{22}	rSn–P	261.6(7)	262.8	—

[a] Refers to B3PW91 calculation with a LanL2DZ basis set on Sn and 6-311+G* on C, P and H atoms. [b] Distances (r) are in pm, angles (∠) and torsions (ϕ) in degrees. See text for parameter definitions and Figure 3 for atom numbering. The figures in parentheses are the estimated standard deviations of the last digits.

Figure 3 Structure of [Sn($P_2C_2Bu^t_2$)], **1b**, with C_2 symmetry showing the atom numbering used in calculations and the GED refinement.

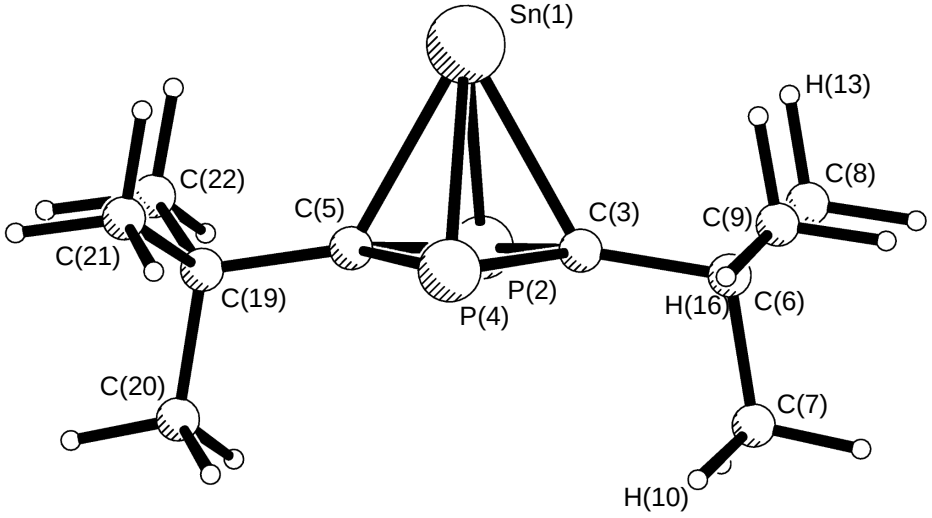

On completion of the SARACEN refinement, the DYNAMITE code[38] was activated within the ed@ed program,[30] upon which the above parameter definitions relating to *r*C–H, ∠C–C–H and the methyl torsions changed. For example, the C–H bond length (p_3) no longer represented the actual bond length for all the C–H distances, but rather the mean of them, while differences between them were updated continually in the course of the refinement.

The success of the final DYNAMITE refinement, for which R_G = 0.049 (R_D = 0.049), can be assessed on the basis of the radial-distribution and experimental – theoretical difference curves (Figure 4) and the molecular-scattering intensity curves (Figure 5). The least-squares correlation matrix is given in Table 6 and coordinates for the GED structure are given in Table 3.1 in the Electronic Appendix (EA).

Obtaining a reliable GED structure determination, as judged by the goodness of fit to the data, makes this an ideal case for calibrating the various calculations that were performed. The calculated geometry of [Sn($P_2C_2Bu^t_2$)] at the B3PW91 level of theory with the LanL2DZ pseudopotential on Sn and the 6-311+G* basis set on all other atoms was close to that determined from the GED experiment. The parameters obtained by using the MP2 level of theory with the SDB-aug-cc-pVTZ basis on the tin atom were

also close to the experimental values, but the geometry optimisation took significantly longer to complete. Subsequent to the determination of the GED structure of **1b** it was decided to test the use of a small-core ECP (aug-cc-pVQZ-PP) on Sn. This resulted in another improvement in the accuracy of the calculations, although in most cases the improvement was quite small. The force field that is required to provide vibrational quantities for use in the GED refinement is much more readily calculated using DFT methods than with MP2. For these reasons, B3PW91/LanL2DZ was used as the method of calculating the geometry of **1b** for use in the refinement.

Table 5 Selected interatomic distances (r_a/pm) and amplitudes of vibration (u_{h1}/pm) for the restrained GED structure of [Sn($P_2C_2Bu^t_2$)], **1b**.[a]

	Atom pair	r_a/pm	u_{h1}/pm[b]	Restraint
$u_{1–9}$	C–H	110.2(3)	7.1(3)	7.7(8)
u_{10}	C(3)–C(6)	152.1(4)	4.0(6)	—
$u_{11–12}$	C(6)–C(8/9)	154.8(2)	4.1(tied to u_{10})	—
u_{13}	C(6)–C(7)	155.6(2)	4.1(tied to u_{10})	—
$u_{14–15}$	P(2)–C(3/5)	180.2(3)	5.2(4)	—
u_{16}	Sn(1)–C(3)	240.7(11)	10.5(11)	10.1(10)
u_{17}	C(3)···C(7)	249.1(10)	7.1(8)	8.0(8)
$u_{18–19}$	C(7)···C(8)	250.6(23)	7.1(tied tou_{17})	—
$u_{20–21}$	C(3)···C(9)	252.6(8)	6.8(tied tou_{17})	—
u_{22}	Sn(1)–P(2)	261.4(7)	7.5(8)	7.7(8)
u_{23}	P(2)···P(4)	269.8(17)	5.1(6)	5.6(6)
u_{24}	P(2)···C(6)	300.0(14)	9.0(7)	8.2(8)
u_{25}	P(2)···C(19)	304.7(16)	9.0(tied tou_{24})	—
u_{26}	P(2)···C(8)	336.7(38)	18.7(18)	19.1(19)
u_{27}	P(2)···C(22)	341.8(39)	18.7(tied tou_{26})	—
u_{28}	Sn(1)···C(6)	352.7(11)	12.1(12)	12.4(12)
u_{29}	P(2)···C(7)	362.0(28)	18.0(25)	—
u_{30}	P(2)···C(20)	369.3(40)	18.0(tied tou_{29})	—
$u_{31–32}$	Sn(1)···C(8/9)	393.5(32)	22.7(17)	—
u_{33}	P(2)···C(9)	424.1(12)	9.8(9)	—
u_{34}	P(2)···C(21)	426.6(14)	9.9(tied tou_{33})	—
u_{35}	Sn(1)···C(7)	480.7(11)	13.8(12)	12.0(12)

[a] Estimated standard deviations, as obtained in the least squares refinement, are given in parentheses. [b] Amplitudes not refined were fixed at the values obtained using the force field calculated at B3PW91/LanL2DZ on Sn and 6-31G* on P, C, and H. Other amplitudes were also included and fixed at this level but are not shown here.

Figure 4 Experimental and difference (experimental – theoretical) radial-distribution curves for [Sn($P_2C_2Bu^t_2$)], **1b**. Before Fourier inversion, the data were multiplied by $s.\exp(-0.00002s^2)/(Z_{Sn} - f_{Sn})(Z_C - f_C)$.

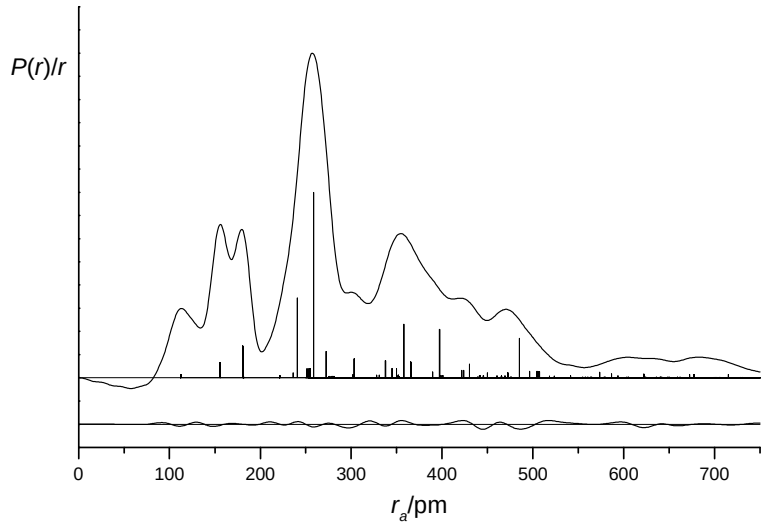

Figure 5 Molecular-scattering intensity and final weighted difference curves for [Sn($P_2C_2Bu^t_2$)], **1b**.

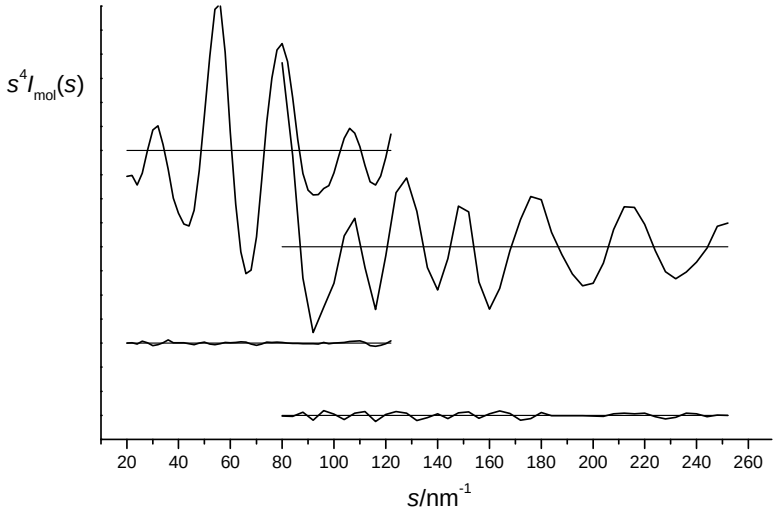

Table 6 Least-squares correlation matrix (×100) for [Sn($P_2C_2Bu^t_2$)], **1b**.[a]

	p_2	p_{10}	p_{21}	u_6	k_1	k_2
p_1	–50				–58	
p_5		–52				
p_{12}				–75		
p_{18}			81			
u_1						62

[a] Only elements with absolute values ≥ 50% are shown; k_1 and k_2 are scale factors.

The R_G values from the SARACEN and DYNAMITE refinements were identical (0.049) and examination of the parameter values from each refinement revealed that those from one were within the ESD range of the other. From this we can conclude that no improvement to the structure or refinement has been gained by using the DYNAMITE method in this particular case, but it is no worse either. As the *tert*-butyl groups are not in close contact with each other in this molecule, it is perhaps not surprising that there is no steric crowding within the groups.

It is important to note that the DYNAMITE and SARACEN refinements return essentially the same parameter and amplitude values. It is very positive to note that if there is no steric crowding in a molecule, activation of the DYNAMITE method will indicate this. Therefore, it is unlikely that a structure will be improved artificially by implementing this method. Also, any improvement in the goodness of fit and any change in parameter values for a refinement can be attributed to better modelling of the light-atom positions via the DYNAMITE method.

In an attempt to understand better the steric properties and structure of **1b**, calculations were performed on various related molecules. All calculations were performed at the B3PW91 level of theory with the 6-31G* basis set on all atoms except for Sn, where LanL2DZ was used where appropriate. Table 7 lists selected parameters for all structures, including **1b,** at this level of computation and Table 3.2 (EA) contains coordinates for **1b**. The geometry of [Sn($P_2C_2H_2$)], **2**, principal geometric parameters for which are included in Table 7 and coordinates in Table 3.3 (EA), differed very little from the *tert*-butyl analogue. With a similar ring deformation and the hydrogen atoms bending away from Sn, the Sn–ring bond lengths were within about 1 pm of those

obtained for **1b**. This suggests that the non-planarity of the ring is caused by the tin atom complexing to the ring atoms and is not a steric effect caused by the *tert*-butyl groups.

Table 7 Comparison of calculated ring parameters for various derivatives of [Sn($P_2C_2Bu^t_2$)], **1b**.[a,b,c]

Parameter	**1b**	**2**	**3**	**4**[d]	**5**
*r*P/C–C	181.2	180.2	169.0 / 192.4	146.5	182.0
*r*M–P/C[e]	263.3	263.7	—	235.1	231.6
*r*M–C	242.6	241.3	—	235.3	221.4
∠C–P/C–C	81.4	80.2	80.7	90.8	81.0
∠P/C–C–P/C	98.0	99.1	99.3	89.2	99.0
ϕX–C–P/C–C	171.4	176.3	180.0	161.4	175.3
ϕC–P/C–C–P/C	8.4	8.9	0.0	0.5	1.0

[a] Complex **2** is [Sn($P_2C_2H_2$)], **3** is [($P_2C_2Bu^t_2$)], **4** is [Sn($C_4Bu^t_2H_2$)] and **5** is [$Li_2P_2C_2Bu^t_2$]. [b] Calculations performed using B3PW91/LanL2DZ/6-31G*. [c] Distances (*r*) are in pm, angles (∠) and torsions (ϕ) in degrees. [d] In this instance atom P has been replaced by a C–H fragment. [e] M refers to Sn in **1b**, **2** and **4** and to Li in **5**. [f] X refers to the *tert*-C atom in **1b**, **3**, **4** and **5** and the H atom in **2**.

The calculated geometry (see Table 7 for parameters; coordinates given in Table 3.4, EA) for neutral diphosphabutadiene ligand, [$P_2C_2Bu^t_2$], **3**, exhibited two separate P–C_{ring} distances (169.0 and 192.4 pm), unlike its tin complex, where only one distance was observed in the calculations and GED refinement. This is as would be expected for a non-aromatic molecule. Notably, this fragment was calculated to be planar, suggesting that the non-planarity of **1b** is caused simply by the Sn–P bond lengths requiring to be longer than Sn–C.

To investigate this further, an analogue with a purely organic ring was explored. For [Sn($C_4Bu^t_2H_2$)], **4**, the cyclobutadiene ring was very nearly planar and again all the bonds within the ring were found to be equal in length. (See Table 3.5, EA, for coordinates and Table 7 for principal parameters.) The Sn–C bonds were calculated to be shorter than for the diphospha derivative, due to the smaller ring involved.

As mentioned in the Introduction, in formal terms complex **1b** should be considered to involve the diphosphabutadiene dianion, $[P_2C_2Bu^t_2]^{2-}$. The dianion $[C_4H_4]^{2-}$ is known to be unstable, existing as a resonance state with a short lifetime, and therefore standard

computational methods cannot be used to model this.[11] The neutral ligand $[Li_2C_4H_4]$ is used instead to express the aromaticity of the cyclobutadiene ring and here we have also calculated the structure of $[Li_2P_2C_2Bu^t_2]$, **5**. The molecule contains an essentially planar ring with all four P–C bonds of equal length (Table 7), suggesting that this ring system is aromatic. (Coordinates for the calculated geometry are given in Table 3.6, EA.) As with $[Li_2C_4H_4]$, this should be thought of as a 2π-aromatic system, because, although there are six π electrons, four of them occupy non-bonding orbitals.

The dilithium salt of the related 1,3-diphosphacyclobutadiene dianion, $[P_2C_2(SiMe_3)_2]^{2-}$, has recently been synthesised and characterised by X-ray crystallography.[10] That study found the P–C bonds to be equivalent (within experimental error) and quoted the ring angles as 83.8(1)° for ∠P–C–P and 96.2(1)° for ∠C–P–C. When these values are compared with those theoretical values obtained for **5** it can be seen that ∠P–C–P is approximately 3° wider in the trimethylsilyl analogue, while ∠C–P–C was narrower by the same amount. For **5** the distance between the lithium atom and the centre of the ring is calculated to be 186.0 pm, considerably shorter than the 206.6(2) pm distance observed for $[Li_2P_2C_2(SiMe_3)_2]$.

The Sn–C bond lengths in other compounds were examined for comparison with the half-sandwich complex, **1b**. In the sandwich complex stannocene, $[Sn(C_5H_5)_2]$, where the cyclopentadienyl groups are not parallel, the bond distance in the gas-phase structure was 270.6(24) pm,[41] and in the X-ray crystal structure they ranged from 256(2) to 285(3) pm,[42] compared to 241.0(11) pm in the present study. In a theoretical study of stannocene, B3PW91 calculations gave an Sn–C bond length of 271.8 pm.[43] It is perhaps not surprising that the Sn–C bonds are longer in stannocene, where the Sn is η^5-coordinated to each ring, as opposed to η^4 in **1b**. In $[Sn(CH_3)_4]$, Sn is bonded to four carbon atoms through simple σ bonds, but in this instance the Sn–C bond length in the gas phase is 214.4(3) pm.[44]

Attempts were made to optimise a geometry for **1b** in which the Sn was less than η^4-coordinated to the ring. No minima were found to correspond to such structures and it was concluded that Sn must interact with each of the ring atoms. This coordination was

also found in the crystal structure,[7] where no parameters were found to be significantly different from those obtained from the GED study.

It might be expected that a compound such as this, with a metal atom exposed on one face of a ring, would exhibit significant intermolecular interactions. In fact any interactions are so small that the crystal and gas-phase structures are effectively indistinguishable. This similarity makes this an ideal molecule for the assessment of computational methods for main-group complexes of this type.

3.4 References

1. K. B. Dillon, F. Mathey and J. F. Nixon, *Phosphorus: The Carbon Copy: From Organophosphorus to Phospha-organic Chemistry*, John Wiley and Sons, Chichester, 1998, and references therein.
2. P. B. Hitchcock, M. J. Maah and J. F. Nixon, *J. Chem. Soc., Chem. Commun.*, 1986, 737.
3. P. Binger, R. Milczarek, R. Mynott, M. Regitz and W. Rösch, *Angew. Chem., Int. Ed. Engl.*, 1986, **25**, 644.
4. F. G. N. Cloke, K. R. Flower, P. B. Hitchcock and J. F. Nixon, *J. Chem. Soc., Chem. Commun.*, 1994, 489.
5. T. Wettling, G. Wolmerhäuser, P. Binger and M. Regitz, *J. Chem. Soc., Chem. Commun.*, 1990, 1541.
6. A. G. Avent, F. G. N. Cloke, K. R. Flower, P. B. Hitchcock, J. F. Nixon and D. M. Vickers, *Angew. Chem., Int. Ed. Engl.*, 1994, **33**, 2330; F. G. N. Cloke, P. B. Hitchcock, J. F. Nixon and D. M. Vickers, *C. R. Chim.*, 2004, **7**, 931.
7. M. D. Francis and P. B. Hitchcock, *Chem. Commun.*, 2002, 86.
8. M. D. Francis and P. B. Hitchcock, *Organometallics*, 2003, **22**, 2891.
9. G. Anderson, J. C. Green and M. D. Francis, *Organometallics*, 2003, **22**, 2897.
10. M. Sebastian, M. Nieger, D. Szieberth, L. Nyulászi and E. Niecke, *Angew. Chem., Int. Ed. Engl.*, 2004, **43**, 637.
11. Y. Jung, T. Heine, P. v. R. Schleyer and M. Head-Gordon, *J. Am. Chem. Soc.*, 2004, **126**, 3132.
12. A. Sekiguchi, T. Matsuo and H. Watanabe, *J. Am. Chem. Soc.*, 2000, **122**, 5652; K. Ishii, N. Kobayashi, T. Matsuo, M. Tanaka and A. Sekiguchi, *J. Am. Chem. Soc.*, 2001, **123**, 5356; A. Sekiguchi, T. Matsuo and M. Tanaka, *Organometallics*, 2002, **21**, 1072.
13. J. M. Lynam, M. C. Copsey, M. Green, J. C. Jeffery, J. E. McGrady, C. A. Russell, J. M. Slattery and A. C. Swain, *Angew. Chem., Int. Ed. Engl.*, 2003, **42**, 2778; D. A.

Pantazis, J. E. McGrady, J. M. Lynam, C. A. Russell and M. Green, *Dalton Trans.*, 2004, 2080.

14. Parallel Quantum Solutions, Fayetteville, AR, USA.
15. M. J. Frisch, G. W. Trucks, H. B. Schlegel, G. E. Scuseria, M. A. Robb, J. R. Cheeseman, V. G. Zakrzewski, J. A. Montgomery, Jr., R. E. Stratmann, J. C. Burant, S. Dapprich, J. M. Millam, A. D. Daniels, K. N. Kudin, M. C. Strain, O. Farkas, J. Tomasi, V. Barone, M. Cossi, R. Cammi, B. Mennucci, C. Pomelli, C. Adamo, S. Clifford, J. Ochterski, G. A. Petersson, P. Y. Ayala, Q. Cui, K. Morokuma, D. K. Malick, A. D. Rabuck, K. Raghavachari, J. B. Foresman, J. Cioslowski, J. V. Ortiz, A. G. Baboul, B. B. Stefanov, G. Liu, A. Liashenko, P. Piskorz, I. Komaromi, R. Gomperts, R. L. Martin, D. J. Fox, T. Keith, M. A. Al-Laham, C. Y. Peng, A. Nanayakkara, C. Gonzalez, M. Challacombe, P. M. W. Gill, B. Johnson, W. Chen, M. W. Wong, J. L. Andres, C. Gonzalez, M. Head-Gordon, E. S. Replogle and J. A. Pople, *Gaussian 98, Revision A.7*, Gaussian, Inc., Pittsburgh, PA, 1998.
16. M. J. Frisch, G. W. Trucks, H. B. Schlegel, G. E. Scuseria, M. A. Robb, J. R. Cheeseman, J. A. Montgomery, Jr., T. Vreven, K. N. Kudin, J. C. Burant, J. M. Millam, S. S. Iyengar, J. Tomasi, V. Barone, B. Mennucci, M. Cossi, G. Scalmani, N. Rega, G. A. Petersson, H. Nakatsuji, M. Hada, M. Ehara, K. Toyota, R. Fukuda, J. Hasegawa, M. Ishida, T. Nakajima, Y. Honda, O. Kitao, H. Nakai, M. Klene, X. Li, J. E. Knox, H. P. Hratchian, J. B. Cross, C. Adamo, J. Jaramillo, R. Gomperts, R. E. Stratmann, O. Yazyev, A. J. Austin, R. Cammi, C. Pomelli, J. W. Ochterski, P. Y. Ayala, K. Morokuma, G. A. Voth, P. Salvador, J. J. Dannenberg, V. G. Zakrzewski, S. Dapprich, A. D. Daniels, M. C. Strain, O. Farkas, D. K. Malick, A. D. Rabuck, K. Raghavachari, J. B. Foresman, J. V. Ortiz, Q. Cui, A. G. Baboul, S. Clifford, J. Cioslowski, B. B. Stefanov, G. Liu, A. Liashenko, P. Piskorz, I. Komaromi, R. L. Martin, D. J. Fox, T. Keith, M. A. Al-Laham, C. Y. Peng, A. Nanayakkara, M. Challacombe, P. M. W. Gill, B. Johnson, W. Chen, M. W. Wong, C. Gonzalez and J. A. Pople, *Gaussian 03, Revision C.01*, Gaussian, Inc., Wallingford, CT, 2004.
17. J. S. Binkley, J. A. Pople, W. J. Hehre, *J. Am. Chem. Soc.*, 1980, **102**, 939; M. S. Gordon, J. S. Binkley, J. A. Pople, W. J. Pietro and W. J. Hehre, *J. Am. Chem. Soc.*,

1982, **104**, 2797; W. J. Pietro, M. M. Francl, W. J. Hehre, D. J. DeFrees, J. A. Pople and J. S. Binkley, *J. Am. Chem. Soc.*, 1982, **104**, 5039.

18. W. J. Hehre, R. Ditchfield and J. A. Pople, *J. Chem. Phys.*, 1972, **56**, 2257; P. C. Hariharan and J. A. Pople, *Theor. Chim. Acta*, 1973, **28**, 213; M. S. Gordon, *Chem. Phys. Lett.*, 1980, **76**, 163.
19. P. J. Hay and W. R. Wadt, *J. Chem. Phys.*, 1985, **82**, 270; W. R. Wadt and P. J. Hay, *J. Chem. Phys.*, 1985, **82**, 284; P. J. Hay and W. R. Wadt, *J. Chem. Phys.*, 1985, **82**, 299.
20. J. P. Perdew, J. A. Chevary, S. H. Vosko, K. A. Jackson, M. R. Pederson, D. J. Singh and C. Fiolhais, *Phys. Rev. B: Condens. Matter*, 1992, **46**, 6671; J. P. Perdew, J. A. Chevary, S. H. Vosko, K. A. Jackson, M. R. Pederson, D. J. Singh and C. Fiolhais, *Phys. Rev. B: Condens. Matter*, 1993, **48**, 4978; J. P. Perdew, K. Burke and W. Yang, *Phys. Rev. B: Condens. Matter*, 1996, **54**, 16533.
21. J. M. L. Martin and A. Sundermann, *J. Chem. Phys.*, 2001, **114**, 3408.
22. A. D. Becke, *J. Chem. Phys.*, 1993, **98**, 5648.
23. J. P. Perdew and Y. Wang, *Phys. Rev. B: Condens. Matter*, 1992, **45**, 13244.
24. C. Lee, W. Yang and R. G. Parr, *Phys. Rev. B: Condens. Matter*, 1992, **37**, 785; B. Miehlich, A. Savin, H. Stoll and H. Preuss, *Chem. Phys. Lett.*, 1989, **157**, 200.
25. J. P. Perdew, K. Burke and M. Ernzerhof, *Phys. Rev. Lett.*, 1996, **77**, 3865; J. P. Perdew, K. Burke and M. Ernzerhof, *Phys. Rev. Lett.*, 1997, **78**, 1396.
26. C. Møller and M. S. Plesset, *Phys. Rev.*, 1934, **46**, 618.
27. V. A. Sipachev, *J. Mol. Struct.* (*THEOCHEM*), 1985, **121**, 143; V. A. Sipachev, *J. Mol. Struct.*, 2001, **567**, 67.
28. C. M. Huntley, G. S. Laurenson and D. W. H. Rankin, *J. Chem. Soc., Dalton Trans.*, 1980, 954.
29. H. Fleischer, D. A. Wann, S. L. Hinchley, K. B. Borisenko, J. R. Lewis, R. J. Mawhorter, H. E. Robertson and D. W. H. Rankin, *Dalton Trans.*, 2005, 3221.
30. S. L. Hinchley, H. E. Robertson, K. B. Borisenko, A. R. Turner, B. F. Johnston, D. W. H. Rankin, M. Ahmadian, J. N. Jones and A. H. Cowley, *Dalton Trans.*, 2004, 2469.

31. A. W. Ross, M. Fink and R. Hilderbrandt, *International Tables for Crystallography*, ed. A. J. C. Wilson, Kluwer Academic Publishers, Dordrecht, Netherlands, 1992, vol. C, p. 245.
32. F. G. N. Cloke, J. C. Green, J. R. Hanks, J. F. Nixon and J. L. Suter, *J. Chem. Soc., Dalton Trans.*, 2000, 3534.
33. R. Bartsch, F. G. N. Cloke, J. C. Green, R. M. Matos, J. F. Nixon, R. J. Suffolk, J. L. Suter and D. J. Wilson, *J. Chem. Soc., Dalton Trans.*, 2001, 1013.
34. G. K. B. Clentsmith, F.G. N. Cloke, J. C. Green, J. Hanks, P. B. Hitchcock and J. F. Nixon, *Angew. Chem., Int. Ed. Engl.*, 2003, **42**, 1038.
35. M. Al-Ktaifani, J. C. Green, P. B. Hitchcock, and J. F. Nixon, *J. Chem. Soc., Dalton Trans.*, 2001, 1726.
36. G. K. B. Clentsmith, F. G. N. Cloke, M. D. Francis, J. C. Green, P. B. Hitchcock, J. F. Nixon, J. L. Suter and D. M. Vickers, *J. Chem. Soc., Dalton Trans.*, 2000, 1715.
37. D. A. Wann, S. L. Hinchley, K. B. Borisenko, H. E. Robertson, M. D. Francis, J. F. Nixon and D. W. H. Rankin, *Dalton Trans.*, 2005, 1972.
38. S. L. Hinchley, M. F. Haddow and D. W. H. Rankin, *Dalton Trans.*, 2004, 384.
39. A. J. Blake, P. T. Brain, H. McNab, J. Miller, C. A. Morrison, S. Parsons, D. W. H. Rankin, H. E. Robertson and B. A. Smart, *J. Phys. Chem.*, 1996, **100**, 12280; P. T. Brain, C. A. Morrison, S. Parsons and D. W. H. Rankin, *J. Chem. Soc., Dalton Trans.*, 1996, 4589; N. W. Mitzel and D. W. H. Rankin, *Dalton Trans.*, 2003, 3650.
40. G. K. B. Clentsmith, F. G. N. Cloke, M. D. Francis, J. C. Green, P. B. Hitchcock, J. F. Nixon, J. L. Suter and D. M. Vickers, *J. Chem. Soc., Dalton Trans.*, 2000, 1715.
41. A. Almenningen, A. Haaland and T. Motzfeldt, *J. Organomet. Chem.*, 1967, **7**, 97.
42. J. L. Atwood, W. E. Hunter, A. H. Cowley, R. A. Jones, C. A. Stewart, *J. Chem. Soc., Chem. Commun.*, 1981, 925.
43. J. D. Smith and T. P. Hanusa, *Organometallics*, 2001, **20**, 3056.
44. M. Nagashima, H. Fujii and M. Kimura, *Bull. Chem. Soc. Jpn.*, 1973, **46**, 3708.

Chapter Four

The molecular structures of the 1,6-disubstituted triptycenes $Sb_2(C_6F_4)_3$ and $Bi_2(C_6F_4)_3$ using gas-phase electron diffraction and *ab initio* and DFT calculations

4.1 Introduction

In stark contrast to the organic cage molecule adamantane, where chemists have succeeded in substituting carbon atoms for a wide variety of non-transition-metal elements, the three-dimensional triptycene molecule had until the 1970s proved far more difficult to substitute. Theoretically, it should be feasible for any element that is capable of approximately tetrahedral coordination geometry to be substituted for the bridgehead carbon atoms. In practise, however, although 1,6-diazatriptycene was first synthesised in 1875, it remained the only known heteroatomic analogue of triptycene for almost 100 years.[1] This owes much to the fact that the nitrogen-substituted molecule is the only substituted triptycene that can be built in a stepwise manner from stable intermediates.[2] Only with the advent of specialist direct synthesis techniques did it become possible to extend the series of analogues to other elements in Group 15.

Fluorinated 1,6-disubstituted triptycenes have many potential applications. $Bi_2(C_6F_4)_3$ is used in the preparation of non-cluster type bismuth compounds for use as imaging contrast agents in a variety of medical imaging techniques and is also listed as having uses in the treatment of gastrointestinal disorders, such as ulcers.[3] $Sb_2(C_6F_4)_3$ has very recently been trialled as a dopant for a perfluorinated graded index polymer fibre (PFGI-POF).[4] In this application the triptycene acts to raise the refractive index of the optical fibre. Although some other perfluorinated molecules proved to be more effective in that role than $Sb_2(C_6F_4)_3$, it demonstrates the industrial demand for novel fluorinated compounds.

Previous diffraction studies on Group 15 1,6-disubstituted fluorinated triptycenes are limited to an X-ray crystallographic study[5] of $As_2(C_6F_4)_3$. This work showed the absence of expected high symmetry, with the substance crystallising in the monoclinic *Cc* space group. Although the aromatic rings are essentially planar, the dihedral angles between the ring planes were found to be 111(2), 125(2) and 125(2)°. Similar deviations from 120° were previously noted in some hydrogen-substituted triptycenes, where the lack of high symmetry was attributed to crystal forces.[6] It has also been noted that although

triptycenes are depicted as totally rigid systems, it may be the case that they behave as rigid aromatic rings that are connected flexibly *via* the bridgehead atoms.[7]

These studies concerning the structures of $Sb_2(C_6F_4)_3$ and $Bi_2(C_6F_4)_3$ as determined by gas-phase electron diffraction and theoretical methods should add to the structural understanding of the Group 15 1,6-disubstituted triptycenes.

4.2 Experimental

4.2.1 Preparation of $Sb_2(C_6F_4)_3$ and $Bi_2(C_6F_4)_3$

Samples of $Sb_2(C_6F_4)_3$ and $Bi_2(C_6F_4)_3$ were prepared by Prof. Alan Massey and co-workers by direct synthesis in a heated, sealed tube where, in each case, the appropriate Group 15 element was reacted with 1,2-$C_6F_4I_2$.[8]

4.2.2 *Ab initio* and DFT studies

All calculations reported in this work were performed using the Gaussian 03 suite of programs,[9] with the resources of the EPSRC National Service for Computational Chemistry Software. Some of the calculations were carried out on a cluster of six HP ES40 computers, where each Alphaserver ES40 machine has four 833 MHz EV68 CPUs and 8 GB of memory connected with a high-speed, low-latency QSW switch forming an Alphaserver SC. Other calculations were performed using a cluster of 22 Linux Opteron nodes. Each Opteron server has twin 2.4 GHz Opteron 250 CPUs and 8 GB of memory connected with a high-speed, low-latency Myrinet network.

Starting coordinates for geometry optimisation calculations for $Sb_2(C_6F_4)_3$ and $Bi_2(C_6F_4)_3$ were created using the GaussView 3.0 package, which allows the symmetry to be constrained to D_{3h}.

For $Sb_2(C_6F_4)_3$, initial low-level calculations were undertaken at the Hartree-Fock level of theory using Pople's 3-21G* basis set[10] (RHF/3-21G*). A geometry optimisation was carried out as well as a frequency calculation to ensure that the calculated structure represented a minimum on the potential energy surface. These calculations were repeated using the 6-31G* basis set[11] on the light atoms (C and F) and, as 6-31G* has

not been coded for Sb, the LanL2DZ basis set[12] on the heavy atoms. In the case of $Bi_2(C_6F_4)_3$ not even the 3-21G* basis set is optimised for Bi and therefore the LanL2DZ basis set was used from the outset with, once again, the 3-21G* and then the 6-31G* basis set on the light atoms. In later calculations the size of the basis set on the light atoms was increased to 6-311G* and further to include a diffuse function on the C and F atoms.[13]

The choice of basis set for use on the heavy atoms is based on their ability to offer a pseudopotential (PP) or effective core potential (ECP), which reduces the number of electrons that are considered explicitly and speeds up the calculations. By doing this, however, there is a concern that the number of electrons considered to be valence electrons is too few to predict the molecular structure accurately. To this end another basis set was tested on these systems. New correlation-consistent basis sets have been developed specifically for the post-*d* block Group 13–15 elements. The basis set used (aug-cc-pVQZ-PP) is a quadruple-ζ one, augmented by diffuse and polarisation functions.[14] It employs a small-core pseudopotential,[15] which for Sb includes 28 core electrons ([Ar] + 4*d*) while the LanL2DZ large core includes 46 electrons in the core ([Kr] + 5*d*). For Bi, the aug-cc-pVQZ-PP ECP includes 60 electrons in the core ([Kr] + 4*d*3*f*) and the LanL2DZ ECP includes 78 electrons ([Xe] + 5*d*4*f*).

Density functional theory (DFT) calculations are known to be very good for predicting the geometries of transition-metal compounds. In Chapters 2 and 3 it was reported that DFT methods can also produce reliable results for use with molecules containing a heavy *p*-block element (Sn).[16] In this chapter several DFT methods have again been tested to compare their results with those obtained experimentally.

Becke's three-parameter hybrid functional[17] was used with the non-local PW91 correlation functional[18] (B3PW91) that performed well for the Sn compound. It was also paired with the LYP functional[19] (B3LYP) and that in turn was used in conjunction with Becke's 1988 exchange functional[20] (BLYP). Calculations were also performed at the MP2 level of theory;[21] all MP2 calculations were frozen core.

Analytical force fields were calculated for both $Sb_2(C_6F_4)_3$ and $Bi_2(C_6F_4)_3$ (RHF/aug-cc-pVQZ-PP/6-31G*). These were used by the SHRINK program[22] to calculate accurate

estimates of the amplitudes of vibration (u_{h1}), some of which were subsequently refined during the electron diffraction refinement, and also to calculate curvilinear corrections (k_{h1}), which are used to counteract the effects of shrinkage that are associated with the GED experiment.[23]

4.2.3 Gas-phase electron diffraction

Data were collected for $Sb_2(C_6F_4)_3$ and $Bi_2(C_6F_4)_3$ using the Edinburgh gas-phase electron diffraction apparatus.[24] An electron wavelength of approximately 6.0 pm was achieved using an accelerating voltage of around 40 kV. Scattering patterns were recorded on Kodak Electron Image films at three nozzle-to-film distances for $Sb_2(C_6F_4)_3$ (94.55, 199.49 and 257.01 mm) and two for $Bi_2(C_6F_4)_3$ (199.49 and 256.88 mm). For $Bi_2(C_6F_4)_3$ it proved impossible to collect data at the shorter distance, at which a higher vapour pressure is generally required. In the case of $Sb_2(C_6F_4)_3$ scattering intensity data were recorded with sample and nozzle temperatures held at 490 and 520 K, respectively, for the shortest distance, 494 and 507 K for the intermediate distance and 483 and 494 K for the longest distance. For $Bi_2(C_6F_4)_3$, the sample and nozzle temperatures were 499 and 516 K, respectively, for the shorter distance and 481 and 514 K for the longer distance.

The GED experiment made use of a new reservoir developed in Edinburgh. The reservoir works on a reverse condenser design, with warm air heating the ampoule rather than a heating tape. This design ensures even heating of the sample and eliminates the possibility of hot or cold spots.

The weighting points for the off-diagonal weight matrices, correlation parameters and scale factors for all camera distances for $Sb_2(C_6F_4)_3$ and $Bi_2(C_6F_4)_3$ are given in Table 1. Also included are the exact electron wavelengths as determined from the scattering patterns for benzene, which were recorded immediately after the patterns for the sample compounds. The scattering intensities were measured using an Epson Expression 1600 Pro flatbed scanner and converted to mean optical densities as a function of the scattering variable, *s*, using an established program.[25] The data-reduction and the least-

squares refinement processes were carried out using the ed@ed program[26] employing the scattering factors of Ross *et al*.[27]

Table 1 Nozzle-to-film distances (mm), weighting functions (nm^{-1}), scale factors, correlation parameters and electron wavelengths (pm) used in the electron diffraction studies of $Sb_2(C_6F_4)_3$ and $Bi_2(C_6F_4)_3$.

	$Sb_2(C_6F_4)_3$			$Bi_2(C_6F_4)_3$	
Nozzle-to-film distance[a]	94.55	199.49	257.01	199.49	256.88
Δs	2	1	1	1	1
s_{min}	170	100	20	52	20
sw_1	190	120	40	65	40
sw_2	258	176	129	181	60
s_{max}	300	205	150	200	74
Scale factor[b]	0.681(11)	0.793(7)	0.758(5)	0.666(8)	0.560(6)
Correlation parameter	–0.413	0.447	0.482	0.315	–0.153
Electron wavelength	6.013	6.013	6.013	6.013	6.013

[a] Determined by reference to the scattering pattern of benzene. [b] Values in parentheses are the estimated standard deviations.

4.3 Results and Discussion

4.3.1 GED study

On the basis of the calculations described previously, a D_{3h}-symmetric model was written to describe the coordinates of $Sb_2(C_6F_4)_3$ for use in the GED refinement. An identical model (except that Bi was substituted for Sb) was used in the refinement of the data collected for $Bi_2(C_6F_4)_3$.

In total 11 independent parameters were required to describe the geometry of $Z_2(C_6F_4)_3$ (Z = Sb, Bi). The molecule has four distinct C–C distances [*r*C(6)–C(1), *r*C(1)–C(2), *r*C(2)–C(3) and *r*C(3)–C(4); see Table 2 and Figure 1 for atom numbering] and these were described using the average of the four (p_1) and three difference parameters ($p_{2–4}$), which were defined as follows:

p_2 = *r*C(6)–C(1) – ({[*r*C(1)–C(2)] + [*r*C(2)–C(3)] + [*r*C(3)–C(4)]}/3),

p_3 = *r*C(1)–C(2) – ({[*r*C(2)–C(3)] + [*r*C(3)–C(4)]}/2), and

p_4 = {[*r*C(2)–C(3)] + [*r*C(3)–C(4)]}/2.

Table 2 Experimental (r_{h1}) and calculated (r_e) geometric parameters for $Z_2(C_6F_4)_3$ (Z = Sb, Bi).[a,b]

	Parameter	$Sb_2(C_6F_4)_3$			$Bi_2(C_6F_4)_3$		
		r_{h1}	r_e	Restraint	r_{h1}	r_e	Restraint
Independent							
p_1	*r*C–C average	139.2(1)	139.8	—	139.3(2)	139.7	—
p_2	*r*C–C difference 1	2.3(4)	1.3	1.3(5)	0.8(5)	0.8	0.8(5)
p_3	*r*C–C difference 2	–0.4(2)	–0.5	–0.5(2)	–0.9(3)	–0.4	–0.4(3)
p_4	*r*C–C difference 3	0.4(2)	0.1	0.1(2)	0.2(2)	0.0	0.0(2)
p_5	*r*C–F average	133.8(2)	133.8	—	133.0(3)	134.0	—
p_6	*r*C–F difference	2.1(4)	1.4	1.4(5)	1.8(5)	1.5	1.8(5)
p_7	*r*Z–C	214.4(1)	213.4	—	222.9(3)	222.9	—
p_8	∠C(2)–C(3)–F	120.5(4)	120.9	—	120.5(5)	121.0	—
p_9	∠C(1)–C(2)–F	121.8(3)	120.6	—	121.9(4)	120.7	—
p_{10}	∠C(6)–C(1)–C(2)	118.7(1)	119.1	—	120.0(2)	119.2	—
p_{11}	∠C(6)–C(1)–Z	124.0(1)	124.1	—	124.8(1)	125.0	—
Dependent							
p_{12}	*r*C(6)–C(1)	140.9(4)	140.8	—	139.9(5)	140.3	—
p_{13}	*r*C(1)–C(2)	138.3(2)	139.2	—	138.5(3)	139.2	—
p_{14}	*r*C(2)–C(3)	138.9(2)	139.7	—	139.5(2)	139.6	—
p_{15}	*r*C(3)–C(4)	138.5(2)	138.6	—	139.3(3)	139.6	—
p_{16}	*r*C(3)–F	132.8(3)	133.1	—	132.1(4)	133.2	—
p_{17}	*r*C(2)–F	134.9(2)	134.5	—	133.9(4)	134.7	—
p_{18}	∠C(1)–C(2)–C(3)	122.1(3)	121.5	—	120.1(4)	121.5	—
p_{19}	∠C(2)–C(3)–C(4)	119.2(1)	119.3	—	119.9(3)	119.3	—
p_{20}	∠C(1)–Z–C(1)′	91.8(1)	91.6	—	90.6(1)	90.4	—

[a] Refers to [MP2/aug-cc-pVQZ-PP/6-311G*] calculation for both $Sb_2(C_6F_4)_3$ and $Bi_2(C_6F_4)_3$. [b] Distances (*r*) are in pm and angles (∠) in degrees. See text for parameter definitions and Figure 1 for atom numbering. The figures in parentheses are the estimated standard deviations of the last digits.

The two different C–F bond lengths were described using the average of and the difference between the two ($p_{5–6}$). The final distance parameter that was employed in the model was *r*Z–C (p_7), where Z is the appropriate Group 15 heteroatom. The four angle parameters that were required to complete the model were ∠C(2)–C(3)–F (p_8), ∠C(1)–C(2)–F (p_9), ∠C(6)–C(1)–C(2) (p_{10}) and ∠C(6)–C(1)–Z (p_{11}).

Figure 1 Gas-phase structure of $Z_2(C_6F_4)_3$ (Z = Sb, Bi) with atom numbering. One ring is numbered explicitly and symmetry-related atoms on the other two rings are denoted C(1)′, C(1)″ etc.

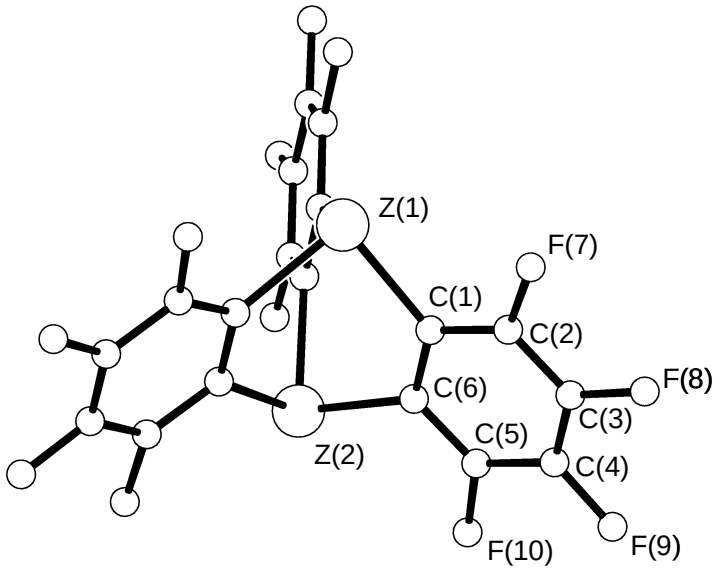

Starting parameters were taken from the results of the MP2/aug-cc-pVQZ-PP/6-311G* calculations and all 11 independent geometric parameters for both compounds were refined using a least-squares refinement method. Restraints were applied, as described in the SARACEN method,[28] only to the four difference parameters used in each model. Additionally, 15 amplitudes of vibration were refined for $Sb_2(C_6F_4)_3$ (two were restrained) and 14 were refined for $Bi_2(C_6F_4)_3$, with four requiring to be restrained. See Table 3 for lists of amplitudes of vibration for both molecules.

Each refinement has an associated goodness of fit that is expressed as an *R* factor. For $Sb_2(C_6F_4)_3$ R_G = 0.055 (R_D = 0.034) and for $Bi_2(C_6F_4)_3$ R_G = 0.061 (R_D = 0.037). The

Table 3 Interatomic distances (r_a) and amplitudes of vibration (u_{h1}) for the restrained GED structures of $Z_2(C_6F_4)_3$ (Z = Sb, Bi).[a]

	Atom pair	$Sb_2(C_6F_4)_3$			$Bi_2(C_6F_4)_3$		
		r_a/pm	u_{h1}/pm[b]	Restraint	r_a/pm	u_{h1}/pm[b]	Restraint
u_1	C(3)–F(8)	133.1(3)	3.6(tied to u_3)	—	132.1(4)	4.4(2)	4.2(4)
u_2	C(2)–F(7)	134.7(2)	3.7(tied to u_3)	—	133.9(4)	4.6(tied to u_1)	—
u_3	C(3)–C(4)	137.9(3)	3.8(2)	4.4(4)	139.3(3)	4.7(tied to u_1)	—
u_4	C(2)–C(1)	138.3(2)	3.9(tied to u_3)	—	138.5(3)	4.8(tied to u_1)	—
u_5	C(3)–C(2)	139.0(2)	3.9(tied to u_3)	—	139.4(2)	4.9(tied to u_1)	—
u_6	C(1)–C(6)	141.4(4)	4.1(tied to u_3)	—	139.8(5)	5.0(tied to u_1)	—
u_7	C(1)–Z(1)	214.4(1)	3.9(2)	—	223.0(3)	5.8(5)	—
u_8	C(3)···F(7)	232.5(4)	5.2(tied to u_{10})	—	234.2(5)	5.6(2)	—
u_9	C(3)···F(9)	235.1(4)	5.2(tied to u_{10})	—	234.4(5)	5.6(tied to u_8)	—
u_{10}	C(2)···F(8)	235.7(5)	5.2(2)	—	235.7(5)	5.7(tied to u_8)	—
u_{11}	C(1)···F(7)	237.9(4)	5.0(tied to u_{10})	—	237.8(5)	5.5(tied to u_8)	—
u_{12}	C(3)···C(5)	238.7(2)	4.6(tied to u_{10})	—	241.0(4)	5.0(tied to u_8)	—
u_{13}	C(2)···C(6)	240.3(3)	4.7(tied to u_{10})	—	240.8(6)	5.1(tied to u_8)	—
u_{14}	C(3)···C(1)	242.3(5)	4.6(tied to u_{10})	—	240.5(6)	5.0(tied to u_8)	—
u_{15}	F(7)···F(8)	265.4(9)	14.7(5)	—	269.4(9)	11.6(4)	11.1(11)
u_{16}	F(7)···F(9)	272.0(14)	15.0(tied to u_{15})	—	268.9(15)	11.8(tied to u_{15})	—
u_{17}	C(2)···C(5)	273.5(5)	8.3(tied to u_{15})	—	277.8(10)	6.5(tied to u_{15})	—
u_{18}	C(3)···C(6)	279.3(4)	8.5(tied to u_{15})	—	277.9(6)	6.7(tied to u_{15})	—
u_{19}	C(2)···Z(1)	303.6(3)	9.5(tied to u_{22})	—	308.2(4)	10.7(tied to u_{22})	—
u_{20}	C(1)···C(1)′	307.2(3)	12.5(tied to u_{22})	—	316.3(5)	14.3(tied to u_{22})	—
u_{21}	C(1)···Z(2)	315.4(2)	8.6(tied to u_{22})	—	323.4(3)	9.6(tied to u_{22})	—
u_{22}	F(7)···Z(1)	316.3(4)	14.9(3)	—	316.1(5)	17.0(4)	—
u_{23}	C(1)···C(6)′	338.1(3)	11.8(fixed)	—	345.8(5)	11.7(tied to u_{26})	—
u_{24}	C(3)···F(10)	358.2(3)	6.1(tied to u_{26})	—	361.1(4)	6.0(tied to u_{26})	—
u_{25}	C(2)···F(9)	360.4(3)	6.1(tied to u_{26})	—	360.7(4)	6.0(tied to u_{26})	—

u_{26}	C(1)···F(8)	362.4(4)	6.1(2)	—		360.9(5)	6.0(4)	—
u_{27}	C(1)···F(10)	364.7(3)	6.1(tied to u_{26})	—		364.1(5)	6.0(tied to u_{26})	—
u_{28}	Z(1)···Z(2)	380.1(2)	7.9(2)	—		393.7(4)	10.5(3)	—
u_{29}	C(2)···F(10)	407.5(5)	6.8(tied to u_{31})	—		411.2(9)	6.5(fixed)	—
u_{30}	C(1)···F(9)	411.7(3)	6.9(tied to u_{31})	—		409.3(6)	6.7(fixed)	—
u_{31}	C(2)···C(1′)	421.3(3)	15.1(8)	—		429.4(4)	15.2(fixed)	—
u_{32}	C(3)···Z(1)	436.4(4)	9.7(6)	—		441.6(5)	9.7(7)	—
u_{33}	C(2)···Z(2)	442.3(2)	9.0(tied to u_{32})	—		451.5(4)	8.8(tied to u_{32})	—
u_{34}	F(8)···F(10)	466.1(5)	9.8(tied to u_{36})	—		467.2(6)	7.9(fixed)	—
u_{35}	C(2)···C(6′)	464.3(4)	18.5(tied to u_{36})	—		472.1(5)	15.6(fixed)	—
u_{36}	C(1)···F(7′)	466.6(4)	23.0(11)	—		472.7(4)	19.2(fixed)	—
u_{37}	C(3)···Z(2)	492.1(4)	12.7(10)	—		499.3(5)	8.2(7)	8.1(8)
u_{38}	C(2)···C(2′)	515.4(5)	23.5(tied to u_{42})	—		522.0(5)	24.6(tied to u_{42})	—
u_{39}	F(7)···F(7′)	526.9(7)	34.6(tied to u_{42})	—		529.1(9)	35.7(tied to u_{42})	—
u_{40}	C(3)···C(1′)	529.6(4)	18.2(tied to u_{42})	—		536.7(6)	19.2(tied to u_{42})	—
u_{41}	F(7)···F(10)	541.2(6)	7.6(tied to u_{42})	—		544.3(9)	7.6(tied to u_{42})	—
u_{42}	F(8)···Z(1)	536.2(5)	11.3(2)	—		541.0(5)	11.9(3)	—
u_{43}	C(2)···F(7′)	537.9(3)	28.8(tied to u_{42})	—		541.9(4)	29.9(tied to u_{42})	—
u_{44}	C(1)···F(10′)	542.2(3)	19.7(tied to u_{42})	—		546.9(4)	20.6(tied to u_{42})	—
u_{45}	F(7)···Z(2)	552.2(3)	9.8(tied to u_{42})	—		559.9(4)	10.1(tied to u_{42})	—
u_{46}	C(3)···C(6′)	547.4(5)	18.3(tied to u_{42})	—		554.3(6)	19.3(tied to u_{42})	—
u_{47}	C(2)···C(5′)	582.9(4)	22.6(tied to u_{42})	—		590.8(6)	23.6(tied to u_{42})	—
u_{48}	F(8)···Z(2)	624.3(3)	9.7(2)	8.4(8)		630.3(5)	10.2(6)	8.5(9)
u_{49}	C(3)···C(2′)	625.6(6)	29.0(tied to u_{48})	—		632.3(7)	25.9(fixed)	—
u_{50}	C(1)···F(8′)	642.6(4)	22.2(tied to u_{48})	—		649.9(5)	21.0(7)	—
u_{51}	C(3)···C(5′)	654.7(5)	28.4(tied to u_{48})	—		661.8(6)	26.8(tied to u_{50})	—
u_{52}	C(2)···F(10′)	660.4(3)	27.0(tied to u_{48})	—		666.3(5)	25.2(tied to u_{50})	—
u_{53}	C(3)···F(7′)	658.5(4)	34.6(tied to u_{48})	—		663.0(5)	32.3(tied to u_{50})	—
u_{54}	C(1)···F(9′)	671.4(4)	21.9(tied to u_{48})	—		677.8(5)	20.7(tied to u_{50})	—
u_{55}	C(3)···F(10′)	712.4(4)	32.3(10)	—		717.1(5)	33.8(tied to u_{59})	—

u_{56}	C(3)···C(3)′	722.5(8)	34.6(tied to u_{55})	—	728.4(10)	36.6(tied to u_{59})	—
u_{57}	C(2)···F(8)′	726.9(5)	33.5(tied to u_{55})	—	733.3(6)	35.4(tied to u_{59})	—
u_{58}	C(3)···C(4)′	735.4(8)	34.3(tied to u_{55})	—	741.4(10)	36.3(tied to u_{59})	—
u_{59}	F(7)···F(8)′	744.0(5)	39.8(tied to u_{55})	—	748.8(5)	41.7(20)	—
u_{60}	F(7)···F(10)′	753.8(6)	27.8(tied to u_{55})	—	757.6(8)	29.1(tied to u_{59})	—
u_{61}	C(2)···F(9)′	775.8(4)	32.1(tied to u_{55})	—	781.9(5)	33.9(tied to u_{59})	—
u_{62}	C(3)···F(8)′	824.8(6)	43.8(tied to u_{63})	—	830.9(8)	44.1(26)	—
u_{63}	F(8)···F(10)′	835.8(3)	38.5(15)	—	839.8(4)	38.4(tied to u_{62})	—
u_{64}	C(3)···F(9)′	846.8(6)	43.1(tied to u_{63})	—	852.7(8)	43.3(tied to u_{62})	—
u_{65}	F(8)···F(8)′	918.6(8)	44.7(fixed)	—	925.0(8)	45.8(fixed)	—
u_{66}	F(8)···F(9)′	957.3(6)	43.2(fixed)	—	962.6(8)	44.3(fixed)	—

[a] Estimated standard deviations, as obtained in the least squares refinement, are given in parentheses. [b] Amplitudes not refined were fixed at the values obtained using the force field calculated at [RHF/aug-cc-pVQZ-PP/6-31G*] for $Sb_2(C_6F_4)_3$ and $Bi_2(C_6F_4)_3$.

success of a refinement can also be gauged from the fit of the radial-distribution and experimental – theoretical difference curves shown as Figures 2 and 3. The least-squares correlation matrices are given in Tables 4 and 5 and the molecular-scattering intensity curves are shown in Figures 4 and 5. Coordinates from the final GED refinements are given in Tables 4.1 and 4.2 in the Electronic Appendix (EA).

It is worth noting that, as is routine nowadays, the scattering factors used were complex (*i.e.* they contain both a real and an imaginary factor).[27] This is particularly important for the refinement of data collected for molecules such as the ones described here. The presence in a molecule of very large atoms (Sb, Bi) with relatively small atoms (C, F) gives rise to a relativistic phase effect. This manifests itself as a double peak in the radial-distribution curve. By using complex scattering factors, the theoretical model can account for the double peak, rather than a single peak, which would lead to huge errors in the structure determination. On close inspection of, for example, Figure 2 it can be seen that the broad peak at about 200–260 pm appears to have a shoulder but that no distances (represented by sticks) are under the shoulder to account for its existence. However, the stick representing the Sb–C distance (214 pm; marked (*) in Figure 2) is positioned in the saddle point of a double peak. The right-hand side of the double peak is overlapped by a stronger peak caused by various distances at about 250 pm. A similar phenomenon is observed for the Bi–C distance in Figure 3, and, in fact, occurs for every distance between Sb or Bi and a lighter atom.

The D_{3h} models that were written for both compounds fit the experimental data excellently. That this high symmetry is observed in the gas phase, contrary to the findings of a crystallographic study of $As_2(C_6F_4)_3$,[5] adds weight to the theory that the distortions observed in 1,6-diarsatriptycene were attributable to packing forces.

Figure 2 Experimental radial-distribution curve and theoretical – experimental difference curve for the refinement of $Sb_2(C_6F_4)_3$. Before Fourier inversion the data were multiplied by $s.\exp(-0.00002s^2)/(Z_{Sb} - f_{Sb})(Z_C - f_C)$. *r*Sb–C, sitting at the saddle point of a partially obscured double peak, is marked (*) for clarity.

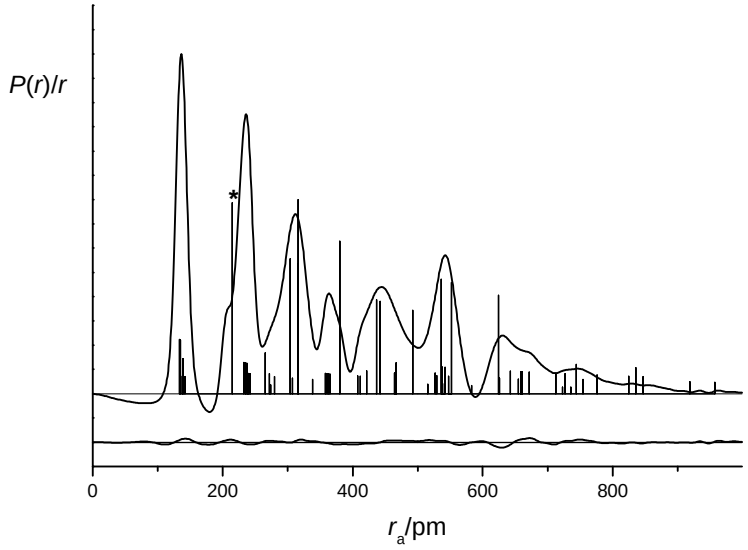

Figure 3 Experimental radial-distribution curve and theoretical – experimental difference curve for the refinement of $Bi_2(C_6F_4)_3$. Before Fourier inversion the data were multiplied by $s.\exp(-0.00002s^2)/(Z_{Bi} - f_{Bi})(Z_C - f_C)$.

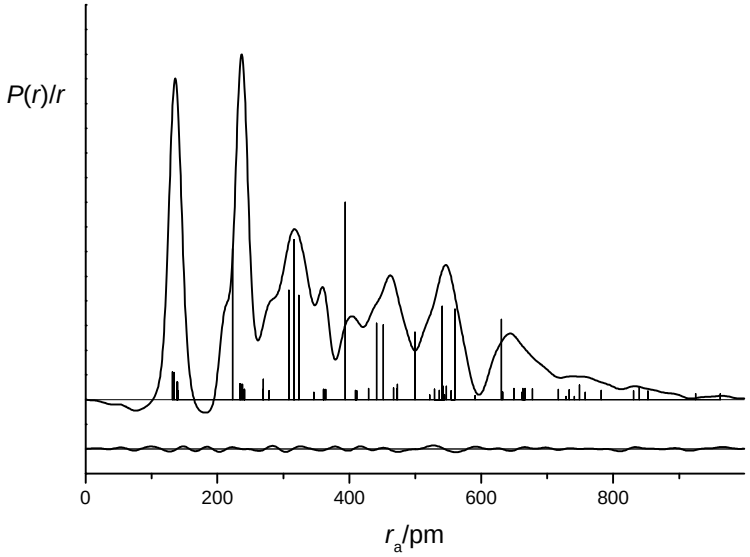

Table 4 Least-squares correlation matrix (×100) for $Sb_2(C_6F_4)_3$.[a]

	p_5	p_9	p_{10}	p_{11}	u_3	u_{10}	u_{28}	u_{32}	u_{36}	u_{37}	k_2	k_3
p_1	–86	–67	–56		–75							
p_2				–75								
p_5					80							
p_7			52			61						
p_9			71									
u_3						68						61
u_7						69						59
u_{10}												69
u_{26}							69					
u_{31}								62	56			
u_{32}									79			
u_{36}										69		
k_1											51	
k_2												62

[a] Only elements with absolute values ≥ 50% are shown; k_1, k_2 and k_3 are scale factors.

Table 5 Least-squares correlation matrix (×100) for $Bi_2(C_6F_4)_3$.[a]

	p_5	p_7	p_{10}	p_{11}	u_1	u_{59}
p_1	–87	–51			–60	
p_2				–58		
p_5					64	
p_9			65			
u_{50}						51

[a] Only elements with absolute values ≥ 50% are shown.

Figure 4 Experimental and difference (experimental – theoretical) molecular-scattering intensities for $Sb_2(C_6F_4)_3$.

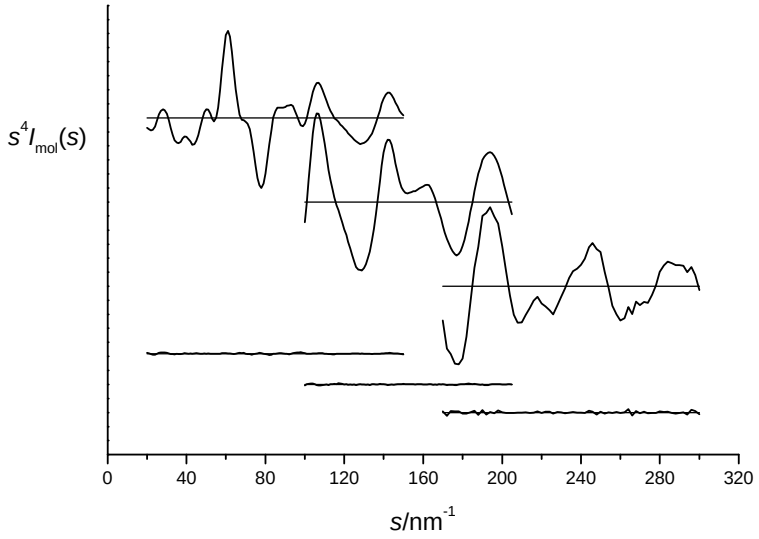

Figure 5 Experimental and difference (experimental – theoretical) molecular-scattering intensities for $Bi_2(C_6F_4)_3$.

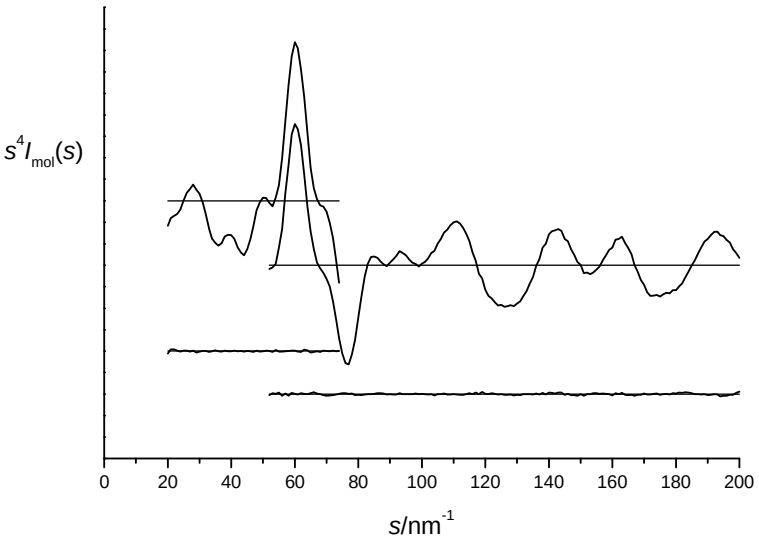

4.3.2 *Ab initio* and DFT calculations

During this project a considerable amount of work has been directed towards calculating accurately the structures of 1,6-disubstituted triptycenes [$Z_2(C_6F_4)_3$] (Z = Sb, Bi). Relatively little work exists where methods of calculation and types of basis set have been tested for all *p*-block elements, hence the need to perform such a comprehensive search for a suitable calculation.

As described in the Experimental section, various levels of theory and pseudopotential basis sets were tested (see Table 6). The validity of these calculations will be assessed using the experimental (GED) structures determined above.

The coordinates for the calculated geometries of $Sb_2(C_6F_4)_3$ using each of MP2, B3PW91, B3LYP and BLYP with both the LanL2DZ and aug-cc-pVQZ-PP ECPs are given in Tables 4.3–4.10 (EA).

All of the methods were reasonably good at calculating the values of the ring parameters and also the C–Sb–C angle, but the calculated Sb–C and Sb···Sb distances were longer than the experimentally determined values in almost every case. For some methods this discrepancy was almost 7 pm for the bonded distance and 9 pm for the non-bonded distance, with the BLYP method performing poorly with both of the pseudopotentials that were tested. The best results were obtained using the MP2/aug-cc-pVQZ-PP/6-311G* combination, giving *r*Sb–C to within 1 pm and *r*Sb···Sb to within approximately 1 pm. A calculation was also performed including a diffuse function on the C and F atoms (6-311+G*) but this was found have little effect (maximum 0.1 pm, 0.1°) on any parameter. Increasing the size of the basis set on Sb to quintuple-ζ (aug-cc-pV5Z-PP) quality had a similarly negligible effect on the structure.

The same set of test calculations was performed to determine the most suitable method for calculating the structure of $Bi_2(C_6F_4)_3$. In this instance, Table 6 shows that the MP2 calculation using the small-core pseudopotential (aug-cc-pVQZ-PP) and the 6-311G* basis set gave a result (224.4 pm) that matched very accurately the GED value for *r*Bi–C [222.9(3) pm] and a Bi···Bi distance that was calculated to be 1.5 pm bnger than the GED value, which one method had overestimated by 10 pm. (Coordinates for all

Table 6 Selected GED parameters (r_{h1}) and calculated parameters (r_e) for $Sb_2(C_6F_4)_3$ and $Bi_2(C_6F_4)_3$ at different levels of theory with the 6-311G* basis set on C and F and comparing the LanL2DZ and aug-cc-pVQZ-PP pseudopotential basis sets on the heavy atoms.[a]

$Sb_2(C_6F_4)_3$	Experimental	Theoretical			
	GED	MP2	B3PW91	B3LYP	BLYP
		LanL2DZ			
*r*Sb–C	214.4(1)	217.1	218.7	219.2	221.2
*r*Sb···Sb	380.6(2)	385.4	384.4	385.6	389.0
∠C–Sb–C	91.8(1)	91.4	91.8	91.8	91.7
*r*C(1)–C(6)	140.9(4)	140.9	140.0	140.4	141.3
*r*C(2)–F	134.9(2)	134.6	134.2	135.0	136.8
		aug-cc-pVQZ-PP			
*r*Sb–C	214.4(1)	213.4	216.7	218.4	221.1
*r*Sb···Sb	380.6(2)	380.1	381.9	384.9	389.8
∠C–Sb–C	91.8(1)	91.6	91.9	91.7	91.5
*r*C(1)–C(6)	140.9(4)	140.8	140.2	140.3	141.2
*r*C(2)–F	134.9(2)	134.5	134.4	135.2	137.1
$Bi_2(C_6F_4)_3$	Experimental	Theoretical			
	GED	MP2	B3PW91	B3LYP	BLYP
		LanL2DZ			
*r*Bi–C	222.9(3)	224.4	225.7	226.4	228.3
*r*Bi···Bi	394.4(4)	398.2	396.1	397.1	400.2
∠C–Bi–C	90.6(1)	90.3	90.9	91.0	90.9
*r*C(1)–C(6)	139.9(5)	140.6	139.8	140.1	141.0
*r*C(2)–F	133.9(4)	135.0	134.7	135.3	137.2
		aug-cc-pVQZ-PP			
*r*Bi–C	222.9(3)	222.9	226.6	225.6	231.6
*r*Bi···Bi	394.4(4)	395.9	397.6	396.2	404.8

∠C–Bi–C	90.6(1)	90.4	90.8	90.9	90.7
*r*C(1)–C(6)	139.9(5)	140.3	139.6	139.8	140.7
*r*C(2)–F	133.9(4)	134.7	134.7	134.6	137.4

[a] Distances are in pm, angles in degrees. See Figure 1 for atom numbering.

methods tested are in Tables 4.11–4.18, EA.) The B3PW91/aug-cc-pVQZ/6-311G* calculation, which performed relatively well for Sb, predicts *r*Bi–C better than most methods but models *r*Bi···Bi relatively poorly (3 pm longer than the GED value).

As with the preceding two chapters, the availability of experimental GED data has allowed conclusions to be drawn as to the suitability of different methods of calculating geometries and has allowed comparison of the use of different basis sets. In this case MP2 calculations proved best, although with the footnote that they were very time-consuming and computationally demanding. However, the most significant finding during this work was the improved performance of the aug-cc-pVQZ-PP ECP over the larger core basis set LanL2DZ. It must be concluded that large-core pseudopotentials should be used with caution as the inclusion of so few electrons in the valence shell can have a sizable effect on the quality of calculated geometries.

4.4 References

1. F. von Dechend and H. Wichelhaus, *Chem. Ber.*, 1875, **8**, 1609.
2. N. P. McCleland and J. B. Whitworth, *J. Chem. Soc.*, 1927, 2753.
3. J. Klaveness, A. Berg, T. Almen, K. Golman, M. Droege and S. Yu, *US Pat.*, 5 817 289, 2000.
4. M. Naritomi, H. Murofushi and N. Nakashimi, *Bull. Chem. Soc. Jpn.*, 2004, **77**, 2121.
5. N. A. A. Al-Jabar, J. Bowen Jones, D. S. Brown, A. H. Colligan, A. G. Massey, J. M. Miller and J. W. Nye, *Appl. Organomet. Chem.*, 1989, **3**, 459.
6. F. J. M. Freijee and C. H. Stam, *Acta Crystallogr., Sect. B: Struct. Crystallogr. Cryst. Chem.*, 1980, **36**, 1247; N. van der Putten and C. H. Stam, *Acta Crystallogr., Sect. B: Struct. Crystallogr. Cryst. Chem.*, 1980, **36**, 1250.
7. C. van Rooyen-Reiss and C. H. Stam, *Acta Crystallogr., Sect. B: Struct. Crystallogr. Cryst. Chem.*, 1980, **36**, 1252.
8. C. M. Woodward, G. Hughes and A. G. Massey, *J. Organomet. Chem.*, 1976, **112**, 9; T. K. Mistry and A. G. Massey, *J. Organomet. Chem.*, 1981, **209**, 45; N. A. A. Al-Jabar and A. G. Massey, *J. Organomet. Chem.*, 1984, **276**, 331; N. A. A. Al-Jabar, A. G. Massey and T. K. Mistry, *Organomet. Synth.*, 1986, **3**, 630.
9. M. J. Frisch, G. W. Trucks, H. B. Schlegel, G. E. Scuseria, M. A. Robb, J. R. Cheeseman, J. A. Montgomery, Jr., T. Vreven, K. N. Kudin, J. C. Burant, J. M. Millam, S. S. Iyengar, J. Tomasi, V. Barone, B. Mennucci, M. Cossi, G. Scalmani, N. Rega, G. A. Petersson, H. Nakatsuji, M. Hada, M. Ehara, K. Toyota, R. Fukuda, J. Hasegawa, M. Ishida, T. Nakajima, Y. Honda, O. Kitao, H. Nakai, M. Klene, X. Li, J. E. Knox, H. P. Hratchian, J. B. Cross, C. Adamo, J. Jaramillo, R. Gomperts, R. E. Stratmann, O. Yazyev, A. J. Austin, R. Cammi, C. Pomelli, J. W. Ochterski, P. Y. Ayala, K. Morokuma, G. A. Voth, P. Salvador, J. J. Dannenberg, V. G. Zakrzewski, S. Dapprich, A. D. Daniels, M. C. Strain, O. Farkas, D. K. Malick, A. D. Rabuck, K. Raghavachari, J. B. Foresman, J. V. Ortiz, Q. Cui, A. G. Baboul, S. Clifford, J. Cioslowski, B. B. Stefanov, G. Liu, A. Liashenko, P. Piskorz, I. Komaromi, R. L.

Martin, D. J. Fox, T. Keith, M. A. Al-Laham, C. Y. Peng, A. Nanayakkara, M. Challacombe, P. M. W. Gill, B. Johnson, W. Chen, M. W. Wong, C. Gonzalez and J. A. Pople, *Gaussian 03, Revision C.01*, Gaussian, Inc., Wallingford, CT, 2004.

10. J. S. Binkley, J. A. Pople and W. J. Hehre, *J. Am. Chem. Soc.*, 1980, **102**, 939; M. S. Gordon, J. S. Binkley, J. A. Pople, W. J. Pietro and W. J. Hehre, *J. Am. Chem. Soc.*, 1982, **104**, 2797; W. J. Pietro, M. M. Francl, W. J. Hehre, D. J. DeFrees, J. A. Pople and J. S. Binkley, *J. Am. Chem. Soc.*, 1982, **104**, 5039.
11. W. J. Hehre, R. Ditchfield and J. A. Pople, *J. Chem. Phys.*, 1972, **56**, 2257; P. C. Hariharan and J. A. Pople, *Theor. Chim. Acta*, 1973, **28**, 213; M. S. Gordon, *Chem. Phys. Lett.*, 1980, **76**, 163.
12. P. J. Hay and W. R. Wadt, *J. Chem. Phys.*, 1985, **82**, 270; W. R. Wadt and P. J. Hay, *J. Chem. Phys.*, 1985, **82**, 284; P. J. Hay and W. R. Wadt, *J. Chem. Phys.*, 1985, **82**, 299.
13. R. Krishnan, J. S. Binkley, R. Seeger and J. A. Pople, *J. Chem. Phys.*, 1980, **72**, 650; A. D. McLean and G. S. Chandler, *J. Chem. Phys.*, 1980, **72**, 5639.
14. K. A. Peterson, *J. Chem. Phys.*, 2003, **119**, 11099.
15. B. Metz, H. Stoll and M. Dolg, *J. Chem. Phys.*, 2000, **113**, 2563.
16. D. A. Wann, S. L. Hinchley, K. B. Borisenko, H. E. Robertson, M. D. Francis, J. F. Nixon and D. W. H. Rankin, *Dalton Trans.*, 2005, 1972.
17. A. D. Becke, *J. Chem. Phys.*, 1993, **98**, 5648.
18. J. P. Perdew, K. Burke and Y. Wang, *Phys. Rev. B: Condens. Matter*, 1996, **54**, 16533.
19. C. Lee, W. Yang and R. G. Parr, *Phys. Rev. B: Condens. Matter*, 1992, **37**, 785; B. Miehlich, A. Savin, H. Stoll and H. Preuss, *Chem. Phys. Lett.*, 1989, **157**, 200.
20. A. D. Becke, *Phys. Rev. A*, 1988, **38**, 3098.
21. C. Møller and M. S. Plesset, *Phys. Rev.*, 1934, **46**, 618.
22. V. A. Sipachev, *J. Mol. Struct.* (*THEOCHEM*), 1985, **121**, 143; V. A. Sipachev, *J. Mol. Struct.*, 2001, **567**, 67.

23. O. Bastiansen and M. Trætteberg, *Acta Crystallogr.*, 1960, **13**, 1108; Y. Morino, S. J. Cyvin, K. Kuchitsu and T. Iijima, *J. Chem. Phys.*, 1962, **36**, 1109; R. Stølevik, H. M. Seip and S. J. Cyvin, *Chem. Phys. Lett.*, 1972, **15**, 263.
24. C. M. Huntley, G. S. Laurenson and D. W. H. Rankin, *J. Chem. Soc., Dalton Trans.*, 1980, 954.
25. H. Fleischer, D. A. Wann, S. L. Hinchley, K. B. Borisenko, J. R. Lewis, R. J. Mawhorter, H. E. Robertson and D. W. H. Rankin, *Dalton Trans.*, 2005, 3221.
26. S. L. Hinchley, H. E. Robertson, K. B. Borisenko, A. R. Turner, B. F. Johnston, D. W. H. Rankin, M. Ahmadian, J. N. Jones and A. H. Cowley, *Dalton Trans.*, 2004, 2469.
27. A. W. Ross, M. Fink and R. Hilderbrandt, *International Tables for Crystallography*, ed. A. J. C. Wilson, Kluwer Academic Publishers, Dordrecht, Netherlands, 1992, vol. C, p.245.
28. A. J. Blake, P. T. Brain, H. McNab, J. Miller, C. A. Morrison, S. Parsons, D. W. H. Rankin, H. E. Robertson and B. A. Smart, *J. Phys. Chem.*, 1996, **100**, 12280; P. T. Brain, C. A. Morrison, S. Parsons and D. W. H. Rankin, *J. Chem. Soc., Dalton Trans.*, 1996, 4589; N. W. Mitzel and D. W. H. Rankin, *Dalton Trans.*, 2003, 3650.

Chapter Five

Molecular structures of $Se(SCH_3)_2$ and $Te(SCH_3)_2$ using gas-phase electron diffraction and *ab initio* and DFT calculations

5.1 Introduction

Trichalcogenides of the type R–Y–Y–Y–R (Y = S, Se, Te; R = H, CH_3, CF_3, *etc.*) can, in principle, be composed of many different conformers. If it is assumed that R can lie either *anti* (*a*) or *gauche* (*g*) to the Y–Y–Y plane, then nine different conformers can be identified. A similar set of conformers was identified for the organic molecule 1,3-dibromopropane (Figure 1),[1] and this diagram can be used to represent the nine conformers of RYYYR, where R is represented by a black ball and all propane hydrogen atoms are removed. However, some of the possible structures are identical because of symmetry, or are enantiomeric pairs that cannot be distinguished using gas-phase electron diffraction (GED) methods. Conformers 6 and 7 are enantiomers, as are 2 and 3, which are identical to 4 and 5, respectively. Only four conformers are, therefore, distinguishable by GED; these are of the type *aa* (C_{2v} symmetry), *ag* (C_1 symmetry), *gg* (C_2 symmetry) and *gg* (C_s symmetry).

Figure 1 The nine possible *anti*/*gauche* conformers of 1,3-dibromopropane. The torsion angles are shown in parenthesis (adapted from Ref. 1).

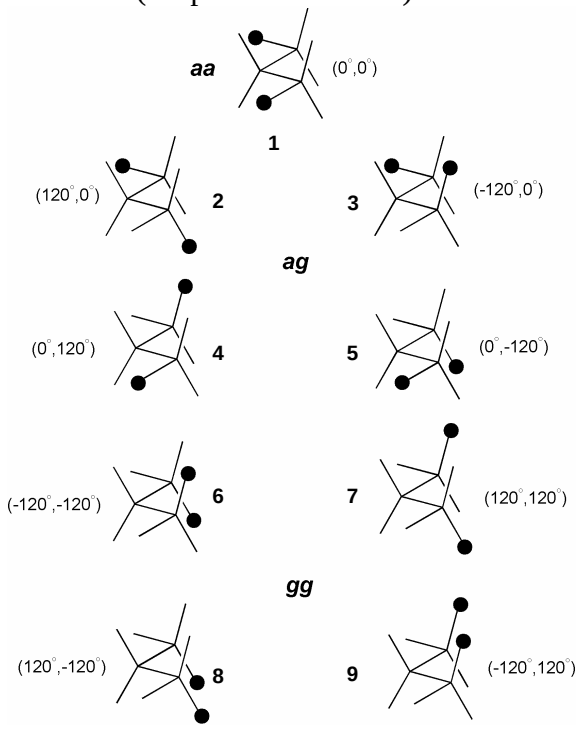

As shown in Figure 1, two conformers of RYYYR exist where both R groups are *gauche* to the YYY plane. In one case (enantiomers 6 and 7) the torsion angles are both of the same sign and move to opposite sides of the YYY plane; this conformation will be denoted as g^+g^+. The pair of identical structures 8 and 9 are of the type g^+g^-, where the R groups lie on the same side of the YYY plane.

According to spectroscopic and quantum chemical studies the simple trisulfane molecule, HSSSH, exists as both g^+g^- and g^+g^+ conformers. Due to the small steric bulk of the hydrogen atoms, the two conformers differ in energy by only 1 kJ mol^{-1} (MP2 calculation with a triple-ζ quality basis set with polarisation functions), in favour of the g^+g^+ conformer.[2]

Two derivatives of trisulfane have previously been studied using gas-phase electron diffraction. Dimethyltrisulfane, CH_3SSSCH_3, was first studied in 1948,[3] and has recently been reinvestigated,[4] because there were huge uncertainties in the original work. A calculation (MP2/6-311+G*) again showed that both g^+g^- and g^+g^+ conformers existed, with the g^+g^+ conformer lower in energy by 7.7 kJ mol^{-1}. The most recent GED study interpreted this as a mixture, which included at least 15% of the g^+g^- conformer.

For bis(trifluoromethyl)trisulfane, CF_3SSSCF_3,[5] an energy gap of 10 kJ mol^{-1} (HF/3-21G*) made it unlikely that both conformers would be observed in the gas phase and the GED data were interpreted on the basis of the g^+g^+ form alone.

Recently, the molecular structures of the 2-seleno and 2-telluro derivatives, $Se(SCH_3)_2$ and $Te(SCH_3)_2$, were determined by single-crystal X-ray diffraction.[6,7] While $Se(SCH_3)_2$ adopts a g^+g^+ conformation, $Te(SCH_3)_2$ exhibits a g^+g^- conformation in the crystalline state. No GED studies have been reported for molecules where the heavier chalcogens (Se, Te) bind to the lighter ones (O, S). The GED structures of $Se(SCH_3)_2$ and $Te(SCH_3)_2$ will, therefore, contribute to the understanding of the structures of these molecules and will also help to evaluate the quality of the calculated structures. GED data will reveal whether there are structural differences between the solid and gaseous states.

5.2 Experimental

5.2.1 Quantum chemical studies

Ab initio and DFT calculations were performed by Dr. Holger Fleischer at Universität Mainz using the Gaussian 98 suite of programs.[8] Geometry optimisations for both $Se(SCH_3)_2$ and $Te(SCH_3)_2$ were performed at the HF and MP2[9] levels of theory. Using DFT methods, Becke's B3 electron-exchange functional[10] and the correlation functional of Lee, Yang and Parr[11] were combined in the B3LYP hybrid functional. Initially, Pople-style all-electron basis sets were used as follows: a split-valence 3-21G* basis set for $Te(SCH_3)_2$,[12] and a split-valence 6-31G* basis set for $Se(SCH_3)_2$.[13] The LanL2DZ(d) basis set, which includes a pseudopotential for the heavy atoms, was subsequently used.[14]

Force fields were calculated at the MP2/LanL2DZ(d) level. These were used to provide estimates of the amplitudes of vibration (u_{h1}) and the curvilinear corrections (k_{h1}), from the SHRINK program,[15] for use in the gas-phase electron diffraction refinements.

5.2.2 Gas-phase electron diffraction

Data were collected for $Se(SCH_3)_2$ and $Te(SCH_3)_2$ using the Edinburgh gas-phase electron diffraction apparatus.[16] An accelerating voltage of around 40 kV was used, representing an electron wavelength of approximately 6.0 pm. Scattering intensities were recorded on Kodak Electron Image films at nozzle-to-film distances of 94.89 and 293.46 mm for $Se(SCH_3)_2$ and 97.51 and 259.65 mm for $Te(SCH_3)_2$. In the case of $Te(SCH_3)_2$ both sets of scattering intensity data were recorded with sample and nozzle temperatures held at 348 and 360 K respectively. For $Se(SCH_3)_2$, data were first collected at the longer nozzle-to-film distance, where sample and nozzle temperatures of 286 and 298 K provided a sufficient vaporisation rate for the GED experiment. In order to collect data at the shorter distance it proved necessary to increase the temperatures to 332 and 343 K.

The weighting points for the off-diagonal weight matrices, correlation parameters and scale factors for both camera distances for $Se(SCH_3)_2$ and $Te(SCH_3)_2$ are given in Table

1. Also included are the exact electron wavelengths as determined from the scattering patterns for benzene, which were recorded immediately after the patterns for the sample compounds. The scattering intensities were measured using an Epson Expression 1600 Pro flatbed scanner and converted to mean optical densities as a function of the scattering variable, *s*. The data reduction and the least-squares refinement processes were carried out using the ed@ed program[17] employing the scattering factors of Ross *et al.*[18]

Table 1 Nozzle-to-film distances (mm), weighting functions (nm^{-1}), scale factors, correlation parameters and electron wavelengths (pm) used in the electron diffraction studies of $Se(SCH_3)_2$ and $Te(SCH_3)_2$.

	$Se(SCH_3)_2$		$Te(SCH_3)_2$	
Nozzle-to-film distance[a]	94.89	293.46	97.51	259.65
Δs	2	2	4	2
s_{min}	80	20	88	20
sw_1	100	40	108	40
sw_2	292	104	220	104
s_{max}	320	120	250	120
Scale factor[b]	0.798(22)	0.736(6)	0.742(22)	0.644(8)
Correlation parameter	0.444	0.436	0.161	–0.124
Electron wavelength	6.020	6.020	6.020	6.020

[a] Determined by reference to the scattering pattern of benzene. [b] Values in parentheses are the estimated standard deviations.

5.3 Results

5.3.1 *Ab initio* and DFT calculations

Ab initio and DFT investigations were performed at various levels of theory (HF, B3LYP, MP2), employing either all-electron basis sets (3-21G* and 6-31G*) or an effective core potential with an appropriate valence basis set as offered by LanL2DZ(d). At all combinations of theory and basis set, and for both compounds, calculations showed that two conformational energy minima existed, representing conformers with methyl groups in *gauche* positions relative to the opposite Y–S bond (*i.e.* with ϕSYSC ≅ 75–90°). In one case the two groups were on the same side of the S–Y–S plane (g^+g^-)

and in the other case they were on opposite sides of the plane (g^+g^+), as shown in Figure 2. These findings are in accordance with those for HSSSH and CH_3SSSCH_3.[2,4] Values for the geometric parameters calculated at all levels are given in Table 2. Coordinates for all calculated structures are given in Tables 5.1–5.8 in the Electronic Appendix (EA).

Figure 2 The g^+g^+ (left) and g^+g^- (right) conformers of $Y(SCH_3)_2$ (Y = Se, Te).

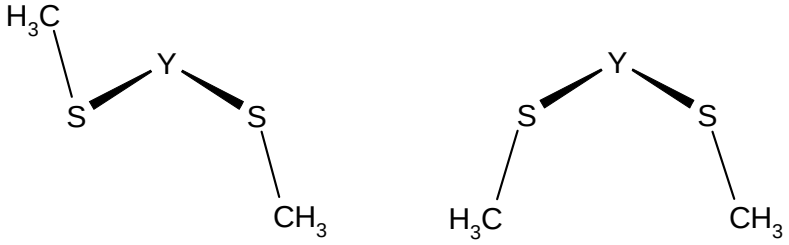

5.3.2 GED study

On the basis of the MP2/LanL2DZ(d) geometry, a model was written describing the structure of $Se(SCH_3)_2$ as a mixture of both conformers. A similar model was used for $Te(SCH_3)_2$ as the only differences between the tellurium and selenium structures were in the values for the bond lengths, angles and torsions and not in the general configurations. The geometry of the g^+g^+ conformers was described in terms of eight independent parameters and had overall C_2 symmetry. (See Figure 3 for atom numbering.) These parameters included three bond lengths, namely *r*Y–S (p_1), *r*S–C (p_2) and *r*C–H (p_3). A single *r*C–H value was used because the three individual MP2/LanL2DZ(d) values differed by only 0.3 pm. The model also required three angle parameters, including ∠S–Y–S (p_4) and ∠Y–S–C (p_5). The difference between the largest and smallest values for ∠S–C–H was 4.3° and, in order to account for this asymmetry in the methyl groups, an average S–C–H angle (p_6) was defined and this angle was used in the model in conjunction with fixed (*i.e.* non-refineable) differences to describe the tilt of the methyl groups. For the selenium molecule these fixed differences were –2.6, +1.7 and +0.9°, for the angles to H(6), H(7) and H(8) respectively, and for the tellurium molecule were –2.9, +1.8 and +1.1°. The two remaining parameters were dihedral angles. ϕC–S–Y–S (p_7) describes the movement of the S–C bond away from the

zero position where it eclipsed the opposite Y–S bond. As p_7 was used to describe the torsions on both sides of the molecule, the methyl groups were moved to opposite sides of the SYS plane. The final parameter was ϕY–S–C–H(6/9) (p_8), which describes the torsion of the methyl groups. The calculated structures show that one C–H bond of each group forms a dihedral angle of approximately 180° with the Y–S bond. From this position, a value of less than 180° represents a rotation in a clockwise direction when viewed along the S–C bond towards CH_3.

Parameters for the g^+g^- conformers were calculated to be similar to those for the g^+g^+ conformers. Therefore, only the sign of p_7 as applied to the one side of the molecule was changed in the model to preserve C_s symmetry. A non-geometric parameter was also included, allowing the abundance of each conformer to be varied.

Figure 3 Gas-phase structure of the g^+g^+ conformer of $Y(SCH_3)_2$ (Y = Se, Te) with atom numbering.

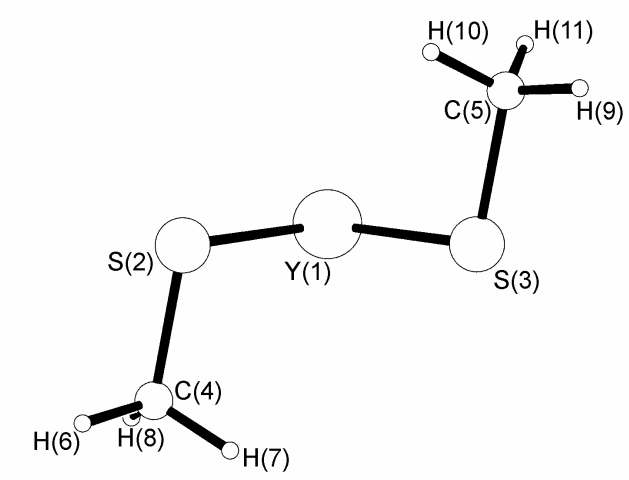

Table 2 Calculated (r_e) geometric parameters and energy differences for the g^+g^+ (C_2 symmetry) and g^+g^- (C_s symmetry) conformers of (*a*) $Se(SCH_3)_2$ and (*b*) $Te(SCH_3)_2$.[a,b]

(*a*)		HF/6-31G*		B3LYP/6-31G*		MP2/6-31G*		MP2/LanL2DZ(d)	
		C_2	C_s	C_2	C_s	C_2	C_s	C_2	C_s
p_1	*r*Se–S	219.1	219.0	222.1	222.0	219.9	219.7	220.9	220.8
p_2	*r*S–C	181.7	181.9	183.7	183.9	181.6	181.9	182.7	182.9
p_3	*r*C–H (mean)	108.1	108.1	109.3	109.3	109.2	109.1	109.6	109.6
p_4	∠S–Se–S	103.7	105.2	105.4	106.9	103.4	105.6	102.6	105.3
p_5	∠Se–S–C	101.9	102.8	101.9	102.7	100.4	101.4	101.1	102.4
p_6	∠S–C–H (mean)	109.3	109.4	109.2	109.3	109.3	109.5	109.2	109.4
p_7	ϕS–Se–S–C	80.3	89.9	81.3	88.5	78.4	87.7	76.0	88.3
p_8	ϕSe–S–C–H(6)	183.8	191.2	184.4	193.2	183.1	194.4	179.8	189.1
ΔE		–6.6		–4.9		–6.1		–7.3	
(*b*)		HF/3-21G*		HF/LanL2DZ(d)		B3LYP/LanL2DZ(d)		MP2/LanL2DZ(d)	
		C_2	C_s	C_2	C_s	C_2	C_s	C_2	C_s
p_1	*r*Te–S	240.3	240.3	238.7	238.7	242.0	242.1	239.3	239.3
p_2	*r*S–C	182.7	182.8	183.0	183.1	184.9	185.0	183.2	183.5
p_3	*r*C–H (mean)	108.0	108.0	108.2	108.2	109.5	109.5	109.6	109.6
p_4	∠S–Te–S	100.4	102.5	101.3	103.2	103.5	105.3	100.3	103.4
p_5	∠Te–S–C	103.6	104.4	103.7	104.5	103.8	104.3	101.9	102.9
p_6	∠S–C–H (mean)	109.3	109.5	109.3	109.4	109.3	109.4	109.3	109.5
p_7	ϕS–Te–S–C	77.2	87.5	78.2	88.5	80.3	88.2	75.7	86.4
p_8	ϕTe–S–C–H(6)	181.1	186.6	181.3	186.3	182.1	188.3	180.1	187.6
ΔE		–5.1		–6.1		–4.2		–5.5	

[a] Distances (*r*) are in pm, angles (∠) and torsions (ϕ) in degrees and energies in kJ mol^{-1}. See text for parameter definitions and Figure 3 for atom numbering. [b] $\Delta E = E(C_2) - E(C_s)$; *E* is the zero-point corrected energy.

With calculations [MP2/LanL2DZ(d)] showing the difference in energy between g^+g^+ and g^+g^- conformers to be approximately 7.3 kJ mol^{-1} when Y = Se and 5.5 kJ mol^{-1} when Y = Te (see Table 2), the probable abundance of each conformer can be calculated using the Boltzmann distribution at the experimental (nozzle) temperatures. It was predicted that $Se(SCH_3)_2$ would exist with around 95% g^+g^+ and 5% g^+g^- (at 298 K) and 93% g^+g^+ and 7% g^+g^- (at 343 K). In the case of $Te(SCH_3)_2$ the g^+g^+ : g^+g^- composition was calculated to be 86 : 14 at 360 K. This already makes it doubtful whether the g^+g^- conformers would be observable in the gas mixture. Another problem is that in terms of the heavy-atom non-bonded distances in both $Se(SCH_3)_2$ and $Te(SCH_3)_2$, the only significant difference that can be expected between the g^+g^+ and g^+g^- conformers is *r*C···C, which is approximately 80 pm longer for theg^+g^+ conformer. Although *r*S···C is, in principle, different for the two conformers, the values lie close together and will be found under the same peak in the GED radial-distribution curve. The peaks in the radial-distribution curve represent the distances between pairs of atoms and the areas of these peaks are proportional to the atomic numbers of the pair of atoms and how often that pairing occurs. For molecules containing very heavy atoms, the consequence of this is that distances from the heavy atoms will dominate the radial-distribution curve. This is the case here, where the relative size of the *r*C···C peak for each conformer is approximately 2% of the size of the largest peak (*r*Se–S) and this ratio is even smaller for the tellurium compound.

On performing least-squares refinements for $Se(SCH_3)_2$, using the model that contained both conformers and a non-geometric parameter to control the abundance of each of the conformers in the mixture, the lowest R_G value was found to be when 100(2)% of the g^+g^+ conformer was present. The structure that was returned for the scenario where 100% of the g^+g^- model was present was almost identical (barring *r*C···C), although the R_G value was higher. The uncertainty associated with the percentage of the g^+g^+ conformer was obtained from Figure 4, where, at a significance level of 95% (for which the R_G ratio is calculated to be 1.016), the value for 2σ was 4%.

For the refinements using the $Te(SCH_3)_2$ data, the lowest R_G value also resulted from the conformer mix where 100% of the g^+g^+ conformer was present. In this case, however,

the value for R_G for 100% of the g^+g^- conformer was only very slightly different. Figure 5 shows that, at the 95% confidence level, 2σ was 64% and that the abundance of conformer g^+g^+ in the GED sample was 100(32)%.

The reported structures of $Se(SCH_3)_2$ and $Te(SCH_3)_2$ will, therefore, be based on g^+g^+ conformers alone.

The processes of refinement for the Se and Te compounds were similar. In both cases eight geometric parameters and seven groups of amplitudes of vibration were refined. (See Table 3 for details of the parameters and Table 4 for the amplitudes of vibration.) For $Se(SCH_3)_2$ flexible restraints were employed, using the SARACEN method,[19] for three geometrical parameters and three amplitudes. For the purposes of SARACEN, the parameter values were set to be those obtained from calculations performed using the MP2 method with the LanL2DZ(d) basis set on all atoms. Similarly, for $Te(SCH_3)_2$, three parameters were restrained, as well as seven amplitudes of vibration.

The success of the final refinements, for which R_G = 0.054 (R_D = 0.042) for $Se(SCH_3)_2$, and R_G = 0.070 (R_D = 0.075) for $Te(SCH_3)_2$, can be assessed on the basis of the radial-distribution and experimental – theoretical difference curves (Figures 6 and 7) and the molecular-scattering intensity curves (Figures 8 and 9). The least-squares correlation matrices are given in Tables 5 and 6.

Figure 4 Variation of R_G ratio with percentage of g^+g^+ conformer of $Se(SCH_3)_2$.

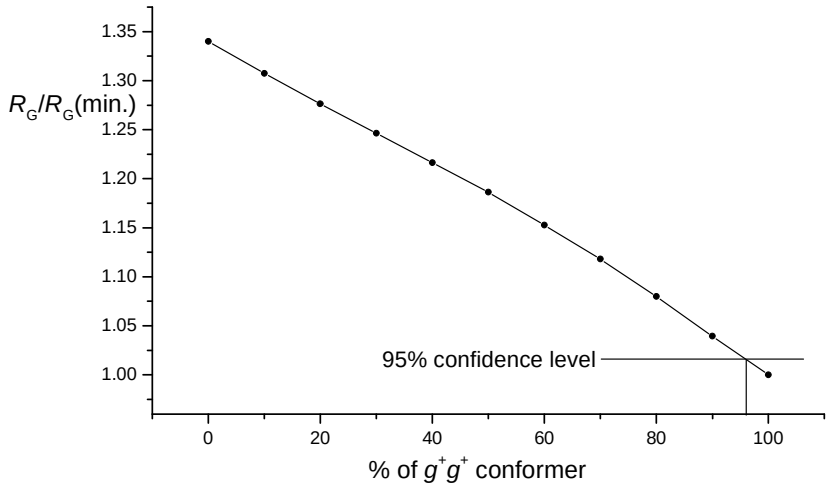

Figure 5 Variation of R_G ratio with percentage of g^+g^+ conformer of $Te(SCH_3)_2$.

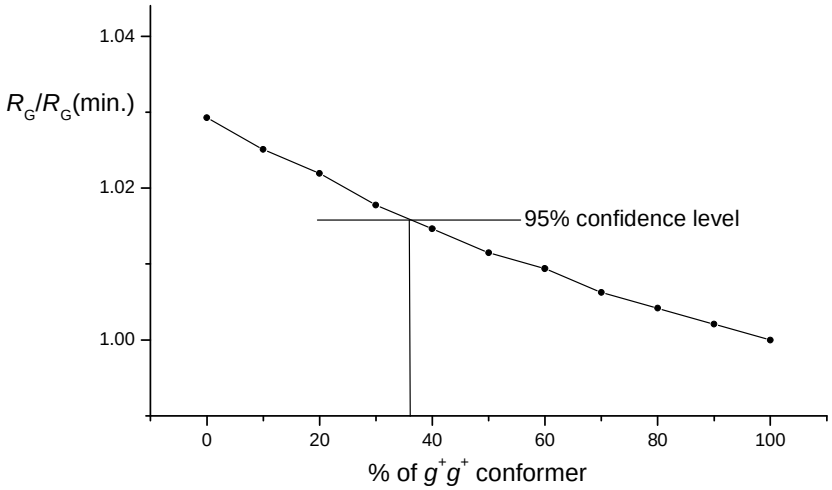

Table 3 GED (r_{h1}) parameters for the g^+g^+ conformers of $Se(SCH_3)_2$ and $Te(SCH_3)_2$ along with XRD parameters for those compounds and selected parameters from a GED study ($r_g/\angle_\alpha$) of $H_3CSSSCH_3$.[a,b]

		$Se(SCH_3)_2$			$Te(SCH_3)_2$			$H_3CSSSCH_3$
		GED	Restraint	XRD[c]	GED	Restraint	XRD[d]	GED[e]
p_1	rY–S	219.1(1)	—	218.9(3)	238.1(2)	—	240.9(3)	204.6(2)
p_2	rS–C	183.2(1)	—	180.9(3)	184.1(3)	—	181.5(5)	181.7(2)
p_3	rC–H	109.6(4)	109.6(10)	—	110.0(6)	109.6(10)	—	108.4(7)
p_4	∠S–Y–S	102.9(3)	—	103.2(5)	98.9(6)	—	98.9(1)	107.3(5)
p_5	∠Y–S–C	100.6(2)	—	102.3(6)	99.7(4)	—	103.8(4)	103.1(5)
p_6	∠S–C–H (mean)	107.4(5)	109.2(10)	—	109.2(9)	109.3(10)	—	112(2)
p_7	ϕS–Y–S–C	87.9(20)	—	79.8(9)	73.0(48)	—	85.7(7)	79(5)
p_8	ϕY–S–C–H(6)	178.8(19)	179.8(20)	—	180.1(19)	180.0(20)	—	—

[a] Distances (r) are in pm, angles (∠) and torsions (ϕ) in degrees. See text for parameter definitions and Figure 3 for atom numbering. The figures in parentheses are the estimated standard deviations of the last digits. [b] Averaged values over crystallographically different parameters. [c] See Ref. 6. [d] See Ref. 7. [e] See Ref. 4.

Table 4 Interatomic distances (r_a) and amplitudes of vibration (u_{h1}) for the restrained GED structures of g^+g^+ $Y(SCH_3)_2$ (Y = Se, Te).[a]

	Atom pair	$Se(SCH_3)_2$			$Te(SCH_3)_2$		
		r_a/pm	u_{h1}/pm[b]	Restraint	r_a/pm	u_{h1}/pm[b]	Restraint
u_1	C(4)–H(8)	109.3(4)	8.4(4)	7.6(8)	110.0(6)	6.5(6)	7.6(8)
u_2	C(4)–H(7)	109.3(4)	8.4(tied to u_1)	—	110.0(6)	6.6(tied to u_1)	—
u_3	C(4)–H(6)	109.3(4)	8.4(tied to u_1)	—	110.0(6)	6.6(tied to u_1)	—
u_4	H(6)···H(7)	180.5(9)	12.3(fixed)	—	179.4(14)	12.3(fixed)	—
u_5	H(6)···H(8)	180.3(9)	12.3(fixed)	—	179.2(14)	12.3(fixed)	—
u_6	H(7)···H(8)	178.9(9)	12.1(fixed)	—	177.6(14)	12.2(fixed)	—
u_7	S(2)–C(4)	183.3(1)	4.5(2)	—	184.1(3)	5.1(4)	5.2(5)
u_8	Y(1)–S(2)	219.0(1)	5.9(1)	—	238.1(2)	5.5(3)	5.5(6)
u_9	S(2)···H(6)	236.8(8)	11.3(fixed)	—	240.5(14)	11.4(fixed)	—
u_{10}	S(2)···H(7)	241.7(11)	10.9(fixed)	—	244.3(13)	10.9(fixed)	—
u_{11}	S(2)···H(8)	241.2(11)	10.9(fixed)	—	244.8(13)	10.9(fixed)	—
u_{12}	Y(1)···C(4)	309.6(4)	11.1(3)	—	323.6(9)	12.7(7)	10.8(11)
u_{13}	Y(1)···H(7)	315.5(22)	23.3(fixed)	—	330.4(26)	25.9(fixed)	—
u_{14}	Y(1)···H(8)	318.9(22)	23.4(fixed)	—	331.2(26)	25.4(fixed)	—
u_{15}	S(2)···H(10)	355.5(49)	39.3(fixed)	—	331.0(129)	48.7(fixed)	—
u_{16}	S(2)···S(3)	341.9(5)	11.2(3)	—	360.6(16)	13.6(9)	14.0(14)
u_{17}	S(2)···C(5)	404.6(34)	29.2(17)	26.0(26)	391.6(97)	32.7(28)	33.7(34)
u_{18}	Y(1)···H(6)	405.2(5)	11.5(fixed)	—	422.0(10)	12.3(fixed)	—
u_{19}	H(7)···H(10)	479.7(105)	57.1(fixed)	—	398.1(33)	70.7(fixed)	—
u_{20}	S(2)···H(11)	448.6(47)	35.7(fixed)	—	430.1(122)	42.9(fixed)	—
u_{21}	C(4)···H(10)	493.4(81)	48.3(fixed)	—	430.2(265)	60.6(fixed)	—
u_{22}	S(2)···H(9)	490.4(33)	30.3(fixed)	—	480.3(90)	38.4(fixed)	—
u_{23}	C(4)···C(5)	522.4(61)	35.7(34)	35.7(36)	475.5(207)	46.9(45)	46.4(46)
u_{24}	H(6)···H(10)	550.9(91)	57.6(fixed)	—	485.0(284)	71.2(fixed)	—

u_{25}	H(7)···H(11)	557.4(61)	44.2(fixed)	—	508.9(231)	55.1(fixed)	—
u_{26}	C(4)···H(11)	576.7(51)	34.6(fixed)	—	540.5(185)	43.6(fixed)	—
u_{27}	C(4)···H(9)	592.9(68)	44.4(fixed)	—	544.3(219)	56.3(fixed)	—
u_{28}	H(8)···H(11)	616.5(50)	34.3(fixed)	—	596.3(152)	40.9(fixed)	—
u_{29}	H(6)···H(9)	657.9(81)	55.8(fixed)	—	605.0(240)	69.4(fixed)	—
u_{30}	H(6)···H(11)	654.1(59)	42.3(fixed)	—	613.8(203)	52.6(fixed)	—

[a] Estimated standard deviations, as obtained in the least-squares refinement, are given in parentheses. [b] Amplitudes not refined were fixed at the values obtained using the force field calculated at MP2/LanL2DZ(d).

Figure 6 Experimental radial-distribution curve and experimental – theoretical difference curve for the refinement of $Se(SCH_3)_2$. Before Fourier inversion the data were multiplied by $s.\exp(-0.00002s^2)/(Z_{Se} - f_{Se})(Z_S - f_S)$.

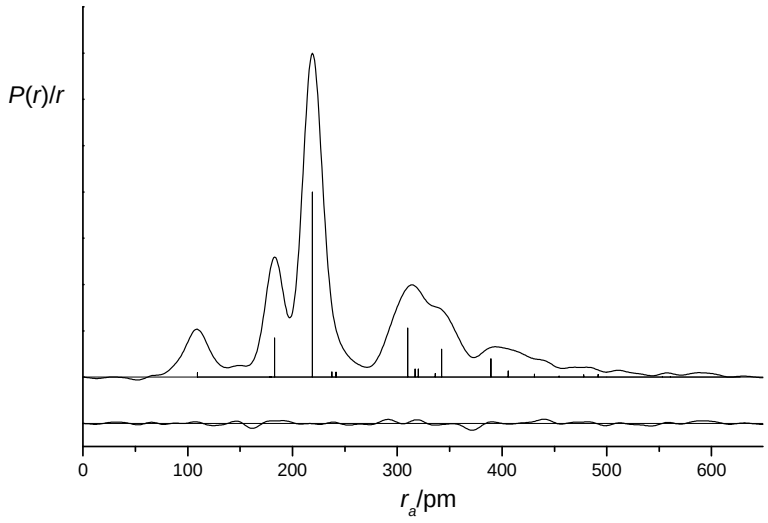

Figure 7 Experimental radial-distribution curve and experimental – theoretical difference curve for the refinement of $Te(SCH_3)_2$. Before Fourier inversion the data were multiplied by $s.\exp(-0.00002s^2)/(Z_{Te} - f_{Te})(Z_S - f_S)$.

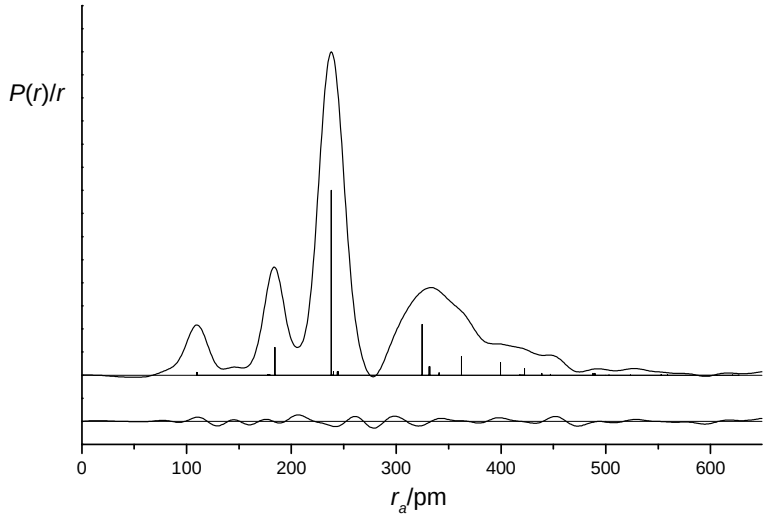

Figure 8 Experimental and difference (experimental – theoretical) molecular-scattering intensities for $Se(SCH_3)_2$.

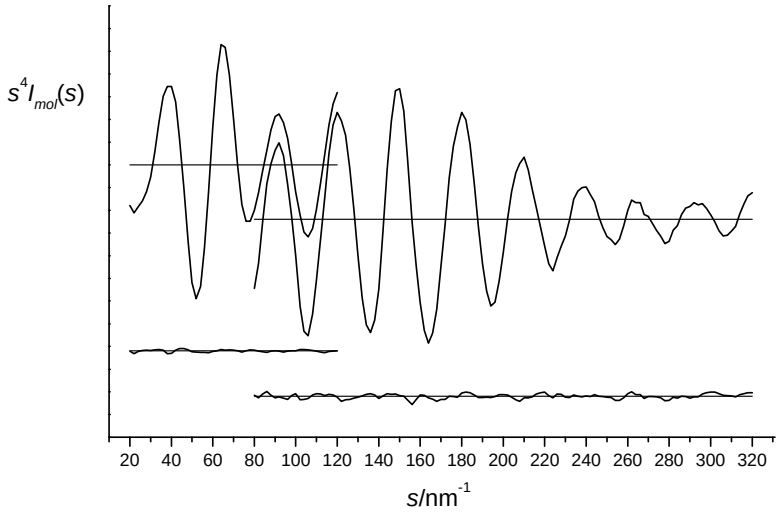

Figure 9 Experimental and difference (experimental – theoretical) molecular-scattering intensities for $Te(SCH_3)_2$.

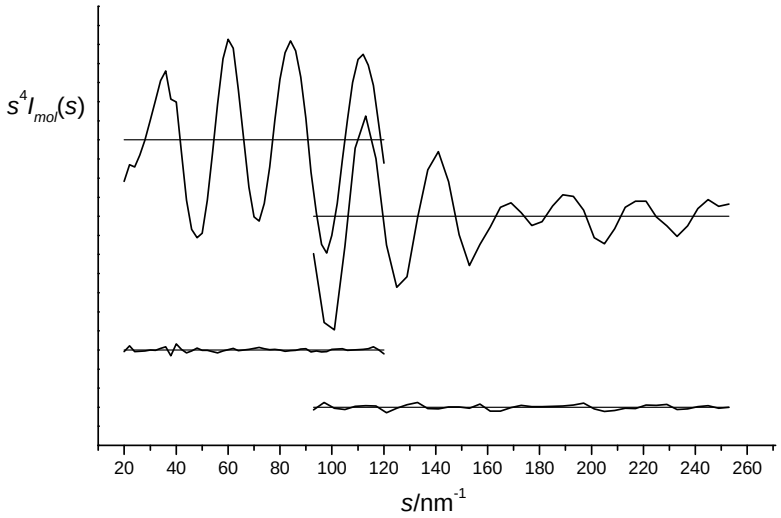

Table 5 Least-squares correlation matrix (×100) for $Se(SCH_3)_2$. [a]

	u_8	k_2
p_2	51	57
u_7	71	76
u_8		93

[a] Only elements with absolute values ≥ 50% are shown; k_2 is a scale factor.

Table 6 Least-squares correlation matrix (×100) for $Te(SCH_3)_2$. [a]

	p_5	p_6	k_1	k_2
p_1		–63		
p_4	63			
u_8			62	72

[a] Only elements with absolute values ≥ 50% are shown; k_1 and k_2 are scale factors.

5.4 Discussion

Comparison of the gas-phase structures of the three compounds $Y(SCH_3)_2$ (Y = S, Se, Te) reveals several differences between parameters that are common to all structures (Table 3). The length of the Y–S bond will, of course, increase upon moving down the group and this is indeed observed from the results of the GED experiments. Also, it can be seen that as Y becomes heavier, the S–C bond becomes longer (and, in this case, weaker) and so it is apparent that the strength of the Y–S bond increases at the cost of the S–C bond. The S–Y–S angles follow an expected trend, becoming smaller as Y becomes heavier. Such a trend has previously been noted, *e.g.* in the series H_2S (92.3°) > H_2Se (91°) > H_2Te (90°).[20] ∠Y–S–C decreases as well when Y becomes heavier, but the differences between angles with different Y atoms are smaller than in the case of ∠S–Y–S. All other common or comparable parameters of the compounds, *i.e.* *r*C–H, ∠S–C–H (mean), ϕS–Y–S–C, and ϕY–S–C–H, show no significant differences.

The crystal structures of $Se(SCH_3)_2$ and $Te(SCH_3)_2$ are interesting because they show that the two compounds have very different solid-state structures.[6,7] Unlike in the gas phase where both molecules appear to adopt a g^+g^+ conformation, $Te(SCH_3)_2$ exhibits a g^+g^- conformation in the crystal. The apparent reason for the different crystal structures is the weaker Lewis acidity of Se(II) compared to Te(II). The weaker intermolecular

interactions in the solid state that are exhibited by $Se(SCH_3)_2$ allow the g^+g^+ conformation to pack well, whereas for the stronger interactions between molecules of $Te(SCH_3)_2$ the opposite is the case.

In terms of geometry optimisation, the density functional method performs the least well for both $Se(SCH_3)_2$ and $Te(SCH_3)_2$, with the exception of the *r*S–C parameter, which is best reproduced at the B3LYP level. The best agreement between theory and experiment is found at the MP2 level.

5.5 References

1. P. E. Farup and R. Stølevik, *Acta Chem. Scand. Ser. A*, 1974, **28**, 680.
2. M. Liedtke, A. H. Saleck, K. M. T. Yamada, G. Winnewisser, D. Cremer, E. Kraka, A. Dolgner, J. Hahn and S. Dobos, *J. Phys. Chem.*, 1993, **97**, 11204.
3. J. Donohue and V. Schomaker, *J. Chem. Phys.*, 1948, **16**, 92.
4. Q. Shen, C. Wells and K. Hagen, *Inorg. Chem.*, 1998, **37**, 3895.
5. M. Gaensslen, R. Minkwitz, W. Molzbeck and H. Oberhammer, *Inorg. Chem.*, 1992, **31**, 4147.
6. H. Fleischer, S. Glang, N. W. Mitzel, D. Schollmeyer and M. Bühl, *Dalton Trans.*, 2004, 3765.
7. H. Fleischer, N. W. Mitzel and D. Schollmeyer, *Eur. J. Inorg. Chem.*, 2003, 815.
8. M. J. Frisch, G. W. Trucks, H. B. Schlegel, G. E. Scuseria, M. A. Robb, J. R. Cheeseman, V. G. Zakrzewski, J. A. Montgomery, Jr., R. E. Stratmann, J. C. Burant, S. Dapprich, J. M. Millam, A. D. Daniels, K. N. Kudin, M. C. Strain, O. Farkas, J. Tomasi, V. Barone, M. Cossi, R. Cammi, B. Mennucci, C. Pomelli, C. Adamo, S. Clifford, J. Ochterski, G. A. Petersson, P. Y. Ayala, Q. Cui, K. Morokuma, D. K. Malick, A. D. Rabuck, K. Raghavachari, J. B. Foresman, J. Cioslowski, J. V. Ortiz, B. B. Stefanov, G. Liu, A. Liashenko, P. Piskorz, I. Komaromi, R. Gomperts, R. L. Martin, D. J. Fox, T. Keith, M. A. Al-Laham, C. Y. Peng, A. Nanayakkara, C. Gonzalez, M. Challacombe, P. M. W. Gill, B. Johnson, W. Chen, M. W. Wong, J. L. Andres, C. Gonzalez, M. Head-Gordon, E. S. Replogle, and J. A. Pople, *Gaussian 98, Revision A.6*, Gaussian, Inc., Pittsburgh, PA, 1998.
9. C. Møller and M. S. Plesset, *Phys. Rev.*, 1934, **46**, 618.
10. A. D. Becke, *J. Chem. Phys.*, 1993, **98**, 5648.
11. C. Lee, W. Yang and R. G. Parr, *Phys. Rev. B: Condens. Matter*, 1988, **37**, 785.
12. J. S. Binkley, J. A. Pople and W. J. Hehre, *J. Am. Chem. Soc.*, 1980, **102**, 939; M. S. Gordon, J. S. Binkley, J. A. Pople, W. J. Pietro and W. J. Hehre, *J. Am. Chem. Soc.*, 1982, **104**, 2797; K. D. Dobbs and W. J. Hehre, *J. Comput. Chem.*, 1986, **7**, 359.

13. P. C. Hariharan and J. A. Pople, *Theor. Chim. Acta*, 1973, **28**, 213; M. M. Francl, W. J. Pietro, W. J. Hehre, J. S. Binkley, M. S. Gordon, D. J. DeFrees and J. A. Pople, *J. Chem. Phys.*, 1982, **77**, 3654; R. C. Binning Jr. and L. A. Curtiss, *J. Comp. Chem.*, 1990, **11**, 1206.
14. P. J. Hay and W. R. Wadt, *J. Chem. Phys.*, 1985, **82**, 270; W. R. Wadt and P. J. Hay, *J. Chem. Phys.*, 1985, **82**, 284; P. J. Hay and W. R. Wadt, *J. Chem. Phys.*, 1985, **82**, 299.
15. V. A. Sipachev, *J. Mol. Struct.* (*THEOCHEM*), 1985, **121**, 143; V. A. Sipachev, *J. Mol. Struct.*, 2001, **567**, 67.
16. C. M. Huntley, G. S. Laurenson and D. W. H. Rankin, *J. Chem. Soc., Dalton Trans.*, 1980, 954.
17. S. L. Hinchley, H. E. Robertson, K. B. Borisenko, A. R. Turner, B. F. Johnston, D. W. H. Rankin, M. Ahmadian, J. N. Jones and A. H. Cowley, *Dalton Trans.*, 2004, 2469.
18. A. W. Ross, M. Fink and R. Hilderbrandt, *International Tables for Crystallography*, ed. A. J. C. Wilson, Kluwer Academic Publishers, Dordrecht, Netherlands, 1992, vol. C, p.245.
19. A. J. Blake, P. T. Brain, H. McNab, J. Miller, C. A. Morrison, S. Parsons, D. W. H. Rankin, H. E. Robertson and B. A. Smart, *J. Phys. Chem.*, 1996, **100**, 12280; P. T. Brain, C. A. Morrison, S. Parsons and D. W. H. Rankin, *J. Chem. Soc., Dalton Trans.*, 1996, 4589; N. W. Mitzel and D. W. H. Rankin, *Dalton Trans.*, 2003, 3650.
20. N. Wiberg, *Hollemann-Wiberg, Lehrbuch der Anorganischen Chemie*, Walter de Gruyter, 101st ed., Berlin, New York, 1995.

Chapter Six

Gas-phase structures of aminodifluorophosphines determined using electron diffraction and computational techniques

6.1 Introduction

With advances in technological ability at relatively low costs, the use of computational methods for structure determination has grown rapidly in recent years. Information gained from performing *ab initio* calculations can be used in a number of different ways to improve upon structures previously determined by experiment alone. Local asymmetry within a molecular structure, often too subtle to be recognised in the past, may now be identified from optimised geometry calculations. Such calculations are useful for predicting the abundances of possible conformers from their relative energies. It is also possible to obtain theoretical harmonic force fields, thus allowing accurate amplitudes of vibration to be used in refinements and to derive vibrational correction terms.

The series of aminodifluorophosphines, $(PF_2)NRR'$ (R, R′ = H, CH_3, SiH_3, GeH_3, PF_2; see Figure 1 for a template structure), has been chosen as an example to show how the use of theoretical methods and gas-phase electron diffraction (GED) can combine to improve upon structures determined by GED alone, and can reveal structural patterns that might otherwise be missed.

Figure 1 Template for aminodifluorophosphines **1**–**8**. R = H for **1**, **3** and **8**, PF_2 for **2**, **5** and **7**, CH_3 for **4** and SiH_3 for **6**. R′ = PF_2 for **1** and **2**, CH_3 for **3** and **4**, SiH_3 for **5**, **6** and **8** and GeH_3 for **7**.

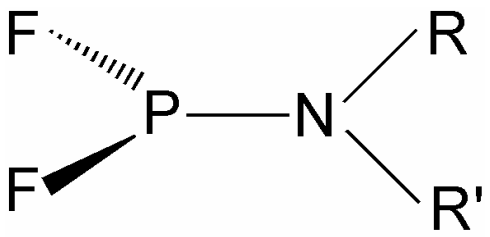

6.2 Experimental

6.2.1 *Ab initio* calculations

All calculations were performed using the Gaussian 98 suite of programs[1] on a Linux 12-processor Parallel Quantum Solutions (PQS) workstation.[2] In each case a thorough search of the potential-energy surface of the molecule was performed at the RHF/3-21G* and RHF/6-31G* levels of theory.[3,4] Allowing for complete rotation about each bond to nitrogen, all stable conformers were identified and calculations were continued to the MP2/6-311+G* level.[5] (All MP2 calculations were frozen core.) For molecules **1**–**8** the coordinates for the geometry calculated at the highest level are given in Tables 6.1–6.8, respectively, in the Electronic Appendix (EA).

For each molecule studied, a force field was calculated (RHF/6-31G*) to provide accurate amplitudes of vibration and vibrational correction terms for use in the refinement of the experimental data. The SHRINK program[6] was employed, using a more reliable curvilinear representation of atomic motions rather than a rectilinear approximation.

6.2.2 Gas-phase electron diffraction

In total, nine members of the aminodifluorophosphine family were revisited during the course of this work. The reanalysis of the GED structures was carried out using the original experimental data. Where necessary the molecular-scattering intensity curves were scanned from the journals and digitised using the UnGraph program.[7] This enabled sets of Cartesian coordinates describing the curves to be obtained and plotted to reconstruct the molecular-intensity curves.

The principles of the SARACEN (Structure Analysis Restrained by *Ab initio* Calculations for Electron diffractioN) method,[8] which is used in refinements throughout the preceding chapters, were also employed. Parameters that are poorly defined by the GED experiment tend to refine to chemically unreasonable values and SARACEN allows flexible restraints to be applied to such parameters, thus allowing their inclusion in the refinement. Each restraint consists of a value (often the starting value for the

parameter taken from the highest-level calculation) and an uncertainty (usually derived from the way that the parameter value differed through a series of calculations).

6.3 Results

Table 1 contains details (nozzle-to-plate distances, weighting functions, scale factors, correlation parameters and electron wavelengths) relating to the original electron diffraction experiments carried out on the eight compounds.

6.3.1 Bis(difluorophosphino)amine (1)

Calculations identified the presence of two conformers of $(PF_2)_2NH$, **1**, and the relative energies of these conformers at different levels of theory and with different basis sets are presented in Table 6.9 (EA). Conformer 1 was calculated to have C_{2v} symmetry and conformer 2 was calculated to have C_s symmetry. From the Boltzmann Law an energy difference of 1.4 kJ mol^{-1} would result in an abundance of 38% of conformer 1 and 64% of conformer 2. This takes into account the double multiplicity exhibited by conformer 2 because of its symmetry.

In order to complete the refinement for **1**, a model was written incorporating the geometries of both of the proposed conformers. The refinement of this combined model was used to determine the composition of the gas-phase sample in terms of conformers 1 and 2. The model was defined by thirteen independent geometric parameters and a weighting parameter to alter the composition of the mixture of conformers. These parameters are listed in Table 6.10 (EA). As the two N–P distances in conformer 1 were calculated to be the same through symmetry, and this length was shared by one of the two distances for conformer 2, a simple average of the two distinct distances and the difference between them were used in the model. For the P–F and N–H bond lengths and the F–P–F angles the values for both conformers were similar enough that a single mean value was assumed in each case when writing the model. In the case of the P–N–H angles, three different values were calculated. In order to describe these, the simple average of all three was taken along with difference 1 (largest – intermediate) and

difference 2 (largest – smallest). The three distinct angles were then described using the following equations:

for the largest angle, P–N–H = [average + {(difference 1)/3} + {(difference 2)/3}],

for the intermediate angle, P–N–H = [average – {2×(difference 1)/3} + {(difference 2)/3}],

and for the smallest angle, P–N–H = [average + {(difference 1)/3} – {2 × (difference 2)/3}].

This approach was also adopted for the N–P–F angles, where the calculations suggested three different values.

Figure 2 Gas-phase structures of all aminodifluorophosphines, **1**–**8**.

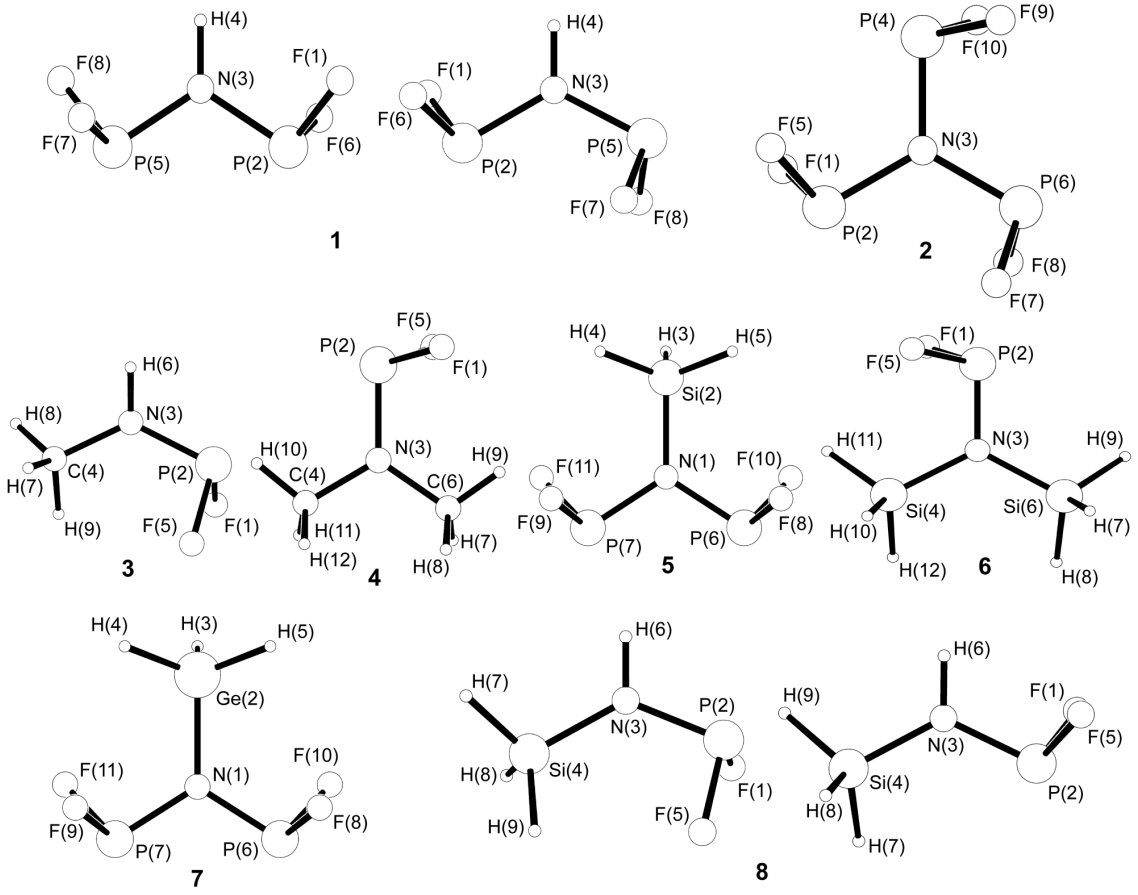

Table 1 Nozzle-to-plate distances (mm), weighting functions (nm^{-1}), scale factors, correlation parameters and electron wavelengths (pm) used in the electron diffraction studies of compounds **1**–**8**.

Compound	Nozzle-to-plate distance[a]	Δs	s_{min}	sw_1	sw_2	s_{max}	Scale factor[b]	Correlation parameter	Electron wavelength[c]
1	288.3	2	34	54	124	146	0.797(11)	0.469	5.719
	128.2	4	52	72	292	340	0.847(9)	0.126	5.707
2	580.0	2	20	32	80	98	0.504(5)	–0.206	5.847
	190.0	4	68	80	260	280	0.505(10)	0.125	5.852
3	500.0	2	28	48	134	156	1.590(14)	–0.014	5.673
	250.0	4	100	120	256	300	1.505(26)	–0.126	5.673
4	500.0	2	28	48	126	148	1.656(30)	0.136	5.791
	250.0	4	104	124	220	252	1.520(71)	–0.023	5.791
5	285.6	2	20	40	80	100	0.900(13)	0.446	5.854
	128.4	4	44	64	220	240	0.960(18)	0.348	5.854
6	284.3	2	24	44	122	144	0.727(13)	0.496	5.799
	128.5	4	60	80	220	260	0.806(14)	0.146	5.799
7	288.3	2	22	42	120	140	0.724(24)	0.442	5.811
	128.2	4	120	140	230	248	0.750(35)	0.363	5.811
8	500.0	2	32	52	122	144	1.327(13)	0.281	5.659
	250.0	4	100	120	200	240	1.324(33)	–0.066	5.659

[a] Determined by reference to the scattering pattern of benzene recorded immediately before or after the sample plates; values taken from the original studies. [b] Values in parentheses are the estimated standard deviations. [c] Values taken from the original studies.

Where differences between parameter values are extremely small, a tight restraint is often warranted and the SARACEN refinement will yield a value close to that of the restraint, and with an ESD close to the uncertainty of the restraints. For this reason mean values are used to describe situations where parameters lie very close in value and the "average and difference" method is used where values are more significantly different.

Two torsion parameters describing the positions of the difluorophosphine groups were also refined, one each for conformers 1 and 2. These torsions were defined as being in the same sense for the PF_2 groups in conformer 1 (*i.e.* the PF_2 groups move to opposite sides of the PNP plane allowing the molecule to distort from C_{2v} to C_2 symmetry) and in the opposite sense for conformer 2 (*i.e.* they move to the same side of the PNP plane for C_s symmetry). The independent parameters and amplitudes of vibration (Table 6.11, EA) were initially refined with a weighting of 0.5, signifying a 50 : 50 mixture of conformers 1 and 2. When the best fit was found for the model at this weighting, the composition was varied, using an *R*-factor loop in which the parameter was stepped by a given increment, to see how the fit was affected. In total thirteen parameters and nine amplitudes of vibration were refined, with flexible restraints applied to seven parameters and five amplitudes using the SARACEN method. Table 2 contains information relating to important geometric parameters.

Although the *ab initio* calculations had predicted symmetry of C_{2v} for conformer 1 and C_s for conformer 2, the refinement allowed the PF_2 groups to rotate and concluded that conformer 1 had C_2 symmetry and conformer 2 had C_1 symmetry (Figure 2).

The structures determined by GED in this work are of the type r_{h1}, in which corrections for curvilinear vibrational motions, calculated using the program SHRINK[6] are applied. Such structures differ from the equilibrium structures calculated *ab initio* only in the anharmonic terms, and in any motion for which the curvature is not modelled adequately by the first-order method used in SHRINK. Discrepancies between theory and experiment therefore arise primarily from one or both of these ways. This is quite possible for large-amplitude torsional motions, so in the molecular models used in the GED analysis, we allow the PF_2 group torsional angles to refine, and do not fix them exactly at the values calculated *ab initio*. The refined values do not therefore represent

any time average of deviations from the mean positions, but are merely fitting parameters, which take account of any deficiencies in the vibrational modelling.

For a composition with 46% of conformer 1 and 54% of conformer 2 present, the lowest R_G value of 0.040 was obtained. Figure 3 shows the radial-distribution curve and the theoretical – experimental difference curve for the joint refinement assuming the abundance of conformer 1 to be 46%. The least-squares correlation matrix for the final refinement is given in Table 6.12 (EA).

Figure 3 Experimental radial-distribution curve and theoretical – experimental difference curve for the refinement of $(PF_2)_2NH$, **1**, as a mixture of two conformers. Before Fourier inversion the data were multiplied by $s.\exp(-0.00002s^2)/(Z_P - f_P)(Z_F - f_F)$.

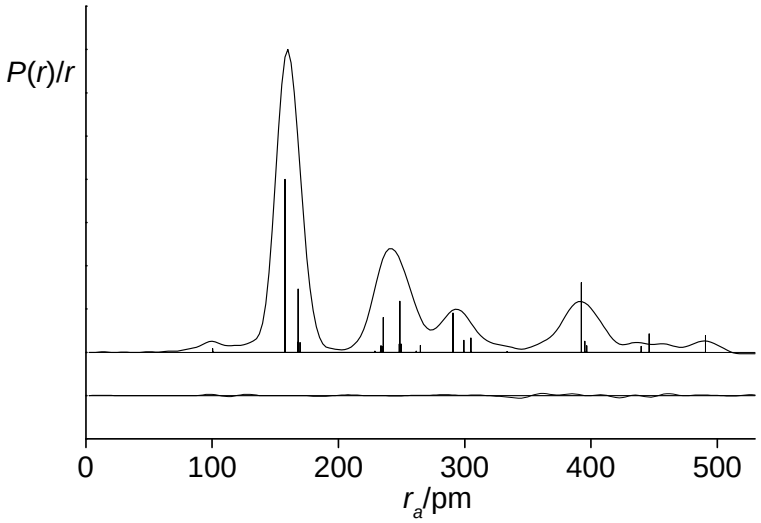

Table 2 Principal bond lengths, angles and torsions[a] for compounds **1**–**8** from new refinements (r_{h1}), the highest-level *ab initio* calculations (r_e) and the original refinements (r_a).

	1	**2**	**3**	**4**	**5**	**6**	**7**	**8**
New refinements, r_{h1}								
P–F	157.8(1)	156.4(1)	163.3(4)	159.2(4)	156.8(2)	158.5(3)	159.5(3)	159.3(2)[b,c]
			163.9(4)		157.2(2)	158.9(3)	160.0(3)	159.5(2)[b]
P–N	168.6(3)	169.2(3)	165.2(9)	164.9(11)	168.9(4)	166.1(11)	169.7(3)	168.0(9)
N–R[d]	102.0(13)	169.2(3)	100.8(19)	146.5(7)	168.9(4)	175.2(3)	169.7(3)	101.4(6)
N–R′[e]	168.6(3)[b]	169.2(3)	150.7(4)	146.5(7)	177.9(10)	176.6(3)	190.8(5)	175.6(7)[b]
	170.0(3)[c]							174.4(7)[c]
P–N–R[d]	121.3(5)[b]	120(fixed)	115.3(3)	120.6(7)	107.4(9)	119.2(5)	114.6(3)	112.1(10)[b]
	120.0(6)[c]							115.4(10)[c]
P–N–R′[e]	117.4(9)[b]	120(fixed)	127.5(6)	124.6(5)	121.9(3)	120.4(9)	122.7(1)	129.1(11)[b]
	122.5(7)[c]							125.9(8)[c]
R–N–R′[d,e]	121.3(5)[b]	120(fixed)	115.5(8)	114.8(10)	121.9(3)	120.4(10)	122.7(1)	115.4(10)[b]
	117.4(8)[c]							118.8(13)[c]
N–P–F	97.5(5)[b]	99.2(6)	99.1(7)	101.4(4)	101.8(4)	100.5(9)	100.9(4)	100.0(5)[b]
	97.3(9)[c]		102.0(7)		99.4(4)	102.1(7)	98.8(4)	98.4(6)[b]
	98.6(7)[c]							99.2(5)[c]
F–P–F	96.9(5)	98.1(9)	92.6(4)	95.3(5)	97.4(5)	96.3(4)	96.6(7)	95.4(5)
Theoretical, r_e								
P–F	161.2[b]	161.2	162.6	163.2	161.4	162.5	161.8	162.4[b,c]
	161.4[c]		163.2		161.8	162.9	162.3	162.6[b]
P–N	169.0	173.5	165.3	165.3	170.1	167.5	169.1	166.6
N–R[d]	102.1[b]	173.5	101.0	146.0	170.1	178.3	169.1	101.3[b]
	101.7[c]							101.8[c]
N–R′[e]	169.0[b]	173.5	146.5	146.0	181.7	178.8	193.6	177.3[b]
	170.4[c]							176.2[c]
P–N–R[d]	118.4[b]	120.0	115.3	120.3	114.8	119.4	116.2	112.4[b]
	114.4[c]							115.6[c]
P–N–R′[e]	123.3[b]	120.0	126.5	124.5	122.6	122.4	121.9	130.0[b]
	128.5[c]							126.4[c]
R–N–R′[d,e]	118.4[b]	120.0	116.6	115.2	122.6	118.1	121.9	117.6[b]
	117.1[c]							118.0[c]

N–P–F	98.8[b]	98.0	99.4	101.0	100.4	98.8	100.4	100.9[b]
	98.0[c]		101.6		97.7	101.3	97.9	99.3[b]
	99.5[c]							100.1[c]
F–P–F	95.2	95.9	93.3	92.8	95.5	94.6	95.0	94.2
Original refinements, r_a								
P–F	158.4(3)	157.4(2)	159.3(4)	158.9(3)	157.0(2)	158.5(3)	159.2(5)	157.4(3)
P–N	168.4(8)	171.2(4)	164.8(7)	164.8(8)	169.1(4)	168.0(4)	169.8(8)	165.7(7)
N–R[d]	97.3(23)	171.2(4)	100.0(fixed)	144.8(6)	169.1(4)	175.5(4)	169.8(8)	99.8
N–R′[e]	168.4(8)	171.2(4)	144.8(12)	144.8(6)	176.7(7)	175.5(4)	188.9(13)	172.0(8)
P–N–R[d]	—	120(fixed)	118.0(fixed)	118.3(6)	117.6(7)	—	114.0(8)	118.8
P–N–R′[e]	122.1(7)	120(fixed)	125.3(20)	118.3(6)	—	—	—	127.9(7)
R–N–R′[d,e]	—	120(fixed)	—	111.8(15)	—	120.0(15)	—	—
N–P–F	98.3(7)	99.0(4)	100.6(4)	97(4)	99.3(3)	99.4(7)	99.6(5)	95.6
F–P–F	95.6(10)	97.1(5)	94.1(8)	99(3)	96.1(5)	96.9(10)	96.5(11)	100.8(12)

[a] Distances are in pm, angles in degrees. The figures in parentheses are the estimated standard deviations of the last digits. [b] Conformer 1. [c] Conformer 2.[d] R = H for **1**, **3** and **8**, P for **2**, **5** and **7**, C for **4** and Si for **6**. [e] R′ = P for **1** and **2**, C for **3** and **4**, Si for **5**, **6** and **8** and Ge for **7**.

Figure 4 is a plot of the change in R_G value with change in the weighting of conformer 1. This plot can be used[9] to obtain an uncertainty associated with the weighting parameter. At a significance level of 95% (for which the R_G ratio is calculated to be 1.016), the abundance of conformer 1 is 46(3)%. This corresponds approximately to an ESD of 2%.

Figure 4 Variations of R_G with percentage of conformer 1 of $(PF_2)_2NH$, **1**.

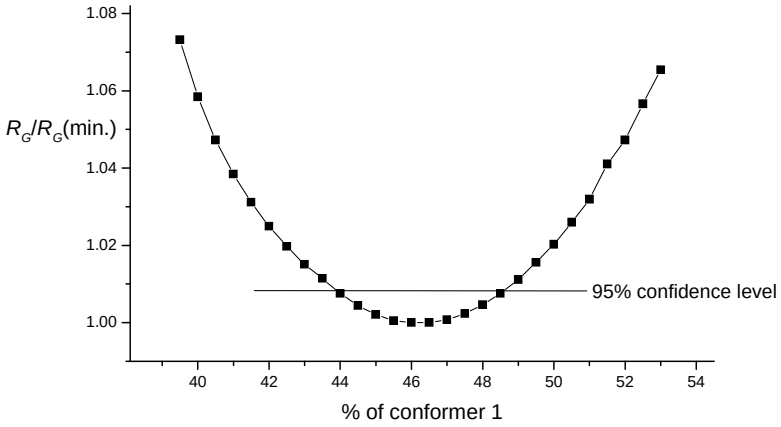

The original GED refinement[10] (R_G = 5.7%) agrees with this work in concluding that there were two distinct conformers of bis(difluorophosphino)amine. In that study, the predominant (lower-energy) form was found to be 72% abundant and had C_{2v} symmetry. In the higher-energy form, one PF_2 group was twisted about 60° away from the C_{2v} position. A study of the vibrational spectrum of this compound in the gas phase also predicted the presence of two conformers by showing two distinct N–H stretches and two N–H deformations.[11] The original refinement was, however, wrong to assume that the P–N–P angles in both conformers were identical. Calculations show that the angles differ by more than 5° between the conformers and one of the most significant improvements made to the refinement has been allowing the P–N–P angles to differ.

6.3.2 Tris(difluorophosphino)amine (2)

A search of the potential-energy surface of $N(PF_2)_3$, **2**, yielded a single conformer. The calculations found the molecule to have a planar nitrogen skeleton, in which all three

phosphorus lone pairs lie perpendicular to the axis of the nitrogen lone-pair orbital. The PF_2 ligands surrounding nitrogen are arranged in a *triskelion* manner (similar to that found on the flag of the Isle of Man) giving the molecule overall C_{3h} symmetry.

The structure of **2** was described in a model in terms of five independent geometric parameters, which are listed in Table 6.13 (EA). It was assumed that all PF_2 groups were identical and had a plane of symmetry and that the NP_3 motif was planar. The model allowed the PF_2 groups to twist away from their C_{3h} positions, all in the same direction, giving the molecule overall C_3 symmetry. All five parameters and nine amplitudes of vibration (Table 6.14, EA) were allowed to refine with four amplitudes requiring to be restrained using the SARACEN method. Table 2 shows the principal bond lengths, angles and torsion and compares these to the original refinement and the highest-level *ab initio* calculation. The gas-phase structure of **2** is shown in Figure 2.

The R_G value obtained for the refinement was 0.049. The goodness of fit can be seen in the experimental – theoretical difference curve shown in Figure 5. The least-squares correlation matrix for the final refinement is given in Table 6.15 (EA).

Figure 5 Experimental radial-distribution curve and theoretical – experimental difference curve for the refinement of $N(PF_2)_3$, **2**. Before Fourier inversion the data were multiplied by $s.\exp(-0.00002s^2)/(Z_P - f_P)(Z_F - f_F)$.

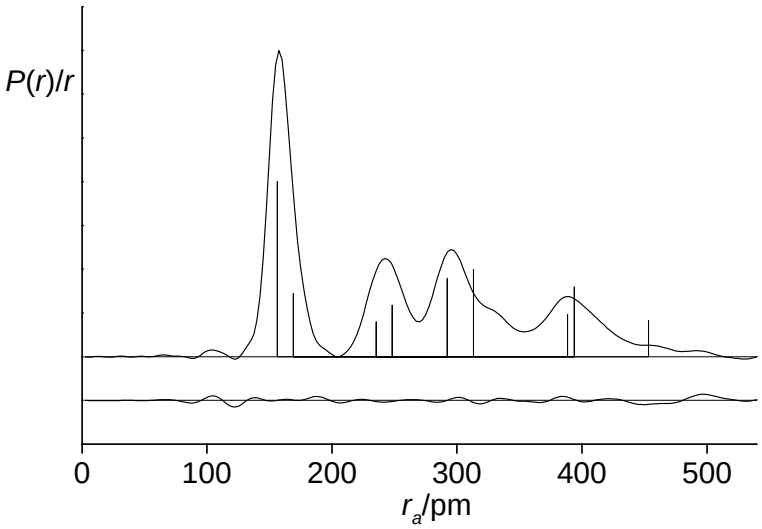

The original refinement,[12] with an R_G value of 0.080, agrees with this work that the molecule has a planar skeleton, which was also the case with the GED structure of the silicon analogue, trisilylamine.[13] A study of $N(PF_2)_3$ using various spectroscopic techniques (IR, Raman, NMR, mass and PE spectroscopies) could not provide a conclusive determination of the positions of the PF_2 groups and, therefore, the overall symmetry.[11] The authors "tentatively suggest" that a mixture of conformers, one with C_s symmetry and the other with C_3 symmetry, may have best fitted the spectroscopic data. This seems unlikely and the C_3 model favoured by GED appears to be more reasonable, with the PF_2 groups rotated slightly (~9°) from the C_{3h} position.

6.3.3 Methylaminodifluorophosphine (3)

Calculations at the RHF/6-31G* level gave rise to two conformers of $(PF_2)NH(CH_3)$, **3**. Both conformers were found to have a slightly pyramidal arrangement of ligands around the central nitrogen, with the total angle around N being approximately 358°. Both structures had C_1 symmetry and the main difference between the two was the orientation of the PF_2 group. In the lower-energy conformer, the fluorine atoms were positioned as far away from the amino hydrogen as possible, *i.e.* with the phosphorus lone pair of electrons approximately eclipsing the N–H bond; the opposite was found for the structure with higher energy, *i.e.* with the phosphorus lone pair *anti* with respect to the N–H bond. The differences in energy between the two conformers at various levels of theory and using different basis sets are shown in Table 6.16 (EA). The energy difference between the two conformers of 7.1 kJ mol^{-1} at the highest level of calculation means that the higher-energy one is likely to be found in a very low abundance in a gas-phase sample. A Boltzmann distribution analysis estimates that the conformer will contribute only around 5% of a gas sample at 296 K. For this reason, a single-conformer refinement was performed for the structure shown in Figure 2.

A model was written describing the geometry of **3** in terms of sixteen independent parameters, listed in Table 6.17 (EA). These parameters include six bond lengths and differences, six angles and differences, and a parameter describing the twist of the PF_2 group away from the position where the P–F(5) bond eclipses the C–N bond. There is

also a parameter for the torsion of the methyl group, about its C–N bond, where the zero position is where the C–H(7) bond eclipses the N–H bond and a positive value is taken as a rotation in the clockwise direction while viewing from N to C. The tilt of the methyl group, so that the centroid of the H···H···H triangle lies either above or below the CNP plane, and where a negative value indicates a move to the opposite side of the plane to the apex of the pyramid, is also included. Lastly there is the parameter describing the drop from the PNC plane of H(6) to make the molecule slightly pyramidal.

Sixteen independent parameters and seven amplitudes of vibration (Table 6.18, EA) were refined, with eight parameters and four amplitudes being restrained using the SARACEN method to prevent them refining to chemically unreasonable values. Table 2 contains details of the principal bond lengths, angles and torsions. The value obtained for the R_G factor was 0.039 and this small value is reflected in the smoothness of the experimental – theoretical difference curve in Figure 6. The least-squares correlation matrix for the final refinement is shown in Table 6.19 (EA).

Figure 6 Experimental radial-distribution curve and theoretical – experimental difference curve for the refinement of $(PF_2)NH(CH_3)$, **3**. Before Fourier inversion the data were multiplied by $s.\exp(-0.00002s^2)/(Z_P - f_P)(Z_F - f_F)$.

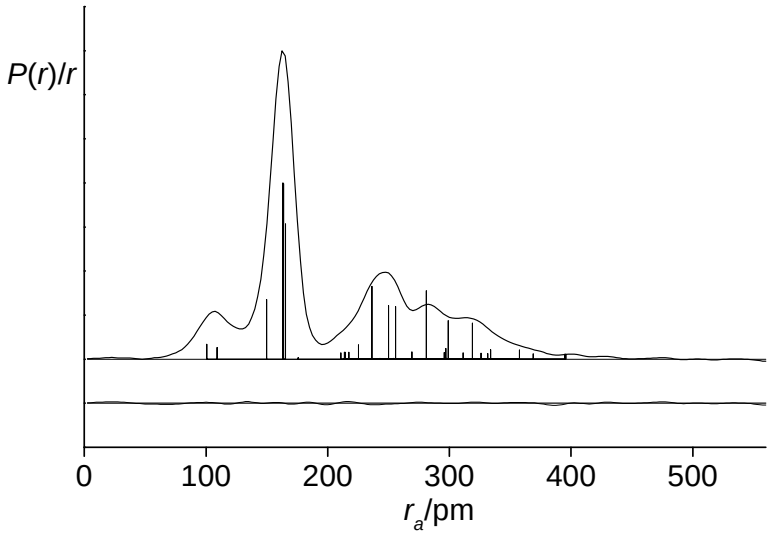

The original refinement[14] failed to quote a value for R_G and it was suspected that the molecule had coplanar bonds to the central nitrogen. This seems to be wrong based on our calculations and refinement. As the infrared spectrum showed two N–H stretches, it was suggested that there were two conformers of **3** present in the sample. However, the intensities of these stretches are in the ratio 10 : 1 and we now believe that any second conformer would be so much higher in energy that it would be unlikely to be observed in the GED experiment, which is unreliable for the determination of amounts less than approximately 20%.

6.3.4 Dimethylaminodifluorophosphine (4)

A thorough search for conformers of $(PF_2)N(CH_3)_2$, **4**, showed only one structure, with overall C_s symmetry and bonds to nitrogen that are coplanar.

Based on calculations (MP2/6-311+G*), a model was written to describe the geometry of the molecule with C_s symmetry in terms of thirteen independent geometric parameters, comprising five bond lengths and differences, five bond angles and three torsion parameters, as shown in Table 6.20a (EA). It was assumed that the $N(CH_3)$ groups had C_{3v} local symmetry and that the PF_2 group had a plane of symmetry. A microwave spectrum[15] for $(PF_2)N(CH_3)_2$ had been recorded and rotational constants, corrected using SHRINK, were included in the refinement as extra data. The refinement was repeated, this time excluding the rotational constants. Although the structure itself changes very little (see Table 6.20b, EA), parameters become less well defined and a need arises to restrain additional torsion parameters, thereby substituting experimental data for theoretical. In particular, the torsion on the PF_2 group is well defined when the microwave data are included but much less so without them. The methyl torsions both show very large ESDs implying that there is little information about their values.

In total thirteen parameters and ten amplitudes of vibration were refined. (For full details see Table 6.21, EA.) Flexible restraints were applied to four parameters and to six amplitudes. Table 2 lists important bond lengths, angles and torsion angles from the least-squares refinement and the molecular structure is shown in Figure 2. The refinement achieved an R_G value of 0.097 with the worst fitting of data coming at longer

distances. The radial-distribution curve and associated experimental – theoretical difference curve are shown in Figure 7. The least-squares correlation matrix for the final refinement is shown in Table 6.22 (EA). For the refinement that was undertaken without the rotational constants, an R_G value of 0.087 was achieved. Despite this modest improvement, we believe that the refinement that includes extra experimental data is better.

Figure 7 Experimental radial-distribution curve and theoretical – experimental difference curve for the refinement of $(PF_2)N(CH_3)_2$, **4**. Before Fourier inversion the data were multiplied by $s.\exp(-0.00002s^2)/(Z_P - f_P)(Z_F - f_F)$.

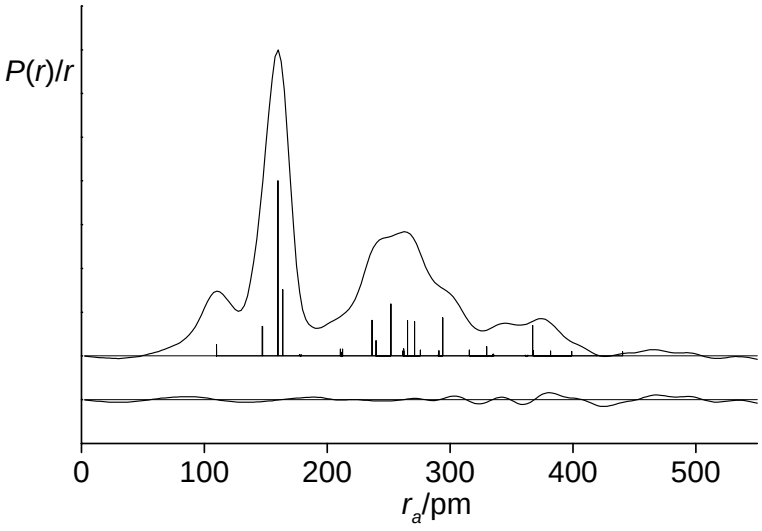

The original GED refinement[16] for **4** gave an R_G value of 0.12 for a structure that was non-planar. (The total angle around N was thought to be 348.4°.) This is in contrast to the microwave structure[15] and an X-ray analysis of the solid phase,[17] both of which show planar structures, as did our calculations and refinement. To probe how easily **4** can become non-planar, calculations were performed (MP2/6-311+G*) where the geometry of the molecule was optimised as the C–N–P–C torsion angle was stepped from 140° to 220°. The torsion angle of 180° represents a molecule that is planar about the nitrogen atom and the most extreme cases correspond to molecules where the sum of the angles at

N was 347°. It was found that while the potential for C–N–P–C was very shallow within 30° of 180° (ΔE = 0.3 kJ mol^{-1}) the energy rose sharply for narrower angles.

6.3.5 Bis(difluorophosphino)silylamine (5)

A search for possible conformers of $(PF_2)_2N(SiH_3)$, **5**, resulted in two structures whose energies differed by 5.3 kJ mol^{-1} (MP2/6-311+G*; see Table 6.23, EA for all energies). Both structures exhibit planar nitrogen centres and differ mainly in the twist of the PF_2 groups. The lower-energy conformer 1 was calculated with C_s symmetry and has the phosphorus lone pairs of electrons pointing towards each other, with the fluorine atoms in the direction of the silyl hydrogens. The higher-energy structure (conformer 2) had C_1 symmetry, with one PF_2 group rotated through 180° from the position seen in the lower-energy conformer. For an energy difference of 5.3 kJ mol^{-1}, a Boltzmann analysis suggests that the composition of a gas-phase sample at the experimental temperature (293 K) will be 95% conformer 1 and 5% conformer 2.

Initially, a model was written to describe **5** in terms of both conformers with a weighting parameter to change the composition of the mixture. However, as it became apparent that the best fit to the experimental data occurred when none of the higher-energy conformer was included, we reverted to a single-conformer model of the C_s-symmetry structure. The model was described in terms of five bond lengths and differences, five angles and differences and two torsion parameters, one each for the PF_2 and silyl twists (see Table 6.24, EA, for a full parameter list). It was assumed that the $N(SiH_3)$ group had local C_{3v} symmetry and that the two PF_2 groups were identical. In total twelve parameters and fourteen amplitudes of vibration (Table 6.25, EA) were refined. Flexible restraints were applied to three parameters and to six amplitudes. The principal refined parameters are listed in Table 2.

The outcome of the refinement for **5** was an R_G value of 0.041 and the structure is shown in Figure 2. The radial-distribution curve, with its associated difference curve (Figure 8), also shows the goodness of fit and suggests that it was indeed correct to ignore the contribution of any other conformer. Table 6.26 (EA) shows the least-squares correlation matrix for the final refinement.

The original refinement,[18] with an R_G value of 0.06, agreed with this study that **5** consists of a single conformer of C_s symmetry.

Figure 8 Experimental radial-distribution curve and theoretical – experimental difference curve for the refinement of $(PF_2)_2N(SiH_3)$, **5**. Before Fourier inversion the data were multiplied by $s.\exp(-0.00002s^2)/(Z_P - f_P)(Z_F - f_F)$.

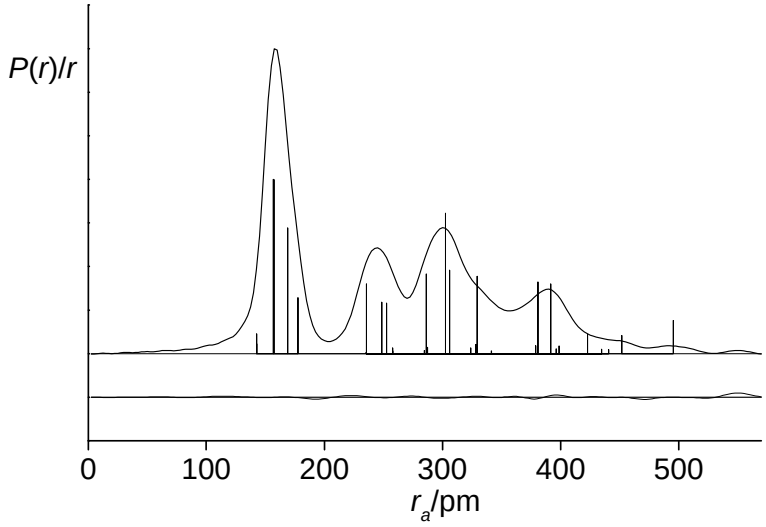

6.3.6 Difluorophosphino(disilyl)amine (6)

A single conformer of $(PF_2)N(SiH_3)_2$, **6**, (Figure 2) was calculated to have C_1 symmetry, having two distinct P–F distances and silyl groups that were twisted to different degrees, therefore precluding C_s symmetry. A model was written describing the structure in terms of fifteen independent geometric parameters, comprising six bond lengths and differences, six bond angles and differences and three torsion parameters, one for each of the silyl groups and one for the PF_2 group. (These are listed in Table 6.27, EA.) The N–Si distances and the P–N–Si and N–P–F angles are defined in terms of an average value and a difference. This results in no symmetry being implied for the molecule as a whole, although the $N(SiH_3)$ groups are defined to possess local C_{3v} symmetry, a good approximation. The silyl torsion parameters are the rotations of the respective groups about their Si–N axes from zero-torsion positions where the Si(4)–H(12) bond for

$Si(4)H_3$ and the Si(6)–H(8) bond for $Si(6)H_3$ eclipse the opposite N–Si bonds. A positive value is defined as rotation in the clockwise direction as viewed from Si to N.

In total fifteen parameters and ten amplitudes of vibrations (Table 6.28, EA) were refined. Flexible restraints were applied to five parameters and to four amplitudes of vibration. Table 2 contains the principal parameters associated with the structure of **6**.

The outcome of the final refinement for $(PF_2)N(SiH_3)_2$ was an R_G value of 0.031. The radial-distribution curve (Figure 9) with its associated difference curve also shows the goodness of the final fit. The least-squares correlation matrix for the final refinement is given in Table 6.29 (EA). The original refinement[18] concluded that the R_G value was 0.08, with the proposed structure in good agreement with that determined here.

Figure 9 Experimental radial-distribution curve and theoretical – experimental difference curve for the refinement of $(PF_2)N(SiH_3)_2$, **6**. Before Fourier inversion the data were multiplied by $s.\exp(-0.00002s^2)/(Z_{Si} - f_{Si})(Z_F - f_F)$.

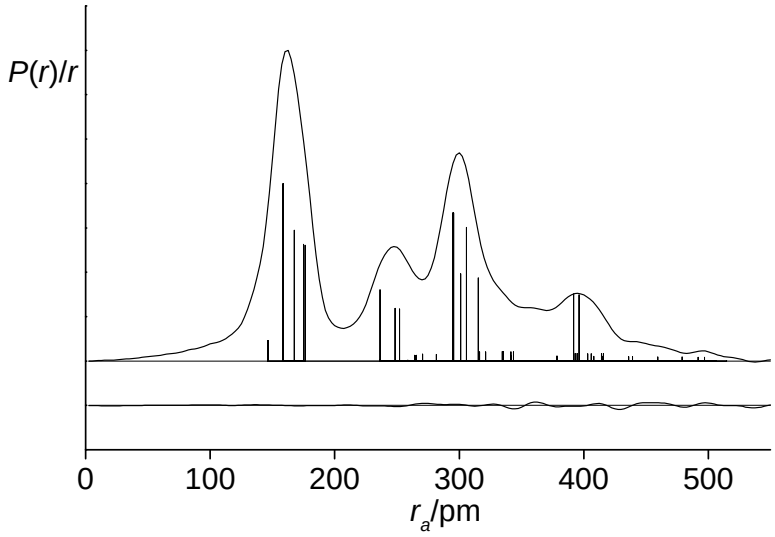

6.3.7 Bis(difluorophosphino)germylamine (7)

An extensive search of the potential-energy surface of $(PF_2)_2N(GeH_3)$, **7**, resulted in the identification of two conformers. A lower-energy conformer with overall C_s symmetry (conformer 1) is close to C_{2v} symmetry for the $GeN(PF_2)_2$ group, while the higher-energy conformer with C_1 symmetry, has one PF_2 group rotated approximately 180°

from the position in conformer 1. The two conformers have significantly different energies (Table 6.30, EA). At the MP2/6-311+G* level, the energy difference between the two conformers was found to be 7.8 kJ mol^{-1}. This corresponds to an composition of approximately 98% conformer 1 and 2% conformer 2, recognising that conformer 1 has a double multiplicity.

The model used for the refinement of **7** therefore described only the C_s-symmetry conformer, in terms of twelve independent parameters (Table 6.31, EA). All twelve independent parameters and twelve significant amplitudes of vibration (Table 6.32, EA) were refined, with flexible restraints applied to five geometric parameters and four amplitudes. Principal parameters are listed in Table 2.

The refinement for **7** revealed the structure shown in Figure 2, with an R_G value of 0.047. The radial-distribution curve and its associated difference curve (Figure 10) show the goodness of fit and the least-squares correlation matrix is shown in Table 6.33 (EA).

The outcome of the original refinement[19] was an R_G value of 0.12. Although the structures obtained from that study and this are very similar, a better fit to the data was produced by removing some of the data from the longer nozzle-to-plate set because there was poor overlap between the data sets.

Figure 10 Experimental radial-distribution curve and theoretical – experimental difference curve for the refinement of $(PF_2)_2N(GeH_3)$, **7**. Before Fourier inversion the data were multiplied by $s.\exp(-0.00002s^2)/(Z_{Ge} - f_{Ge})(Z_F - f_F)$.

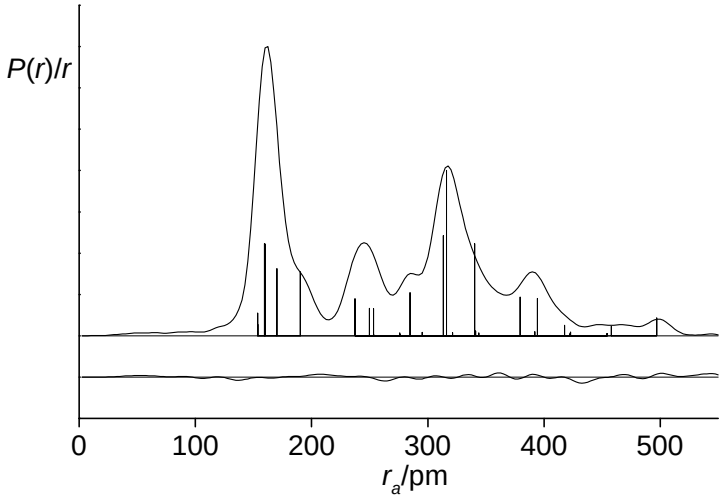

6.3.8 Silylaminodifluorophosphine (8)

An extensive search of the potential-energy surface of $(PF_2)NH(SiH_3)$, **8**, revealed the presence of two conformers (Figure 2), the relative energies of which are shown in Table 6.34 (EA). Conformer 1 was calculated to have C_1 symmetry and conformer 2 to have C_s symmetry. A Boltzmann analysis of the composition of the sample at the experimental temperature (273 K) indicates that an energy difference of 0.5 kJ mol^{-1} will result in a sample composed of 71% of conformer 1 and 29% of conformer 2, allowing for the double multiplicity of conformer 2.

A model was written incorporating the geometries of both of the proposed conformers. The refinement of this combined model would be used to determine the composition of the gas-phase sample in terms of conformers 1 and 2. The joint model was defined by 23 independent geometric parameters and a conformer-weighting parameter. (Full details are given in Table 6.35, EA.) To account for the major differences between the two conformers, average values and differences were used for most of the bond-length and angle parameters. Two torsion parameters describing the positions of the difluorophosphine groups were also refined, one each for conformers 1 and 2. The parameters and amplitudes (Table 6.36, EA) were initially refined with a weighting of 0.5, signifying a 50 : 50 mixture of conformers 1 and 2. When the best fit had been found for the model at this weighting, the composition was varied, using an *R*-factor loop in which the parameter was stepped by a given increment, to see how the fit was affected. An uncertainty associated with the refined percentage of conformer 1 was obtained[9] from Figure 11. At a significance level of 95% (for which the R_G ratio is calculated to be 1.016), the abundance of conformer 1 is 54(+2/–5)%. The principal bond lengths, angles and torsions for **8** are given in Table 2.

For a composition with 54% of conformer 1 and 46% of conformer 2 present, the lowest R_G value of 0.049 was obtained. Figure 12 shows the radial-distribution curve and the theoretical – experimental difference curve for the joint refinement assuming the abundance of conformer 1 to be 54%. A least-squares correlation matrix is given in Table 6.37 (EA).

The original GED refinement[20] gave an R_G value of 0.098 and was interpreted in terms of two conformers, similar to those in this discussion.

Figure 11 Variations of R_G with percentage of conformer 1 of $(PF_2)NH(SiH_3)$, **8**.

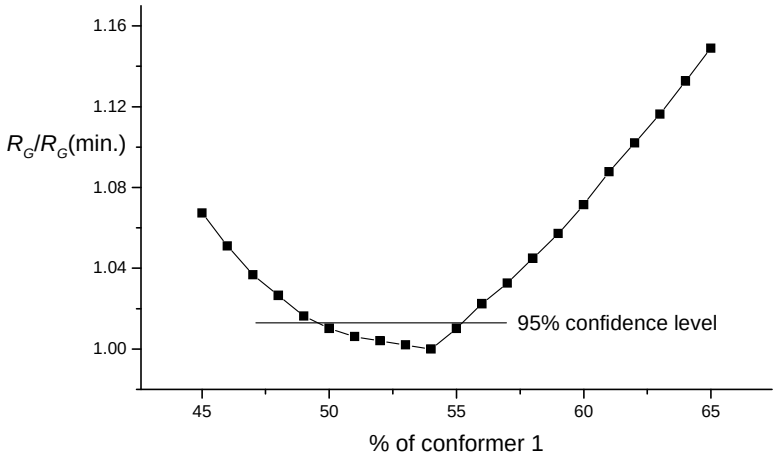

Figure 12 Experimental radial-distribution curve and theoretical – experimental difference curve for the refinement of $(PF_2)NH(SiH_3)$, **8**, as a mixture of two conformers. Before Fourier inversion the data were multiplied by $s.\exp(-0.00002s^2)/(Z_P - f_P)(Z_F - f_F)$.

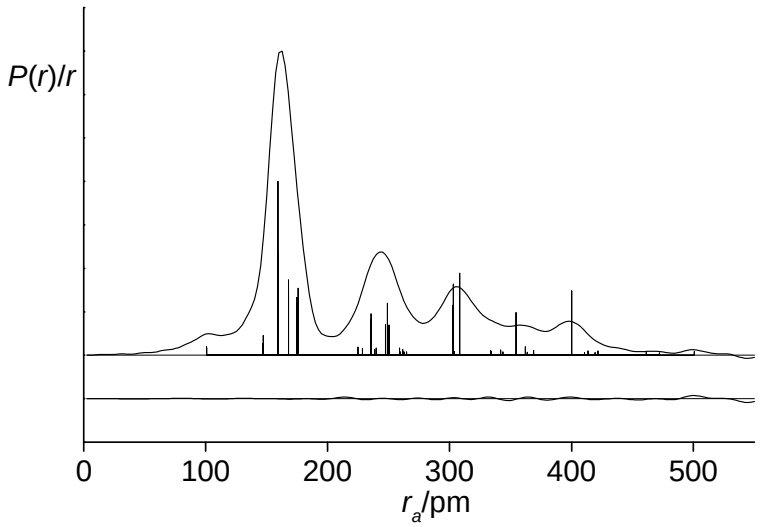

6.4 Discussion

It was clear from studying the original gas-phase structures of the eight aminodifluorophosphines that, while they mostly achieved the same conformations that we have found in this work, numerous assumptions had been made. The use of structures calculated *ab initio* and, consequently, the SARACEN method of restraining parameters, rather than fixing them, has allowed more complete structure determinations. Figure 13 shows the improvement in the R_G values for seven of the eight compounds that were revisited and the average value has dropped from approximately 8.8% to 5.1%. The case of $(PF_2)NH(CH_3)$, **3**, has been omitted because the R_G value for the original refinement was not published. Another benefit of the inclusion of the new methods was a general lowering of the uncertainties associated with the refined parameter values. As a result, the structures are more precise than those previously published.

Figure 13 Comparison of original and new *R* factors for all compounds except **3**, for which no original *R* factor was recorded.

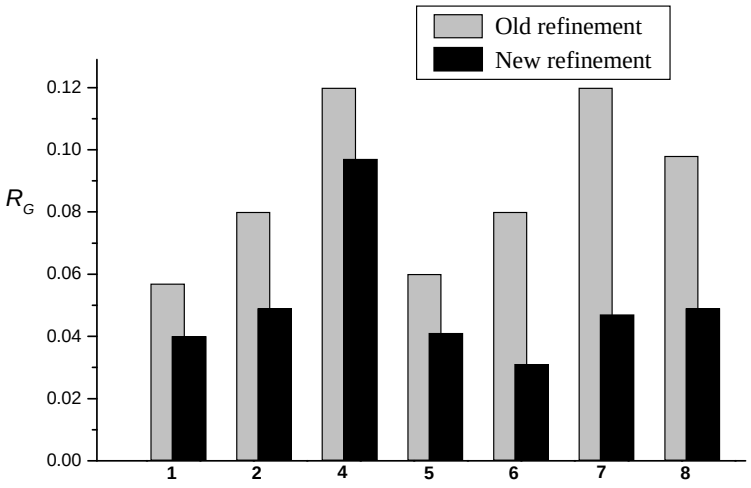

From consulting Table 2, trends can be observed in some of the bond lengths common to all the r_{h1} structures. In some instances, these trends were obscured by inaccuracies or uncertainties in the original structures. $N(PF_2)_3$, **2**, with only the three difluorophosphine

groups attached to the central nitrogen atom, is a good compound to use as a reference. The N–P bonds in **2** are, at 173.5 pm, longer than in any of the other molecules except $(GeH_3)N(PF_2)_2$, **7**. $N(PF_2)_3$ also displays some of the shortest P–F bonds seen in the series of compounds. Conversely, the four compounds that contain only one difluorophosphine group have amongst the longest P–F bond lengths and have values for the N–P bond distance that are up to 4 pm shorter than those found in **2**. These findings are consistent with the nitrogen lone pair of electrons delocalising onto P. The PF_2 groups will compete for the lone pair of electrons and so we see longer P–N bonds for molecules with more PF_2 groups. It is also noticeable that long P–N bonds in a molecule correlate with shorter P–F bonds.

All of the structures determined are either planar at N or deviate from planarity by only a few degrees. It is therefore valid to say that, in all cases, the lone pair of electrons on the nitrogen will lie at approximately 90° to the P–N bonds. It is also reasonable to say that the phosphorus lone pair will lie on the inverse of the centroid of the N···F···F triangle, as described in the method of Hinchley *et al.*[21] Thus, a value can be calculated that corresponds to the dihedral angle formed between the nitrogen lone pair (Nlp) and that on the phosphorus (Plp). These values for ϕNlp–N–P–Plp are given in Table 3 and the values around 90° indicate orthogonality between the lone pairs. As the lone pairs of electrons are not experimentally observable, and approximations have been made, no uncertainty has been quoted for any of the Nlp–N–P–Plp dihedral angles.

Table 3 Experimentally derived torsional angles[a] describing the position of the PF_2 groups in terms of the phosphorus lone pair of electrons in relation to the nitrogen lone pair (see text for full definition).

Compound	Conformer	Torsional angle
$(PF_2)_2NH$	1	74.3
	2	89.1 [P(2)] and 89.3 [P(5)]
$N(PF_2)_3$		81.3 (all)
$(PF_2)NH(CH_3)$		71.4
$(PF_2)N(CH_3)_2$		86.5
$(PF_2)_2N(SiH_3)$		80.4 (both)
$(PF_2)N(SiH_3)_2$		84.1
$(PF_2)_2N(GeH_3)$		80.1 (both)
$(PF_2)NH(SiH_3)$	1	61.6
	2	86.1

[a] Angles in degrees.

6.5 References

1. M. J. Frisch, G. W. Trucks, H. B. Schlegel, G. E. Scuseria, M. A. Robb, J. R. Cheeseman, V. G. Zakrzewski, J. A. Montgomery, Jr., R. E. Stratmann, J. C. Burant, S. Dapprich, J. M. Millam, A. D. Daniels, K. N. Kudin, M. C. Strain, O. Farkas, J. Tomasi, V. Barone, M. Cossi, R. Cammi, B. Mennucci, C. Pomelli, C. Adamo, S. Clifford, J. Ochterski, G. A. Petersson, P. Y. Ayala, Q. Cui, K. Morokuma, D. K. Malick, A. D. Rabuck, K. Raghavachari, J. B. Foresman, J. Cioslowski, J. V. Ortiz, A. G. Baboul, B. B. Stefanov, G. Liu, A. Liashenko, P. Piskorz, I. Komaromi, R. Gomperts, R. L. Martin, D. J. Fox, T. Keith, M. A. Al-Laham, C. Y. Peng, A. Nanayakkara, C. Gonzalez, M. Challacombe, P. M. W. Gill, B. Johnson, W. Chen, M. W. Wong, J. L. Andres, C. Gonzalez, M. Head-Gordon, E. S. Replogle, and J. A. Pople, *Gaussian 98, Revision A.7*, Gaussian, Inc., Pittsburgh, PA, 1998.
2. Parallel Quantum Solutions, Fayetteville, AR, USA.
3. J. S. Binkley, J. A. Pople and W. J. Hehre, *J. Am. Chem. Soc.*, 1980, **102**, 939; M. S. Gordon, J. S. Binkley, J. A. Pople, W. J. Pietro and W. J. Hehre, *J. Am. Chem. Soc*., 1982, **104**, 2797; W. J. Pietro, M. M. Francl, W. J. Hehre, D. J. DeFrees, J. A. Pople and J. S. Binkley, *J. Am. Chem. Soc.*, 1982, **104**, 5039.
4. W. J. Hehre, R. Ditchfield and J. A. Pople, *J. Chem. Phys.*, 1972, **56**, 2257; P. C. Hariharan and J. A. Pople, *Theor. Chim. Acta*, 1973, **28**, 213; M. S. Gordon, *Chem. Phys. Lett*., 1980, **76**, 163.
5. A. D. McLean and G. S. Chandler, *J. Chem. Phys.*, 1980, **72**, 5639; R. Krishnan, J. S. Binkley, R. Seeger and J. A. Pople, *J. Chem. Phys.*, 1980, **72**, 650.
6. V. A. Sipachev, *J. Mol. Struct.* (*THEOCHEM*), 1985, **121**, 143.
7. UnGraph, Version 4.0, Biosoft® Professional Software, Inc.
8. A. J. Blake, P. T. Brain, H. McNab, J. Miller, C. A. Morrison, S. Parsons, D. W. H. Rankin, H. E. Robertson and B. A. Smart, *J. Phys. Chem.*, 1996, **100**, 12280; P. T. Brain, C. A. Morrison, S. Parsons and D. W. H. Rankin, *J. Chem. Soc., Dalton Trans.*, 1996, 4589; N. W. Mitzel and D. W. H. Rankin, *Dalton Trans.*, 2003, 3650.
9. W. C. Hamilton, *Acta Crystallogr*., 1965, **18**, 502.

10. C. M. Huntley, G. S. Laurenson and D. W. H. Rankin, *J. Chem. Soc., Dalton Trans.*, 1980, 954.
11. D. E. J. Arnold and D. W. H. Rankin, *J. Chem. Soc., Dalton Trans.*, 1975, 889.
12. D. E. J. Arnold, D. W. H. Rankin, M. R. Todd and R. Seip, *J. Chem. Soc., Dalton Trans.*, 1979, 1290.
13. K. Hedberg, *J. Am. Chem. Soc.*, 1955, **77**, 6491; B. Beagley and A. R. Conrad, *J. Chem. Soc., Faraday Trans.*, 1970, 2740.
14. G. S. Laurenson and D. W. H. Rankin, *J. Mol. Struct.*, 1979, **54**, 111.
15. P. Forti, D. Damiani and P. G. Favero, *J. Am. Chem. Soc.*, 1973, **95**, 756.
16. G. C. Holywell, D. W. H. Rankin, B. Beagley and J. M. Freeman, *J. Chem. Soc. A*, 1971, 785.
17. E. D. Morris, Jr. and C. E. Nordman, *Inorg. Chem.*, 1969, **8**, 1673.
18. G. S. Laurenson and D. W. H. Rankin, *J. Chem. Soc., Dalton Trans.*, 1981, 425.
19. G. S. Laurenson and D. W. H. Rankin, *J. Chem. Soc., Dalton Trans.*, 1981, 1047.
20. D. E. J. Arnold, E. A. V. Ebsworth, H. F. Jessop and D. W. H. Rankin, *J. Chem. Soc., Dalton Trans.*, 1972, 1681.
21. S. L. Hinchley, H. E. Robertson, D. W. H. Rankin and W.-W. du Mont, *J. Chem. Soc., Dalton Trans.*, 2002, 378.

Chapter Seven

Towards equilibrium structures in crystals

7.1 Introduction

Equilibrium structures, *i.e.* structures such as those in a theoretical vibrationless state at the bottom of a potential energy well, are the ultimate goal of the structural chemist. Equilibrium structures are also what we calculated using *ab initio* and DFT calculations in the preceding chapters in this thesis.

In the field of gas-phase structure determination a lot of research has been done, in many different groups around the world, to determine corrections that, when applied to experimental distances, will yield values for geometrical parameters as close as possible to the equilibrium values. As shown in Chapter 1, distances obtained from gas-phase electron diffraction (GED) are vibrationally averaged and one of the fundamental corrections made to GED structures accounts for the artificial shortening of non-bonded distances caused by vibrations.

Vibrational averaging of distances is not a phenomenon that is unique to gas-phase structure determination. In crystals vibrations take place within molecules and, additionally, there is motion of molecules relative to one another, known as libration.

It has long been recognised that when the motions of two atoms in a crystal are very different the bond length between them appears shorter than its equilibrium value.[1] As was the case for gas-phase structures, attempts have been made to account for this effect. As early as 1956 Cruickshank published equations for determining the anisotropic thermal motions of individual atoms in crystals by three-dimensional Fourier refinement methods.[2] In 1964 Busing and Levy determined estimates of corrections for thermal effects by calculating the mean separations of pairs of atoms rather than estimating the equilibrium positions of individual atoms.[3] More recently attempts have been made to account for the effects of motion in crystals by Jeffrey and Ruble *et al*. They derived correction terms experimentally from comparison of the components of the thermal ellipsoids at different temperatures and extrapolating to 0 K. Using this method they studied several systems including deuterated benzene,[4] adenosine[5] and benzamide.[6] Bürgi *et al.* developed a method of visualising and analysing molecular motions in crystals.[7] The program PEANUT[8] allows limited information to be obtained relating to

coupling between motions. However, because many vibrational and librational motions are highly correlated, none of these methods allowed a full treatment of all motions.

A recent project carried out in the GED group in Edinburgh involved the novel use of molecular dynamics (MD) simulations to determine correction parameters to be applied to the experimental gas-phase structure of the sodium chloride dimer, Na_2Cl_2, thus allowing an experimental equilibrium structure to be obtained.[9]

If MD simulations on an isolated molecule can be used to model the vibrations in a gas, then using solid-state MD simulations (plane-wave DFT) on a periodic solid may allow the effects of vibrations and librations on average nuclear positions in crystals, relative to equilibrium positions, to be derived. The differences, when applied to coordinates obtained experimentally by neutron diffraction, should yield experimental equilibrium structures. This chapter describes the early stages of a study involving MD simulations, which should lead towards the determination of equilibrium structures in crystals.

7.2 Phase I ammonia – the test case

The solid-state structure of phase I ammonia was studied using MD simulations by Murshed Siddick, a colleague at the University of Edinburgh, as part of his PhD project.[10] His aim was to investigate the nature of hydrogen bonding in crystals. However, the existence of a complete data set made it prudent to begin our investigations with this simple four-atom molecule.

7.2.1 Computational method

The structure of crystalline phase I ammonia has been determined by X-ray diffraction studies.[11] The crystallographic unit cell (see Figure 1) contains four molecules in a cubic cell, space group $P2_13$, a = 513.05(8) pm, $V = 135.05\times10^6$ pm^3. Starting from this unit cell geometry and space group, the theoretical 0 K equilibrium structure was optimised at ambient pressure using the standard plane-wave DFT package CASTEP.[12] The electronic core was described using the standard pseudopotential supplied with the package and the PBE functional was used as both the exchange and correlation

functional.[13] During the optimisation process the unit-cell parameters and atomic positions were alternately optimised until an energy convergence criterion was met (maximum energy change per atom = 5×10^{-6} eV).

Figure 1 The crystallographic unit cell for phase I NH_3.

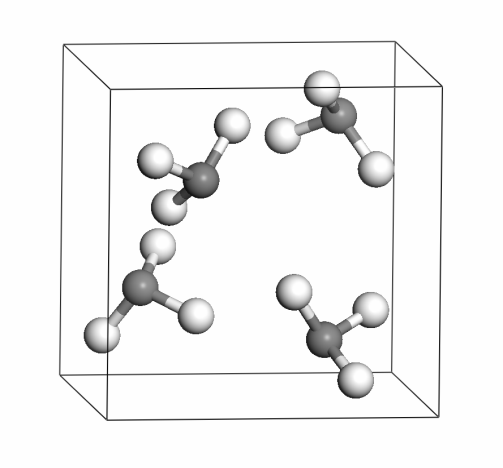

This calculated equilibrium structure formed the starting point for the MD simulation using a 2×2×2 supercell (constructed from the optimised unit cell, see Figure 2).

Figure 2 The 2×2×2 supercell for NH_3, used to model librations whose periodic length is too great to be modelled by the 1×1×1 cell.

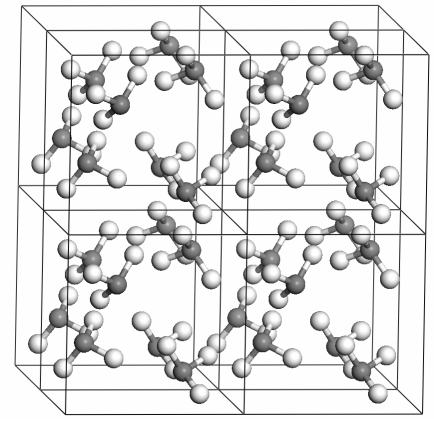

Although the crystallographic unit cell has a high degree of symmetry, the MD simulation was run with P1 symmetry so that the crystal structure disorder could be fully

observed. It was necessary to run the simulation on a system larger than the unit cell in order to visualise lattice vibrations that have a periodic length greater than that of the unit cell. Of course, there will always be vibrations with even longer wavelengths. Data were collected in time steps of 0.5 fs for approximately 5 ps. The initial temperature of the simulation was 200 K and the system stabilised to around 100 K within about 1 ps (see Figure 3).

Figure 3 The total energy and temperature of the MD simulation of a 2×2×2 supercell of phase I NH_3.

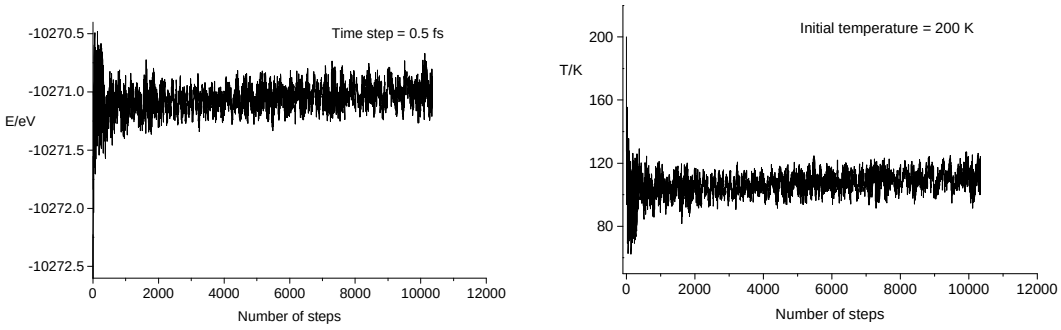

7.2.2 Results and discussion

Data were collected from the MD simulation every 0.5 fs for approximately 4 ps after the temperature of the system had stabilised. At each of those geometries the coordinates were recorded for all 128 atoms in the 2×2×2 supercell. These coordinates were then averaged over the many thousands of time steps to give the average position of each atom in the supercell. The eight values for each atomic position were then averaged, leaving a single unit cell with average *x*, *y* and *z* coordinates for 16 atoms. From these positions, values for each of the 12 N–H distances were calculated. The average value for *r*N–H was 101.950 pm and the difference between the longest and shortest bond was 0.154 pm. This value is, as expected, shorter than the bond length for the minimum energy structure calculated earlier (102.879 pm).

In fact, the asymmetric unit for phase I ammonia consists only of one N atom and one H atom, and so the positions were averaged once more to leave just two atoms. These

values were then subtracted from the values of the calculated equilibrium positions. The resultant Δx, Δy and Δz components form the correction that should be applied to the experimental structure. Table 1 lists the vibrationally averaged coordinates from the MD simulation alongside those from the calculated equilibrium structure, the components of the correction, the coordinates from the neutron diffraction crystal structure and the vibrationally corrected crystal structure.

Table 1 The vibrationally averaged coordinates from the MD simulation for phase I ammonia along with the equivalent coordinates from the calculated equilibrium structure and the neutron diffraction crystal structure.[a]

Atomic coordinate	MD simulation	Equilibrium structure	Calculated correction[b]	Crystal structure[c]	Corrected structure
x_N	0.2011(5)	0.1959	–0.0052(10)	0.2108(11)	0.2056(15)
x_H	0.3557(5)	0.3499	–0.0058(9)	0.3694(13)	0.3636(16)
y_H	0.2702(6)	0.2695	–0.0007(10)	0.2694(10)	0.2687(14)
z_H	0.0990(6)	0.0925	–0.0065(10)	0.1141(11)	0.1076(15)

[a] All coordinates are fractional coordinates. [b] A correction has been calculated by subtracting the vibrationally averaged coordinates from the equilibrium coordinates and applied to the experimental crystal structure. [c] From Ref. 14.

As expected the average position of the hydrogen atom lay closer to the nitrogen position in the vibrationally averaged structure than it did in the calculated equilibrium structure. In theory, this difference in positions between the two structures is the correction that must be applied to the atomic positions determined by neutron diffraction to give an experimental equilibrium structure. The available neutron diffraction data for ND_3 were collected at three separate temperatures (2, 77 and 180 K).[14] The corrections listed in Table 1 were applied to the 77 K data as that is the closest temperature to that at which the MD simulation stabilised. In fact, the difference in the rN–H as determined at 77 and 180 K was only 0.1 pm. The coordinates for the corrected experimental structure give an N–H bond length of 101.2 pm, a value that is equal to the neutron diffraction bond length determined at 2 K. Unfortunately, because the MD simulated data deals with NH_3 and the neutron diffraction experiment used ND_3, these corrections can only purport to be a good approximation.

The uncertainties on the vibrationally averaged coordinates from the MD simulation are the standard deviations of the positions of the atoms in the averaged 1×1×1 cell. Similarly, the uncertainties on the correction factors are the standard deviations of the values for all atoms in the unit cell. The ESDs on the corrected coordinates are the root-mean-squares of the uncertainties on the corrections and the experimental positions.

7.3 Application of the new method to an aromatic ring system

1,2,4,5-tetrachlorobenzene-d_2 was chosen as the next system to be studied using the method developed above. The relative rigidity of the benzene ring means that the components of the thermal parameters arising from the intramolecular vibrations are relatively small, with the largest contributions arising from the deformation modes involving the chlorine and hydrogen substituents. In contrast, the heaviest atoms are peripheral, and librational modes involving molecular rotations will involve large motions of these atoms, on curved paths. The effects that we are studying will therefore be maximised. The molecular symmetry will allow averaging of data for related molecular fragments, increasing the statistical significance of the results.

The size of the crystallographic unit cell is crucial when deciding if it is possible to perform MD simulations. Although there are no experimental data for $C_6D_2Cl_4$, an X-ray diffraction study of the hydrogen isotopomer, $C_6H_2Cl_4$, shows that there are only two molecules in the crystallographic unit cell, which has a cell volume of 376.3×10^6 pm^3 (see Figure 4).[15] There is no reason to believe that the structure of $C_6D_2Cl_4$ will differ significantly and the calculations, although rather time-consuming, will be feasible.

The deuterated compound has been chosen for two separate reasons. First, as accurate neutron diffraction data are required for comparison with the averaged theoretical structure, it is preferable to use a deuterated molecule, because the neutron scattering ability of D is far superior to that of H. The second reason for choosing a deuterated molecule is that the time step for the MD simulation is determined by the highest frequency vibrational mode. For $C_6D_2Cl_4$ this mode (a C–D stretch) occurs at a much

lower frequency than its C–H analogue, and thus the calculation time is reduced by almost one third. This amounts to a significant saving of time and money over the course of such a simulation.

Figure 4 Crystallographic unit cell for 1,2,4,5-tetrachlorobenzene. There are two molecules within the unit cell, both lying across cell boundaries.

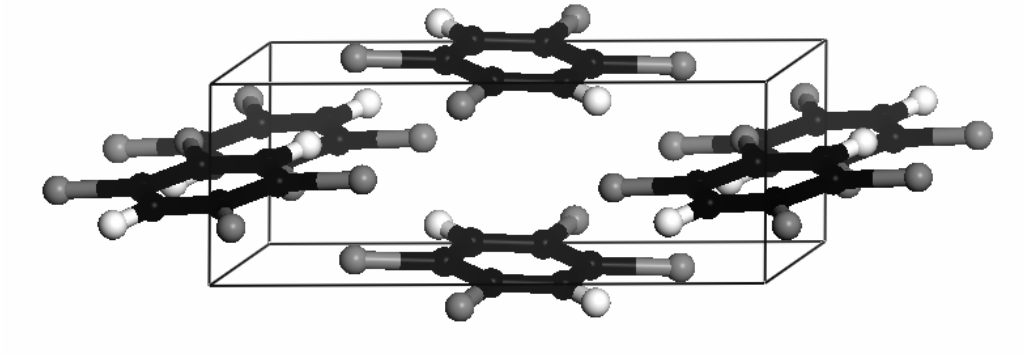

7.3.1 Computational method

Calculations were performed using the VASP 4.4 MD simulation code[16] with the resources of the Edinburgh Parallel Computing Centre (EPCC) on the machine Lomond (a Sun Fire 15K server with 52 UltraSPARC III processors). Initial calculations had been carried out using a Pentium 3 dual-processor 800 MHz workstation but were prohibitively slow. The PW91 functional was used to provide both exchange and correlation for the DFT calculations. A series of pseudopotentials was used to model the wavefunction towards the nuclear region and periodic plane-wave basis sets were used to describe the valence electrons.

Starting values for atomic coordinates and cell parameters were adapted from those determined by the X-ray diffraction study of $C_6H_2Cl_4$.[15] This showed that there were two molecules in the monoclinic unit cell (space group $P2_1/n$) with a = 379.56(12) pm, b = 1051.75(19) pm, c = 956.48(13) pm, β = 99.723°. The lattice parameters and atoms were then alternately allowed to optimise to give the calculated equilibrium structure.

The length of the a axis in the crystallographic unit cell of $C_6H_2Cl_4$ is significantly shorter than either the b or c axis. An attempt to run a simulation on a 1×1×1 cell failed

when the molecules in the cell began to move far from the positions that they had adopted in the experimental structure. Using a 2×1×1 cell yielded similarly poor results, but when a 3×1×1 supercell (see Figure 5) was used the energy remained relatively constant and the atoms moved very little from their experimental positions.

The time step used for the production phase of the MD simulation was determined with reference to the highest energy vibration, which is the C–D stretching motion. From this a time step of 0.9 fs was calculated.

Figure 5 3×1×1 supercell for 1,2,4,5-tetrachlorobenzene-d_2 used in the MD simulation as viewed along the *a*, *b* and *c* axes (from left to right).

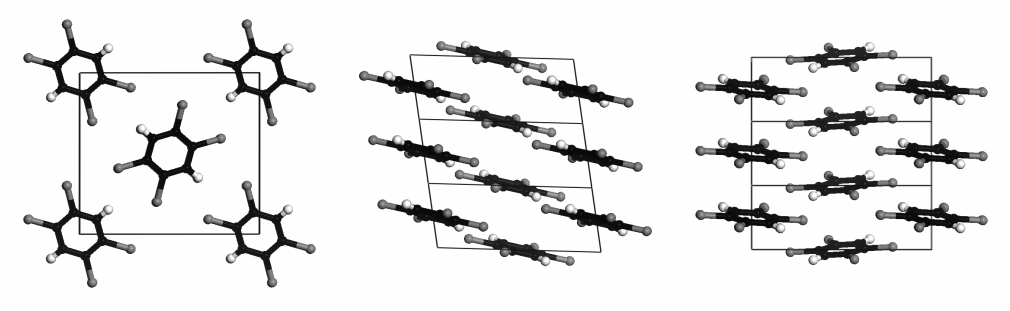

7.3.2 Results and discussion

Data were collected for a period of about 2.5 ps, a simulation that took approximately 2000 hours of processor time. Figure 6 shows that the simulation, which was started at a temperature of 200 K, settled to around 100 K after approximately 700 cycles. All coordinates calculated after this point in the simulation were used to determine the average positions of the atoms compared to the equilibrium positions.

As was the case in the ammonia example, the size of the supercell used in the simulation will have to be increased to include acoustic phonon waves that will have a longer wavelength than the length of the cell boundaries. In this case the cell will be scaled up to 6×2×2 and this simulation might require in the region of 20000 hours CPU time. The ability of the supercomputer to assign a large number of processors to any job (currently up to 48 processors per user) means that this simulation is feasible. An application has been submitted to the EPCC requesting this additional time on Lomond. As these data

are not yet available, a cursory attempt will be made to obtain a correction from the 3×1×1 data, although it is expected that the errors will be significant.

Figure 6 The total energy and temperature of the MD simulation of a 3×1×1 supercell of $C_6D_2Cl_4$.

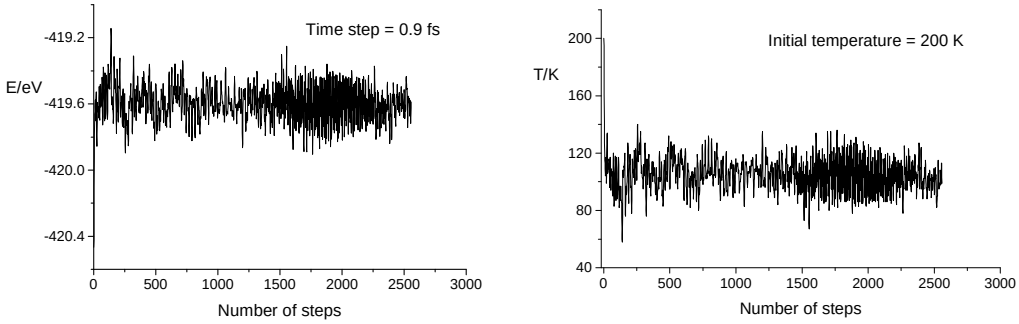

The coordinates that were calculated for approximately 1700 cycles of the MD simulation were averaged to give the mean position for each of the 72 atoms in the 3×1×1 supercell. These positions were further averaged to leave the 24 atoms of the crystallographic unit cell. The asymmetric unit consists of half of one molecule as shown in Figure 7. The coordinates were, therefore, averaged once more to leave just six atoms.

Figure 7 Atom numbering used for $C_6D_2Cl_4$ and $C_6H_2Cl_4$. The dashed line indicates that half of the molecule makes up the asymmetric unit.

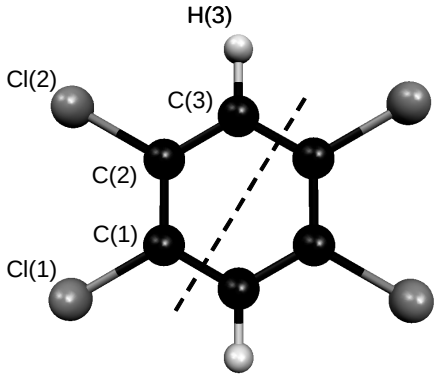

As was demonstrated for NH_3, the atomic positions in the vibrationally averaged structure are subtracted from the calculated equilibrium coordinates to give the corrections, which can then be applied to the neutron diffraction structure (see Table 2). An application has been submitted to the ISIS neutron facility at the Rutherford Appleton Laboratory, where it is hoped that time will be granted so that single-crystal neutron diffraction data can be collected for $C_6D_2Cl_4$. As these data are not presently available it is not possible to implement the correction fully. An attempt has been made to apply the corrections to the X-ray diffraction data that exist, but that introduces an entirely different problem related to the fundamentally different quantities that are measured in X-ray diffraction. This topic is discussed in detail in Chapter 8. Also by applying the correction in this manner, there is once again the problem of having experimental and simulation data for different isotopomers.

Table 2 The coordinates for the asymmetric portion $C_6D_2Cl_4$.[a]

Atomic coordinate	MD simulation	Equilibrium structure	Calculated correction[b]	Crystal structure[c]	Corrected structure
$x_{C(1)}$	0.07489(566)	0.07226	–0.00263(189)	0.0675(5)	0.06487(189)
$y_{C(1)}$	0.46801(9)	0.46663	–0.00138(71)	0.4674(2)	0.46602(71)
$z_{C(1)}$	0.36281(1293)	0.36218	–0.00063(8)	0.3662(2)	0.36557(8)
$x_{C(2)}$	0.97167(548)	0.97441	0.00274(183)	0.9810(4)	0.98374(183)
$y_{C(2)}$	0.37257(5)	0.37139	–0.00118(70)	0.3735(2)	0.37232(70)
$z_{C(2)}$	0.45364(1289)	0.45552	0.00188(8)	0.4577(2)	0.45958(8)
$x_{C(3)}$	0.89747(547)	0.90320	0.00573(195)	0.9115(5)	0.91723(195)
$y_{C(3)}$	0.40498(2)	0.40508	0.00010(70)	0.4067(2)	0.40680(70)
$z_{C(3)}$	0.59018(1288)	0.59283	0.00265(8)	0.5916(2)	0.59425(8)
$x_{Cl(1)}$	0.16799(554)	0.16382	–0.00417(230)	0.1518(1)	0.14763(230)
$y_{Cl(1)}$	0.43061(5)	0.42738	–0.00323(50)	0.4294(1)	0.42617(50)
$z_{Cl(1)}$	0.19292(1289)	0.19109	–0.00183(9)	0.2000(1)	0.19817(9)
$x_{Cl(2)}$	0.93959(566)	0.94590	0.00631(201)	0.9582(2)	0.96451(201)
$y_{Cl(2)}$	0.21381(12)	0.21049	–0.00332(64)	0.2162(1)	0.21288(64)
$z_{Cl(2)}$	0.39983(1289)	0.40356	0.00373(15)	0.4080(1)	0.41173(15)
$x_{H(3)}$	0.81863(538)	0.82876	0.01013(234)	0.836(7)	0.84613(234)
$y_{H(3)}$	0.33051(2)	0.33111	0.00060(80)	0.342(3)	0.34260(80)
$z_{H(3)}$	0.66052(1288)	0.66465	0.00413(23)	0.651(3)	0.65513(23)

[a] All coordinates are fractional coordinates. See Figure 7 for atom numbering. [b] The correction was calculated by subtracting the vibrationally averaged coordinates from the equilibrium coordinates and applied to the experimental crystal structure. [c] From Ref. 15.

Bond lengths derived from the calculated equilibrium and MD-simulated vibrationally averaged coordinates show, as expected, that there is a shortening of bonded distances due to atomic motion. Table 3 compares several bond lengths and angles from these two structures. It can be seen that the difference for the C–C bond lengths (0.6 pm) is much smaller than that for the C–Cl distances, where the bonds are shorter by up to 1.6 pm. The C–H bond length remains essentially unchanged. Also, the angles within the asymmetric unit are identical in the equilibrium and averaged MD structures. This signifies that that the MD process, while allowing the angles to change during the simulation, does so by equal amounts either side of the equilibrium angle. Distances from the crystal coordinates both before and after the corrections have been applied are also given in Table 3. However, as mentioned earlier, these values are not derived from nuclear positions and so no comparison is possible other than to say that the application of a correction acts to lengthen the vibrationally averaged (and, therefore, shortened) bonds.

Table 3 Comparison of selected structural parameters from asymmetric units for the averaged MD simulation structure and the equilibrium structure.[a]

Parameter	MD simulation	Equilibrium structure	Crystal structure[b]	Corrected structure[c]
*r*C(1)–C(2)	140.2	140.8	137.2	138.0
*r*C(2)–C(3)	139.6	140.2	136.8	137.5
*r*C(1)–Cl(1)	173.0	174.4	168.8	170.1
*r*C(2)–Cl(2)	172.6	174.2	170.0	171.6
*r*C–H	108.8	108.7	94.5	94.4
∠C(1)–C(2)–C(3)	120.1	120.1	119.6	119.6
∠C(1)–C(2)–Cl(2)	120.8	120.8	121.3	121.3
∠C(2)–C(1)–Cl(1)	121.1	121.1	120.6	120.6

[a] Distances (*r*) are in pm, angles (∠) are in degrees. [b] Determined from the atomic coordinates given in Ref. 15. [c] From the coordinates of the crystal structure after correction using the difference between the MD average structure and the calculated equilibrium structure.

From the averaged MD coordinates it is striking how much the standard deviations vary between the *x*/*a*, *y*/*b* and *z*/*c* axes (views along these axes are shown in Figure 5). In the case of the *y* axis, the molecules in the crystal seem to be very well aligned and this

could be the reason that their positions changed very little during the production phase of the MD simulation. On the other hand, the values obtained for the *x* and *z* axes showed a much larger variation during the simulation. It should also be noted that the large uncertainties on the *x* and *z* axes are similar for different atoms. This suggests that the whole molecule is moving considerably in those two directions. By performing further MD studies on this and other molecules, it is hoped that this phenomenon can be more clearly understood.

This short chapter demonstrates the potential of MD simulations to provide corrections to account for the effects of vibrations and (some) librations on crystal structures. The method described has by no means been perfected and many possible setbacks have been identified. However, this is simply the first step on a long journey towards determining accurate equilibrium crystal structures. If that goal can be realised the consequences for crystallography could be far-reaching. The future course for this work is outlined in Chapter 8.

7.4 References

1. G. E. Bacon, *Neutron Diffraction*, Oxford University Press, Oxford, 1975.
2. D. W. J. Cruickshank, *Acta Crystallogr.*, 1956, **9**, 747.
3. W. R. Busing and H. A. Levy, *Acta Crystallogr.*, 1964, **17**, 142.
4. G. A. Jeffrey, J. R. Ruble, R. K. McMullan and J. A. Pople, *Proc. R. Soc. London, Ser. A*, 1987, **414**, 47.
5. W. T. Klooster, J. R. Ruble, B. M. Craven and R. K. McMullan, *Acta Crystallogr., Sect. B: Struct. Sci.*, 1991, **47**, 376.
6. Q. Gao, G. A. Jeffrey and J. R. Ruble, *Acta Crystallogr., Sect. B: Struct. Sci.*, 1991, **47**, 742.
7. W. Hummel, A Raselli and H.-B. Bürgi, *Acta Crystallogr., Sect. B: Struct. Sci.*, 1990, **46**, 683.
8. W. Hummel, J. Hauser and H.-B. Bürgi, *J. Mol. Graphics*, 1990, **8**, 214.
9. P. D. McCaffrey, C. A. Morrison and D. W. H. Rankin, unpublished work.
10. M. M. Siddick, personal communication.
11. R. Boese, N. Niederprüm, D. Bläser, A. Maulitz, M. Y. Antipin and P. R. Mallison, *J. Phys. Chem. B*, 1997, **101**, 5794.
12. M. C. Payne, M. P. Teter, D. C. Allen, T. A. Arias and J. D. Joannopoulos, *Rev. Mod. Phys.*, 1992, **64**, 1045.
13. J. P. Perdew and Y. Wang, *Phys. Rev. B: Condens. Matter*, 1992, **45**, 13244.
14. A. W. Hewat and C. Riekel, *Acta Crystallogr., Sect. A: Cryst. Phys., Diffr., Theor. Gen. Cryst.*, 1979, **35**, 569.
15. G. Kresse and J. Furthmüller, *Comput. Mater. Sci.*, 1996, **6**, 15.
16. D. G. Anderson, A. J. Blake, R. Blom, S. Cradock and D. W. H. Rankin, *Acta Chem. Scand.*, 1991, **45**, 158.

Chapter Eight

Conclusions, recommendations and future work

8.1 Experimental determination of gas-phase structures

The structures of seven molecules containing heavy *p*-block elements have been determined by gas-phase electron diffraction (GED) using the SARACEN[1] and DYNAMITE[2] methods of refinement. For some of the larger molecules the process of collecting GED data tested the Edinburgh apparatus to its limits. The ability to collect data for some of the larger molecules, where temperatures in excess of 500 K were required to obtain a suitable vapour pressure, was aided greatly by the use of the air-heated reservoir.[3]

It had been hoped to study further examples of the main-group metal polyphospholyl complexes described in Chapters 2 and 3, but those compounds failed to vaporise when heated to the limits of the apparatus or began to decompose at higher temperatures. Samples that were run but for which data could not be collected included [Ga($P_3C_2Bu^t_2$)] and [Cr($P_3C_3Bu^t_3$)($CO)_3$]. In fact, preparations have been reported for each of the following complexes:[4]

- [M($P_3C_3Bu^t_3$)($CO)_3$] (M = Cr, Mo, W)
- [M($P_2C_3Bu^t_3$)] (M = Ga, In, Tl)
- [M($P_3C_2Bu^t_2$)] (M = Ga, In, Tl)
- [M($P_2C_2Bu^t_2$)] (M = Ge, Sn, Pb)

As most of these molecules have a reasonable degree of symmetry (with the exception of the sterically crowded half-sandwich complexes of [$P_2C_3Bu^t_3$]) they are ideal for study by GED. Of particular interest would be the degree of ring deformation experienced by the aromatic [$P_2C_2Bu^t_2$] ring when complexed with Group 14 metals that are both larger and smaller than Sn. This could give a further insight into whether this deformation is purely due to the difference in Sn–C and Sn–P bond lengths.

For all of the molecules studied in this thesis geometrical parameters have been refined with the inclusion of curvilinear corrections to account for the shrinkage effect.[5] The r_a and r_{h1} notation has been used accurately throughout this work. Unfortunately this is not the case in all GED publications. In the field of structural chemistry many different experimental and theoretical distances are measured and often it is not made clear what is being reported. It is now commonplace to use the SHRINK program[6] and calculated harmonic force fields to determine these corrections and it is hoped that the r_{h1} notation will become more widely used. This recommendation was made at a recent European Electron Diffraction Symposium where it was well received.

8.2 Theoretical determination of gas-phase structures

As explained in Chapter 1, the complete determination of structures from GED data is often not possible without the aid of extra sources of information, and the use of theoretical methods for this purpose is almost ubiquitous. Chapter 6 demonstrated the advances in accuracy and precision of structure that can be made by refining amplitudes of vibration and including corrections to counteract the structural effects of vibrational averaging. Using the SARACEN method[1] the *R*-factors of eight members of the aminodifluorophosphine family were significantly improved and geometrical parameters that were previously constrained were allowed to refine, subject to flexible restraints.

Computed structures and the use of SARACEN were certainly necessary for full determinations of the structures of the heavy main-group compounds described in Chapters 2–5. With this dependence on calculated parameters it becomes very important for the electron diffractionist to have a thorough understanding of the accuracy of those theoretical parameters. Supercomputers are now more accessible than ever and software packages such as Gaussian 03[7] allow any experimental chemist to obtain theoretical results with which to corroborate their findings. Many different *ab initio* and DFT methods are available and great care has been taken in this work to ensure that the methods used provide accurate structures.

It is well documented[8] that, in general, MP2 calculations are less good for transition-metal complexes than DFT methods, which can produce results that are commensurate with experiment. MP2 calculations would be expected to give reasonable results for molecules composed of main-group elements and the findings of this work broadly agree with that hypothesis. As for the use of DFT, the calculations performed during this degree show that DFT methods can give results that are comparable in accuracy to those determined using MP2. They also highlight the vast differences in values that can be obtained from different DFT methods.

That MP2 should give good results for geometry optimisations of *p*-block molecules and that the use DFT calculations is rather hit-and-miss is no great surprise. Of more interest are the results of the other computational trial that was carried out. The use of pseudopotential basis sets is necessary to speed up calculations of molecules with heavy atoms by replacing the core electrons by a potential and thus allowing fewer valence electron to be considered explicitly in the calculation. Until recently these pseudopotentials were of the large-core type where very few electrons were included in the calculation. New small-core pseudopotentials are now available and an investigation was performed to determine whether this could affect the accuracy of a calculation. It showed that, while using the aug-cc-pVQZ ECP did not universally improve the accuracy of results, for many of the molecules tested the inclusion of more electrons in the valence shell was necessary.

8.3 Experimental equilibrium structures in the solid state

In Chapter 7 it was demonstrated that molecular dynamics (MD) simulation have a potential use in solid-state structure determination. Although this work is at a very early stage, the results obtained are exciting and have the potential to lead to a fundamental advance in determining equilibrium crystal structures.

Using the methods described in Chapter 7, it is hoped that MD simulations can be performed on a larger crystal array for $C_6D_2Cl_4$ and that single-crystal neutron

diffraction data can be collected for this compound. This will allow a much more accurate correction to be applied than that attempted previously.

It is hoped that this method can be extended to many more molecules. In the long term, it is recognised that this method of determining thermal corrections is both time-consuming and expensive. If, for example, studies performed on other substituted benzenes give results that show correlation with those results for $C_6D_2Cl_4$, it might be possible to derive a semi-empirical correction that can be applied without the need to perform MD simulations every time. This could then be extended to include other classes of molecules.

8.3.1 Monte Carlo simulations

While the initial study focussed on the use of MD simulations to observe the motion of atoms and molecules in solid-state matter, it is acknowledged that Monte Carlo simulations might also be applicable. A future development of this work will involve the use of Monte Carlo simulations to investigate whether the results obtained are similar to those from MD and, if so, whether the simulations are any quicker and less computationally demanding.

8.3.2 Representations of thermal motion in crystals

The use of ellipsoids to describe the thermal motions of atoms in crystals is very common. However, intuition suggests that it is more likely for an atom to move around a curved trajectory than an ellipsoid. One outcome of the use of MD simulations to view crystal vibrations could be to determine a more realistic shape that can be used to represent atomic motion.

By plotting the many positions adopted by an atom during the MD simulation, it should be possible to map a surface that has, for instance, a banana or bowl shape. If a mathematical function could be determined for the shape of this surface it would allow this advance to be incorporated into crystallography at the cost of only one or two extra parameters to describe the shape. If the experimental data were good enough, these extra parameters describing the curvature could be refined. These could then be correlated

with the vibrational corrections, which could thus be determined directly from the experimental data. This opens the possibility of determining equilibrium structures rapidly and routinely.

8.3.3 Crystal structures by X-ray diffraction

So far the crystal structures discussed have been derived from neutron diffraction data. Obtaining neutron diffraction data can be a very costly process, unlike obtaining X-ray diffraction data, which is now commonplace. However, X-ray diffraction locates centres of electron density and not the nuclear positions determined by neutron diffraction so correcting for vibrations and librations, as described for $C_6D_2Cl_4$ in Chapter 7, will only yield a corrected centre of electron density.

A more significant advance would be to determine equilibrium nuclear structures from X-ray diffraction data. To do that the difference in position between the centre of electron density and the nucleus would have to be calculated. Quantum chemical calculations have the ability to determine any molecular property including electron density. It is, however, difficult to accurately partition the electron density between atoms. Methods are available and it needs to be explored to see which method works best.

8.4 References

1. A. J. Blake, P. T. Brain, H. McNab, J. Miller, C. A. Morrison, S. Parsons, D. W. H. Rankin, H. E. Robertson and B. A. Smart, *J. Phys. Chem.*, 1996, **100**, 12280; P. T. Brain, C. A. Morrison, S. Parsons and D. W. H. Rankin, *J. Chem. Soc., Dalton Trans.*, 1996, 4589; N. W. Mitzel and D. W. H. Rankin, *Dalton Trans.*, 2003, 3650.
2. S. L. Hinchley, M. F. Haddow and D. W. H. Rankin, *Dalton Trans.*, 2004, 384.
3. J. T. Schirlin, *Ph.D. Thesis*, University of Edinburgh, 2004.
4. K. B. Dillon, F. Mathey and J. F. Nixon, *Phosphorus: The Carbon Copy: From Organophosphorus to Phospha-organic Chemistry*, John Wiley and Sons, Chichester, 1998, and references therein.
5. O. Bastiansen and M. Trætteberg, *Acta Crystallogr.*, 1960, **13**, 1108; Y. Morino, S. J. Cyvin, K. Kuchitsu and T. Iijima, *J. Chem. Phys.*, 1962, **36**, 1109; R. Stølevik, H. M. Seip and S. J. Cyvin, *Chem. Phys. Lett.*, 1972, **15**, 263.
6. V. A. Sipachev, *J. Mol. Struct.* (*THEOCHEM*), 1985, **121**, 143; V. A. Sipachev, *J. Mol. Struct.*, 2001, **567**, 67.
7. M. J. Frisch, G. W. Trucks, H. B. Schlegel, G. E. Scuseria, M. A. Robb, J. R. Cheeseman, J. A. Montgomery, Jr., T. Vreven, K. N. Kudin, J. C. Burant, J. M. Millam, S. S. Iyengar, J. Tomasi, V. Barone, B. Mennucci, M. Cossi, G. Scalmani, N. Rega, G. A. Petersson, H. Nakatsuji, M. Hada, M. Ehara, K. Toyota, R. Fukuda, J. Hasegawa, M. Ishida, T. Nakajima, Y. Honda, O. Kitao, H. Nakai, M. Klene, X. Li, J. E. Knox, H. P. Hratchian, J. B. Cross, C. Adamo, J. Jaramillo, R. Gomperts, R. E. Stratmann, O. Yazyev, A. J. Austin, R. Cammi, C. Pomelli, J. W. Ochterski, P. Y. Ayala, K. Morokuma, G. A. Voth, P. Salvador, J. J. Dannenberg, V. G. Zakrzewski, S. Dapprich, A. D. Daniels, M. C. Strain, O. Farkas, D. K. Malick, A. D. Rabuck, K. Raghavachari, J. B. Foresman, J. V. Ortiz, Q. Cui, A. G. Baboul, S. Clifford, J. Cioslowski, B. B. Stefanov, G. Liu, A. Liashenko, P. Piskorz, I. Komaromi, R. L. Martin, D. J. Fox, T. Keith, M. A. Al-Laham, C. Y. Peng, A. Nanayakkara, M. Challacombe, P. M. W. Gill, B. Johnson, W. Chen, M. W. Wong, C. Gonzalez and J. A. Pople, *Gaussian 03, Revision C.01*, Gaussian, Inc., Wallingford, CT, 2004.

8. N. Fey, *J. Chem. Technol. Biotechnol.*, 1999, **74**, 852, and references therein.

Appendix A

Publications

Structure by theory and experiment: one nationality, two languages.
S. L. Hinchley, D. A. Wann and D. W. H. Rankin, *Int. J. Quantum Chem.*, 2005, **101**, 878.

The molecular structure of [Sn($P_2C_2Bu^t_2$)] using gas-phase electron diffraction and DFT calculations.
D. A. Wann, S. L. Hinchley, K. B. Borisenko, H. E. Robertson, M. D. Francis, J. F. Nixon and D. W. H. Rankin, *Dalton Trans.*, 2005, 1972.

Gas-phase structures of aminodifluorophosphines determined using electron diffraction data and computational techniques.
D. A. Wann, S. L. Hinchley and D. W. H. Rankin, *Dalton Trans.*, 2005, 2572.

Molecular structures of $Se(SCH_3)_2$ and $Te(SCH_3)_2$ using gas-phase electron diffraction and ab initio and DFT geometry optimisations.
H. Fleischer, D. A. Wann, S. L. Hinchley, K. B. Borisenko, J. R. Lewis, R. J. Mawhorter and D. W. H. Rankin, *Dalton Trans.*, 2005, 3221.

Molecular structures of the 1,6-disubstituted triptycenes $Sb_2(C_6F_4)_3$ and $Bi_2(C_6F_4)_3$ using gas-phase electron diffraction and ab initio and DFT calculations.
D. A. Wann, S. L. Hinchley, H. E. Robertson, N. A. A. Al-Jabar, A. G. Massey and D. W. H. Rankin, submitted for publication.

The molecular structures of [In($P_3C_2Bu^t_2$)] and [In($P_2C_3Bu^t_3$)] using gas-phase electron diffraction and ab initio and DFT calculations.
D. A. Wann, H. E. Robertson, M. D. Francis, J. F. Nixon and D. W. H. Rankin, manuscript in preparation.

Appendix B

Conferences and courses attended

Conferences

10th European Symposium on Gas Electron Diffraction
St. Petersburg, Russia, June 2003
Poster presentation: *Conformations of aminodifluorophosphines revisited*

Universities of Scotland Inorganic Club
University of Strathclyde, Glasgow, September 2003
Poster presentation: *Conformations of aminodifluorophosphines revisited*

20th Austin Symposium on Molecular Structure
Austin, TX, USA, March 2004
Poster presentation: *Structures of main-group metal complexes: a challenge for theory?*

16th International Conference on Phosphorus Chemistry
Birmingham, July 2004
Poster presentation: *Structure and bonding of main-group metal phospholyl complexes*

Universities of Scotland Inorganic Club
Heriott-Watt University, Edinburgh, September 2004
Oral presentation: *Structure by theory and experiment: main-group metal complexes*

11th European Symposium on Gas Electron Diffraction
Blaubeuren, Germany, June 2005
Oral presentation: *Towards equilibrium structures for gas-phase molecules and crystals*

Younger European Chemists' Conference
Brno, Czech Republic, September 2005
Poster presentation: *Improved modelling of solid-state atomic movement: a dynamic approach*

Universities of Scotland Inorganic Club

University of Glasgow, September 2005

Poster presentation: *Improved modelling of solid-state atomic movement: a dynamic approach*

Courses

- Making a poster, 2002
- Introduction to UNIX, 2002
- Introduction to FORTRAN 90, 2002
- Introduction to HTML and authoring on the web, 2003
- More HTML, 2003
- An introduction to CGI scripts and HTML forms, 2004
- Unix 2: enhancing your UNIX skills, 2004
- Scientific paper production, 2004
- Interviewing skills, 2004
- UK GRADschool, London, August 2004
- Researcher in Residence, Introduction, Glasgow, September 2004
- Even more HTML, 2005
- Dreamweaver, 2005
- LaTeX: a document preparation system, 2005
- UNIX 3: shell programming, 2005
- Departmental colloquia, 2002 – 2005
- Inorganic section meetings, 2002 – 2004
- Materials, Structure and Chemical Physics section talks, 2004 – 2005

Electronic Appendix – Chapter Two
Tables 2.1 – 2.28

Table 2.1 Calculated (MP2/aug-cc-pVQZ-PP/6-311+G*) coordinates for [In($P_3C_2Bu^t_2$)], **1**.

Atom	*x*	*y*	*z*
In(1)	1.8621	–0.4318	0.0000
P(2)	–1.1399	–0.7528	0.0000
C(3)	–0.6220	0.2334	1.3583
P(4)	0.1455	1.7701	1.0638
P(5)	0.1455	1.7701	–1.0638
C(6)	–0.6220	0.2334	–1.3583
C(7)	–0.9543	–0.2222	2.8036
C(8)	–2.3890	0.2446	3.1252
C(9)	–0.8888	–1.7523	2.9574
H(10)	–3.1103	–0.1952	2.4457
H(11)	–2.6616	–0.0461	4.1358
H(12)	–2.4772	1.3228	3.0519
H(13)	0.1027	–2.1343	2.7361
H(14)	–1.1251	–2.0272	3.9805
H(15)	–1.5931	–2.2644	2.3140
C(16)	–0.9543	–0.2222	–2.8036
C(17)	0.0017	0.3942	–3.8381
C(18)	–0.8888	–1.7523	–2.9574
C(19)	–2.3890	0.2446	–3.1252
H(20)	1.0320	0.1072	–3.6541
H(21)	–0.2635	0.0476	–4.8318
H(22)	–0.0438	1.4760	–3.8496
H(23)	–1.5931	–2.2644	–2.3140
H(24)	–1.1251	–2.0272	–3.9805
H(25)	0.1027	–2.1343	–2.7361
H(26)	–2.4772	1.3228	–3.0519
H(27)	–2.6616	–0.0461	–4.1358
H(28)	–3.1103	–0.1952	–2.4457
C(29)	0.0017	0.3942	3.8381
H(30)	1.0320	0.1072	3.6541
H(31)	–0.0438	1.4760	3.8496
H(32)	–0.2635	0.0476	4.8318

Energy = –1600.700456 Hartrees.
All coordinates are in Å.

Table 2.2 Calculated (MP2/LanL2DZ/6-311+G*) coordinates for [In($P_3C_2Bu^t_2$)], **1**.

Atom	*x*	*y*	*z*
In(1)	1.7986	–0.4221	0.0000
P(2)	–1.1451	–0.8009	0.0000
C(3)	–0.5987	0.2031	1.3450
P(4)	0.0913	1.8082	1.0633
P(5)	0.0913	1.8082	–1.0633
C(6)	–0.5987	0.2031	–1.3450
C(7)	–0.9012	–0.2360	2.7849
C(8)	–2.2887	0.3122	3.1588
C(9)	–0.9141	–1.7650	2.9193
H(10)	–3.0540	–0.0733	2.4775
H(11)	–2.5528	0.0146	4.1805
H(12)	–2.3009	1.4054	3.1029
H(13)	0.0486	–2.1945	2.6219
H(14)	–1.1009	–2.0413	3.9630
H(15)	–1.6944	–2.2259	2.3076
C(16)	–0.9012	–0.2360	–2.7849
C(17)	0.1372	0.3171	–3.7696
C(18)	–0.9141	–1.7650	–2.9193
C(19)	–2.2887	0.3122	–3.1588
H(20)	1.1445	–0.0306	–3.5150
H(21)	–0.0951	–0.0285	–4.7830
H(22)	0.1497	1.4101	–3.7843
H(23)	–1.6944	–2.2259	–2.3076
H(24)	–1.1009	–2.0413	–3.9630
H(25)	0.0486	–2.1945	–2.6219
H(26)	–2.3009	1.4054	–3.1029
H(27)	–2.5528	0.0146	–4.1805
H(28)	–3.0540	–0.0733	–2.4775
C(29)	0.1372	0.3171	3.7696
H(30)	1.1445	–0.0306	3.5150
H(31)	0.1497	1.4101	3.7843
H(32)	–0.0951	–0.0285	4.7830

Energy = –1415.1029211 Hartrees.
All coordinates are in Å.

Table 2.3 Calculated (B3PW91/aug-cc-pVQZ-PP/6-311+G*) coordinates for [In($P_3C_2Bu^t_2$)], **1**.

Atom	*x*	*y*	*z*
In(1)	1.7764	–0.4753	0.0000
P(2)	–1.1577	–0.7420	0.0000
C(3)	–0.6009	0.2431	1.3565
P(4)	0.2268	1.7700	1.0708
P(5)	0.2268	1.7700	–1.0708
C(6)	–0.6009	0.2431	–1.3565
C(7)	–0.9291	–0.2002	2.7946
C(8)	–2.3313	0.3402	3.1383
C(9)	–0.9408	–1.7306	2.9290
H(10)	–3.0874	–0.0557	2.4545
H(11)	–2.6110	0.0522	4.1577
H(12)	–2.3593	1.4316	3.0739
H(13)	0.0334	–2.1614	2.6770
H(14)	–1.1744	–2.0137	3.9606
H(15)	–1.6885	–2.1969	2.2822
C(16)	–0.9291	–0.2002	–2.7946
C(17)	0.0767	0.3633	–3.8080
C(18)	–0.9408	–1.7306	–2.9290
C(19)	–2.3313	0.3402	–3.1383
H(20)	1.0942	0.0183	–3.5982
H(21)	–0.1866	0.0336	–4.8181
H(22)	0.0904	1.4564	–3.8117
H(23)	–1.6885	–2.1969	–2.2822
H(24)	–1.1744	–2.0137	–3.9606
H(25)	0.0334	–2.1614	–2.6770
H(26)	–2.3593	1.4316	–3.0739
H(27)	–2.6110	0.0522	–4.1577
H(28)	–3.0874	–0.0557	–2.4545
C(29)	0.0767	0.3633	3.8080
H(30)	1.0942	0.0183	3.5982
H(31)	0.0904	1.4564	3.8117
H(32)	–0.1866	0.0336	4.8181

Energy = –1606.133005 Hartrees.
All coordinates are in Å.

Table 2.4 Calculated (B3PW91/LanL2DZ/6-311+G*) coordinates for [In($P_3C_2Bu^t_2$)], **1**.

Atom	*x*	*y*	*z*
In(1)	1.7917	–0.4541	0.0000
P(2)	–1.1526	–0.7617	0.0000
C(3)	–0.6087	0.2350	1.3530
P(4)	0.1740	1.7855	1.0699
P(5)	0.1740	1.7855	–1.0699
C(6)	–0.6087	0.2350	–1.3530
C(7)	–0.9217	–0.2148	2.7918
C(8)	–2.3296	0.3045	3.1427
C(9)	–0.9076	–1.7451	2.9251
H(10)	–3.0826	–0.1013	2.4612
H(11)	–2.6009	0.0110	4.1627
H(12)	–2.3731	1.3953	3.0796
H(13)	0.0727	–2.1589	2.6677
H(14)	–1.1306	–2.0327	3.9577
H(15)	–1.6505	–2.2239	2.2820
C(16)	–0.9217	–0.2148	–2.7918
C(17)	0.0823	0.3624	–3.7993
C(18)	–0.9076	–1.7451	–2.9251
C(19)	–2.3296	0.3045	–3.1427
H(20)	1.1027	0.0295	–3.5840
H(21)	–0.1713	0.0301	–4.8110
H(22)	0.0829	1.4555	–3.8019
H(23)	–1.6505	–2.2239	–2.2820
H(24)	–1.1306	–2.0327	–3.9577
H(25)	0.0727	–2.1589	–2.6677
H(26)	–2.3731	1.3953	–3.0796
H(27)	–2.6009	0.0110	–4.1627
H(28)	–3.0826	–0.1013	–2.4612
C(29)	0.0823	0.3624	3.7993
H(30)	1.1027	0.0295	3.5840
H(31)	0.0829	1.4555	3.8019
H(32)	–0.1713	0.0301	4.8110

Energy = –1417.764842 Hartrees.
All coordinates are in Å.

Table 2.5 Calculated (B3LYP/aug-cc-pVQZ-PP/6-311+G*) coordinates for [In($P_3C_2Bu^t_2$)], **1**.

Atom	*x*	*y*	*z*
In(1)	1.8321	–0.4573	0.0000
P(2)	–1.1546	–0.7588	0.0000
C(3)	–0.6130	0.2347	1.3642
P(4)	0.1905	1.7803	1.0767
P(5)	0.1905	1.7803	–1.0767
C(6)	–0.6130	0.2347	–1.3642
C(7)	–0.9492	–0.2110	2.8085
C(8)	–2.3634	0.3210	3.1479
C(9)	–0.9519	–1.7477	2.9527
H(10)	–3.1138	–0.0805	2.4623
H(11)	–2.6448	0.0311	4.1657
H(12)	–2.4002	1.4114	3.0838
H(13)	0.0266	–2.1739	2.7132
H(14)	–1.1918	–2.0247	3.9838
H(15)	–1.6901	–2.2241	2.3043
C(16)	–0.9492	–0.2110	–2.8085
C(17)	0.0485	0.3610	–3.8357
C(18)	–0.9519	–1.7477	–2.9527
C(19)	–2.3634	0.3210	–3.1479
H(20)	1.0689	0.0201	–3.6377
H(21)	–0.2234	0.0304	–4.8425
H(22)	0.0578	1.4529	–3.8399
H(23)	–1.6901	–2.2241	–2.3043
H(24)	–1.1918	–2.0247	–3.9838
H(25)	0.0266	–2.1739	–2.7132
H(26)	–2.4002	1.4114	–3.0838
H(27)	–2.6448	0.0311	–4.1657
H(28)	–3.1138	–0.0805	–2.4623
C(29)	0.0485	0.3610	3.8357
H(30)	1.0689	0.0201	3.6377
H(31)	0.0578	1.4529	3.8399
H(32)	–0.2234	0.0304	4.8425

Energy = –1606.384649 Hartrees.
All coordinates are in Å.

Table 2.6 Calculated (B3LYP/LanL2DZ/6-311+G*) coordinates for [In($P_3C_2Bu^t_2$)], **1**.

Atom	*x*	*y*	*z*
In(1)	0.0000	–1.8388	–0.4413
P(2)	0.0000	1.1487	–0.7779
C(3)	–1.3605	0.6169	0.2250
P(4)	–1.0756	–0.1484	1.7901
P(5)	1.0756	–0.1484	1.7901
C(6)	1.3605	0.6169	0.2250
C(7)	–2.8070	0.9405	–0.2221
C(8)	–3.1756	2.3297	0.3532
C(9)	–2.9426	0.9908	–1.7585
H(10)	–2.4965	3.1033	–0.0139
H(11)	–4.1940	2.6054	0.0600
H(12)	–3.1252	2.3299	1.4448
H(13)	–2.6770	0.0337	–2.2166
H(14)	–3.9778	1.2149	–2.0329
H(15)	–2.3105	1.7603	–2.2064
C(16)	2.8070	0.9405	–0.2221
C(17)	3.8178	–0.0961	0.3096
C(18)	2.9426	0.9908	–1.7585
C(19)	3.1756	2.3297	0.3532
H(20)	3.5986	–1.0996	–0.0668
H(21)	4.8284	0.1680	–0.0160
H(22)	3.8257	–0.1445	1.4004
H(23)	2.3105	1.7603	–2.2064
H(24)	3.9778	1.2149	–2.0329
H(25)	2.6770	0.0337	–2.2166
H(26)	3.1252	2.3299	1.4448
H(27)	4.1940	2.6054	0.0601
H(28)	2.4965	3.1033	–0.0139
C(29)	–3.8178	–0.0961	0.3096
H(30)	–3.5986	–1.0996	–0.0667
H(31)	–3.8257	–0.1445	1.4004
H(32)	–4.8284	0.1680	–0.0160

Energy = –1418.040660 Hartrees.
All coordinates are in Å.

Table 2.7 Calculated (BLYP/aug-cc-pVQZ-PP/6-311+G*) coordinates for [In($P_3C_2Bu^t_2$)], **1**.

Atom	*x*	*y*	*z*
In(1)	1.8655	–0.4610	0.0000
P(2)	–1.1623	–0.7727	0.0000
C(3)	–0.6193	0.2329	1.3783
P(4)	0.1962	1.7942	1.0898
P(5)	0.1962	1.7942	–1.0898
C(6)	–0.6193	0.2329	–1.3783
C(7)	–0.9687	–0.2116	2.8325
C(8)	–2.3996	0.3230	3.1606
C(9)	–0.9688	–1.7605	2.9850
H(10)	–3.1475	–0.0856	2.4661
H(11)	–2.6904	0.0345	4.1834
H(12)	–2.4387	1.4194	3.0913
H(13)	0.0196	–2.1866	2.7563
H(14)	–1.2207	–2.0359	4.0208
H(15)	–1.7025	–2.2442	2.3260
C(16)	–0.9687	–0.2116	–2.8325
C(17)	0.0261	0.3716	–3.8754
C(18)	–0.9688	–1.7605	–2.9850
C(19)	–2.3996	0.3230	–3.1606
H(20)	1.0549	0.0294	–3.6873
H(21)	–0.2565	0.0436	–4.8875
H(22)	0.0339	1.4702	–3.8740
H(23)	–1.7025	–2.2442	–2.3260
H(24)	–1.2207	–2.0359	–4.0208
H(25)	0.0196	–2.1866	–2.7563
H(26)	–2.4387	1.4194	–3.0913
H(27)	–2.6904	0.0345	–4.1834
H(28)	–3.1475	–0.0856	–2.4661
C(29)	0.0261	0.3716	3.8754
H(30)	1.0549	0.0294	3.6873
H(31)	0.0339	1.4702	3.8740
H(32)	–0.2565	0.0436	4.8875

Energy = –1605.985849 Hartrees.
All coordinates are in Å.

Table 2.8 Calculated (BLYP/LanL2DZ/6-311+G*) coordinates for [In($P_3C_2Bu^t_2$)], **1**.

Atom	*x*	*y*	*z*
In(1)	0.0000	–1.8605	–0.4530
P(2)	0.0000	1.1583	–0.7855
C(3)	–1.3747	0.6182	0.2259
P(4)	–1.0893	–0.1715	1.8008
P(5)	1.0893	–0.1715	1.8008
C(6)	1.3747	0.6182	0.2259
C(7)	–2.8312	0.9584	–0.2181
C(8)	–3.1873	2.3616	0.3682
C(9)	–2.9747	1.0155	–1.7665
H(10)	–2.4983	3.1345	–0.0016
H(11)	–4.2105	2.6491	0.0782
H(12)	–3.1320	2.3577	1.4661
H(13)	–2.7208	0.0509	–2.2308
H(14)	–4.0147	1.2543	–2.0373
H(15)	–2.3312	1.7832	–2.2174
C(16)	2.8312	0.9584	–0.2181
C(17)	3.8590	–0.0778	0.3190
C(18)	2.9747	1.0155	–1.7665
C(19)	3.1873	2.3616	0.3682
H(20)	3.6499	–1.0882	–0.0635
H(21)	4.8745	0.1991	–0.0033
H(22)	3.8624	–0.1297	1.4163
H(23)	2.3312	1.7832	–2.2174
H(24)	4.0147	1.2543	–2.0373
H(25)	2.7208	0.0509	–2.2308
H(26)	3.1320	2.3577	1.4661
H(27)	4.2105	2.6491	0.0782
H(28)	2.4983	3.1345	–0.0016
C(29)	–3.8590	–0.0778	0.3190
H(30)	–3.6499	–1.0882	–0.0635
H(31)	–3.8624	–0.1298	1.4163
H(32)	–4.8745	0.1991	–0.0033

Energy = –1417.734964 Hartrees.
All coordinates are in Å.

Table 2.9 Calculated (PW91PW91/aug-cc-pVQZ-PP/6-311+G*) coordinates for [In($P_3C_2Bu^t_2$)], **1**.

Atom	*x*	*y*	*z*
In(1)	1.7775	–0.4844	0.0000
P(2)	–1.1709	–0.7448	0.0000
C(3)	–0.6044	0.2468	1.3639
P(4)	0.2394	1.7813	1.0796
P(5)	0.2394	1.7813	–1.0796
C(6)	–0.6044	0.2468	–1.3639
C(7)	–0.9318	–0.1980	2.8059
C(8)	–2.3433	0.3380	3.1490
C(9)	–0.9356	–1.7349	2.9404
H(10)	–3.0997	–0.0651	2.4603
H(11)	–2.6229	0.0476	4.1742
H(12)	–2.3756	1.4350	3.0822
H(13)	0.0471	–2.1610	2.6874
H(14)	–1.1708	–2.0214	3.9771
H(15)	–1.6831	–2.2060	2.2866
C(16)	–0.9318	–0.1980	–2.8059
C(17)	0.0742	0.3743	–3.8235
C(18)	–0.9356	–1.7349	–2.9404
C(19)	–2.3433	0.3380	–3.1490
H(20)	1.0987	0.0312	–3.6132
H(21)	–0.1908	0.0440	–4.8395
H(22)	0.0832	1.4735	–3.8230
H(23)	–1.6831	–2.2060	–2.2866
H(24)	–1.1708	–2.0214	–3.9771
H(25)	0.0471	–2.1610	–2.6874
H(26)	–2.3756	1.4350	–3.0822
H(27)	–2.6229	0.0476	–4.1742
H(28)	–3.0997	–0.0651	–2.4603
C(29)	0.0742	0.3743	3.8235
H(30)	1.0987	0.0312	3.6132
H(31)	0.0832	1.4735	3.8230
H(32)	–0.1908	0.0440	4.8395

Energy = –1606.150777 Hartrees.
All coordinates are in Å.

Table 2.10 Calculated (PW91PW91/LanL2DZ/6-311+G*) coordinates for [In($P_3C_2Bu^t_2$)], **1**.

Atom	*x*	*y*	*z*
In(1)	1.7881	–0.4647	0.0000
P(2)	–1.1671	–0.7681	0.0000
C(3)	–0.6115	0.2342	1.3601
P(4)	0.1883	1.7926	1.0787
P(5)	0.1883	1.7926	–1.0787
C(6)	–0.6115	0.2342	–1.3601
C(7)	–0.9223	–0.2122	2.8049
C(8)	–2.2959	0.3889	3.1896
C(9)	–0.9975	–1.7477	2.9272
H(10)	–3.0870	0.0358	2.5125
H(11)	–2.5666	0.0969	4.2167
H(12)	–2.2727	1.4870	3.1394
H(13)	–0.0467	–2.2205	2.6378
H(14)	–1.2119	–2.0307	3.9693
H(15)	–1.7895	–2.1761	2.2967
C(16)	–0.9223	–0.2122	–2.8049
C(17)	0.1386	0.3007	–3.7988
C(18)	–0.9975	–1.7477	–2.9272
C(19)	–2.2959	0.3889	–3.1896
H(20)	1.1382	–0.0915	–3.5567
H(21)	–0.1141	–0.0250	–4.8194
H(22)	0.2026	1.3980	–3.8053
H(23)	–1.7895	–2.1761	–2.2967
H(24)	–1.2119	–2.0307	–3.9693
H(25)	–0.0467	–2.2205	–2.6378
H(26)	–2.2727	1.4870	–3.1394
H(27)	–2.5666	0.0969	–4.2167
H(28)	–3.0870	0.0358	–2.5125
C(29)	0.1386	0.3007	3.7988
H(30)	1.1382	–0.0915	3.5567
H(31)	0.2026	1.3980	3.8053
H(32)	–0.1141	–0.0250	4.8194

Energy = –1417.797746 Hartrees.
All coordinates are in Å.

Table 2.11 Calculated (PBE1PBE/aug-cc-pVQZ-PP/6-311+G*) coordinates for [In($P_3C_2Bu^t_2$)], **1**.

Atom	*x*	*y*	*z*
In(1)	1.7560	–0.4790	0.0000
P(2)	–1.1622	–0.7341	0.0000
C(3)	–0.5992	0.2469	1.3524
P(4)	0.2311	1.7686	1.0679
P(5)	0.2311	1.7686	–1.0679
C(6)	–0.5992	0.2469	–1.3524
C(7)	–0.9183	–0.1986	2.7877
C(8)	–2.3149	0.3396	3.1395
C(9)	–0.9291	–1.7258	2.9168
H(10)	–3.0742	–0.0554	2.4587
H(11)	–2.5880	0.0492	4.1599
H(12)	–2.3425	1.4311	3.0770
H(13)	0.0435	–2.1554	2.6559
H(14)	–1.1551	–2.0115	3.9493
H(15)	–1.6816	–2.1895	2.2736
C(16)	–0.9183	–0.1986	–2.7877
C(17)	0.0915	0.3615	–3.7933
C(18)	–0.9291	–1.7258	–2.9168
C(19)	–2.3149	0.3396	–3.1395
H(20)	1.1076	0.0178	–3.5752
H(21)	–0.1656	0.0284	–4.8039
H(22)	0.1040	1.4547	–3.7995
H(23)	–1.6816	–2.1895	–2.2736
H(24)	–1.1551	–2.0115	–3.9493
H(25)	0.0435	–2.1554	–2.6559
H(26)	–2.3425	1.4311	–3.0770
H(27)	–2.5880	0.0492	–4.1599
H(28)	–3.0742	–0.0554	–2.4587
C(29)	0.0915	0.3615	3.7933
H(30)	1.1076	0.0178	3.5752
H(31)	0.1040	1.4547	3.7995
H(32)	–0.1656	0.0284	4.8039

Energy = –1605.404600 Hartrees.
All coordinates are in Å.

Table 2.12 Calculated (PBE1PBE/LanL2DZ/6-311+G*) coordinates for [In($P_3C_2Bu^t_2$)], **1**.

Atom	*x*	*y*	*z*
In(1)	1.7785	–0.4524	0.0000
P(2)	–1.1560	–0.7632	0.0000
C(3)	–0.6106	0.2319	1.3487
P(4)	0.1666	1.7818	1.0664
P(5)	0.1666	1.7818	–1.0664
C(6)	–0.6106	0.2319	–1.3487
C(7)	–0.9119	–0.2161	2.7864
C(8)	–2.2767	0.3736	3.1762
C(9)	–0.9790	–1.7422	2.9052
H(10)	–3.0653	0.0204	2.5057
H(11)	–2.5406	0.0796	4.1980
H(12)	–2.2596	1.4660	3.1292
H(13)	–0.0333	–2.2086	2.6112
H(14)	–1.1840	–2.0259	3.9425
H(15)	–1.7693	–2.1714	2.2837
C(16)	–0.9119	–0.2161	–2.7864
C(17)	0.1454	0.2955	–3.7694
C(18)	–0.9790	–1.7422	–2.9052
C(19)	–2.2767	0.3736	–3.1762
H(20)	1.1402	–0.0897	–3.5231
H(21)	–0.0993	–0.0329	–4.7845
H(22)	0.2042	1.3870	–3.7800
H(23)	–1.7693	–2.1714	–2.2837
H(24)	–1.1840	–2.0259	–3.9425
H(25)	–0.0333	–2.2086	–2.6112
H(26)	–2.2596	1.4660	–3.1292
H(27)	–2.5406	0.0796	–4.1980
H(28)	–3.0653	0.0204	–2.5057
C(29)	0.1454	0.2955	3.7694
H(30)	1.1402	–0.0897	3.5231
H(31)	0.2042	1.3870	3.7800
H(32)	–0.0993	–0.0329	4.7845

Energy = –1417.130152 Hartrees.
All coordinates are in Å.

Table 2.13 Calculated (B3PW91/aug-cc-pVQZ-PP/6-311+G*) coordinates for [In($P_2C_3Bu^t_3$)], **2**.

Atom	*x*	*y*	*z*
In(1)	–0.4412	–0.0215	1.8344
C(2)	–1.6389	0.0093	–0.6490
P(3)	–0.7023	1.4812	–0.5774
C(4)	0.9305	0.7082	–0.4626
C(5)	0.9277	–0.7082	–0.5079
P(6)	–0.7055	–1.4705	–0.6196
C(7)	–3.1604	0.0075	–0.8290
C(8)	–3.4530	–0.0948	–2.3391
C(9)	–3.8094	–1.1908	–0.1205
C(10)	–3.7969	1.2967	–0.2918
H(11)	–4.5336	–0.0928	–2.5208
H(12)	–3.0391	–1.0161	–2.7584
H(13)	–3.0148	0.7472	–2.8823
H(14)	–3.6385	–1.1581	0.9604
H(15)	–4.8918	–1.1877	–0.2872
H(16)	–3.4201	–2.1436	–0.4899
H(17)	–3.4100	2.1856	–0.7980
H(18)	–4.8808	1.2744	–0.4453
H(19)	–3.6138	1.4190	0.7804
C(20)	2.0856	1.7550	–0.4699
C(21)	2.5217	1.9856	–1.9317
C(22)	1.6022	3.1250	0.0573
C(23)	3.3019	1.4199	0.4057
H(24)	1.6817	2.3583	–2.5249
H(25)	3.3202	2.7349	–1.9743
H(26)	2.8849	1.0786	–2.4140
H(27)	1.2225	3.0584	1.0813
H(28)	2.4458	3.8226	0.0601
H(29)	0.8197	3.5695	–0.5603
H(30)	3.8422	0.5282	0.1014
H(31)	4.0133	2.2510	0.3621
H(32)	3.0103	1.3020	1.4542
C(33)	2.0952	–1.7407	–0.4885
C(34)	3.1534	–1.4440	–1.5657
C(35)	1.5961	–3.1640	–0.8213
C(36)	2.7315	–1.8548	0.9107
H(37)	2.6897	–1.3983	–2.5556
H(38)	3.8906	–2.2534	–1.5850
H(39)	3.7000	–0.5177	–1.4117
H(40)	0.8694	–3.5391	–0.0968
H(41)	2.4505	–3.8487	–0.8078
H(42)	1.1411	–3.2223	–1.8139
H(43)	3.0948	–0.9090	1.3056
H(44)	3.5764	–2.5522	0.8855
H(45)	2.0027	–2.2539	1.6237

Energy = –1460.692899 Hartrees.
All coordinates are in Å.

Table 2.14 Calculated (B3PW91/LanL2DZ/6-311+G*) coordinates for [In($P_2C_3Bu^t_3$)], **2**.

Atom	*x*	*y*	*z*
In(1)	0.4280	–0.0234	1.8451
C(2)	1.6405	0.0102	–0.6474
P(3)	0.7093	–1.4709	–0.6290
C(4)	–0.9212	–0.7076	–0.5099
C(5)	–0.9238	0.7096	–0.4629
P(6)	0.7065	1.4834	–0.5846
C(7)	3.1617	0.0079	–0.8255
C(8)	3.7976	1.2976	–0.2890
C(9)	3.8092	–1.1887	–0.1129
C(10)	3.4544	–0.0971	–2.3350
H(11)	4.8819	1.2744	–0.4397
H(12)	3.6116	1.4218	0.7825
H(13)	3.4127	2.1862	–0.7973
H(14)	3.4197	–2.1425	–0.4795
H(15)	4.8917	–1.1866	–0.2780
H(16)	3.6366	–1.1524	0.9677
H(17)	3.0152	0.7436	–2.8794
H(18)	4.5349	–0.0949	–2.5173
H(19)	3.0403	–1.0192	–2.7522
C(20)	–2.0892	–1.7390	–0.4945
C(21)	–3.1444	–1.4402	–1.5739
C(22)	–1.5904	–3.1620	–0.8296
C(23)	–2.7277	–1.8554	0.9035
H(24)	–2.6767	–1.3885	–2.5616
H(25)	–3.8791	–2.2517	–1.5999
H(26)	–3.6946	–0.5164	–1.4178
H(27)	–0.8624	–3.5382	–0.1070
H(28)	–2.4447	–3.8467	–0.8148
H(29)	–1.1377	–3.2193	–1.8232
H(30)	–3.0874	–0.9097	1.3018
H(31)	–3.5752	–2.5496	0.8755
H(32)	–2.0013	–2.2597	1.6161
C(33)	–2.0793	1.7552	–0.4741
C(34)	–2.5108	1.9829	–1.9374
C(35)	–1.5990	3.1263	0.0533
C(36)	–3.2967	1.4192	0.3995
H(37)	–3.3108	2.7304	–1.9844
H(38)	–1.6691	2.3563	–2.5277
H(39)	–2.8695	1.0743	–2.4198
H(40)	–1.2224	3.0614	1.0785
H(41)	–2.4434	3.8229	0.0529
H(42)	–0.8151	3.5714	–0.5621
H(43)	–3.8356	0.5271	0.0944
H(44)	–4.0087	2.2497	0.3555
H(45)	–3.0057	1.3011	1.4482

Energy = –1272.328338 Hartrees.
All coordinates are in Å.

Table 2.15 Calculated (B3LYP/aug-cc-pVQZ-PP/6-311+G*) coordinates for [In($P_2C_3Bu^t_3$)], **2**.

Atom	*x*	*y*	*z*
In(1)	–0.4675	–0.0246	1.8814
C(2)	–1.6415	0.0096	–0.6609
P(3)	–0.7006	1.4839	–0.5814
C(4)	0.9406	0.7092	–0.4618
C(5)	0.9380	–0.7081	–0.5084
P(6)	–0.7033	–1.4723	–0.6286
C(7)	–3.1678	0.0085	–0.8651
C(8)	–3.4417	–0.0819	–2.3867
C(9)	–3.8355	–1.1988	–0.1746
C(10)	–3.8215	1.2969	–0.3266
H(11)	–4.5192	–0.0781	–2.5827
H(12)	–3.0232	–0.9989	–2.8086
H(13)	–2.9972	0.7639	–2.9173
H(14)	–3.6858	–1.1747	0.9090
H(15)	–4.9140	–1.1901	–0.3607
H(16)	–3.4444	–2.1500	–0.5428
H(17)	–3.4305	2.1916	–0.8168
H(18)	–4.9016	1.2710	–0.5004
H(19)	–3.6607	1.4108	0.7494
C(20)	2.1035	1.7621	–0.4743
C(21)	2.5350	1.9965	–1.9443
C(22)	1.6277	3.1396	0.0621
C(23)	3.3328	1.4233	0.3939
H(24)	1.6952	2.3739	–2.5333
H(25)	3.3361	2.7420	–1.9889
H(26)	2.8930	1.0902	–2.4298
H(27)	1.2629	3.0743	1.0907
H(28)	2.4725	3.8344	0.0543
H(29)	0.8393	3.5864	–0.5434
H(30)	3.8717	0.5358	0.0805
H(31)	4.0417	2.2555	0.3493
H(32)	3.0511	1.2985	1.4435
C(33)	2.1142	–1.7456	–0.4966
C(34)	3.1692	–1.4461	–1.5862
C(35)	1.6184	–3.1788	–0.8269
C(36)	2.7671	–1.8598	0.9028
H(37)	2.6982	–1.3975	–2.5718
H(38)	3.9053	–2.2554	–1.6135
H(39)	3.7171	–0.5218	–1.4349
H(40)	0.8965	–3.5564	–0.1009
H(41)	2.4759	–3.8582	–0.8145
H(42)	1.1621	–3.2417	–1.8174
H(43)	3.1300	–0.9147	1.2960
H(44)	3.6147	–2.5524	0.8678
H(45)	2.0487	–2.2642	1.6221

Energy = –1460.9674256 Hartrees.
All coordinates are in Å.

Table 2.16 Calculated (B3LYP/LanL2DZ/6-311+G*) coordinates for [In($P_2C_3Bu^t_3$)], **2**.

Atom	*x*	*y*	*z*
In(1)	–0.4512	–0.0202	1.8804
C(2)	–1.6440	0.0081	–0.6539
P(3)	–0.7058	1.4839	–0.5874
C(4)	0.9329	0.7089	–0.4605
C(5)	0.9308	–0.7093	–0.5045
P(6)	–0.7080	–1.4749	–0.6275
C(7)	–3.1704	0.0059	–0.8549
C(8)	–3.4457	–0.0910	–2.3754
C(9)	–3.8363	–1.1983	–0.1571
C(10)	–3.8233	1.2962	–0.3199
H(11)	–4.5233	–0.0878	–2.5709
H(12)	–3.0274	–1.0099	–2.7934
H(13)	–3.0011	0.7523	–2.9098
H(14)	–3.6840	–1.1690	0.9259
H(15)	–4.9152	–1.1906	–0.3408
H(16)	–3.4458	–2.1512	–0.5215
H(17)	–3.4346	2.1891	–0.8151
H(18)	–4.9039	1.2688	–0.4901
H(19)	–3.6589	1.4150	0.7550
C(20)	2.0960	1.7611	–0.4803
C(21)	2.5205	1.9908	–1.9528
C(22)	1.6235	3.1403	0.0551
C(23)	3.3283	1.4231	0.3838
H(24)	1.6782	2.3679	–2.5383
H(25)	3.3226	2.7347	–2.0038
H(26)	2.8738	1.0824	–2.4376
H(27)	1.2633	3.0778	1.0854
H(28)	2.4688	3.8344	0.0419
H(29)	0.8327	3.5865	–0.5477
H(30)	3.8658	0.5352	0.0692
H(31)	4.0372	2.2551	0.3361
H(32)	3.0499	1.2992	1.4343
C(33)	2.1076	–1.7457	–0.4968
C(34)	3.1565	–1.4466	–1.5922
C(35)	1.6109	–3.1793	–0.8243
C(36)	2.7673	–1.8593	0.8995
H(37)	2.6790	–1.3939	–2.5745
H(38)	3.8897	–2.2582	–1.6264
H(39)	3.7087	–0.5246	–1.4421
H(40)	0.8900	–3.5562	–0.0968
H(41)	2.4683	–3.8589	–0.8117
H(42)	1.1535	–3.2438	–1.8141
H(43)	3.1300	–0.9138	1.2919
H(44)	3.6160	–2.5502	0.8602
H(45)	2.0533	–2.2654	1.6222

Energy = –1272.626858 Hartrees.
All coordinates are in Å.

Table 2.17 Calculated (BLYP/aug-cc-pVQZ-PP/6-311+G*) coordinates for [In($P_2C_3Bu^t_3$)], **2**.

Atom	*x*	*y*	*z*
In(1)	0.4794	–0.0172	1.9154
C(2)	1.6545	0.0075	–0.6674
P(3)	0.7077	–1.4895	–0.6237
C(4)	–0.9510	–0.7157	–0.5068
C(5)	–0.9537	0.7129	–0.4639
P(6)	0.7048	1.4970	–0.5876
C(7)	3.1898	0.0051	–0.8877
C(8)	3.8554	1.3105	–0.3678
C(9)	3.8724	–1.2034	–0.1845
C(10)	3.4502	–0.1046	–2.4245
H(11)	4.9402	1.2823	–0.5543
H(12)	3.7054	1.4377	0.7149
H(13)	3.4564	2.2047	–0.8670
H(14)	3.4749	–2.1649	–0.5386
H(15)	4.9554	–1.1964	–0.3838
H(16)	3.7337	–1.1656	0.9068
H(17)	2.9954	0.7388	–2.9637
H(18)	4.5322	–0.1009	–2.6331
H(19)	3.0265	–1.0332	–2.8326
C(20)	–2.1342	–1.7655	–0.4997
C(21)	–3.1891	–1.4704	–1.6090
C(22)	–1.6293	–3.2120	–0.8201
C(23)	–2.8065	–1.8736	0.9054
H(24)	–2.7077	–1.4282	–2.5972
H(25)	–3.9306	–2.2839	–1.6367
H(26)	–3.7399	–0.5383	–1.4660
H(27)	–0.9086	–3.5855	–0.0809
H(28)	–2.4910	–3.8972	–0.8113
H(29)	–1.1613	–3.2803	–1.8120
H(30)	–3.1879	–0.9227	1.2848
H(31)	–3.6502	–2.5814	0.8689
H(32)	–2.0866	–2.2626	1.6417
C(33)	–2.1232	1.7787	–0.4859
C(34)	–2.5422	2.0177	–1.9729
C(35)	–1.6460	3.1648	0.0644
C(36)	–3.3744	1.4373	0.3719
H(37)	–3.3451	2.7706	–2.0259
H(38)	–1.6902	2.3932	–2.5577
H(39)	–2.9017	1.1063	–2.4630
H(40)	–1.2930	3.0943	1.1036
H(41)	–2.4930	3.8675	0.0471
H(42)	–0.8424	3.6116	–0.5331
H(43)	–3.9130	0.5468	0.0433
H(44)	–4.0857	2.2761	0.3217
H(45)	–3.1055	1.3053	1.4306

Energy = –1460.4540112 Hartrees.
All coordinates are in Å.

Table 2.18 Calculated (BLYP/LanL2DZ/6-311+G*) coordinates for [In($P_2C_3Bu^t_3$)], **2**.

Atom	*x*	*y*	*z*
In(1)	0.4600	–0.0111	1.9025
C(2)	1.6578	0.0053	–0.6558
P(3)	0.7135	–1.4929	–0.6165
C(4)	–0.9432	–0.7171	–0.5004
C(5)	–0.9454	0.7121	–0.4609
P(6)	0.7112	1.4967	–0.5909
C(7)	3.1939	0.0017	–0.8703
C(8)	3.8578	1.3085	–0.3521
C(9)	3.8733	–1.2043	–0.1597
C(10)	3.4581	–0.1135	–2.4056
H(11)	4.9434	1.2788	–0.5332
H(12)	3.7024	1.4401	0.7292
H(13)	3.4622	2.2013	–0.8567
H(14)	3.4774	–2.1671	–0.5119
H(15)	4.9570	–1.1979	–0.3545
H(16)	3.7298	–1.1625	0.9307
H(17)	3.0045	0.7278	–2.9489
H(18)	4.5405	–0.1108	–2.6117
H(19)	3.0350	–1.0435	–2.8112
C(20)	–2.1271	–1.7663	–0.4967
C(21)	–3.1758	–1.4718	–1.6116
C(22)	–1.6208	–3.2131	–0.8142
C(23)	–2.8057	–1.8736	0.9053
H(24)	–2.6883	–1.4258	–2.5966
H(25)	–3.9145	–2.2876	–1.6458
H(26)	–3.7308	–0.5420	–1.4699
H(27)	–0.9017	–3.5860	–0.0732
H(28)	–2.4824	–3.8984	–0.8060
H(29)	–1.1513	–3.2827	–1.8052
H(30)	–3.1893	–0.9228	1.2826
H(31)	–3.6489	–2.5818	0.8651
H(32)	–2.0895	–2.2615	1.6456
C(33)	–2.1150	1.7775	–0.4907
C(34)	–2.5275	2.0105	–1.9801
C(35)	–1.6407	3.1657	0.0572
C(36)	–3.3688	1.4376	0.3636
H(37)	–3.3312	2.7620	–2.0396
H(38)	–1.6734	2.3852	–2.5622
H(39)	–2.8830	1.0969	–2.4687
H(40)	–1.2915	3.0988	1.0978
H(41)	–2.4881	3.8677	0.0346
H(42)	–0.8352	3.6114	–0.5386
H(43)	–3.9066	0.5470	0.0340
H(44)	–4.0797	2.2765	0.3105
H(45)	–3.1027	1.3064	1.4231

Energy = –1272.206169 Hartrees.
All coordinates are in Å.

Table 2.19 Calculated (PW91PW91/aug-cc-pVQZ-PP/6-311+G*) coordinates for [In($P_2C_3Bu^t_3$)], **2**.

Atom	*x*	*y*	*z*
In(1)	0.4416	–0.0151	1.8414
C(2)	1.6475	0.0082	–0.6532
P(3)	0.7108	–1.4844	–0.6198
C(4)	–0.9324	–0.7134	–0.5113
C(5)	–0.9357	0.7106	–0.4679
P(6)	0.7071	1.4928	–0.5860
C(7)	3.1731	0.0053	–0.8307
C(8)	3.8105	1.3063	–0.3053
C(9)	3.8235	–1.1902	–0.1048
C(10)	3.4690	–0.1151	–2.3459
H(11)	4.9005	1.2832	–0.4584
H(12)	3.6238	1.4403	0.7711
H(13)	3.4196	2.1936	–0.8243
H(14)	3.4302	–2.1515	–0.4661
H(15)	4.9120	–1.1893	–0.2713
H(16)	3.6487	–1.1440	0.9811
H(17)	3.0283	0.7253	–2.9013
H(18)	4.5560	–0.1152	–2.5259
H(19)	3.0523	–1.0465	–2.7557
C(20)	–2.1026	–1.7497	–0.4872
C(21)	–3.1712	–1.4534	–1.5634
C(22)	–1.6004	–3.1786	–0.8215
C(23)	–2.7358	–1.8615	0.9211
H(24)	–2.7104	–1.4091	–2.5615
H(25)	–3.9124	–2.2675	–1.5761
H(26)	–3.7191	–0.5208	–1.4063
H(27)	–0.8672	–3.5525	–0.0937
H(28)	–2.4587	–3.8683	–0.8062
H(29)	–1.1439	–3.2356	–1.8201
H(30)	–3.1108	–0.9111	1.3112
H(31)	–3.5769	–2.5731	0.9029
H(32)	–1.9949	–2.2482	1.6380
C(33)	–2.0948	1.7598	–0.4755
C(34)	–2.5374	1.9852	–1.9434
C(35)	–1.6073	3.1372	0.0473
C(36)	–3.3135	1.4247	0.4079
H(37)	–3.3403	2.7386	–1.9857
H(38)	–1.6938	2.3569	–2.5431
H(39)	–2.9041	1.0704	–2.4224
H(40)	–1.2240	3.0725	1.0766
H(41)	–2.4545	3.8400	0.0476
H(42)	–0.8192	3.5781	–0.5767
H(43)	–3.8584	0.5282	0.1024
H(44)	–4.0277	2.2615	0.3667
H(45)	–3.0163	1.3046	1.4610

Energy = –1460.662320 Hartrees.
All coordinates are in Å.

Table 2.20 Calculated (PW91PW91/LanL2DZ/6-311+G*) coordinates for [In($P_2C_3Bu^t_3$)], **2**.

Atom	*x*	*y*	*z*
In(1)	0.4289	–0.0150	1.8455
C(2)	1.6488	0.0084	–0.6509
P(3)	0.7143	–1.4857	–0.6273
C(4)	–0.9265	–0.7131	–0.5122
C(5)	–0.9292	0.7116	–0.4682
P(6)	0.7112	1.4947	–0.5946
C(7)	3.1745	0.0048	–0.8240
C(8)	3.8104	1.3064	–0.2987
C(9)	3.8218	–1.1888	–0.0925
C(10)	3.4730	–0.1189	–2.3379
H(11)	4.9011	1.2821	–0.4465
H(12)	3.6185	1.4429	0.7765
H(13)	3.4228	2.1931	–0.8213
H(14)	3.4291	–2.1511	–0.4515
H(15)	4.9108	–1.1890	–0.2552
H(16)	3.6432	–1.1389	0.9927
H(17)	3.0325	0.7201	–2.8957
H(18)	4.5601	–0.1191	–2.5167
H(19)	3.0567	–1.0510	–2.7463
C(20)	2.0970	–1.7486	–0.4899
C(21)	–3.1646	–1.4507	–1.5666
C(22)	–1.5950	–3.1770	–0.8271
C(23)	–2.7300	–1.8625	0.9181
H(24)	–2.7016	–1.4003	–2.5633
H(25)	–3.9028	–2.2674	–1.5846
H(26)	–3.7163	–0.5211	–1.4063
H(27)	–0.8602	–3.5523	–0.1017
H(28)	–2.4531	–3.8669	–0.8103
H(29)	–1.1414	–3.2328	–1.8270
H(30)	–3.1028	–0.9123	1.3111
H(31)	–3.5725	–2.5725	0.8989
H(32)	–1.9898	–2.2520	1.6342
C(33)	–2.0888	1.7596	–0.4789
C(34)	–2.5297	1.9801	–1.9476
C(35)	–1.6032	3.1388	0.0413
C(36)	–3.3064	1.4246	0.4058
H(37)	–3.3339	2.7320	–1.9936
H(38)	–1.6856	2.3516	–2.5468
H(39)	–2.8935	1.0634	–2.4248
H(40)	–1.2206	3.0771	1.0709
H(41)	–2.4514	3.8405	0.0395
H(42)	–0.8153	3.5797	–0.5829
H(43)	–3.8511	0.5277	0.1014
H(44)	–4.0211	2.2610	0.3654
H(45)	–3.0070	1.3049	1.4584

Energy = –1272.312675 Hartrees.
All coordinates are in Å.

Table 2.21 Calculated (PBE1PBE/aug-cc-pVQZ-PP/6-311+G*) coordinates for [In($P_2C_3Bu^t_3$)], **2**.

Atom	*x*	*y*	*z*
In(1)	0.4347	–0.0200	1.8161
C(2)	1.6365	0.0091	–0.6488
P(3)	0.7058	–1.4692	–0.6230
C(4)	–0.9229	–0.7074	–0.5114
C(5)	–0.9256	0.7072	–0.4663
P(6)	0.7027	1.4796	–0.5822
C(7)	3.1559	0.0071	–0.8152
C(8)	3.7847	1.2947	–0.2756
C(9)	3.7955	–1.1873	–0.0998
C(10)	3.4612	–0.0978	–2.3184
H(11)	4.8700	1.2717	–0.4182
H(12)	3.5898	1.4190	0.7944
H(13)	3.4021	2.1820	–0.7880
H(14)	3.4089	–2.1404	–0.4716
H(15)	4.8794	–1.1843	–0.2562
H(16)	3.6134	–1.1521	0.9793
H(17)	3.0278	0.7436	–2.8664
H(18)	4.5435	–0.0963	–2.4894
H(19)	3.0505	–1.0199	–2.7391
C(20)	–2.0887	–1.7350	–0.4835
C(21)	–3.1555	–1.4366	–1.5465
C(22)	–1.5941	–3.1539	–0.8242
C(23)	–2.7078	–1.8515	0.9195
H(24)	–2.7009	–1.3859	–2.5405
H(25)	–3.8896	–2.2488	–1.5615
H(26)	–3.7038	–0.5128	–1.3840
H(27)	–0.8611	–3.5313	–0.1071
H(28)	–2.4490	–3.8378	–0.8052
H(29)	–1.1477	–3.2083	–1.8210
H(30)	–3.0591	–0.9051	1.3243
H(31)	–3.5576	–2.5431	0.8998
H(32)	–1.9727	–2.2599	1.6208
C(33)	–2.0801	1.7478	–0.4669
C(34)	–2.5309	1.9710	–1.9214
C(35)	–1.5942	3.1182	0.0463
C(36)	–3.2819	1.4156	0.4242
H(37)	–3.3318	2.7181	–1.9574
H(38)	–1.6972	2.3449	–2.5228
H(39)	–2.8955	1.0616	–2.3980
H(40)	–1.2023	3.0573	1.0662
H(41)	–2.4396	3.8135	0.0549
H(42)	–0.8199	3.5608	–0.5831
H(43)	–3.8260	0.5217	0.1332
H(44)	–3.9938	2.2464	0.3853
H(45)	–2.9754	1.3041	1.4693

Energy = –1459.889363 Hartrees.
All coordinates are in Å.

Table 2.22 Calculated (PBE1PBE/LanL2DZ/6-311+G*) coordinates for [In($P_2C_3Bu^t_3$)], **2**.

Atom	*x*	*y*	*z*
In(1)	0.4223	–0.0245	1.8325
C(2)	1.6379	0.0110	–0.6488
P(3)	0.7094	–1.4685	–0.6357
C(4)	–0.9166	–0.7061	–0.5149
C(5)	–0.9191	0.7093	–0.4668
P(6)	0.7065	1.4825	–0.5887
C(7)	3.1567	0.0088	–0.8150
C(8)	3.7854	1.2968	–0.2769
C(9)	3.7957	–1.1839	–0.0963
C(10)	3.4603	–0.0987	–2.3180
H(11)	4.8708	1.2732	–0.4178
H(12)	3.5889	1.4228	0.7927
H(13)	3.4040	2.1838	–0.7908
H(14)	3.4083	–2.1380	–0.4646
H(15)	4.8796	–1.1821	–0.2524
H(16)	3.6133	–1.1450	0.9827
H(17)	3.0250	0.7413	–2.8666
H(18)	4.5422	–0.0969	–2.4911
H(19)	3.0490	–1.0217	–2.7361
C(20)	–2.0828	–1.7325	–0.4924
C(21)	–3.1461	–1.4313	–1.5580
C(22)	–1.5885	–3.1509	–0.8359
C(23)	–2.7046	–1.8522	0.9090
H(24)	–2.6867	–1.3744	–2.5495
H(25)	–3.8780	–2.2453	–1.5805
H(26)	–3.6976	–0.5100	–1.3934
H(27)	–0.8541	–3.5296	–0.1209
H(28)	–2.4431	–3.8350	–0.8159
H(29)	–1.1443	–3.2039	–1.8337
H(30)	–3.0518	–0.9061	1.3181
H(31)	–3.5575	–2.5399	0.8860
H(32)	–1.9724	–2.2669	1.6097
C(33)	–2.0740	1.7486	–0.4708
C(34)	–2.5190	1.9703	–1.9271
C(35)	–1.5918	3.1195	0.0444
C(36)	–3.2777	1.4144	0.4168
H(37)	–3.3214	2.7154	–1.9676
H(38)	–1.6831	2.3456	–2.5246
H(39)	–2.8784	1.0597	–2.4050
H(40)	–1.2036	3.0590	1.0657
H(41)	–2.4381	3.8137	0.0501
H(42)	–0.8157	3.5635	–0.5817
H(43)	–3.8199	0.5201	0.1239
H(44)	–3.9905	2.2444	0.3775
H(45)	–2.9727	1.3021	1.4624

Energy = –1271.618689 Hartrees.
All coordinates are in Å.

Table 2.23 Selected interatomic distances (r_a/pm) and amplitudes of vibration (u_{h1}/pm) for the restrained GED structure of [In($P_3C_2Bu^t_2$)], **1**.[a]

	Atom pair	r_a/pm	u_{h1}/pm[b]	Restraint
u_1	C(9)–H(15)	109.4(4)	7.8(6)	7.9(8)
u_2	C(9)–H(13)	109.4(4)	7.9(tied to u_1)	—
u_3	C(8)–H(10)	109.4(4)	7.7(tied to u_1)	—
u_4	C(17)–H(20)	109.5(4)	7.4(tied to u_1)	—
u_5	C(19)–H(26)	109.5(4)	7.4(tied to u_1)	—
u_6	C(18)–H(23)	109.5(4)	7.4(tied to u_1)	—
u_7	C(8)–H(11)	109.5(4)	7.4(tied to u_1)	—
u_8	C(18)–H(24)	109.5(4)	7.4(tied to u_1)	—
u_9	C(9)–H(14)	109.5(4)	7.4(tied to u_1)	—
u_{10}	C(7)–C(29)	153.8(3)	5.8(5)	5.8(6)
u_{11}	C(7)–C(9)	153.9(3)	5.8(tied to u_{10})	—
u_{12}	C(3)–C(7)	154.3(3)	5.3(tied to u_{10})	—
u_{13}	C(7)–C(8)	154.4(3)	5.9(tied to u_{10})	—
u_{14}	C(3)–P(4)	176.6(4)	5.0(5)	5.1(5)
u_{15}	P(2)–C(3)	177.2(4)	5.0(tied to u_{14})	—
u_{16}	P(4)–P(5)	213.3(11)	5.8(5)	5.4(5)
u_{17}	C(8)···C(29)	246.1(40)	7.4(tied tou_{18})	—
u_{18}	C(9)···C(29)	248.2(17)	6.8(7)	—
u_{19}	C(8)···C(9)	249.8(17)	7.3(tied tou_{18})	—
u_{20}	C(3)···C(8)	251.3(12)	7.5(tied to u_{18})	—
u_{21}	C(3)···C(29)	256.2(11)	7.0(tied tou_{18})	—
u_{22}	C(3)···C(9)	257.7(13)	7.1(tied tou_{18})	—
u_{23}	C(3)···C(6)	272.0(10)	5.4(tied tou_{18})	—
u_{24}	In(1)–C(3)	282.8(10)	14.2(tied to u_{27})	—
u_{25}	P(2)···C(7)	285.8(17)	7.2(tied tou_{27})	—
u_{26}	P(4)···C(7)	287.2(15)	7.1(tied tou_{27})	—
u_{27}	In(1)–P(4)	292.5(14)	13.4(7)	14.5(15)
u_{28}	In(1)–P(2)	293.2(20)	13.3(tied to u_{27})	—
u_{29}	C(3)···P(5)	298.5(8)	6.0(tied tou_{27})	—
u_{30}	P(2)···P(4)	306.5(9)	5.4(tied tou_{27})	—
u_{31}	P(4)···C(29)	313.7(24)	20.5(tied to u_{27})	—
u_{32}	P(2)···C(8)	331.3(73)	42.7(tied to u_{27})	—
u_{33}	P(2)···C(9)	335.5(43)	22.9(tied to u_{27})	—
u_{34}	P(4)···C(8)	370.4(57)	42.0(tied tou_{35})	—
u_{35}	In(1)···C(7)	389.5(14)	19.6(15)	—
u_{36}	In(1)···C(9)	405.6(49)	48.2(tied tou_{35})	—
u_{37}	In(1)···C(17)	445.4(78)	60.5(59)	57.6(58)
u_{38}	C(3)···C(19)	475.1(40)	22.5(tied tou_{40})	—
u_{39}	C(3)···C(18)	487.2(26)	14.4(tied tou_{40})	—
u_{40}	In(1)···C(8)	508.1(21)	20.3(13)	—
u_{41}	P(4)···C(17)	509.8(17)	13.2(tied tou_{40})	—
u_{42}	P(4)···C(19)	519.2(23)	21.3(tied tou_{40})	—
u_{43}	C(3)···C(17)	520.0(12)	12.6(tied tou_{40})	—
u_{44}	P(4)···C(18)	540.6(20)	13.6(tied tou_{40})	—
u_{45}	C(7)···C(16)	558.6(25)	9.1(tied tou_{40})	—

[a] Estimated standard deviations, as obtained in the least squares refinement, are given in parentheses. [b] Amplitudes not refined were fixed at the values obtained using the force field calculated at the RHF level with aug-cc-pVQZ on In and 6-31G* on P, C, and H. Other amplitudes were also included and fixed at this level but are not shown here.

Table 2.24 Experimental (GED) coordinates for [In($P_3C_2Bu^t_2$)], **1**.

Atom	*x*	*y*	*z*
In(1)	0.0000	–1.6433	2.4312
P(2)	0.0000	0.0000	0.0000
C(3)	1.3598	–1.1347	0.0000
P(4)	1.0661	–2.8755	0.0000
P(5)	–1.0661	–2.8755	0.0000
C(6)	–1.3598	–1.1347	0.0000
C(7)	2.7992	–0.5833	–0.0788
C(8)	3.0295	–0.0123	–1.4952
C(9)	3.0759	0.5294	0.9484
H(10)	2.3267	0.7967	–1.7229
H(11)	4.0437	0.3905	–1.5920
H(12)	2.9010	–0.7821	–2.2641
H(13)	2.9360	0.1777	1.9765
H(14)	4.1069	0.8880	0.8543
H(15)	2.4163	1.3950	0.8218
C(16)	–2.7992	–0.5833	–0.0788
C(17)	–3.8534	–1.6861	0.1183
C(18)	–3.0759	0.5294	0.9484
C(19)	–3.0295	–0.0123	–1.4952
H(20)	–3.7544	–2.1763	1.0931
H(21)	–4.8620	–1.2630	0.0568
H(22)	–3.7821	–2.4763	–0.6373
H(23)	–2.4163	1.3950	0.8218
H(24)	–4.1069	0.8880	0.8543
H(25)	–2.9360	0.1777	1.9765
H(26)	–2.9010	–0.7821	–2.2641
H(27)	–4.0437	0.3905	–1.5920
H(28)	–2.3267	0.7967	–1.7229
C(29)	3.8534	–1.6861	0.1183
H(30)	3.7544	–2.1763	1.0931
H(31)	3.7821	–2.4763	–0.6373
H(32)	4.8620	–1.2630	0.0568

All coordinates are in Å.

Table 2.25 Selected interatomic distances (r_a/pm) and amplitudes of vibration (u_{h1}/pm) for the best-fit GED structure of [In($P_2C_3Bu^t_3$)], **2**.[a]

	Atom pair	r_a/pm	u_{h1}/pm[b]	Restraint
$u_{1–27}$	C–H	109.2(1)	8.1(5)	—
u_{28}	C(4)–C(5)	141.4(2)	4.3(4)	—
u_{29}	C(2)–C(7)	153.8(2)	4.8(tied to u_{28})	—
u_{30}	C(5)–C(33)	153.8(2)	5.0(tied to u_{28})	—
u_{31}	C(4)–C(20)	153.8(2)	5.0(tied to u_{28})	—
u_{32}	C(20)–C(21)	153.9(2)	4.8(tied to u_{28})	—
u_{33}	C(33)–C(36)	153.9(2)	4.8(tied to u_{28})	—
u_{34}	C(33)–C(34)	153.9(2)	4.8(tied to u_{28})	—
u_{35}	C(20)–C(23)	153.9(2)	4.8(tied to u_{28})	—
u_{36}	C(7)–C(9)	153.9(2)	4.8(tied to u_{28})	—
u_{37}	C(7)–C(10)	153.9(2)	4.7(tied to u_{28})	—
u_{38}	C(33)–C(35)	153.9(2)	4.8(tied to u_{28})	—
u_{39}	C(7)–C(8)	153.9(2)	4.8(tied to u_{28})	—
u_{40}	C(20)–C(22)	153.9(2)	4.8(tied to u_{28})	—
u_{41}	C(2)–P(6)	178.4(11)	5.1(5)	—
u_{42}	C(2)–P(3)	178.5(11)	5.0(tied to u_{41})	—
u_{43}	C(5)–P(6)	184.9(8)	5.5(tied to u_{41})	—
u_{44}	P(3)–C(4)	184.9(8)	5.5(tied to u_{41})	—
u_{45}	C(22)···C(23)	241.8(3)	17.3(tied tou_{71})	—
u_{46}	C(34)···C(35)	241.9(3)	17.4(tied tou_{71})	—
u_{47}	C(35)···C(36)	243.0(3)	18.0(tied tou_{71})	—
u_{48}	C(21)···C(22)	244.7(3)	18.6(tied tou_{71})	—
u_{49}	C(2)···C(8)	247.1(3)	18.6(tied tou_{71})	—
u_{50}	C(5)···C(34)	247.6(3)	20.5(tied tou_{71})	—
u_{51}	C(9)···C(10)	248.3(3)	18.0(tied tou_{71})	—
u_{52}	C(8)···C(10)	248.5(3)	18.4(tied tou_{71})	—
u_{53}	C(8)···C(9)	248.6(3)	18.4(tied tou_{71})	—
u_{54}	C(21)···C(23)	251.4(3)	19.4(tied tou_{71})	—
u_{55}	C(5)···C(36)	252.3(3)	19.4(tied tou_{71})	—
u_{56}	C(4)···C(22)	253.0(3)	17.1(tied tou_{71})	—
u_{57}	C(4)···C(23)	253.1(3)	19.5(tied tou_{71})	—
u_{58}	C(2)···C(10)	253.3(3)	17.3(tied tou_{71})	—
u_{59}	C(34)···C(36)	253.3(3)	19.6(tied tou_{71})	—
u_{60}	C(2)···C(9)	253.6(3)	17.6(tied tou_{71})	—
u_{61}	C(4)···C(21)	254.0(3)	19.6(tied tou_{71})	—
u_{62}	C(5)···C(35)	259.7(3)	17.0(tied tou_{71})	—
u_{63}	In(1)–C(2)	261.8(16)	28.6(tied to u_{71})	—
u_{64}	C(5)···C(20)	267.9(3)	16.3(tied tou_{71})	—
u_{65}	C(4)···C(33)	268.8(3)	16.4(tied tou_{71})	—
u_{66}	C(23)···C(36)	269.3(49)	42.3(tied tou_{71})	—
u_{67}	C(2)···C(5)	271.1(8)	15.0(tied tou_{71})	—
u_{68}	C(2)···C(4)	271.1(8)	15.0(tied tou_{71})	—
u_{69}	P(3)···C(5)	276.1(6)	13.7(tied tou_{71})	—
u_{70}	C(4)···P(6)	276.2(6)	13.6(tied tou_{71})	—
u_{71}	In(1)–P(3)	277.7(12)	26.2(9)	—

u_{72}	In(1)–P(6)	277.7(12)	26.6(tied to u_{71})	—
u_{73}	In(1)–C(4)	279.3(22)	30.2(tied to u_{71})	—
u_{74}	In(1)–C(5)	279.4(22)	29.9(tied to u_{71})	—
u_{75}	P(6)···C(33)	280.4(12)	17.0(tied tou_{71})	—
u_{76}	P(3)···C(20)	281.9(12)	17.2(tied tou_{71})	—
u_{77}	P(3)···C(22)	285.8(20)	25.9(tied tou_{71})	—
u_{78}	P(6)···C(7)	290.2(11)	17.6(tied tou_{71})	—
u_{79}	P(3)···C(7)	290.2(11)	17.5(tied tou_{71})	—
u_{80}	P(6)···C(35)	295.2(22)	23.6(tied tou_{71})	—
u_{81}	P(3)···P(6)	300.2(19)	13.0(tied tou_{71})	—
u_{82}	C(5)···C(23)	321.0(22)	25.8(tied tou_{71})	—
u_{83}	P(3)···C(10)	325.9(36)	34.3(tied tou_{71})	—
u_{84}	C(4)···C(34)	337.2(31)	27.5(tied tou_{71})	—
u_{85}	C(20)···C(36)	340.0(52)	11.1(tied tou_{88})	—
u_{86}	C(5)···C(21)	342.5(28)	9.6(tied tou_{88})	—
u_{87}	C(20)···C(33)	346.2(4)	6.9(tied tou_{88})	—
u_{88}	In(1)···C(9)	347.9(43)	26.6(54)	—
u_{89}	C(23)···C(33)	348.8(49)	10.0(tied tou_{88})	—
u_{90}	P(3)···C(9)	353.7(37)	10.0(tied tou_{88})	—
u_{91}	In(1)···C(7)	361.7(25)	13.1(tied tou_{88})	—
u_{92}	P(6)···C(34)	363.7(48)	10.5(tied tou_{88})	—
u_{93}	C(21)···C(34)	374.2(70)	17.3(tied tou_{88})	—
u_{94}	P(3)···C(21)	374.9(39)	14.3(tied tou_{88})	—
u_{95}	P(6)···C(9)	384.1(43)	27.5(tied tou_{88})	—
u_{96}	In(1)···C(33)	386.3(24)	13.5(tied tou_{88})	—
u_{97}	In(1)···C(20)	386.5(25)	13.7(tied tou_{88})	—
u_{98}	C(5)···C(22)	390.2(7)	6.2(tied tou_{88})	—
u_{99}	C(21)···C(33)	390.8(59)	12.9(tied tou_{88})	—
u_{100}	C(20)···C(34)	391.4(66)	10.6(tied tou_{88})	—
u_{101}	C(4)···C(35)	396.3(9)	5.9(tied tou_{88})	—
u_{102}	C(21)···C(36)	399.5(131)	15.4(tied tou_{105})	—
u_{103}	P(3)···C(23)	400.4(32)	11.6(tied tou_{105})	—
u_{104}	P(6)···C(36)	402.9(31)	15.0(tied tou_{105})	—
u_{105}	In(1)···C(23)	405.0(43)	30.1(27)	—
u_{106}	P(6)···C(10)	406.0(23)	10.4(tied tou_{105})	—
u_{107}	In(1)···C(36)	410.9(51)	27.9(tied tou_{105})	—
u_{108}	C(2)···C(33)	413.9(8)	7.4(tied tou_{105})	—
u_{109}	P(3)···C(8)	414.4(19)	26.1(tied tou_{105})	—
u_{110}	C(2)···C(20)	414.7(8)	7.5(tied tou_{105})	—
u_{111}	C(23)···C(34)	416.4(129)	15.3(tied tou_{105})	—
u_{112}	C(5)···C(7)	421.5(8)	7.5(tied tou_{105})	—
u_{113}	C(4)···C(7)	421.5(8)	7.5(tied tou_{105})	—
u_{114}	In(1)···C(22)	421.6(54)	27.6(tied tou_{105})	—
u_{115}	P(6)···C(20)	427.9(7)	7.2(tied tou_{105})	—
u_{116}	In(1)···C(35)	427.9(55)	22.8(tied tou_{105})	—
u_{117}	P(3)···C(33)	428.2(7)	7.3(tied tou_{105})	—
u_{118}	In(1)···C(8)	441.8(41)	16.0(tied tou_{105})	—
u_{119}	C(2)···C(22)	455.4(11)	10.4(tied tou_{105})	—
u_{120}	C(2)···C(35)	464.2(10)	10.2(tied tou_{105})	—

u_{121}	C(5)···C(8)	468.5(9)	15.7(tied to u_{105})	—
u_{122}	C(22)···C(36)	474.6(26)	39.2(tied to u_{139})	—
u_{123}	C(23)···C(35)	483.5(38)	24.9(tied to u_{139})	—
u_{124}	C(2)···C(34)	487.2(27)	27.0(tied to u_{139})	—
u_{125}	C(22)···C(33)	488.9(13)	19.3(tied to u_{139})	—
u_{126}	C(20)···C(35)	491.5(15)	18.1(tied to u_{139})	—
u_{127}	P(3)···C(36)	492.1(11)	23.9(tied to u_{139})	—
u_{128}	C(4)···C(9)	492.1(14)	20.7(tied to u_{139})	—
u_{129}	P(6)···C(23)	493.6(8)	21.4(tied to u_{139})	—
u_{130}	P(3)···C(34)	493.9(12)	25.8(tied to u_{139})	—
u_{131}	C(2)···C(21)	497.5(19)	31.4(tied to u_{139})	—
u_{132}	P(6)···C(21)	500.7(15)	27.0(tied to u_{139})	—
u_{133}	C(5)···C(9)	503.2(18)	21.7(tied to u_{139})	—
u_{134}	C(4)···C(8)	507.5(10)	30.1(tied to u_{139})	—
u_{135}	C(5)···C(10)	511.0(11)	18.2(tied to u_{139})	—
u_{136}	C(2)···C(23)	511.7(21)	21.8(tied to u_{139})	—
u_{137}	C(2)···C(36)	512.8(18)	25.8(tied to u_{139})	—
u_{138}	P(6)···C(22)	518.5(8)	16.1(tied to u_{139})	—
u_{139}	In(1)···C(34)	518.6(23)	31.3(22)	—
u_{140}	In(1)···C(21)	522.2(23)	29.5(tied to u_{139})	—
u_{141}	P(3)···C(35)	526.3(9)	16.0(tied to u_{139})	—
u_{142}	C(22)···C(34)	540.4(58)	25.9(tied to u_{139})	—
u_{143}	C(21)···C(35)	540.6(55)	39.3(tied to u_{139})	—
u_{144}	C(7)···C(33)	556.2(9)	15.8(tied to u_{139})	—
u_{145}	C(7)···C(20)	557.2(9)	15.8(tied to u_{139})	—

[a] Estimated standard deviations, as obtained in the least squares refinement, are given in parentheses. [b] Amplitudes not refined were fixed at the values obtained using the force field calculated at the RHF level with aug-cc-pVQZ on In and 6-31G* on P, C, and H. Other amplitudes were also included and fixed at this level but are not shown here.

Table 2.27 Selected interatomic distances (r_a/pm) and amplitudes of vibration (u_{h1}/pm) for the restrained GED structure of [In($P_2C_3Bu^t_3$)], **2**.[a]

	Atom pair	r_a/pm	u_{h1}/pm[b]	Restraint
$u_{1–27}$	C–H	109.3(6)	7.7(9)	7.6(8)
u_{28}	C(4)–C(5)	140.9(8)	4.6(6)	4.8(5)
u_{29}	C(2)–C(7)	153.1(6)	5.1(tied to u_{28})	—
u_{30}	C(5)–C(33)	153.2(6)	5.3(tied to u_{28})	—
u_{31}	C(4)–C(20)	153.2(6)	5.3(tied to u_{28})	—
u_{32}	C(20)–C(21)	153.3(6)	5.1(tied to u_{28})	—
u_{33}	C(33)–C(36)	153.3(6)	5.1(tied to u_{28})	—
u_{34}	C(33)–C(34)	153.3(6)	5.1(tied to u_{28})	—
u_{35}	C(20)–C(23)	153.3(6)	5.1(tied to u_{28})	—
u_{36}	C(7)–C(9)	153.3(6)	5.1(tied to u_{28})	—
u_{37}	C(7)–C(10)	153.3(6)	5.1(tied to u_{28})	—
u_{38}	C(33)–C(35)	153.3(6)	5.1(tied to u_{28})	—
u_{39}	C(7)–C(8)	153.3(6)	5.1(tied to u_{28})	—
u_{40}	C(20)–C(22)	153.3(6)	5.2(tied to u_{28})	—
u_{41}	C(2)–P(6)	173.6(8)	5.1(6)	5.1(5)
u_{42}	C(2)–P(3)	173.6(8)	5.1(tied to u_{41})	—
u_{43}	C(5)–P(6)	176.0(16)	5.5(tied to u_{41})	—
u_{44}	P(3)–C(4)	176.0(16)	5.5(tied to u_{41})	—
u_{45}	C(22)···C(23)	242.8(22)	6.0(8)	7.5(8)
u_{46}	C(34)···C(35)	242.1(22)	6.1(tied tou_{45})	—
u_{47}	C(35)···C(36)	244.5(22)	6.3(tied tou_{45})	—
u_{48}	C(21)···C(22)	244.8(22)	6.5(tied tou_{45})	—
u_{49}	C(2)···C(8)	248.7(20)	6.5(tied tou_{45})	—
u_{50}	C(5)···C(34)	249.3(23)	7.2(tied tou_{45})	—
u_{51}	C(9)···C(10)	248.6(21)	6.3(tied tou_{45})	—
u_{52}	C(8)···C(10)	244.0(66)	6.4(tied tou_{45})	—
u_{53}	C(8)···C(9)	248.6(21)	6.4(tied tou_{45})	—
u_{54}	C(21)···C(23)	245.2(7)	6.8(tied tou_{45})	—
u_{55}	C(5)···C(36)	253.9(22)	6.8(tied tou_{45})	—
u_{56}	C(4)···C(22)	254.7(19)	6.0(tied tou_{45})	—
u_{57}	C(4)···C(23)	255.1(19)	6.8(tied tou_{45})	—
u_{58}	C(2)···C(10)	254.7(20)	6.1(tied tou_{45})	—
u_{59}	C(34)···C(36)	248.4(67)	6.9(tied tou_{45})	—
u_{60}	C(2)···C(9)	255.0(20)	6.2(tied tou_{45})	—
u_{61}	C(4)···C(21)	255.9(18)	6.9(tied tou_{45})	—
u_{62}	C(5)···C(35)	260.4(23)	6.0(tied tou_{45})	—
u_{63}	In(1)–C(2)	276.5(12)	13.8(14)	12.4(12)
u_{64}	C(5)···C(20)	267.9(14)	7.9(tied tou_{63})	—
u_{65}	C(4)···C(33)	268.8(14)	7.9(tied tou_{63})	—
u_{66}	C(23)···C(36)	272.0(103)	21.8(tied tou_{88})	—
u_{67}	C(2)···C(5)	261.9(19)	7.2(tied tou_{63})	—
u_{68}	C(2)···C(4)	261.9(19)	7.2(tied tou_{63})	—
u_{69}	P(3)···C(5)	268.3(13)	6.6(tied tou_{63})	—
u_{70}	C(4)···P(6)	268.3(13)	6.6(tied tou_{63})	—
u_{71}	In(1)–P(3)	286.1(9)	14.5(10)	11.4(11)

u_{72}	In(1)–P(6)	286.2(9)	14.7(tied to u_{71})	—
u_{73}	In(1)–C(4)	280.3(29)	16.7(tied to u_{71})	—
u_{74}	In(1)–C(5)	280.4(29)	16.5(tied to u_{71})	—
u_{75}	P(6)···C(33)	272.8(21)	8.2(tied tou_{63})	—
u_{76}	P(3)···C(20)	274.4(21)	8.3(tied tou_{63})	—
u_{77}	P(3)···C(22)	294.1(43)	12.5(tied tou_{63})	—
u_{78}	P(6)···C(7)	286.4(11)	7.6(tied tou_{71})	—
u_{79}	P(3)···C(7)	286.4(11)	7.5(tied tou_{71})	—
u_{80}	P(6)···C(35)	289.7(43)	10.3(tied tou_{71})	—
u_{81}	P(3)···P(6)	291.9(14)	7.2(tied tou_{71})	—
u_{82}	C(5)···C(23)	314.5(30)	13.3(tied tou_{88})	—
u_{83}	P(3)···C(10)	313.3(36)	14.9(tied tou_{88})	—
u_{84}	C(4)···C(34)	331.3(42)	14.1(tied tou_{88})	—
u_{85}	C(20)···C(36)	351.8(79)	16.9(tied tou_{88})	—
u_{86}	C(5)···C(21)	354.2(43)	14.7(tied tou_{88})	—
u_{87}	C(20)···C(33)	345.8(39)	10.5(tied tou_{88})	—
u_{88}	In(1)···C(9)	395.1(82)	40.6(40)	36.4(36)
u_{89}	C(23)···C(33)	328.9(59)	15.2(tied tou_{88})	—
u_{90}	P(3)···C(9)	407.1(34)	15.2(tied tou_{88})	—
u_{91}	In(1)···C(7)	373.3(25)	19.9(tied tou_{88})	—
u_{92}	P(6)···C(34)	368.1(66)	16.0(tied tou_{88})	—
u_{93}	C(21)···C(34)	385.5(156)	26.4(tied tou_{88})	—
u_{94}	P(3)···C(21)	351.2(73)	21.8(tied tou_{88})	—
u_{95}	P(6)···C(9)	315.4(49)	42.0(tied tou_{88})	—
u_{96}	In(1)···C(33)	378.5(33)	20.6(tied tou_{88})	—
u_{97}	In(1)···C(20)	378.6(33)	20.9(tied tou_{88})	—
u_{98}	C(5)···C(22)	385.8(26)	9.4(tied tou_{88})	—
u_{99}	C(21)···C(33)	415.0(99)	19.7(tied tou_{88})	—
u_{100}	C(20)···C(34)	374.4(93)	16.2(tied tou_{88})	—
u_{101}	C(4)···C(35)	396.7(24)	9.0(tied tou_{88})	—
u_{102}	C(21)···C(36)	443.1(138)	15.2(tied tou_{105})	—
u_{103}	P(3)···C(23)	404.5(31)	11.4(tied tou_{105})	—
u_{104}	P(6)···C(36)	389.1(45)	14.8(tied tou_{105})	—
u_{105}	In(1)···C(23)	416.4(88)	29.6(34)	30.4(30)
u_{106}	P(6)···C(10)	421.6(28)	10.3(tied tou_{105})	—
u_{107}	In(1)···C(36)	389.6(67)	27.5(tied tou_{105})	—
u_{108}	C(2)···C(33)	403.9(17)	7.3(tied tou_{105})	—
u_{109}	P(3)···C(8)	361.8(64)	25.8(tied tou_{105})	—
u_{110}	C(2)···C(20)	404.6(17)	7.4(tied tou_{105})	—
u_{111}	C(23)···C(34)	360.8(142)	15.1(tied tou_{105})	—
u_{112}	C(5)···C(7)	410.9(18)	7.4(tied tou_{105})	—
u_{113}	C(4)···C(7)	410.9(18)	7.4(tied tou_{105})	—
u_{114}	In(1)···C(22)	396.9(69)	27.2(tied tou_{105})	—
u_{115}	P(6)···C(20)	418.7(14)	7.1(tied tou_{105})	—
u_{116}	In(1)···C(35)	435.4(74)	22.5(tied tou_{105})	—
u_{117}	P(3)···C(33)	419.1(14)	7.2(tied tou_{105})	—
u_{118}	In(1)···C(8)	506.3(24)	15.8(tied tou_{105})	—
u_{119}	C(2)···C(22)	453.4(34)	10.3(tied tou_{105})	—
u_{120}	C(2)···C(35)	455.2(39)	10.1(tied tou_{105})	—

u_{121}	C(5)···C(8)	479.0(39)	15.4(tied to u_{105})	—
u_{122}	C(22)···C(36)	467.6(80)	25.7(tied to u_{139})	—
u_{123}	C(23)···C(35)	475.3(63)	16.4(tied to u_{139})	—
u_{124}	C(2)···C(34)	485.9(48)	17.8(tied to u_{139})	—
u_{125}	C(22)···C(33)	480.5(40)	12.7(tied to u_{139})	—
u_{126}	C(20)···C(35)	493.6(37)	118.9(tied to u_{139})	—
u_{127}	P(3)···C(36)	486.7(33)	157.0(tied to u_{139})	—
u_{128}	C(4)···C(9)	504.8(27)	136.0(tied to u_{139})	—
u_{129}	P(6)···C(23)	483.8(29)	140.9(tied to u_{139})	—
u_{130}	P(3)···C(34)	484.4(30)	169.7(tied to u_{139})	—
u_{131}	C(2)···C(21)	482.0(47)	206.1(tied to u_{139})	—
u_{132}	P(6)···C(21)	498.8(27)	177.1(tied to u_{139})	—
u_{133}	C(5)···C(9)	473.6(31)	142.6(tied to u_{139})	—
u_{134}	C(4)···C(8)	481.7(33)	19.8(tied to u_{139})	—
u_{135}	C(5)···C(10)	506.9(27)	119.4(tied to u_{139})	—
u_{136}	C(2)···C(23)	510.1(30)	143.2(tied to u_{139})	—
u_{137}	C(2)···C(36)	501.1(36)	169.2(tied to u_{139})	—
u_{138}	P(6)···C(22)	510.4(27)	105.7(tied to u_{139})	—
u_{139}	In(1)···C(34)	513.1(33)	205.5(20)	204.0(200)
u_{140}	In(1)···C(21)	518.2(34)	193.5(tied to u_{139})	—
u_{141}	P(3)···C(35)	519.1(29)	105.1(tied to u_{139})	—
u_{142}	C(22)···C(34)	525.4(90)	170.2(tied to u_{139})	—
u_{143}	C(21)···C(35)	562.7(99)	258.1(tied to u_{139})	—
u_{144}	C(7)···C(33)	545.3(20)	103.6(tied to u_{139})	—
u_{145}	C(7)···C(20)	546.4(20)	104.0(tied to u_{139})	—

[a] Estimated standard deviations, as obtained in the least squares refinement, are given in parentheses. [b] Amplitudes not refined were fixed at the values obtained using the force field calculated at the RHF level with aug-cc-pVQZ on In and 6-31G* on P, C, and H. Other amplitudes were also included and fixed at this level but are not shown here.

Table 2.28 Experimental (GED) coordinates for the restrained structure of [In($P_2C_3Bu^t_3$)], **2**.

Atom	*x*	*y*	*z*
In(1)	–1.3202	0.0000	2.4325
C(2)	0.0000	0.0000	0.0000
P(3)	–0.9357	–1.4610	0.0000
C(4)	–2.5235	–0.7038	0.0000
C(5)	–2.5235	0.7038	0.0000
P(6)	–0.9357	1.4610	0.0000
C(7)	1.5315	0.0000	0.0000
C(8)	2.0181	0.1168	–1.4475
C(9)	2.1219	1.1587	0.8089
C(10)	2.1161	–1.3133	0.5283
H(11)	3.1124	0.1199	–1.4851
H(12)	1.6536	1.0446	–1.9009
H(13)	1.6536	–0.7262	–2.0438
H(14)	1.7966	1.1025	1.8530
H(15)	3.2162	1.1246	0.7852
H(16)	1.7966	2.1194	0.3964
H(17)	1.7885	–2.1553	–0.0904
H(18)	3.2105	–1.2789	0.5145
H(19)	1.7885	–1.4923	1.5577
C(20)	–3.6690	–1.7203	0.0000
C(21)	–4.1008	–2.1495	–1.4053
C(22)	–3.3108	–3.0083	0.7471
C(23)	–4.9282	–1.1987	0.6985
H(24)	–3.2641	–2.6124	–1.9390
H(25)	–4.9197	–2.8744	–1.3503
H(26)	–4.4429	–1.2840	–1.9824
H(27)	–3.0674	–2.7904	1.7923
H(28)	–4.1512	–3.7100	0.7266
H(29)	–2.4446	–3.4922	0.2838
H(30)	–5.2970	–0.2959	0.2003
H(31)	–5.7203	–1.9544	0.6759
H(32)	–4.7133	–0.9537	1.7439
C(33)	–3.6519	1.7393	0.0000
C(34)	–4.3705	1.6960	–1.3517
C(35)	–3.2348	3.2038	0.1643
C(36)	–4.6800	1.4695	1.1026
H(37)	–5.1837	2.4289	–1.3774
H(38)	–3.6730	1.9244	–2.1644
H(39)	–4.7947	0.7021	–1.5289
H(40)	–2.7107	3.3489	1.1147
H(41)	–4.1138	3.8567	0.1506
H(42)	–2.5667	3.5058	–0.6490
H(43)	–5.1358	0.4829	0.9689
H(44)	–5.4739	2.2234	1.0795
H(45)	–4.2027	1.4996	2.0877

All coordinates are in Å.

Electronic Appendix – Chapter Three
Tables 3.1 – 3.6

Table 3.1 GED coordinates for [Sn($P_2C_2Bu^t_2$)], **1b**.[a]

Atom	*x*	*y*	*z*
Sn(1)	0.0000	2.2002	0.0000
P(2)	0.0000	0.0000	1.3626
C(3)	1.1809	0.0986	0.0000
P(4)	0.0000	0.0000	–1.3626
C(5)	–1.1809	0.0986	0.0000
C(6)	2.7139	–0.1401	0.0000
C(7)	2.9627	–1.6776	0.0009
C(8)	3.3627	0.4916	–1.2673
C(9)	3.3649	0.4990	1.2625
H(10)	4.0667	–1.9066	0.0111
H(11)	2.5158	–2.1588	–0.9161
H(12)	2.4985	–2.1599	0.9082
H(13)	4.4785	0.3295	–1.2714
H(14)	3.1718	1.6022	–1.3060
H(15)	2.9405	0.0327	–2.2067
H(16)	4.4815	0.3422	1.2625
H(17)	2.9488	0.0412	2.2052
H(18)	3.1689	1.6088	1.2982
C(19)	–2.7139	–0.1401	0.0000
C(20)	–2.9627	–1.6776	–0.0009
C(21)	–3.3627	0.4916	1.2671
C(22)	–3.3649	0.4990	–1.2625
H(23)	–4.0667	–1.9066	–0.0111
H(24)	–2.5158	–2.1581	0.9161
H(25)	–2.4985	–2.1599	–0.9082
H(26)	–4.4785	0.3295	1.2714
H(27)	–3.1718	1.6022	1.3060
H(28)	–2.9405	0.0327	2.2067
H(29)	–4.4815	0.3422	–1.2625
H(30)	–2.9488	0.0412	–2.2052
H(31)	–3.1689	1.6088	–1.2982

[a] All coordinates are r_a in Å.

Table 3.2 Calculated coordinates (B3PW91/LanL2DZ/6-31G*) for [Sn($P_2C_2Bu^t_2$)], **1b**.

Atom	*x*	*y*	*z*
Sn(1)	0.0000	0.0000	1.5772
P(2)	1.3678	0.0000	–0.6732
C(3)	0.0000	–1.1813	–0.5416
P(4)	–1.3678	–0.0000	–0.6732
C(5)	–0.0000	1.1813	–0.5416
C(6)	0.0000	–2.6845	–0.7173
C(7)	0.0000	–2.9910	–2.2308
C(8)	1.2554	–3.3041	–0.0845
C(9)	–1.2553	–3.3043	–0.0845
H(10)	0.8868	–2.5675	–2.7158
H(11)	0.0001	–4.0747	–2.4041
H(12)	–0.8867	–2.5675	–2.7158
H(13)	1.2710	–3.1461	1.0005
H(14)	1.2852	–4.3848	–0.2700
H(15)	2.1710	–2.8689	–0.5029
H(16)	–2.1709	–2.8689	–0.5028
H(17)	–1.2850	–4.3849	–0.2699
H(18)	–1.2709	–3.1461	1.0005
C(19)	–0.0000	2.6845	–0.7173
C(20)	–0.0000	2.9910	–2.2308
C(21)	–1.2554	3.3041	–0.0845
C(22)	1.2553	3.3043	–0.0845
H(23)	–0.8868	2.5675	–2.7158
H(24)	–0.0001	4.0747	–2.4041
H(25)	0.8867	2.5675	–2.7158
H(26)	–1.2710	3.1461	1.0005
H(27)	–1.2852	4.3848	–0.2700
H(28)	–2.1710	2.8689	–0.5029
H(29)	2.1709	2.8689	–0.5028
H(30)	1.2850	4.3849	–0.2699
H(31)	1.2709	3.1461	1.0005

Energy = –1077.502038 Hartrees (corrected for ZPE).
All coordinates are in Å.

Table 3.3 Calculated coordinates (B3PW91/LanL2DZ/6-31G*) for [Sn($P_2C_2H_2$)], **2**.

Atom	*x*	*y*	*z*
Sn(1)	0.0000	0.0000	1.0351
P(2)	0.0000	1.3710	–1.2177
C(3)	1.1613	0.0000	–1.0797
P(4)	0.0000	–1.3710	–1.2177
C(5)	–1.1613	0.0000	–1.0797
H(6)	2.2453	0.0000	–1.1341
H(7)	–2.2453	0.0000	–1.1341

Energy = –763.324630 Hartrees (corrected for ZPE).
All coordinates are in Å.

Table 3.4 Calculated coordinates (B3PW91/6-31G*) for [$P_2C_2Bu^t_2$], **3**.

Atom	*x*	*y*	*z*
P(1)	1.3795	–0.0122	0.0000
C(2)	–0.1428	1.1642	0.0000
P(3)	–1.3797	0.0122	0.0000
C(4)	0.1428	–1.1642	0.0000
C(5)	–0.1458	2.6577	0.0000
C(6)	–1.5778	3.2086	0.0000
C(7)	0.6035	3.1488	1.2573
C(8)	0.6035	3.1488	–1.2573
H(9)	–2.1292	2.8754	0.8870
H(10)	–1.5679	4.3049	0.0000
H(11)	–2.1292	2.8754	–0.8869
H(12)	1.6307	2.7673	1.2871
H(13)	0.6508	4.2447	1.2601
H(14)	0.0925	2.8242	2.1701
H(15)	0.0925	2.8242	–2.1701
H(16)	0.6508	4.2447	–1.2601
H(17)	1.6307	2.7673	–1.2871
C(18)	0.1458	–2.6577	0.0000
C(19)	1.5778	–3.2086	0.0000
C(20)	–0.6035	–3.1488	1.2573
C(21)	–0.6035	–3.1488	–1.2573
H(22)	2.1292	–2.8754	0.8870
H(23)	1.5679	–4.3049	0.0000
H(24)	2.1292	–2.8754	–0.8869
H(25)	–1.6307	–2.7673	1.2871
H(26)	–0.6508	–4.2447	1.2601
H(27)	–0.0925	–2.8242	2.1701
H(28)	–0.0925	–2.8242	–2.1701
H(29)	–0.6508	–4.2447	–1.2601
H(30)	–1.6307	–2.7673	–1.2871

Energy = –1074.038806 Hartrees (corrected for ZPE).
All coordinates are in Å.

Table 3.5 Calculated coordinates (B3PW91/LanL2DZ/6-31G*) for [Sn($C_4Bu^t_2H_2$)], **4**.

Atom	*x*	*y*	*z*
Sn(1)	–1.5890	–0.0002	0.0057
C(2)	0.5256	–1.0284	–0.0020
C(3)	0.5163	0.0000	–1.0447
C(4)	0.5253	1.0285	–0.0020
C(5)	0.5231	0.0000	1.0410
C(6)	0.8581	0.0002	–2.5111
C(7)	2.3981	0.0004	–2.6389
C(8)	0.3008	–1.2557	–3.1956
C(9)	0.3005	1.2560	–3.1955
H(10)	2.8300	–0.8858	–2.1604
H(11)	2.6990	0.0005	–3.6945
H(12)	2.8298	0.8866	–2.1603
H(13)	–0.7948	–1.2682	–3.1648
H(14)	0.6139	–1.2909	–4.2464
H(15)	0.6640	–2.1687	–2.7091
H(16)	0.6634	2.1691	–2.7089
H(17)	0.6136	1.2914	–4.2462
H(18)	–0.7951	1.2683	–3.1647
C(19)	0.8750	0.0000	2.5050
C(20)	2.4158	0.0002	2.6223
C(21)	0.3221	1.2557	3.1933
C(22)	0.3224	–1.2560	3.1931
H(23)	2.8443	0.8865	2.1408
H(24)	2.7240	0.0002	3.6758
H(25)	2.8445	–0.8859	2.1407
H(26)	–0.7737	1.2680	3.1699
H(27)	0.6423	1.2910	4.2418
H(28)	0.6817	2.1688	2.7042
H(29)	0.6823	–2.1689	2.7040
H(30)	0.6427	–1.2913	4.2417
H(31)	–0.7734	–1.2686	3.1698
H(32)	0.6564	–2.1033	–0.0026
H(33)	0.6559	2.1034	–0.0024

Energy = –472.194130 Hartrees (corrected for ZPE).
All coordinates are in Å.

Table 3.6 Calculated coordinates (B3PW91/6-31G*) for [$Li_2(P_2C_2Bu^t_2)$], **5**.

Atom	*x*	*y*	*z*
Li(1)	0.0000	0.0000	–1.9281
P(2)	0.0000	–1.3843	–0.0649
C(3)	1.1816	0.0000	–0.0807
P(4)	0.0000	1.3843	–0.0648
C(5)	–1.1816	0.0000	–0.0807
C(6)	2.6982	0.0000	0.0140
C(7)	3.1455	0.0000	1.4933
C(8)	3.2746	–1.2534	–0.6636
C(9)	3.2746	1.2535	–0.6635
H(10)	2.7667	–0.8930	2.0093
H(11)	4.2399	–0.0000	1.5919
H(12)	2.7667	0.8928	2.0093
H(13)	3.0331	–1.2653	–1.7339
H(14)	4.3670	–1.2903	–0.5611
H(15)	2.8640	–2.1688	–0.2205
H(16)	2.8640	2.1688	–0.2204
H(17)	4.3670	1.2903	–0.5611
H(18)	3.0331	1.2654	–1.7338
C(19)	–2.6982	0.0000	0.0140
C(20)	–3.1455	0.0000	1.4933
C(21)	–3.2746	1.2535	–0.6635
C(22)	–3.2746	–1.2534	–0.6636
H(23)	–2.7667	0.8929	2.0093
H(24)	–4.2399	0.0000	1.5919
H(25)	–2.7667	–0.8930	2.0093
H(26)	–3.0331	1.2654	–1.7338
H(27)	–4.3670	1.2903	–0.5610
H(28)	–2.8640	2.1688	–0.2204
H(29)	–2.8640	–2.1688	–0.2205
H(30)	–4.3670	–1.2903	–0.5611
H(31)	–3.0331	–1.2653	–1.7339
Li(32)	0.0000	–0.0000	1.7920

Energy = –1089.185305 Hartrees (corrected for ZPE).
All coordinates are in Å.

Electronic Appendix – Chapter Four
Tables 4.1 – 4.18

Table 4.1 Experimental (GED) coordinates for $Sb_2(C_6F_4)_3$.[a]

Atom	*x*	*y*	*z*
C(1)	0.0000	4.2028	0.6926
C(2)	0.0000	2.9899	1.3693
C(3)	0.0000	1.7772	0.7043
C(4)	0.0000	1.7772	–0.7043
C(5)	0.0000	2.9899	–1.3693
C(6)	0.0000	4.2028	–0.6926
F(7)	0.0000	5.3485	1.3640
F(8)	0.0000	3.0618	2.7161
F(9)	0.0000	3.0618	–2.7161
F(10)	0.0000	5.3485	–1.3640
C(1)′	–3.6398	–2.1014	0.6926
C(2)′	–2.5894	–1.4950	1.3693
C(3)′	–1.5391	–0.8886	0.7043
C(4)′	–1.5391	–0.8886	–0.7043
C(5)′	–2.5894	–1.4950	–1.3693
C(6)′	–3.6398	–2.1014	–0.6926
F(7)′	–4.6319	–2.6742	1.3640
F(8)′	–2.6516	–1.5309	2.7161
F(9)′	–2.6516	–1.5309	–2.7161
F(10)′	–4.6319	–2.6742	–1.3640
C(1)″	3.6398	–2.1014	0.6926
C(2)″	2.5894	–1.4950	1.3693
C(3)″	1.5391	–0.8886	0.7043
C(4)″	1.5391	–0.8886	–0.7043
C(5)″	2.5894	–1.4950	–1.3693
C(6)″	3.6398	–2.1014	–0.6926
F(7)″	4.6319	–2.6742	1.3640
F(8)″	2.6516	–1.5309	2.7161
F(9)″	2.6516	–1.5309	–2.7161
F(10)″	4.6319	–2.6742	–1.3640
Sb(1)	0.0000	0.0000	1.9029
Sb(2)	0.0000	0.0000	–1.9029

[a] All coordinates in Å.

Table 4.2 Experimental (GED) coordinates for $Bi_2(C_6F_4)_3$.[a]

Atom	*x*	*y*	*z*
C(1)	0.0000	4.2386	0.6966
C(2)	0.0000	3.0298	1.3921
C(3)	0.0000	1.8304	0.6994
C(4)	0.0000	1.8304	–0.6994
C(5)	0.0000	3.0298	–1.3921
C(6)	0.0000	4.2386	–0.6966
F(7)	0.0000	5.3880	1.3481
F(8)	0.0000	3.0744	2.7309
F(9)	0.0000	3.0744	–2.7309
F(10)	0.0000	5.3880	–1.3481
C(1)′	3.6707	–2.1193	0.6966
C(2)′	–2.6239	–1.5149	1.3921
C(3)′	–1.5852	–0.9152	0.6994
C(4)′	–1.5852	–0.9152	–0.6994
C(5)′	–2.6239	–1.5149	–1.3921
C(6)′	–3.6707	–2.1193	–0.6966
F(7)′	–4.6661	–2.6940	1.3481
F(8)′	–2.6625	–1.5372	2.7309
F(9)′	–2.6625	–1.5372	–2.7309
F(10)′	–4.6661	–2.6940	–1.3481
C(1)″	3.6707	–2.1193	0.6966
C(2)″	2.6239	–1.5149	1.3921
C(3)″	1.5852	–0.9152	0.6994
C(4)″	1.5852	–0.9152	–0.6994
C(5)″	2.6239	–1.5149	–1.3921
C(6)″	3.6707	–2.1193	–0.6966
F(7)″	4.6661	–2.6940	1.3481
F(8)″	2.6625	–1.5372	2.7309
F(9)″	2.6625	–1.5372	–2.7309
F(10)″	4.6661	–2.6940	–1.3481
Bi(1)	0.0000	0.0000	1.9722
Bi(2)	0.0000	0.0000	–1.9722

[a] All coordinates in Å.

Table 4.3 Calculated [MP2/LanL2DZ/6-311G*] coordinates for $Sb_2(C_6F_4)_3$.[a]

Atom	*x*	*y*	*z*
C(1)	0.0000	4.2340	0.6958
C(2)	0.0000	3.0149	1.3756
C(3)	0.0000	1.7943	0.7046
C(4)	0.0000	1.7943	–0.7046
C(5)	0.0000	3.0149	–1.3756
C(6)	0.0000	4.2340	–0.6958
F(7)	0.0000	5.3878	1.3598
F(8)	0.0000	3.0692	2.7204
F(9)	0.0000	3.0692	–2.7204
F(10)	0.0000	5.3878	–1.3598
C(1)′	–3.6668	–2.1170	0.6958
C(2)′	–2.6110	–1.5075	1.3756
C(3)′	–1.5539	–0.8971	0.7046
C(4)′	–1.5539	–0.8971	–0.7046
C(5)′	–2.6110	–1.5075	–1.3756
C(6)′	–3.6668	–2.1170	–0.6958
F(7)′	–4.6659	–2.6939	1.3598
F(8)′	–2.6580	–1.5346	2.7204
F(9)′	–2.6580	–1.5346	–2.7204
F(10)′	–4.6659	–2.6939	–1.3598
C(1)″	3.6668	–2.1170	0.6958
C(2)″	2.6110	–1.5075	1.3756
C(3)″	1.5539	–0.8971	0.7046
C(4)″	1.5539	–0.8971	–0.7046
C(5)″	2.6110	–1.5075	–1.3756
C(6)″	3.6668	–2.1170	–0.6958
F(7)″	4.6659	–2.6939	1.3598
F(8)″	2.6580	–1.5346	2.7204
F(9)″	2.6580	–1.5346	–2.7204
F(10)″	4.6659	–2.6939	–1.3598
Sb(1)	0.0000	0.0000	1.9271
Sb(2)	0.0000	0.0000	–1.9271

[a] All coordinates in Å.

Energy = –1890.60154 Hartrees (corrected for ZPE).

Table 4.4 Calculated [MP2/aug-cc-pVQZ-PP/6-311G*] coordinates for $Sb_2(C_6F_4)_3$.[a]

Atom	*x*	*y*	*z*
C(1)	0.0000	1.7667	0.7040
C(2)	0.0000	2.9823	1.3820
C(3)	0.0000	4.2004	0.6979
C(4)	0.0000	4.2004	–0.6979
C(5)	0.0000	2.9823	–1.3820
C(6)	0.0000	1.7667	–0.7040
F(7)	0.0000	3.0162	2.7267
F(8)	0.0000	5.3553	1.3589
F(9)	0.0000	5.3553	–1.3589
F(10)	0.0000	3.0162	–2.7267
C(1)′	–3.6376	–2.1002	–0.6979
C(2)′	–3.6376	–2.1002	0.6979
C(3)′	–2.5828	–1.4912	1.3820
C(4)′	–1.5300	–0.8833	0.7040
C(5)′	–1.5300	–0.8833	–0.7040
C(6)′	–2.5828	–1.4912	–1.3820
F(7)′	–4.6378	–2.6777	1.3589
F(8)′	–2.6121	–1.5081	2.7267
F(9)′	–2.6121	–1.5081	–2.7267
F(10)′	–4.6378	–2.6777	–1.3589
C(1)″	2.5828	–1.4912	1.3820
C(2)″	1.5300	–0.8833	0.7040
C(3)″	1.5300	–0.8833	–0.7040
C(4)″	2.5828	–1.4912	–1.3820
C(5)″	3.6376	–2.1002	–0.6979
C(6)″	3.6376	–2.1002	0.6979
F(7)″	4.6378	–2.6777	1.3589
F(8)″	2.6121	–1.5081	2.7267
F(9)″	2.6121	–1.5081	–2.7267
F(10)″	4.6378	–2.6777	–1.3589
Sb(1)	0.0000	0.0000	1.9006
Sb(2)	0.0000	0.0000	–1.9006

[a] All coordinates in Å.

Energy = –2353.72102 Hartrees (corrected for ZPE).

Table 4.5 Calculated [B3PW91/LanL2DZ/6-311G*] coordinates for $Sb_2(C_6F_4)_3$.[a]

Atom	*x*	*y*	*z*
C(1)	0.0000	4.2240	0.6932
C(2)	0.0000	3.0097	1.3718
C(3)	0.0000	1.8000	0.7003
C(4)	0.0000	1.8000	–0.7003
C(5)	0.0000	3.0097	–1.3718
C(6)	0.0000	4.2240	–0.6932
F(7)	0.0000	5.3750	1.3561
F(8)	0.0000	3.0531	2.7144
F(9)	0.0000	3.0531	–2.7144
F(10)	0.0000	5.3750	–1.3561
C(1)′	–3.6580	–2.1120	0.6932
C(2)′	–2.6065	–1.5048	1.3718
C(3)′	–1.5589	–0.9000	0.7003
C(4)′	–1.5589	–0.9000	–0.7003
C(5)′	–2.6065	–1.5048	–1.3718
C(6)′	–3.6580	–2.1120	–0.6932
F(7)′	–4.6549	–2.6875	1.3561
F(8)′	–2.6441	–1.5266	2.7144
F(9)′	–2.6441	–1.5266	–2.7144
F(10)′	–4.6549	–2.6875	–1.3561
C(1)″	3.6580	–2.1120	0.6932
C(2)″	2.6065	–1.5048	1.3718
C(3)″	1.5589	–0.9000	0.7003
C(4)″	1.5589	–0.9000	–0.7003
C(5)″	2.6065	–1.5048	–1.3718
C(6)″	3.6580	–2.1120	–0.6932
F(7)″	4.6549	–2.6875	1.3561
F(8)″	2.6441	–1.5266	2.7144
F(9)″	2.6441	–1.5266	–2.7144
F(10)″	4.6549	–2.6875	–1.3561
Sb(1)	0.0000	0.0000	1.9099
Sb(2)	0.0000	0.0000	–1.9099

[a] All coordinates in Å.

Energy = –2364.43391 Hartrees (corrected for ZPE).

Table 4.6 Calculated [B3PW91/aug-cc-pVQZ-PP/6-311G*] coordinates for $Sb_2(C_6F_4)_3$.[a]

Atom	*x*	*y*	*z*
C(1)	0.0000	4.2236	0.6933
C(2)	0.0000	3.0091	1.3708
C(3)	0.0000	1.7987	0.7009
C(4)	0.0000	1.7987	–0.7009
C(5)	0.0000	3.0091	–1.3708
C(6)	0.0000	4.2236	–0.6933
F(7)	0.0000	5.3743	1.3563
F(8)	0.0000	3.0518	2.7140
F(9)	0.0000	3.0518	–2.7140
F(10)	0.0000	5.3743	–1.3563
C(1)′	–3.6578	–2.1118	0.6933
C(2)′	–2.6059	–1.5045	1.3708
C(3)′	–1.5577	–0.8993	0.7009
C(4)′	–1.5577	–0.8993	–0.7009
C(5)′	–2.6059	–1.5045	–1.3708
C(6)′	–3.6578	–2.1118	–0.6933
F(7)′	–4.6543	–2.6872	1.3563
F(8)′	–2.6429	–1.5259	2.7140
F(9)′	–2.6429	–1.5259	–2.7140
F(10)′	–4.6543	–2.6872	–1.3563
C(1)″	3.6578	–2.1118	0.6933
C(2)″	2.6059	–1.5045	1.3708
C(3)″	1.5577	–0.8993	0.7009
C(4)″	1.5577	–0.8993	–0.7009
C(5)″	2.6059	–1.5045	–1.3708
C(6)″	3.6578	–2.1118	–0.6933
F(7)″	4.6543	–2.6872	1.3563
F(8)″	2.6429	–1.5259	2.7140
F(9)″	2.6429	–1.5259	–2.7140
F(10)″	4.6543	–2.6872	–1.3563
Sb(1)	0.0000	0.0000	1.9097
Sb(2)	0.0000	0.0000	–1.9097

[a] All coordinates in Å.

Energy = –2364.43391 Hartrees (corrected for ZPE).

Table 4.7 Calculated [B3LYP/LanL2DZ/6-311G*] coordinates for $Sb_2(C_6F_4)_3$.[a]

Atom	*x*	*y*	*z*
C(1)	0.0000	4.2462	0.6932
C(2)	0.0000	3.0303	1.3714
C(3)	0.0000	1.8173	0.7021
C(4)	0.0000	1.8173	–0.7021
C(5)	0.0000	3.0303	–1.3714
C(6)	0.0000	4.2462	–0.6932
F(7)	0.0000	5.4011	1.3610
F(8)	0.0000	3.0769	2.7205
F(9)	0.0000	3.0769	–2.7205
F(10)	0.0000	5.4011	–1.3610
C(1)′	–3.6773	–2.1231	0.6932
C(2)′	–2.6243	–1.5151	1.3714
C(3)′	–1.5738	–0.9086	0.7021
C(4)′	–1.5738	–0.9086	–0.7021
C(5)′	–2.6243	–1.5151	–1.3714
C(6)′	–3.6773	–2.1231	–0.6932
F(7)′	–4.6775	–2.7006	1.3610
F(8)′	–2.6647	–1.5384	2.7205
F(9)′	–2.6647	–1.5384	–2.7205
F(10)′	–4.6775	–2.7006	–1.3610
C(1)″	3.6773	–2.1231	0.6932
C(2)″	2.6243	–1.5151	1.3714
C(3)″	1.5738	–0.9086	0.7021
C(4)″	1.5738	–0.9086	–0.7021
C(5)″	2.6243	–1.5151	–1.3714
C(6)″	3.6773	–2.1231	–0.6932
F(7)″	4.6775	–2.7006	1.3610
F(8)″	2.6647	–1.5384	2.7205
F(9)″	2.6647	–1.5384	–2.7205
F(10)″	4.6775	–2.7006	–1.3610
Sb(1)	0.0000	0.0000	1.9279
Sb(2)	0.0000	0.0000	–1.9279

[a] All coordinates in Å.

Energy = –1895.18126 Hartrees (corrected for ZPE).

Table 4.8 Calculated [B3LYP/aug-cc-pVQZ-PP/6-311G*] coordinates for $Sb_2(C_6F_4)_3$.[a]

Atom	*x*	*y*	*z*
C(1)	0.0000	4.2387	0.6940
C(2)	0.0000	3.0221	1.3704
C(3)	0.0000	1.8100	0.7016
C(4)	0.0000	1.8100	–0.7016
C(5)	0.0000	3.0221	–1.3704
C(6)	0.0000	4.2387	–0.6940
F(7)	0.0000	5.3939	1.3613
F(8)	0.0000	3.0625	2.7220
F(9)	0.0000	3.0625	–2.7220
F(10)	0.0000	5.3939	–1.3613
C(1)′	–3.6708	–2.1193	0.6940
C(2)′	–2.6172	–1.5111	1.3704
C(3)′	–1.5675	–0.9050	0.7016
C(4)′	–1.5675	–0.9050	–0.7016
C(5)′	–2.6172	–1.5111	–1.3704
C(6)′	–3.6708	–2.1193	–0.6940
F(7)′	–4.6713	–2.6970	1.3613
F(8)′	–2.6522	–1.5312	2.7220
F(9)′	–2.6522	–1.5312	–2.7220
F(10)′	–4.6713	–2.6970	–1.3613
C(1)″	3.6708	–2.1193	0.6940
C(2)″	2.6172	–1.5111	1.3704
C(3)″	1.5675	–0.9050	0.7016
C(4)″	1.5675	–0.9050	–0.7016
C(5)″	2.6172	–1.5111	–1.3704
C(6)″	3.6708	–2.1193	–0.6940
F(7)″	4.6713	–2.6970	1.3613
F(8)″	2.6522	–1.5312	2.7220
F(9)″	2.6522	–1.5312	–2.7220
F(10)″	4.6713	–2.6970	–1.3613
Sb(1)	0.0000	0.0000	1.9244
Sb(2)	0.0000	0.0000	–1.9244

[a] All coordinates in Å.

Energy = –2365.08049 Hartrees (corrected for ZPE).

Table 4.9 Calculated [BLYP/LanL2DZ/6-311G*] coordinates for $Sb_2(C_6F_4)_3$.[a]

Atom	*x*	*y*	*z*
C(1)	0.0000	4.2799	0.6992
C(2)	0.0000	3.0539	1.3826
C(3)	0.0000	1.8324	0.7066
C(4)	0.0000	1.8324	–0.7066
C(5)	0.0000	3.0539	–1.3826
C(6)	0.0000	4.2799	–0.6992
F(7)	0.0000	5.4504	1.3739
F(8)	0.0000	3.1013	2.7493
F(9)	0.0000	3.1013	–2.7493
F(10)	0.0000	5.4504	–1.3739
C(1)′	–3.7065	–2.1399	0.6992
C(2)′	–2.6448	–1.5270	1.3826
C(3)′	–1.5869	–0.9162	0.7066
C(4)′	–1.5869	–0.9162	–0.7066
C(5)′	–2.6448	–1.5270	–1.3826
C(6)′	–3.7065	–2.1399	–0.6992
F(7)′	–4.7202	–2.7252	1.3739
F(8)′	–2.6858	–1.5506	2.7493
F(9)′	–2.6858	–1.5506	–2.7493
F(10)′	–4.7202	–2.7252	–1.3739
C(1)″	3.7065	–2.1399	0.6992
C(2)″	2.6448	–1.5270	1.3826
C(3)″	1.5869	–0.9162	0.7066
C(4)″	1.5869	–0.9162	–0.7066
C(5)″	2.6448	–1.5270	–1.3826
C(6)″	3.7065	–2.1399	–0.6992
F(7)″	4.7202	–2.7252	1.3739
F(8)″	2.6858	–1.5506	2.7493
F(9)″	2.6858	–1.5506	–2.7493
F(10)″	4.7202	–2.7252	–1.3739
Sb(1)	0.0000	0.0000	1.9452
Sb(2)	0.0000	0.0000	–1.9452

[a] All coordinates in Å.

Energy = –1894.87117 Hartrees (corrected for ZPE).

Table 4.10 Calculated [BLYP/aug-cc-pVQZ-PP/6-311G*] coordinates for $Sb_2(C_6F_4)_3$.[a]

Atom	*x*	*y*	*z*
C(1)	0.0000	4.2760	0.7001
C(2)	0.0000	3.0491	1.3807
C(3)	0.0000	1.8290	0.7059
C(4)	0.0000	1.8290	–0.7059
C(5)	0.0000	3.0491	–1.3807
C(6)	0.0000	4.2760	–0.7001
F(7)	0.0000	5.4468	1.3743
F(8)	0.0000	3.0876	2.7515
F(9)	0.0000	3.0876	–2.7515
F(10)	0.0000	5.4468	–1.3743
C(1)′	–3.7031	–2.1380	0.7001
C(2)′	–2.6406	–1.5245	1.3807
C(3)′	–1.5839	–0.9145	0.7059
C(4)′	–1.5839	–0.9145	–0.7059
C(5)′	–2.6406	–1.5245	–1.3807
C(6)′	–3.7031	–2.1380	–0.7001
F(7)′	–4.7171	–2.7234	1.3743
F(8)′	–2.6739	–1.5438	2.7515
F(9)′	–2.6739	–1.5438	–2.7515
F(10)′	–4.7171	–2.7234	–1.3743
C(1)″	3.7031	–2.1380	0.7001
C(2)″	2.6406	–1.5245	1.3807
C(3)″	1.5839	–0.9145	0.7059
C(4)″	1.5839	–0.9145	–0.7059
C(5)″	2.6406	–1.5245	–1.3807
C(6)″	3.7031	–2.1380	–0.7001
F(7)″	4.7171	–2.7234	1.3743
F(8)″	2.6739	–1.5438	2.7515
F(9)″	2.6739	–1.5438	–2.7515
F(10)″	4.7171	–2.7234	–1.3743
Sb(1)	0.0000	0.0000	1.9483
Sb(2)	0.0000	0.0000	–1.9483

[a] All coordinates in Å.

Energy = –2364.56211 Hartrees (corrected for ZPE).

Table 4.11 Calculated [MP2/LanL2DZ/6-311G*] coordinates for $Bi_2(C_6F_4)_3$.[a]

Atom	*x*	*y*	*z*
C(1)	0.0000	4.2777	0.6963
C(2)	0.0000	3.0576	1.3733
C(3)	0.0000	1.8377	0.7032
C(4)	0.0000	1.8377	–0.7032
C(5)	0.0000	3.0576	–1.3733
C(6)	0.0000	4.2777	–0.6963
F(7)	0.0000	5.4329	1.3602
F(8)	0.0000	3.1060	2.7224
F(9)	0.0000	3.1060	–2.7224
F(10)	0.0000	5.4329	–1.3602
C(1)′	–3.7046	–2.1389	0.6963
C(2)′	–2.6479	–1.5288	1.3733
C(3)′	–1.5915	–0.9188	0.7032
C(4)′	–1.5915	–0.9188	–0.7032
C(5)′	–2.6479	–1.5288	–1.3733
C(6)′	–3.7046	–2.1389	–0.6963
F(7)′	–4.7051	–2.7165	1.3602
F(8)′	–2.6899	–1.5530	2.7224
F(9)′	–2.6899	–1.5530	–2.7224
F(10)′	–4.7051	–2.7165	–1.3602
C(1)″	3.7046	–2.1389	0.6963
C(2)″	2.6479	–1.5288	1.3733
C(3)″	1.5915	–0.9188	0.7032
C(4)″	1.5915	–0.9188	–0.7032
C(5)″	2.6479	–1.5288	–1.3733
C(6)″	3.7046	–2.1389	–0.6963
F(7)″	4.7051	–2.7165	1.3602
F(8)″	2.6899	–1.5530	2.7224
F(9)″	2.6899	–1.5530	–2.7224
F(10)″	4.7051	–2.7165	–1.3602
Bi(1)	0.0000	0.0000	1.9912
Bi(2)	0.0000	0.0000	–1.9912

[a] All coordinates in Å.

Energy = –1890.67381 Hartrees (corrected for ZPE)

Table 4.12 Calculated [MP2/aug-cc-pVTZ-PP/6-311G*] coordinates for $Bi_2(C_6F_4)_3$.[a]

Atom	*x*	*y*	*z*
C(1)	0.0000	4.2594	0.6980
C(2)	0.0000	3.0414	1.3806
C(3)	0.0000	1.8267	0.7016
C(4)	0.0000	1.8267	–0.7016
C(5)	0.0000	3.0414	–1.3806
C(6)	0.0000	4.2594	–0.6980
F(7)	0.0000	5.4161	1.3583
F(8)	0.0000	3.0773	2.7274
F(9)	0.0000	3.0773	–2.7274
F(10)	0.0000	5.4161	–1.3583
C(1)′	–3.6888	–2.1297	0.6980
C(2)′	–2.6339	–1.5207	1.3806
C(3)′	–1.5820	–0.9133	0.7016
C(4)′	–1.5820	–0.9133	–0.7016
C(5)′	–2.6339	–1.5207	–1.3806
C(6)′	–3.6888	–2.1297	–0.6980
F(7)′	–4.6905	–2.7081	1.3583
F(8)′	–2.6651	–1.5387	2.7274
F(9)′	–2.6651	–1.5387	–2.7274
F(10)′	–4.6905	–2.7081	–1.3583
C(1)″	3.6888	–2.1297	0.6980
C(2)″	2.6339	–1.5207	1.3806
C(3)″	1.5820	–0.9133	0.7016
C(4)″	1.5820	–0.9133	–0.7016
C(5)″	2.6339	–1.5207	–1.3806
C(6)″	3.6888	–2.1297	–0.6980
F(7)″	4.6905	–2.7081	1.3583
F(8)″	2.6651	–1.5387	2.7274
F(9)″	2.6651	–1.5387	–2.7274
F(10)″	4.6905	–2.7081	–1.3583
Bi(1)	0.0000	0.0000	1.9793
Bi(2)	0.0000	0.0000	–1.9793

[a] All coordinates in Å.

Energy = –2307.87495 Hartrees (corrected for ZPE)

Table 4.13 Calculated [B3PW91/LanL2DZ/6-311G*] coordinates for $Bi_2(C_6F_4)_3$.[a]

Atom	*x*	*y*	*z*
C(1)	0.0000	4.2823	0.6933
C(2)	0.0000	3.0668	1.3689
C(3)	0.0000	1.8572	0.6989
C(4)	0.0000	1.8572	–0.6989
C(5)	0.0000	3.0668	–1.3689
C(6)	0.0000	4.2823	–0.6933
F(7)	0.0000	5.4335	1.3578
F(8)	0.0000	3.1078	2.7148
F(9)	0.0000	3.1078	–2.7148
F(10)	0.0000	5.4335	–1.3578
C(1)′	–3.7086	–2.1412	0.6933
C(2)′	–2.6560	–1.5334	1.3689
C(3)′	–1.6083	–0.9286	0.6989
C(4)′	–1.6083	–0.9286	–0.6989
C(5)′	–2.6560	–1.5334	–1.3689
C(6)′	–3.7086	–2.1412	–0.6933
F(7)′	–4.7056	–2.7168	1.3578
F(8)′	–2.6914	–1.5539	2.7148
F(9)′	–2.6914	–1.5539	–2.7148
F(10)′	–4.7056	–2.7168	–1.3578
C(1)″	3.7086	–2.1412	0.6933
C(2)″	2.6560	–1.5334	1.3689
C(3)″	1.6083	–0.9286	0.6989
C(4)″	1.6083	–0.9286	–0.6989
C(5)″	2.6560	–1.5334	–1.3689
C(6)″	3.7086	–2.1412	–0.6933
F(7)″	4.7056	–2.7168	1.3578
F(8)″	2.6914	–1.5539	2.7148
F(9)″	2.6914	–1.5539	–2.7148
F(10)″	4.7056	–2.7168	–1.3578
Bi(1)	0.0000	0.0000	1.9807
Bi(2)	0.0000	0.0000	–1.9807

[a] All coordinates in Å.

Energy = –1894.58547 Hartrees (corrected for ZPE)

Table 4.14 Calculated [B3PW91/aug-cc-pVTZ-PP/6-311G*] coordinates for $Bi_2(C_6F_4)_3$.[a]

Atom	*x*	*y*	*z*
C(1)	0.0000	4.2841	0.6938
C(2)	0.0000	3.0690	1.3694
C(3)	0.0000	1.8610	0.6982
C(4)	0.0000	1.8610	–0.6982
C(5)	0.0000	3.0690	–1.3694
C(6)	0.0000	4.2841	–0.6938
F(7)	0.0000	5.4367	1.3562
F(8)	0.0000	3.1058	2.7164
F(9)	0.0000	3.1058	–2.7164
F(10)	0.0000	5.4367	–1.3562
C(1)′	–3.7147	–2.1409	0.6938
C(2)′	–2.6612	–1.5352	1.3692
C(3)′	–1.6140	–0.9330	0.6981
C(4)′	–1.6140	–0.9330	–0.6981
C(5)′	–2.6612	–1.5352	–1.3692
C(6)′	–3.7147	–2.1409	–0.6938
F(7)′	–4.7140	–2.7149	1.3567
F(8)′	–2.6933	–1.5532	2.7162
F(9)′	–2.6933	–1.5532	–2.7162
F(10)′	–4.7140	–2.7149	–1.3567
C(1)″	3.7147	–2.1409	0.6938
C(2)″	2.6612	–1.5352	1.3692
C(3)″	1.6140	–0.9330	0.6981
C(4)″	1.6140	–0.9330	–0.6981
C(5)″	2.6612	–1.5352	–1.3692
C(6)″	3.7147	–2.1409	–0.6938
F(7)″	4.7140	–2.7149	1.3567
F(8)″	2.6933	–1.5532	2.7162
F(9)″	2.6933	–1.5532	–2.7162
F(10)″	4.7140	–2.7149	–1.3567
Bi(1)	0.0000	0.0000	1.9882
Bi(2)	0.0000	0.0000	–1.9882

[a] All coordinates in Å.

Energy = –2313.03393 Hartrees (corrected for ZPE)

Table 4.15 Calculated [B3LYP/LanL2DZ/6-311G*] coordinates for $Bi_2(C_6F_4)_3$.[a]

Atom	*x*	*y*	*z*
C(1)	0.0000	4.2929	0.6939
C(2)	0.0000	3.0759	1.3700
C(3)	0.0000	1.8641	0.7003
C(4)	0.0000	1.8641	–0.7003
C(5)	0.0000	3.0759	–1.3700
C(6)	0.0000	4.2929	–0.6939
F(7)	0.0000	5.4495	1.3614
F(8)	0.0000	3.1166	2.7225
F(9)	0.0000	3.1166	–2.7225
F(10)	0.0000	5.4495	–1.3614
C(1)′	–3.7178	–2.1465	0.6939
C(2)′	–2.6638	–1.5379	1.3700
C(3)′	–1.6144	–0.9321	0.7003
C(4)′	–1.6144	–0.9321	–0.7003
C(5)′	–2.6638	–1.5379	–1.3700
C(6)′	–3.7178	–2.1465	–0.6939
F(7)′	–4.7194	–2.7247	1.3614
F(8)′	–2.6990	–1.5583	2.7225
F(9)′	–2.6990	–1.5583	–2.7225
F(10)′	–4.7194	–2.7247	–1.3614
C(1)″	3.7178	–2.1465	0.6939
C(2)″	2.6638	–1.5379	1.3700
C(3)″	1.6144	–0.9321	0.7003
C(4)″	1.6144	–0.9321	–0.7003
C(5)″	2.6638	–1.5379	–1.3700
C(6)″	3.7178	–2.1465	–0.6939
F(7)″	4.7194	–2.7247	1.3614
F(8)″	2.6990	–1.5583	2.7225
F(9)″	2.6990	–1.5583	–2.7225
F(10)″	4.7194	–2.7247	–1.3614
Bi(1)	0.0000	0.0000	1.9857
Bi(2)	0.0000	0.0000	–1.9857

[a] All coordinates in Å.

Energy = –1895.26698 Hartrees (corrected for ZPE)

Table 4.16 Calculated [B3LYP/aug-cc-pVTZ-PP/6-311G*] coordinates for $Bi_2(C_6F_4)_3$.[a]

Atom	*x*	*y*	*z*
C(1)	0.0000	4.3062	0.6945
C(2)	0.0000	3.0892	1.3696
C(3)	0.0000	1.8790	0.6993
C(4)	0.0000	1.8790	–0.6993
C(5)	0.0000	3.0892	–1.3696
C(6)	0.0000	4.3062	–0.6945
F(7)	0.0000	5.4635	1.3610
F(8)	0.0000	3.1255	2.7238
F(9)	0.0000	3.1255	–2.7238
F(10)	0.0000	5.4635	–1.3610
C(1)′	–3.7293	–2.1531	0.6945
C(2)′	–2.6753	–1.5446	1.3696
C(3)′	–1.6273	–0.9395	0.6993
C(4)′	–1.6273	–0.9395	–0.6993
C(5)′	–2.6753	–1.5446	–1.3696
C(6)′	–3.7293	–2.1531	–0.6945
F(7)′	–4.7315	–2.7317	1.3610
F(8)′	–2.7067	–1.5627	2.7238
F(9)′	–2.7067	–1.5627	–2.7238
F(10)′	–4.7315	–2.7317	–1.3610
C(1)″	3.7293	–2.1531	0.6945
C(2)″	2.6753	–1.5446	1.3696
C(3)″	1.6273	–0.9395	0.6993
C(4)″	1.6273	–0.9395	–0.6993
C(5)″	2.6753	–1.5446	–1.3696
C(6)″	3.7293	–2.1531	–0.6945
F(7)″	4.7315	–2.7317	1.3610
F(8)″	2.7067	–1.5627	2.7238
F(9)″	2.7067	–1.5627	–2.7238
F(10)″	4.7315	–2.7317	–1.3610
Bi(1)	0.0000	0.0000	2.0010
Bi(2)	0.0000	0.0000	–2.0010

[a] All coordinates in Å.

Energy = –2313.80950 Hartrees (corrected for ZPE)

Table 4.17 Calculated [BLYP/LanL2DZ/6-311G*] coordinates for $Bi_2(C_6F_4)_3$.[a]

Atom	*x*	*y*	*z*
C(1)	0.0000	4.3264	0.6997
C(2)	0.0000	3.0996	1.3807
C(3)	0.0000	1.8796	0.7049
C(4)	0.0000	1.8796	–0.7049
C(5)	0.0000	3.0996	–1.3807
C(6)	0.0000	4.3264	–0.6997
F(7)	0.0000	5.4989	1.3741
F(8)	0.0000	3.1406	2.7518
F(9)	0.0000	3.1406	–2.7518
F(10)	0.0000	5.4989	–1.3741
C(1)′	–3.7467	–2.1632	0.6997
C(2)′	–2.6843	–1.5498	1.3807
C(3)′	–1.6278	–0.9398	0.7049
C(4)′	–1.6278	–0.9398	–0.7049
C(5)′	–2.6843	–1.5498	–1.3807
C(6)′	–3.7467	–2.1632	–0.6997
F(7)′	–4.7621	–2.7494	1.3741
F(8)′	–2.7198	–1.5703	2.7518
F(9)′	–2.7198	–1.5703	–2.7518
F(10)′	–4.7621	–2.7494	–1.3741
C(1)″	3.7467	–2.1632	0.6997
C(2)″	2.6843	–1.5498	1.3807
C(3)″	1.6278	–0.9398	0.7049
C(4)″	1.6278	–0.9398	–0.7049
C(5)″	2.6843	–1.5498	–1.3807
C(6)″	3.7467	–2.1632	–0.6997
F(7)″	4.7621	–2.7494	1.3741
F(8)″	2.7198	–1.5703	2.7518
F(9)″	2.7198	–1.5703	–2.7518
F(10)″	4.7621	–2.7494	–1.3741
Bi(1)	0.0000	0.0000	2.0012
Bi(2)	0.0000	0.0000	–2.0012

[a] All coordinates in Å.

Energy = –1894.96409 Hartrees (corrected for ZPE)

Table 4.18 Calculated [BLYP/aug-cc-pVTZ-PP/6-311G*] coordinates for $Bi_2(C_6F_4)_3$.[a]

Atom	*x*	*y*	*z*
C(1)	0.0000	4.3476	0.7006
C(2)	0.0000	3.1205	1.3799
C(3)	0.0000	1.9026	0.7035
C(4)	0.0000	1.9026	–0.7035
C(5)	0.0000	3.1205	–1.3799
C(6)	0.0000	4.3476	–0.7006
F(7)	0.0000	5.5203	1.3745
F(8)	0.0000	3.1549	2.7535
F(9)	0.0000	3.1549	–2.7535
F(10)	0.0000	5.5203	–1.3745
C(1)′	–3.7652	–2.1738	0.7006
C(2)′	–2.7024	–1.5602	1.3799
C(3)′	–1.6477	–0.9513	0.7035
C(4)′	–1.6477	–0.9513	–0.7035
C(5)′	–2.7024	–1.5602	–1.3799
C(6)′	–3.7652	–2.1738	–0.7006
F(7)′	–4.7808	–2.7602	1.3745
F(8)′	–2.7323	–1.5775	2.7535
F(9)′	–2.7323	–1.5775	–2.7535
F(10)′	–4.7808	–2.7602	–1.3745
C(1)″	3.7652	–2.1738	0.7006
C(2)″	2.7024	–1.5602	1.3799
C(3)″	1.6477	–0.9513	0.7035
C(4)″	1.6477	–0.9513	–0.7035
C(5)″	2.7024	–1.5602	–1.3799
C(6)″	3.7652	–2.1738	–0.7006
F(7)″	4.7808	–2.7602	1.3745
F(8)″	2.7323	–1.5775	2.7535
F(9)″	2.7323	–1.5775	–2.7535
F(10)″	4.7808	–2.7602	–1.3745
Bi(1)	0.0000	0.0000	2.0242
Bi(2)	0.0000	0.0000	–2.0242

[a] All coordinates in Å.

Energy = –2313.34741 Hartrees (corrected for ZPE)

Electronic Appendix – Chapter Five
Tables 5.1 – 5.8

Table 5.1 Calculated [HF/6-31G*] coordinates for $Se(SCH_3)_2$.

	g^+g^+			g^+g^-		
Atom	*x*	*y*	*z*	*x*	*y*	*z*
Se(1)	0.0000	0.0000	0.9131	0.7851	–0.5180	0.0000
S(2)	0.0000	1.7226	–0.4399	–0.5327	–0.3343	1.7392
S(3)	0.0000	–1.7226	–0.4399	–0.5327	–0.3343	–1.7392
C(4)	1.7525	1.8317	–0.9083	–0.5327	1.4560	2.0579
C(5)	–1.7525	–1.8317	–0.9083	–0.5327	1.4560	–2.0579
H(6)	1.8519	2.7117	–1.5315	–1.0023	1.5946	3.0239
H(7)	2.0494	0.9590	–1.4722	–1.1035	1.9863	1.3094
H(8)	2.3749	1.9370	–0.0317	0.4772	1.8383	2.0932
H(9)	–1.8519	–2.7117	–1.5315	–1.0023	1.5946	–3.0239
H(10)	–2.0494	–0.9590	–1.4722	–1.1035	1.9863	–1.3094
H(11)	–2.3749	–1.9370	–0.0317	0.4772	1.8383	–2.0932

Sum of electronic and zero-point energies = –3271.7673 Hartree for g^+g^+
Sum of electronic and zero-point energies = –3271.7648 Hartree for g^+g^-
All coordinates in Å.

Table 5.2 Calculated [B3LYP/6-31G*] coordinates for $Se(SCH_3)_2$.

	g^+g^+			g^+g^-		
Atom	*x*	*y*	*z*	*x*	*y*	*z*
Se(1)	0.0000	0.0000	0.9035	0.7786	–0.5343	0.0000
S(2)	0.0000	1.7671	–0.4424	–0.5284	–0.3323	1.7835
S(3)	0.0000	–1.7671	–0.4424	–0.5284	–0.3323	–1.7835
C(4)	1.7767	1.9032	–0.8869	–0.5284	1.4822	2.0796
C(5)	–1.7767	–1.9032	–0.8869	–0.5284	1.4822	–2.0796
H(6)	1.8762	2.8084	–1.4941	–0.9545	1.6326	3.0765
H(7)	2.0893	1.0370	–1.4744	–1.1477	1.9998	1.3438
H(8)	2.3931	1.9935	0.0098	0.4901	1.8749	2.0572
H(9)	–1.8762	–2.8084	–1.4941	–0.9545	1.6326	–3.0765
H(10)	–2.0893	–1.0370	–1.4744	–1.1477	1.9998	–1.3438
H(11)	–2.3931	–1.9935	0.0098	0.4901	1.8749	–2.0572

Sum of electronic and zero-point energies = –3275.5371 Hartree for g^+g^+
Sum of electronic and zero-point energies = –3275.5353 Hartree for g^+g^-
All coordinates in Å.

Table 5.3 Calculated [MP2/6-31G*] coordinates for $Se(SCH_3)_2$.

	g^+g^+			g^+g^-		
Atom	*x*	*y*	*z*	*x*	*y*	*z*
Se(1)	0.0000	0.0000	0.9232	0.7822	–0.5325	0.0000
S(2)	0.0000	1.7256	–0.4402	–0.5311	–0.3297	1.7499
S(3)	0.0000	–1.7256	–0.4402	–0.5311	–0.3297	–1.7499
C(4)	1.7501	1.7597	–0.9251	–0.5311	1.4725	1.9940
C(5)	–1.7501	–1.7597	–0.9251	–0.5311	1.4725	–1.9940
H(6)	1.8847	2.6288	–1.5742	–0.9423	1.6575	2.9898
H(7)	2.0079	0.8549	–1.4780	–1.1568	1.9722	1.2534
H(8)	2.3907	1.8559	–0.0479	0.4858	1.8638	1.9460
H(9)	–1.8847	–2.6288	–1.5742	–0.9423	1.6575	–2.9898
H(10)	–2.0079	–0.8549	–1.4780	–1.1568	1.9722	–1.2534
H(11)	–2.3907	–1.8559	–0.0479	0.4858	1.8638	–1.9460

Sum of electronic and zero-point energies = –3272.3901 Hartree for g^+g^+
Sum of electronic and zero-point energies = –3272.3878 Hartree for g^+g^-
All coordinates in Å.

Table 5.4 Calculated [MP2/LanL2DZ(d)] coordinates for $Se(SCH_3)_2$.

	g^+g^+			g^+g^-		
Atom	*x*	*y*	*z*	*x*	*y*	*z*
Se(1)	0.0000	0.0000	1.4507	1.1046	–1.1369	0.0000
S(2)	0.0000	1.7242	0.0700	–0.2184	–0.9287	1.7553
S(3)	0.0000	–1.7242	0.0700	–0.2184	–0.9287	–1.7553
C(4)	1.7391	1.7273	–0.4886	–0.2184	0.8792	2.0339
C(5)	–1.7391	–1.7273	–0.4886	–0.2184	0.8792	–2.0339
H(6)	1.8402	2.5629	–1.1938	–0.7258	1.0416	2.9942
H(7)	1.9719	0.7879	–1.0032	–0.7713	1.4006	1.2452
H(8)	2.4202	1.8761	0.3561	0.8044	1.2658	2.0966
H(9)	–1.8402	–2.5629	–1.1938	–0.7258	1.0416	–2.9942
H(10)	–1.9719	–0.7879	–1.0032	–0.7713	1.4006	–1.2452
H(11)	–2.4202	–1.8761	0.3561	0.8044	1.2658	–2.0966

Sum of electronic and zero-point energies = –108.6376 Hartree for g^+g^+
Sum of electronic and zero-point energies = –108.6348 Hartree for g^+g^-
All coordinates in Å.

Table 5.5 Calculated [HF/3-21G*] coordinates for $Te(SCH_3)_2$.

	g^+g^+			g^+g^-		
Atom	*x*	*y*	*z*	*x*	*y*	*z*
Te(1)	0.0000	0.0000	0.8631	0.7249	–0.4791	0.0000
S(2)	0.0000	1.8461	–0.6751	–0.7522	–0.1929	1.8735
S(3)	0.0000	–1.8461	–0.6751	–0.7522	–0.1929	–1.8735
C(4)	1.7324	1.9249	–1.2512	–0.7522	1.6096	2.1794
C(5)	–1.7324	–1.9249	–1.2512	–0.7522	1.6096	–2.1794
H(6)	1.7927	2.7595	–1.9377	–1.3144	1.7654	3.0912
H(7)	1.9986	1.0167	–1.7707	–1.2369	2.1370	1.3722
H(8)	2.4062	2.0910	–0.4245	0.2523	1.9812	2.3135
H(9)	–1.7927	–2.7595	–1.9377	–1.3144	1.7654	–3.0912
H(10)	–1.9986	–1.0167	–1.7707	–1.2369	2.1370	–1.3722
H(11)	–2.4062	–2.0910	–0.4245	0.2523	1.9812	–2.3135

Sum of electronic and zero-point energies = –7453.3400 Hartree for g^+g^+
Sum of electronic and zero-point energies = –7453.3381 Hartree for g^+g^-
All coordinates in Å.

Table 5.6 Calculated [HF/LanL2DZ(d)] coordinates for $Te(SCH_3)_2$.

	g^+g^+			g^+g^-		
Atom	*x*	*y*	*z*	*x*	*y*	*z*
Te(1)	0.0000	0.0000	1.5593	0.7158	–0.4677	0.0000
S(2)	0.0000	1.8457	0.0463	–0.7426	–0.2038	1.8714
S(3)	0.0000	–1.8457	0.0463	–0.7426	–0.2038	–1.8714
C(4)	1.7402	1.9488	–0.5096	–0.7426	1.5969	2.2006
C(5)	–1.7402	–1.9488	–0.5096	–0.7426	1.5969	–2.2006
H(6)	1.7925	2.7941	–1.1857	–1.3074	1.7346	3.1152
H(7)	2.0233	1.0497	–1.0384	–1.2281	2.1375	1.4005
H(8)	2.4050	2.1152	0.3261	0.2622	1.9687	2.3436
H(9)	–1.7925	–2.7941	–1.1857	–1.3074	1.7346	–3.1152
H(10)	–2.0233	–1.0497	–1.0384	–1.2281	2.1375	–1.4005
H(11)	–2.4050	–2.1152	0.3261	0.2622	1.9687	–2.3436

Sum of electronic and zero-point energies = –106.8570 Hartree for g^+g^+
Sum of electronic and zero-point energies = –106.8547 Hartree for g^+g^-
All coordinates in Å.

Table 5.7 Calculated [B3LYP/LanL2DZ(d)] coordinates for $Te(SCH_3)_2$.

	g^+g^+			g^+g^-		
Atom	*x*	*y*	*z*	*x*	*y*	*z*
Te(1)	0.0000	0.0000	0.8306	0.7096	–0.4695	0.0000
S(2)	0.0000	1.9006	–0.6669	–0.7362	–0.2093	1.9239
S(3)	0.0000	–1.9006	–0.6669	–0.7362	–0.2093	–1.9239
C(4)	1.7702	2.0597	–1.1756	–0.7362	1.6106	2.2542
C(5)	–1.7702	–2.0597	–1.1756	–0.7362	1.6106	–2.2542
H(6)	1.8208	2.9385	–1.8298	–1.2597	1.7446	3.2087
H(7)	2.0894	1.1749	–1.7334	–1.2762	2.1502	1.4710
H(8)	2.4177	2.2147	–0.3082	0.2823	1.9977	2.3453
H(9)	–1.8208	–2.9385	–1.8298	–1.2597	1.7446	–3.2087
H(10)	–2.0894	–1.1749	–1.7334	–1.2762	2.1502	–1.4710
H(11)	–2.4177	–2.2147	–0.3082	0.2823	1.9977	–2.3453

Sum of electronic and zero-point energies = –108.0849 Hartree for g^+g^+
Sum of electronic and zero-point energies = –108.0833 Hartree for g^+g^-
All coordinates in Å.

Table 5.8 Calculated [MP2/LanL2DZ(d)] coordinates for $Te(SCH_3)_2$.

	g^+g^+			g^+g^-		
Atom	*x*	*y*	*z*	*x*	*y*	*z*
Te(1)	0.0000	0.0000	1.5906	0.7151	–0.4788	0.0000
S(2)	0.0000	1.8374	0.0571	–0.7419	–0.1993	1.8775
S(3)	0.0000	–1.8374	0.0571	–0.7419	–0.1993	–1.8775
C(4)	1.7375	1.8447	–0.5247	–0.7419	1.6180	2.1307
C(5)	–1.7375	–1.8447	–0.5247	–0.7419	1.6180	–2.1307
H(6)	1.8205	2.6722	–1.2415	–1.2855	1.7955	3.0680
H(7)	1.9745	0.9021	–1.0309	–1.2623	2.1283	1.3132
H(8)	2.4312	2.0111	0.3063	0.2780	2.0051	2.2260
H(9)	–1.8205	–2.6722	–1.2415	–1.2855	1.7955	–3.0680
H(10)	–1.9745	–0.9021	–1.0309	–1.2623	2.1283	–1.3132
H(11)	–2.4312	–2.0111	0.3063	0.2780	2.0051	–2.2260

Sum of electronic and zero-point energies = –107.4617 Hartree for g^+g^+
Sum of electronic and zero-point energies = –107.4596 Hartree for g^+g^-
All coordinates in Å.

Electronic Appendix – Chapter Six
Tables 6.1 – 6.37

Table 6.1 Calculated coordinates (MP2/6-311+G*) for $(PF_2)_2NH$, **1**.[a]

Atom	*x*	*y*	*z*	*x*	*y*	*z*
	Conformer 1			Conformer 2		
F(1)	1.191304	2.207765	0.317265	0.238235	2.127617	1.193300
P(2)	0.000000	1.487595	–0.496470	0.672879	1.130863	0.000000
N(3)	0.000000	0.000000	0.306499	–0.714215	0.141188	0.000000
H(4)	0.000000	0.000000	1.327023	–1.617129	0.609400	0.000000
P(5)	0.000000	–1.487600	–0.496470	–0.803535	–1.546773	0.000000
F(6)	–1.191300	2.207765	0.317265	0.238235	2.127617	–1.193300
F(7)	–1.191300	–2.207770	0.317265	0.238235	–1.869787	–1.190799
F(8)	1.191304	–2.207770	0.317265	0.238235	–1.869787	1.190799

[a] All coordinates are in Å.
Energy (conformer 1) = –1135.730774 Hartrees (corrected for ZPE).
Energy (conformer 2) = –1135.730246 Hartrees (corrected for ZPE).

Table 6.2 Calculated coordinates (MP2/6-311+G*) for $N(PF_2)_3$, **2**.[a]

Atom	*x*	*y*	*z*
F(1)	–2.224081	0.000000	1.197249
P(2)	–1.526447	0.824086	0.000000
N(3)	0.000000	0.000000	0.000000
P(4)	0.049545	–1.733985	0.000000
F(5)	–2.224081	0.000000	–1.197249
P(6)	1.476903	0.909899	0.000000
F(7)	1.112041	1.926111	–1.197249
F(8)	1.112041	1.926111	1.197249
F(9)	1.112041	–1.926111	–1.197249
F(10)	1.112041	–1.926111	1.197249

[a] All coordinates are in Å.
Energy = –1675.413140 Hartrees (corrected for ZPE).

Table 6.3 Calculated coordinates (MP2/6-311+G*) for $(PF_2)_2N(CH_3)$, **3**.[a]

Atom	*x*	*y*	*z*
F(1)	0.000000	0.197714	0.000000
P(2)	–0.350633	1.641093	0.000000
N(3)	–1.432932	1.765135	0.000000
C(4)	0.077857	2.111656	0.883753
F(5)	0.077857	2.111656	–0.883753
H(6)	0.141730	–0.673522	–1.444226
H(7)	0.141730	–0.673522	1.444226
H(8)	1.143700	0.310612	–2.244236
H(9)	1.143700	0.310612	2.244236

[a] All coordinates are in Å.
Energy = –1174.876073 Hartrees (corrected for ZPE).

Table 6.4 Calculated coordinates (MP2/6-311+G*) for $(PF_2)N(CH_3)_2$, **4**.[a]

Atom	*x*	*y*	*z*
F(1)	0.806615	–1.157644	1.181750
P(2)	–0.287281	–0.892397	0.000000
N(3)	–0.359339	0.758955	0.000000
C(4)	0.806615	1.638409	0.000000
F(5)	0.806615	–1.157644	–1.181750
C(6)	–1.649603	1.439324	0.000000
H(7)	–2.461609	0.709458	0.000000
H(8)	–1.749187	2.069649	0.889646
H(9)	–1.749187	2.069649	–0.889646
H(10)	1.722692	1.048265	0.000000
H(11)	0.800375	2.273722	–0.891241
H(12)	0.800375	2.273722	0.891241

[a] All coordinates are in Å.
Energy = –674.325963 Hartrees (corrected for ZPE).

Table 6.5 Calculated coordinates (MP2/6-311+G*) for $(PF_2)_2N(SiH_3)$, **5**.[a]

Atom	*x*	*y*	*z*
N(1)	0.000000	0.032862	0.000000
Si(2)	1.558362	0.966990	0.000000
H(3)	1.247875	2.407303	0.000000
H(4)	2.283153	0.573417	1.219905
H(5)	2.283153	0.573417	–1.219905
P(6)	–0.809254	–0.397499	–1.432682
P(7)	–0.809254	–0.397499	1.432682
F(8)	0.341230	–1.262883	–2.162204
F(9)	0.341230	–1.262883	2.162204
F(10)	–0.527543	0.963046	–2.261954
F(11)	–0.527543	0.963046	2.261954

[a] All coordinates are in Å.
Energy = –1425.916665 Hartrees (corrected for ZPE).

Table 6.6 Calculated coordinates (MP2/6-311+G*) for $(PF_2)N(SiH_3)_2$, **6**.[a]

Atom	*x*	*y*	*z*
F(1)	0.448546	–0.022328	–0.014131
P(2)	1.979641	–0.916111	–0.051546
N(3)	2.613023	–0.909885	1.284910
Si(4)	1.686348	–2.301396	–0.475629
F(5)	2.883335	–0.249390	–1.014964
Si(6)	0.515793	1.759151	0.117663
H(7)	0.568377	2.366618	–1.228139
H(8)	1.776392	2.057792	0.836200
H(9)	–0.650854	2.246945	0.873854
H(10)	–0.996167	–0.858720	–0.149474
H(11)	–1.805630	0.193818	–1.092772
H(12)	–1.751037	–0.413391	1.219345

[a] All coordinates are in Å.
Energy = –1176.410768 Hartrees (corrected for ZPE).

Table 6.7 Calculated coordinates (MP2/6-311+G*) for $(PF_2)_2N(GeH_3)$, **7**.[a]

Atom	*x*	*y*	*z*
N(1)	0.000000	0.345760	0.000000
Ge(2)	0.150968	–1.583908	0.000000
H(3)	1.652005	–1.903379	0.000000
H(4)	–0.559790	–2.043292	1.278446
H(5)	–0.559790	–2.043292	–1.278446
P(6)	–0.028422	1.239345	–1.435633
P(7)	–0.028422	1.239345	1.435633
F(8)	–1.314291	0.579610	–2.163563
F(9)	–1.314291	0.579610	2.163563
F(10)	1.063694	0.368965	–2.262268
F(11)	1.063694	0.368965	2.262268

[a] All coordinates are in Å.
Energy = –3212.340503 Hartrees (corrected for ZPE).

Table 6.8 Calculated coordinates (MP2/6-311+G*) for $(PF_2)NH(SiH_3)$, **8**.[a]

Atom	*x*	*y*	*z*	*x*	*y*	*z*
	Conformer 1			Conformer 2		
F(1)	–1.277250	–1.058928	–0.744811	–1.685340	1.190126	–0.206605
P(2)	–1.115763	–0.042228	0.510584	–0.826723	0.000008	0.490017
N(3)	0.511608	–0.197864	0.834609	0.521368	–0.000087	–0.487631
Si(4)	1.910563	0.012673	–0.234181	2.200075	0.000006	0.047439
F(5)	–1.072533	1.289045	–0.421928	–1.685434	–1.190069	–0.206556
H(6)	0.692475	–0.402325	1.810236	0.338477	–0.000151	–1.488620
H(7)	2.479756	1.370297	–0.093976	2.158222	–0.000512	1.523446
H(8)	2.924839	–0.981404	0.178869	2.895378	–1.202569	–0.459129
H(9)	1.458283	–0.216579	–1.616969	2.895095	1.203124	–0.458233

[a] All coordinates are in Å.
Energy (conformer 1) = –886.225399 Hartrees (corrected for ZPE).
Energy (conformer 2) = –886.225209 Hartrees (corrected for ZPE).

Table 6.9 Relative energies (kJ mol^{-1}) of the two conformers of bis(difluorophosphino)amine, **1**.

Level/basis set	Conformer 1	Conformer 2
RHF/3-21G*	0	0.6
RHF/6-31G*	0	0.9
MP2/6-31G*	0	1.3
MP2/6-31+G*	0	1.3
MP2/6-311G*	0	1.9
MP2/6-311+G*	0	1.4

Table 6.10 Refined and calculated geometric parameters (r_{h1} structure) for $(PF_2)_2NH$, **1**, from the GED study.[a,b]

No.	Parameter	GED (r_{h1})	MP2/6-311+G*	Restraint
Independent				
p_1	N–P average	169.3(3)	169.7	—
p_2	N–P difference	1.4(2)	1.4	1.4(2)
p_3	P–F mean	157.8(1)	161.4	—
p_4	N–H mean	102.0(13)	101.9	101.9(14)
p_5	N–P–F average	97.8(6)	98.8	—
p_6	N–P–F difference 1	1.1(6)	0.7	0.7(6)
p_7	N–P–F difference 2	1.3(6)	1.5	1.5(6)
p_8	F–P–F mean	96.9(5)	95.2	—
p_9	P–N–H average	119.6(3)	116.6	116.6(10)
p_{10}	P–N–H difference 1	1.3(6)	1.3	1.3(5)
p_{11}	P–N–H difference 2	3.9(11)	4.0	4.0(10)
p_{12}	P–N–P–F(6)	124.3(10)	131.6	—
p_{13}	P′–N′–P′–F′(6)	144.0(77)	131.6	—
p_{14}	Weight conformer 1	0.46(3)[c]	0.38	—
Dependent				
p_{15}	N–P–F(1)	97.5(5)	98.8	—
p_{16}	N′–P′–F′(1)	97.3(9)	98.0	—
p_{17}	N′–P′–F′(6)	98.6(7)	99.5	—
p_{18}	N–P	168.6(3)	169.1	—
p_{19}	N′–P′	170.0(3)	170.4	—
p_{20}	P–N–H	121.3(5)	118.4	—
p_{21}	P′(2)–N′–H′	120.0(6)	117.1	—
p_{22}	P′(5)–N′–H′	117.4(8)	114.4	—
p_{23}	P–N–P	117.4(9)	123.3	—
p_{24}	P′–N′–P′	122.5(7)	128.5	—

[a] Distances are in pm, angles in degrees. See text for parameter definitions and Figure 2 for atom numbering. The figures in parentheses are the estimated standard deviations of the last digits. [b] *Z′* denotes an atom from the second conformer. [c] Standard deviation obtained from values of *R* factor as the weight was varied. See Figure 4.

Table 6.11 Selected interatomic distances (r_a/pm) and amplitudes of vibration (u_{h1}/pm) for the restrained GED structure of $(PF_2)_2NH$, **1**.[a]

No.	Atom pair	r_a/pm	u_{h1}/pm[b]	Restraint
u_1	F(1)–P(2)	157.7(1)	5.2(2)	—
u_2	P(2)–N(3)	168.6(6)	4.7(tied to u_1)	—
u_3	F(1)...F(6)	239.4(8)	9.4(tied to u_4)	—
u_4	F(1)...N(3)	244.7(4)	13.3(7)	—
u_5	P(2)...P(5)	286.5(5)	10.0(9)	—
u_6	F(1)...P(5)	392.5(4)	10.5(7)	—
u_7	F(1)...F(8)	487.1(13)	13.5(14)	17.2(17)
u_8	F(1)...F(7)	424.3(9)	13.0(10)	10.4(10)
u_9	P′(5)–F′(7)	157.7(1)	5.3(tied to u_1)	—
u_{10}	F′(1)–P′(2)	158.2(1)	5.2(tied to u_1)	—
u_{11}	N′(3)–P′(5)	168.6(5)	4.7(tied to u_1)	—
u_{12}	P′(2)–N′(3)	170.0(5)	4.8(tied to u_1)	—
u_{13}	F′(7)...F′(8)	239.4(10)	10.0(tied to u_4)	—
u_{14}	F′(1)...N′(3)	245.5(14)	13.5(tied to u_4)	—
u_{15}	N′(3)...F′(7)	246.7(10)	13.0(tied to u_1)	—
u_{16}	P′(2)...P′(5)	295.3(9)	7.7(tied to u_5)	—
u_{17}	P′(2)...F′(7)	309.4(54)	16.8(14)	16.6(17)
u_{18}	F′(1)...F′(8)	376.1(29)	23.7(33)	33.1(33)
u_{19}	F′(1)...F′(7)	342.1(12)	20.4(19)	18.5(19)

[a] Estimated standard deviations, as obtained in the least squares refinement, are given in parentheses. Atom pairs u_9 to u_{19} inclusive relate to the second conformer; atoms from conformer 2 denoted by Z′. [b] Amplitudes not refined were fixed at the values obtained using the RHF/6-31G* force field.

Table 6.12 Least-squares correlation matrix (×100) for $(PF_2)_2NH$, **1**.[a]

	p_1	p_6	p_8	p_{12}	p_{13}	u_4	u_5	k_1	k_2
p_5		52	–77	52		–70			
p_6					54				
p_8				–60		66			
p_9	60								
p_{11}							–60		
u_1								72	54
u_4								50	50
k_1									70

[a] Only elements with absolute values ≥ 50% are shown; k_1 and k_2 are scale factors.

Table 6.13 Refined and calculated geometric parameters (r_{h1} structure) for $N(PF_2)_3$, **2**, from the GED study.[a]

No.	Parameter	GED (r_{h1})	MP2/6-311+G*	Restraint
Independent				
p_1	N–P	169.2(3)	173.5	—
p_2	P–F	156.4(1)	161.2	—
p_3	N–P–F	99.2(6)	98.0	—
p_4	F–P–F	98.1(9)	95.9	—
p_5	F(1)–P(2)–N–P(4)	41.5(15)	48.6	—

[a] Distances are in pm, angles in degrees. See text for parameter definitions and Figure 2 for atom numbering. The figures in parentheses are the estimated standard deviations of the last digits.

Table 6.14 Selected interatomic distances (r_a/pm) and amplitudes of vibration (u_{h1}/pm) for the restrained GED structure of $N(PF_2)_3$, **2**.[a]

No.	Atom pair	r_a/pm	u_{h1}/pm[b]	Restraint
u_1	F(5)–P(2)	156.4(1)	3.9(3)	—
u_2	P(4)...P(2)	292.2(5)	9.6(5)	—
u_3	N(3)–P(2)	169.1(3)	5.0(5)	4.7(5)
u_4	P(4)...F(1)	313.4(10)	20.9(9)	16.4(16)
u_5	P(6)...F(5)	393.4(6)	19.2(16)	—
u_6	F(1)...F(5)	236.0(15)	7.9(13)	—
u_7	F(5)...N(3)	247.5(10)	9.7(14)	—
u_8	F(7)...F(5)	388.9(14)	24.1(27)	26.4(26)
u_9	F(8)...F(5)	452.7(10)	22.1(12)	15.9(16)

[a] Estimated standard deviations, as obtained in the least-squares refinement, are given in parentheses. [b] Amplitudes not refined were fixed at the values obtained using the RHF/6-31G* force field.

Table 6.15 Least-squares correlation matrix (×100) for $N(PF_2)_3$, **2**.[a]

	p_4	p_5	u_3	u_4	u_6	u_7	u_8	k_1
p_1				58				
p_2			50					
p_3	–72	79			–83	–71		
p_4		–52			62	90		
p_5					–72	–56		
u_1			65					63
u_5							–86	
u_6						59		

[a] Only elements with absolute values ≥ 50% are shown; k_1 is a scale factor.

Table 6.16 Energy differences (kJ mol^{-1}) between the two conformers of $(PF_2)NH(CH_3)$, **3**, for the various calculations.

Level/Basis Set	Conformer 1	Conformer 2
RHF/3-21G*	0	5.2
RHF/6-31G*	0	5.5
MP2/6-31G*	0	6.2
MP2/6-31+G*	0	6.9
MP2/6-311G*	0	6.4
MP2/6-311+G*	0	7.1

Table 6.17 Refined and calculated geometric parameters (r_{h1} structure) for $(PF_2)NH(CH_3)$, **3**, from the GED study.[a]

No.	Parameter	GED (r_{h1})	MP2/6-311+G*	Restraint
Independent				
p_1	N–P	165.2(9)	165.3	165.3(12)
p_2	P–F average	163.6(3)	162.9	162.9(3)
p_3	P–F difference	0.3(1)	0.3	0.3(1)
p_4	N–C	150.7(4)	144.8	—
p_5	N–H	100.8(19)	101.0	—
p_6	C–H mean	109.8(8)	109.1	—
p_7	N–P–F average	100.6(3)	100.5	—
p_8	N–P–F difference	1.4(7)	1.1	1.1(7)
p_9	F–P–F	92.6(4)	93.3	—
p_{10}	P–N–C	127.5(6)	126.5	—
p_{11}	P–N–H	115.3(3)	115.3	115.3(3)
p_{12}	H–C–H mean	107.8(9)	108.8	108.8(10)
p_{13}	C–N–P–F(5)	–29.0(48)	–44.3	—
p_{14}	CH_3 torsion	–91.2(207)	—	—
p_{15}	CH_3 tilt	–1.5(20)	—	–2.0(20)
p_{16}	H(6) drop	15.8(20)	—	16.0(20)
Dependent				
p_{17}	P–F(1)	163.3(4)	162.6	—
p_{18}	P–F(5)	163.9(4)	163.2	—
p_{19}	N–P–F(1)	99.1(7)	99.4	—
p_{20}	N–P–F(5)	102.0(7)	101.6	—
p_{21}	C–N–H	115.5(8)	116.6	—
p_{22}	N–C–H(7)	110.3(13)	111.8	—

[a] Distances are in pm, angles in degrees. See text for parameter definitions and Figure 2 for atom numbering. The figures in parentheses are the estimated standard deviations of the last digits.

Table 6.18 Selected interatomic distances (r_a/pm) and amplitudes of vibration (u_{h1}/pm) for the restrained GED structure of $(PF_2)NH(CH_3)$, **3**.[a]

No.	Atom pair	r_a/pm	u_{h1}/pm[b]	Restraint
u_1	F(1)–P(2)	163.2(4)	5.2(1)	4.1(4)
u_2	N(3)–P(2)	165.1(9)	5.7(tied to u_1)	—
u_3	P(2)–F(5)	163.9(4)	5.4(tied to u_1)	—
u_4	N(3)–C(4)	150.7(4)	4.9(4)	4.7(5)
u_5	C(4)–H(7)	109.6(8)	8.0(7)	7.5(8)
u_6	C(4)–H(8)	109.6(8)	7.9(tied to u_5)	—
u_7	C(4)–H(9)	109.6(8)	7.9(tied to u_5)	—
u_8	F(1)...N(3)	249.7(13)	6.2(8)	—
u_9	F(1)...C(4)	320.0(35)	14.8(15)	15.1(15)
u_{10}	F(1)...F(5)	236.5(5)	6.2(6)	—
u_{11}	P(2)...C(4)	281.0(6)	8.5(7)	—
u_{12}	F(5)...N(3)	255.6(13)	6.5(tied to u_8)	—
u_{13}	C(4)...F(5)	298.0(31)	16.8(tied to u_9)	—

[a] Estimated standard deviations, as obtained in the least-squares refinement, are given in parentheses. [b] Amplitudes not refined were fixed at the values obtained using the RHF/6-31G* force field.

Table 6.19 Least-squares correlation matrix (×100) for $(PF_2)NH(CH_3)$, **3**.[a]

	p_1	p_5	p_7	p_9	p_{10}	p_{14}	p_{15}	u_1	u_5	u_8	u_{11}	k_1	k_2
p_1					–51			–55					
p_2	–98	–74	55		50			54					
p_4													–54
p_5									67				
p_6							–70						
p_7	–60			–51	50						–54		
p_8										–78			
p_9	71												
p_{13}						65					54		
u_1												51	
k_1													60

[a] Only elements with absolute values ≥ 50% are shown; k_1 and k_2 are scale factors.

Table 6.20a Refined and calculated geometric parameters (r_{h1} structure) for $(PF_2)N(CH_3)_2$, **4**, from the GED study, including rotational constants.[a]

No.	Parameter	GED (r_{h1})	MP2/6-311+G*	Restraint
Independent				
p_1	N–P	164.9(11)	165.3	165.3(14)
p_2	P–F	159.2(4)	163.2	—
p_3	N–C average	146.5(7)	146.0	—
p_4	N–C difference	0.2(1)	0.2	0.2(1)
p_5	C–H mean	108.9(8)	109.5	—
p_6	N–P–F	101.4(4)	101.0	—
p_7	F–P–F	95.3(5)	92.8	—
p_8	P–N–C average	122.6(5)	122.4	—
p_9	P–N–C difference	4.0(8)	4.2	4.2(9)
p_{10}	H–C–H mean	109.0(7)	109.0	109.0(8)
p_{11}	C(4)–N–P–F(5)	–52.1(8)	–47.5	—
p_{12}	C(4)H_3 torsion	–0.3(148)	0.0	—
p_{13}	C(6)H_3 torsion	1.2(171)	0.0	—
Dependent				
p_{14}	C(4)–N	146.5(7)	146.0	—
p_{15}	C(6)–N	146.6(7)	145.9	—
p_{16}	P–N–C(4)	124.6(5)	124.5	—
p_{17}	P–N–C(6)	120.6(7)	120.3	—
p_{18}	C–N–C	114.8(10)	115.2	—
p_{19}	N–C–H(10)	110.0(7)	110.2	—

[a] Distances are in pm, angles in degrees. See text for parameter definitions and Figure 2 for atom numbering. The figures in parentheses are the estimated standard deviations of the last digits.

Table 6.20b Refined and calculated geometric parameters (r_{h1} structure) for $(PF_2)N(CH_3)_2$, **4**, from the GED study, excluding rotational constants.[a]

No.	Parameter	GED (r_{h1})	MP2/6-311+G*	Restraint
Independent				
p_1	N–P	164.3(11)	165.3	165.3(14)
p_2	P–F	159.4(4)	163.2	—
p_3	N–C average	146.3(7)	146.0	—
p_4	N–C difference	0.2(1)	0.2	0.2(1)
p_5	C–H mean	109.7(8)	109.5	—
p_6	N–P–F	102.2(5)	101.0	—
p_7	F–P–F	95.7(8)	92.8	—
p_8	P–N–C average	123.5(7)	122.4	—
p_9	P–N–C difference	4.3(9)	4.2	4.2(9)
p_{10}	H–C–H mean	108.7(7)	109.0	109.0(8)
p_{11}	C(4)–N–P–F(5)	–57.3(28)	–47.5	—
p_{12}	C(4)H_3 torsion	0.0(19)	0.0	0.0(20)
p_{13}	C(6)H_3 torsion	0.3(19)	0.0	0.0(20)
Dependent				
p_{14}	C(4)–N	146.2(7)	145.9	—
p_{15}	C(6)–N	146.4(7)	146.0	—
p_{16}	P–N–C(4)	125.7(8)	124.5	—
p_{17}	P–N–C(6)	121.3(9)	120.3	—
p_{18}	C–N–C	113.0(14)	115.2	—
p_{19}	N–C–H(10)	110.2(7)	110.2	—

[a] Distances are in pm, angles in degrees. See text for parameter definitions and Figure 2 for atom numbering. The figures in parentheses are the estimated standard deviations of the last digits.

Table 6.21 Selected interatomic distances (r_a/pm) and amplitudes of vibration (u_{h1}/pm) for the restrained GED structure of $(PF_2)N(CH_3)_2$, **4**.[a]

No.	Atom pair	r_a/pm	u_{h1}/pm[b]	Restraint
u_1	C(6)–H(7)	108.5(8)	8.8(tied to u_4)	—
u_2	C(4)–H(10)	108.6(8)	8.8(tied to u_4)	—
u_3	C(6)–H(8)	108.5(8)	9.0(tied to u_4)	—
u_4	C(4)–H(11)	108.5(8)	8.9(10)	—
u_5	N(3)–C(4)	146.5(7)	4.6(4)	4.6(5)
u_6	N(3)–C(6)	146.7(7)	4.7(tied to u_5)	—
u_7	F(1)–P(2)	159.1(4)	5.0(6)	—
u_8	P(2)–N(3)	164.6(11)	4.1(4)	4.2(4)
u_9	F(1)...F(5)	235.4(11)	6.7(6)	6.6(7)
u_{10}	F(1)...N(3)	250.3(8)	9.3(8)	9.2(9)
u_{11}	P(2)...C(4)	264.7(40)	7.9(6)	8.0(8)
u_{12}	P(2)...C(6)	270.2(30)	7.6(tied to u_{11})	—
u_{13}	F(1)...C(6)	293.5(43)	11.0(16)	—
u_{14}	P(2)...H(11)	329.4(45)	29.9(26)	29.0(29)
u_{15}	P(2)...H(8)	330.1(104)	34.5(tied to u_{14})	—
u_{16}	F(1)...C(4)	363.8(25)	16.7(20)	—

[a] Estimated standard deviations, as obtained in the least-squares refinement, are given in parentheses. [b] Amplitudes not refined were fixed at the values obtained using the RHF/6-31G* force field.

Table 6.22 Least-squares correlation matrix (×100) for $(PF_2)N(CH_3)_2$, **4**.[a]

	p_1	p_2	p_6	p_8	p_{11}	u_7
p_1		–84	–58	–51		–73
p_2						57
p_3	–54					66
p_7					–90	
p_{11}				–51		

[a] Only elements with absolute values ≥ 50% are shown.

Table 6.23 Energy differences (kJ mol^{-1}) between the two conformers of $(PF_2)_2N(SiH_3)$, **5**, for the various calculations.

Level/basis set	Conformer 1	Conformer 2
RHF/3-21G*	0	7.0
RHF/6-31G*	0	4.0
MP2/6-31G*	0	5.4
MP2/6-311G*	0	5.7
MP2/6-311+G*	0	5.3

Table 6.24 Refined and calculated geometric parameters (r_{h1} structure) for $(PF_2)_2N(SiH_3)$, **5**, from the GED study.[a]

No.	Parameter	GED (r_{h1})	MP2/6-311+G*	Restraint
Independent				
p_1	N–P	169.0(4)	170.1	—
p_2	P–F average	157.0(1)	161.6	—
p_3	P–F difference	0.4(3)	0.4	0.4(2)
p_4	N–Si	177.7(10)	181.7	—
p_5	Si–H mean	142.9(16)	147.3	—
p_6	N–P–F average	100.6(4)	99.0	—
p_7	N–P–F difference	2.4(3)	2.4	2.4(3)
p_8	F–P–F	97.4(5)	95.5	—
p_9	P(6)–N–Si	121.9(3)	122.6	—
p_{10}	H–Si–H mean	111.5(8)	111.6	111.6(8)
p_{11}	Si–N–P(6)–F(8)	58.5(11)	58.7	—
p_{12}	SiH_3 torsion	16.2(21)	0.0	—
Dependent				
p_{13}	P(6)–F(8)	156.8(2)	161.8	—
p_{14}	P(6)–F(10)	157.2(2)	162.3	—
p_{15}	N–P(6)–F(8)	101.8(4)	100.4	—
p_{16}	N–P(6)–F(10)	99.4(4)	97.9	—
p_{17}	P–N–P	116.1(6)	116.2	—
p_{18}	N–Si–H(3)	107.3(9)	106.5	—

[a] Distances are in pm, angles in degrees. See text for parameter definitions and Figure 2 for atom numbering. The figures in parentheses are the estimated standard deviations of the last digits.

Table 6.25 Selected interatomic distances (r_a/pm) and amplitudes of vibration (u_{h1}/pm) for the restrained GED structure of $(PF_2)_2N(SiH_3)$, **5**.[a]

No.	Atom pair	r_a/pm	u_{h1}/pm[b]	Restraint
u_1	N(1)–Si(2)	177.7(10)	5.0(5)	4.9(5)
u_2	N(1)–P(6)	169.0(4)	4.4(4)	4.5(5)
u_3	Si(2)–H(3)	142.8(17)	8.3(9)	8.4(8)
u_4	Si(2)–H(4)	142.8(17)	8.3(tied to u_3)	—
u_5	P(6)–F(8)	156.7(2)	4.5(3)	—
u_6	P(6)–F(10)	157.1(2)	4.5(tied to u_5)	—
u_7	N(1)...F(8)	252.6(6)	9.1(tied to u_8)	—
u_8	N(1)...F(10)	248.4(6)	9.2(12)	—
u_9	Si(2)...P(6)	302.5(4)	9.0(5)	—
u_{10}	Si(2)...F(8)	329.2(13)	16.9(14)	—
u_{11}	Si(2)...F(10)	306.8(16)	18.6(15)	17.6(18)
u_{12}	P(6)...P(7)	286.2(7)	7.1(6)	6.8(7)
u_{13}	P(6)...F(9)	381.7(12)	16.9(6)	—
u_{14}	P(6)...F(11)	391.5(7)	13.8(tied to u_{13})	—
u_{15}	F(8)...F(9)	424.2(33)	22.6(24)	24.0(24)
u_{16}	F(8)...F(10)	235.6(10)	7.2(10)	—
u_{17}	F(8)...F(11)	495.1(11)	19.7(19)	—
u_{18}	F(10)...F(11)	451.7(19)	15.2(29)	—

[a] Estimated standard deviations, as obtained in the least-squares refinement, are given in parentheses. [b] Amplitudes not refined were fixed at the values obtained using the RHF/6-31G* force field.

Table 6.26 Least-squares correlation matrix (×100) for $(PF_2)_2N(SiH_3)$, **5**.[a]

	p_1	p_9	u_1	u_5	u_8	u_{12}	u_{16}	k_1	k_2
p_1			55	–76					
p_4	–63	–91		65	56		56	54	
p_5								–55	
p_6							–58		
p_8					93		77	57	
p_9	65			–64	–55		–56		
u_5								52	
u_8							85	63	
u_9						71			
u_{16}								57	
k_1									69

[a] Only elements with absolute values ≥ 50% are shown; k_1 and k_2 are scale factors.

Table 6.27 Refined and calculated geometric parameters (r_{h1} structure) for $(PF_2)N(SiH_3)_2$, **6**, from the GED study.[a]

No.	Parameter	GED (r_{h1})	MP2/6-311+G*	Restraint
Independent				
p_1	N–P	166.1(10)	167.5	—
p_2	P–F average	158.7(3)	162.7	—
p_3	P–F difference	0.4(4)	0.3	0.3(4)
p_4	N–Si average	175.9(3)	178.1	—
p_5	N–Si difference	1.4(1)	1.4	1.4(1)
p_6	Si–H mean	146.0(5)	147.8	—
p_7	N–P–F average	101.3(6)	100.1	—
p_8	N–P–F difference	1.5(10)	2.4	2.4(12)
p_9	F–P–F	96.3(4)	94.6	—
p_{10}	P–N–Si average	119.8(5)	120.9	—
p_{11}	P–N–Si difference	–1.2(11)	3.0	3.0(15)
p_{12}	H–Si–H mean	111.0(9)	110.3	110.3(10)
p_{13}	Si(4)–N–P–F(5)	–55.5(29)	–59.3	—
p_{14}	$Si(4)H_3$ torsion	52.7(203)	86.0	—
p_{15}	$Si(6)H_3$ torsion	61.0(96)	20.0	—
Dependent				
p_{16}	P–F(1)	158.9(3)	162.9	—
p_{17}	P–F(5)	158.5(3)	162.5	—
p_{18}	N–P–F(1)	100.5(9)	98.8	—
p_{19}	N–P–F(5)	102.1(7)	101.3	—
p_{20}	Si–N–Si	120.4(10)	118.1	—
p_{21}	N–Si(4)	176.6(3)	178.8	—
p_{22}	N–Si(6)	175.2(3)	177.3	—
p_{23}	P–N–Si(4)	119.2(5)	119.4	—
p_{24}	P–N–Si(6)	120.4(9)	122.4	—

[a] Distances are in pm, angles in degrees. See text for parameter definitions and Figure 2 for atom numbering. The figures in parentheses are the estimated standard deviations of the last digits.

Table 6.28 Selected interatomic distances (r_a/pm) and amplitudes of vibration (u_{h1}/pm) for the restrained GED structure of $(PF_2)N(SiH_3)_2$, **6**.[a]

No.	Atom pair	r_a/pm	u_{h1}/pm[b]	Restraint
u_1	F(1)–P(2)	158.6(3)	4.4(tied to u_3)	—
u_2	N(3)–P(2)	167.9(10)	4.6(4)	4.4(4)
u_3	P(2)–F(5)	158.2(3)	4.3(4)	—
u_4	N(3)–Si(4)	176.1(4)	5.4(tied to u_5)	—
u_5	N(3)–Si(6)	174.7(4)	5.2(5)	—
u_6	Si(4)–H(10)	145.9(6)	8.2(7)	8.5(9)
u_7	Si(4)–H(11)	145.9(6)	8.2(tied to u_6)	—
u_8	Si(4)–H(12)	145.9(6)	8.2(tied to u_6)	—
u_9	Si(6)–H(7)	145.9(6)	8.2(tied to u_6)	—
u_{10}	Si(6)–H(8)	145.9(6)	8.2(tied to u_6)	—
u_{11}	Si(6)–H(9)	145.9(6)	8.2(tied to u_6)	—
u_{12}	F(1)...N(3)	248.4(12)	8.2(6)	7.1(7)
u_{13}	F(1)...Si(4)	301.5(38)	18.1(tied to u_{20})	—
u_{14}	F(1)...F(5)	236.2(8)	7.6(9)	—
u_{15}	F(1)...Si(6)	396.5(18)	11.7(tied to u_{21})	—
u_{16}	P(2)...Si(4)	295.8(8)	9.0(tied to u_{17})	—
u_{17}	P(2)...Si(6)	294.5(13)	9.2(5)	—
u_{18}	N(3)...F(5)	251.7(12)	8.1(tied to u_{12})	—
u_{19}	Si(4)...F(5)	316.5(33)	15.2(15)	17.4(17)
u_{20}	Si(4)...Si(6)	305.8(11)	7.5(7)	—
u_{21}	F(5)...Si(6)	391.0(33)	17.6(10)	—

[a] Estimated standard deviations, as obtained in the least-squares refinement, are given in parentheses. [b] Amplitudes not refined were fixed at the values obtained using the RHF/6-31G* force field.

Table 6.29 Least-squares correlation matrix (×100) for $(PF_2)N(SiH_3)_2$, **6**.[a]

	p_1	p_{10}	u_5	u_6	u_{12}	u_{17}	u_{19}	u_{20}	u_{21}	k_1	k_2
p_1		–65	72								
p_2				–69							
p_4	–81		–55								
p_7	–68		–51								
p_9					66						
p_{10}						75		59			
p_{11}								–52			
p_{13}		58				62	59	55	63		
u_3				67							
u_5										50	
u_{17}								76			
u_{19}								52			
k_1											67

[a] Only elements with absolute values ≥ 50% are shown; k_1 and k_2 are scale factors.

Table 6.30 Energy differences (kJ mol^{-1}) between the two conformers of $(PF_2)_2N(GeH_3)$, **7**, for the various calculations.

Level/basis set	Conformer 1	Conformer 2
RHF/3-21G*	0	11.9
RHF/6-31G*	0	8.0
MP2/6-31G*	0	9.2
MP2/6-31+G*	0	8.8
MP2/6-311G*	0	8.7
MP2/6-311+G*	0	7.8

Table 6.31 Refined and calculated geometric parameters (r_{h1} structure) for $(PF_2)_2N(GeH_3)$, **7**, from the GED study.[a]

No.	Parameter	GED (r_{h1})	MP2/6-311+G*	Restraint
Independent				
p_1	N–P	169.7(3)	169.1	—
p_2	P–F average	159.7(2)	162.1	—
p_3	P–F difference	0.6(5)	0.5	0.5(5)
p_4	N–Ge	190.8(5)	193.6	—
p_5	Ge–H mean	154.0(8)	153.4	153.4(9)
p_6	N–P–F average	99.8(3)	99.1	—
p_7	N–P–F difference	2.1(4)	2.4	2.4(4)
p_8	F–P–F	96.6(7)	95.0	—
p_9	P(6)–N–Ge	122.7(1)	121.9	—
p_{10}	H–Ge–H mean	112.3(14)	113.0	113.0(15)
p_{11}	Ge–N–P(6)–F(8)	59.5(8)	58.3	—
p_{12}	GeH_3 torsion	8.8(44)	9.0	—
Dependent				
p_{13}	P(6)–F(8)	159.5(3)	161.8	—
p_{14}	P(6)–F(10)	160.0(3)	162.3	—
p_{15}	N–P(6)–F(8)	100.9(4)	100.4	—
p_{16}	N–P(6)–F(10)	98.8(4)	97.9	—
p_{17}	P–N–P	114.5(3)	116.2	—
p_{18}	N–Ge–H(3)	106.5(16)	106.5	—

[a] Distances are in pm, angles in degrees. See text for parameter definitions and Figure 2 for atom numbering. The figures in parentheses are the estimated standard deviations of the last digits.

Table 6.32 Selected interatomic distances (r_a/pm) and amplitudes of vibration (u_{h1}/pm) for the restrained GED structure of $(PF_2)_2N(GeH_3)$, **7**.[a]

No.	Atom pair	r_a/pm	u_{h1}/pm[b]	Restraint
u_1	N(1)–Ge(2)	190.7(5)	6.5(6)	—
u_2	N(1)–P(6)	169.7(3)	4.6(4)	4.4(4)
u_3	Ge(2)–H(3)	153.8(8)	8.9(9)	8.8(9)
u_4	Ge(2)–H(4)	153.8(8)	8.8(tied to u_3)	—
u_5	P(6)–F(8)	159.4(3)	4.9(2)	—
u_6	P(6)–F(10)	159.9(3)	5.0(tied to u_5)	—
u_7	N(1)...F(8)	253.4(6)	9.5(12)	—
u_8	N(1)...F(10)	250.0(7)	9.4(tied to u_7)	—
u_9	Ge(2)...P(6)	315.7(4)	8.1(4)	7.2(7)
u_{10}	Ge(2)...F(8)	340.5(10)	11.8(9)	—
u_{11}	Ge(2)...F(10)	314.8(11)	15.5(16)	18.2(18)
u_{12}	P(6)...P(7)	285.0(5)	6.1(8)	—
u_{13}	P(6)...F(9)	380.2(11)	12.5(9)	—
u_{14}	P(6)...F(11)	394.1(8)	10.1(tied to u_{13})	—
u_{15}	F(8)...F(10)	238.4(12)	6.8(8)	—
u_{16}	F(8)...F(11)	497.3(11)	12.0(14)	—

[a] Estimated standard deviations, as obtained in the least-squares refinement, are given in parentheses. [b] Amplitudes not refined were fixed at the values obtained using the RHF/6-31G* force field.

Table 6.33 Least-squares correlation matrix (×100) for $(PF_2)_2N(GeH_3)$, **7**.[a]

	p_9	u_2	u_5	u_7	u_{10}	u_{11}	u_{12}	u_{13}	u_{15}	k_2
p_1			–60							
p_2		66								
p_4	–64									51
p_6							–51		–70	
p_8				91						
p_{11}					–64			–61		
u_9						–63	–52			
u_{11}							59			

[a] Only elements with absolute values ≥ 50% are shown; k_2 is a scale factor.

Table 6.34 Energy differences (kJ mol^{-1}) between the two conformers of $(PF_2)NH(SiH_3)$, **8**, for the calculations at different levels of theory.

Level/basis set	Conformer 1	Conformer 2
RHF/3-21G*	0	4.8
RHF/6-31G*	0	4.1
MP2/6-31G*	0	1.7
MP2/6-311G*	0	0.4
MP2/6-311+G*	0	0.5

Table 6.35 Refined and calculated geometric parameters (r_{h1} structure) for $(PF_2)NH(SiH_3)$, **8**, from the GED study.[a,b]

No.	Parameter	GED (r_{h1})	MP2/6-311+G*	Restraint
Independent				
p_1	P–F average	159.3(2)	162.4	—
p_2	P–F difference 1	0.3(2)	0.3	0.3(3)
p_3	P–F difference 2	0.2(1)	0.2	0.2(2)
p_4	N–P–F average	99.2(4)	100.1	—
p_5	N–P–F difference 1	0.8(5)	0.8	0.8(6)
p_6	N–P–F difference 2	1.6(4)	1.6	1.6(4)
p_7	F–P–F mean	95.4(5)	94.2	—
p_8	F(5)–P(2)–N(3)–Si(4)	–20.1(39)	–41.3	—
p_9	F′(1)–P′(2)–N′(3)–Si′(4)	127.6(26)	131.9	—
p_{10}	H–Si–H mean	110.1(9)	110.3	110.3(10)
p_{11}	Si–H mean	147.7(3)	147.7	147.7(3)
p_{12}	SiH_3 torsion 1	–36.0(48)	2.0	—
p_{13}	SiH_3 torsion 2	26.3(47)	60.0	—
p_{14}	SiH_3 rock 1	1.9(19)	2.0	2.0(20)
p_{15}	SiH_3 rock 2	–1.7(19)	–2.0	–2.0(20)
p_{16}	N–H mean	101.4(6)	101.5	101.5(6)
p_{17}	N–Si average	175.0(7)	176.8	—
p_{18}	N–Si difference	1.1(1)	1.1	1.1(1)
p_{19}	N–P mean	168.0(9)	166.6	—
p_{20}	P–N–Si average	127.5(5)	128.2	—
p_{21}	P–N–Si difference	3.2(16)	3.6	3.4(17)
p_{22}	P–N–H average	113.7(8)	113.9	113.9(8)
p_{23}	P–N–H difference	3.3(13)	3.2	3.2(14)
p_{24}	Weight conformer 1	0.54(+2/–5)[c]	0.54	—
Dependent				
p_{25}	P–F(1)	159.2(3)	162.4	—
p_{26}	P–F(5)	159.5(2)	162.6	—
p_{27}	P′–F′	159.3(2)	162.5	—
p_{28}	N–P–F(1)	100.0(5)	100.9	—
p_{29}	N–P–F(5)	98.4(6)	99.3	—
p_{30}	N′–P′–F′	99.2(5)	100.1	—
p_{31}	N–Si	175.6(7)	177.3	—
p_{32}	N′–Si′	174.4(7)	176.2	—
p_{33}	P–N–Si	129.1(8)	130.0	—
p_{34}	P′–N′–Si′	125.9(11)	126.4	—
p_{35}	P–N–H	112.1(10)	112.4	—
p_{36}	P′–N′–H′	115.4(10)	115.6	—

[a] Distances are in pm, angles in degrees. See text for parameter definitions and Figure 2 for atom numbering. The figures in parentheses are the estimated standard deviations of the last digits. [b] *Z′* denotes an atom from the second conformer. [c] Error determined from *R*-factor plot (Figure 11) as the weight was varied.

Table 6.36 Selected interatomic distances (r_a/pm) and amplitudes of vibration (u_{h1}/pm) for the restrained GED structure of $(PF_2)NH(SiH_3)$, **8**.[a]

No.	Atom pair	r_a/pm	u_{h1}/pm[b]	Restraint
u_1	F(1)–P(2)	159.2(3)	3.9(3)	4.0(4)
u_2	P(2)–N(3)	167.9(10)	4.3(4)	4.3(4)
u_3	P(2)–F(5)	159.4(2)	3.9(tied to u_1)	—
u_4	N(3)–Si(4)	175.6(7)	4.4(4)	4.7(5)
u_5	Si(4)–H(7)	147.5(3)	8.8(8)	8.6(9)
u_6	Si(4)–H(8)	147.5(3)	8.8(tied to u_5)	—
u_7	Si(4)–H(9)	147.5(3)	8.8(tied to u_5)	—
u_8	F(1)...N(3)	250.4(7)	8.2(8)	—
u_9	F(1)...Si(4)	354.7(40)	19.2(33)	—
u_{10}	F(1)...F(5)	235.6(10)	7.4(tied to u_{20})	—
u_{11}	P(2)...Si(4)	308.3(10)	11.3(5)	—
u_{12}	N(3)...F(5)	247.4(9)	8.8(tied to u_8)	—
u_{13}	Si(4)...F(5)	303.8(28)	21.6(20)	21.5(22)
u_{14}	F′(1)–P′(2)	159.3(2)	3.9(tied to u_1)	—
u_{15}	P′(2)–N′(3)	167.9(10)	4.4(tied to u_2)	—
u_{16}	N′(3)–Si′(4)	174.5(7)	4.4(tied to u_4)	—
u_{17}	Si′(4)–H′(7)	147.5(3)	8.6(tied to u_5)	—
u_{18}	Si′(4)–H′(8)	147.5(3)	8.7(tied to u_5)	—
u_{19}	F′(1)...N′(3)	249.0(8)	8.5(tied to u_8)	—
u_{20}	F′(1)...F′(5)	235.5(10)	7.3(6)	6.7(7)
u_{21}	P′(2)...Si′(4)	303.0(15)	11.7(tied to u_{11})	—

[a] Estimated standard deviations, as obtained in the least-squares refinement, are given in parentheses. Atom pairs u_{14} to u_{21} inclusive relate to the second conformer; atoms from conformer 2 are denoted by Z'. [b] Amplitudes not refined were fixed at the values obtained using the RHF/6-31G* force field.

Table 6.37 Least-squares correlation matrix (×100) for $(PF_2)NH(SiH_3)$, **8**.[a]

	p_{17}	p_{19}	u_1	u_8	u_{20}	k_2
p_1	67	–77	56			
p_4	51	–70	56			
p_7				80		
p_{17}		–79	61			
p_{19}			–78			
u_8					54	
k_1						53

[a] Only elements with absolute values ≥ 50% are shown; k_1 and k_2 are scale factors.